JOHANNES GUTENBERG UNIVERSITÄT MAINZ

The molecular role of the adhesion GPCR ADGRV1 in brain astrocytes

Dissertation

Submitted to the

Faculty of Biology (FB10)

In partial fulfilment of requirements for the

„Doctor rerum naturalium“

Johannes Gutenberg-Universität Mainz

Baran Enes Güler

Mainz, May 2024

Dekan	:	Univ.-Prof. Dr. Eckhard Thines, Institute of Biotechnology and Drug Research
1. Gutachter	:	Univ.-Prof. Dr. Uwe Wolfrum, Institute of Molecular Physiology
2. Gutachter	:	Prof. Dr. Martin Heine Institute of Developmental Biology and Neurobiology

Date of thesis defense:

“Homo sum, humani nihil a me alienum puto”

Publius Terentius

I. Explanatory notes

The present doctoral work is a cumulative thesis consisting of four essential articles:

Publication I

Güler BE, Krzysko J and Wolfrum U (2021). Isolation and culturing of primary mouse astrocytes for the analysis of focal adhesion dynamics. STAR Protoc. Dec 8;2(4):100954. doi: 10.1016/j.xpro.2021.100954. PMID: 34917973; PMCID: PMC8669101.

Publication II

Kusuluri DK, Güler BE, Knapp B, Horn N, Boldt K, Ueffing M, Aust G and Wolfrum U (2021). Adhesion G protein-coupled receptor VLGR1/ADGRV1 regulates cell spreading and migration by mechanosensing at focal adhesions. iScience. Mar 8;24(4):102283. doi: 10.1016/j.isci.2021.102283. PMID: 33851099; PMCID: PMC8024656.

Publication III

Güler, BE, Linnert J and Wolfrum U (2023). Monitoring paxillin in astrocytes reveals the significance of the adhesion G protein coupled receptor VLGR1/ADGRV1 for focal adhesion assembly. Basic Clin Pharmacol Toxicol. 133(4):301-312. doi: 10.1111/bcpt.13860. Epub 2023 Mar 30. PMID: 36929698.

Preprint I

Güler BE, Zorin M, Linnert J, Nagel-Wolfrum K and Wolfrum U (2024). The adhesion GPCR ADGRV1 controls glutamate homeostasis in hippocampal astrocytes supporting neuron development: first insights into to pathophysiology of ADGRV1-associated epilepsy. bioRxiv 2024.04.25.591120; doi: https://doi.org/10.1101/2024.04.25.591120.

In addition to the publications compiled for this dissertation, I have contributed to the following scientific work:

PUBLICATIONS

Knapp B, Roedig J, Roedig H, Krzysko J, Horn N, **Güler BE**, Kusuluri DK, Yildirim A, Boldt K, Ueffing M, Liebscher I, Wolfrum U (2022). Affinity proteomics identifies interaction partners and defines novel insights into the function of the adhesion GPCR VLGR1/ADGRV1. Molecules. May 12;27(10):3108. doi: 10.3390/molecules27103108. PMID: 35630584; PMCID: PMC9146371.

Krzysko J, Maciag F, Mertens A, **Güler BE**, Linnert J, Boldt K, Ueffing M, Nagel-Wolfrum K, Heine M, Wolfrum U (2022). The adhesion GPCR VLGR1/ADGRV1 regulates the Ca2+ homeostasis at mitochondria-associated ER membranes. Cells. Sep 7;11(18):2790. doi: 10.3390/cells11182790. PMID: 36139365; PMCID: PMC9496679.

Linnert J, **Güler BE**, Krzysko J, Wolfrum U (2023). The adhesion G protein-coupled receptor VLGR1/ADGRV1 controls autophagy. Basic Clin Pharmacol Toxicol. 2023 Oct;133(4):313-330. doi: 10.1111/bcpt.13869. PMID: 37002809.

Linnert J, Knapp B, **Güler BE**, Boldt K, Ueffing M, Wolfrum U (2023). Usher syndrome proteins ADGRV1 (USH2C) and CIB2 (USH1J) interact and share a common interactome containing TRiC/CCT-BBS chaperonins. Front Cell Dev Biol. 22;11:1199069. doi: 10.3389/fcell.2023.1199069. PMID: 37427378; PMCID: PMC10323441.

Wolfrum U, Linnert J, **Güler BE**, Klein J, Fritze JS, Wenck N, Nagel-Wolfrum K (2024), Identification of unexpected pathomechanisms underlying the human Usher syndrome. In: Retinal Degenerative Diseases - Mechanisms and Experimental Therapy. Advances in Experimental Medicine and Biology. Springer, Boston, MA. Eds, Bowes Rickman C, Grimm C, Anderson RE, Ash J, Hollyfield J, Pierce EA (under review).

List of Abbreviations

aGPCR	Adhesion G protein-coupled receptor ADGRV1
ATP	Adenosine triphosphate
Calxß	Calx-beta
cAMP	Cyclic adenosine monophosphate
CTF	C-terminal fragment
DAPI	4,6-Diamidino-2-Phenylindol
ECD	Extracellular domain
ECL	Extracellular loops
ECM	Extracellular matrix
ER	Endoplasmic reticulum
FAK	Focal adhesion kinase
FAs	Focal adhesions
FRAP	Fluoresence recovery after photobleaching
GAIN	GPCR autoproteolysis-inducing (domain)
GPS	PCR proteolysis site
GPCR	G protein-coupled receptor
GTP	Guanosine triphosphate
ICD	Intracellular domain
ICL	Intracellular loops
KD	Knockdown
min	Minute
MT	Microtubule
NTF	N-terminal fragment
PN	Postnatal Day
PBM	PDZ-Binding motif
PDZ	Domain, named after PDZ containing proteins PSD95, DLG-1, and ZO-1
PTX	Pentraxin
s	Second
TAP	Tandem affinity purification
TM	Transmembrane
USH	Human Usher Syndrome
WT	Wild type

INDEX

1. Introduction

This study focuses on the Very Large G protein-coupled receptor (VLGR1), recently renamed as Adhesion G protein-coupled receptor V1 (ADGRV1) (Scholz et al., 2019). ADGRV1 belongs to the adhesion GPCR family within the broader category of G protein-coupled receptors (GPCRs). Also known as the USH2C protein, ADGRV1 is associated with the human Usher syndrome (USH), the prevailing hereditary cause of deaf-blindness in humans. Within the Usher syndrome protein network, ADGRV1 dynamically interacts with other proteins in hair and photoreceptor cells. Additionally, human pathogenic variants in the *ADGRV1* gene are known to result in various forms of epilepsy. In the past, ADGRV1 was identified within membrane adhesion complexes at synapses and as part of fibrous connections in mechanosensitive hair cells and retinal photoreceptor cells. Although ADGRV1 is ubiquitously expressed in humans and mice during development, it is most prominently expressed in astrocytes. This study aims to uncover the previously unknown role of ADGRV1 in the central nervous system, particularly in astrocytes, thereby deepening and expanding our understanding of the pathomechanisms related to this adhesion GPCR (aGPCR).

1.1 Adhesion G protein-coupled receptors (aGPCRs)

GPCRs are one of the largest protein families having more than 800 members in the human proteome (Fredriksson et al., 2003). This protein superfamily can be divided into five subfamilies by using sequence similarity which are Class A: Rhodopsin receptors, Class B: secretin receptors, Class C: Glutamate receptors, Class E: Adhesion receptors and Class F: frizzled/taste2 (Odoemelam et al., 2020). The structural basis of all GPCR families consists of similar protein domains. The extracellular N-terminal fragment (NTF) which plays a critical role in ligand identification and selection, the 7-Transmembrane domain (7TM) and the C-terminal fragment (CTF). The CTF forms binding sites for G proteins or arrestins and interacts with regulatory proteins such as GPCR kinases. The 7TM helical core, located between the extracellular and intracellular regions, transmits, and transforms signals from ligands through distinct structural changes. Depending on the activation mechanisms, GPCRs show different structural composition and size in their extracellular N-terminus and intracellular C-terminus (Rosenbaum et al., 2009). GPCRs are essential to cellular communication by facilitating the transmission of extracellular signals into the cell. These signals can be conveyed through neurotransmitters, hormones, odorants/taste compounds, or light and mechano-stimulation. Sensing extracellular cues can either activate or inhibit several signalling pathways via canonical signal transduction. Signal transduction typically involves heterotrimeric G proteins

(Rosenbaum et al., 2009; Glukhova et al., 2018). Heterotrimeric G proteins are composed of α, β, and γ subunits bound to the guanine nucleotide. Even though most of the GPCRs can transduce extracellular cues by more than one subunit, they preferably engage to single type of G protein (Chaudhary and Kim 2021). Different G protein coupling by GPCRs initiates different downstream signalling cascades (Jang et al., 2023).

The group of Adhesion GPCRs (aGPCRs), which consist of 33 members, constitute the second largest GPCR family (Figure 1) (Favara et al., 2014). The classification of aGPCRs has evolved over time and initially, they were grouped with the Secretin receptors based on their structural similarities (Hamann et al. 2015). However, subsequent genetic studies have revealed that aGPCRs form a distinct subfamily within the GPCR superfamily, with their own unique characteristics and functions. Unlike other GPCRs, aGPCRs are often characterized by their notably long extracellular NTFs, which encompass numerous protein-binding domains responsible for facilitating cell-cell and cell-matrix adhesions (Hamann et al., 2015). Like other GPCRs, aGPCRs contain a seven-transmembrane helix domain (7TM) except for ADGRG7 which was recently identified as the first eight transmembrane helices containing aGPCRs (Kuhn et al., 2024).

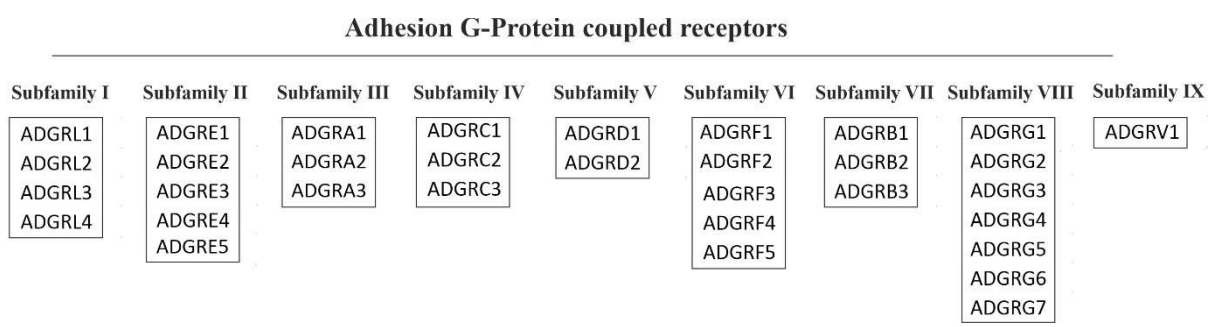

Figure 1. aGPCR family members. Phylogenetically aGPCRs are divided into 9 subfamilies from Family I to Family IX (Scholz et al., 2019).

aGPCRs possess a distinctive GAIN (GPCR autoproteolysis-inducing) protein domain situated at the N-terminus of their 7TM. This GAIN domain encompasses the GPCR proteolytic site (GPS), where autolytic cleavage occurs resulting in the formation of two functional protein subunits (Sakurai et al., 2022). The N-terminal fragment (NTF) remains extracellular, while the C-terminal fragment remains associated with the cell membrane (Araç et al., 2012). These fragments typically exist as dimers; however, they can also independently engage in signalling functions and, notably, form heterodimers with fragments from other aGPCRs (Hu et al., 2014a; Hamann et al., 2015; Knapp et al., 2019). It is worth highlighting that the C-terminal fragments of many aGPCRs exhibit higher receptor activity than the full-length proteins (Okajima et al.,

2010; Paavola et al., 2011; Knapp et al., 2019). In this context, the initial ~10 amino acids at the N-terminus of the C-terminal fragment, known as the "*Stachel sequence*" play an important role. Following the dissociation or a conformational change of the NTF, the tethered agonist is released and can activate the receptor by binding to the transmembrane domain (Figure 2) (Liebscher et al., 2014; Stoveken et al., 2015; Demberg et al., 2017). Consequently, the NTF serves to inhibit receptor activity by masking the tethered agonist sequence prior to cleavage.

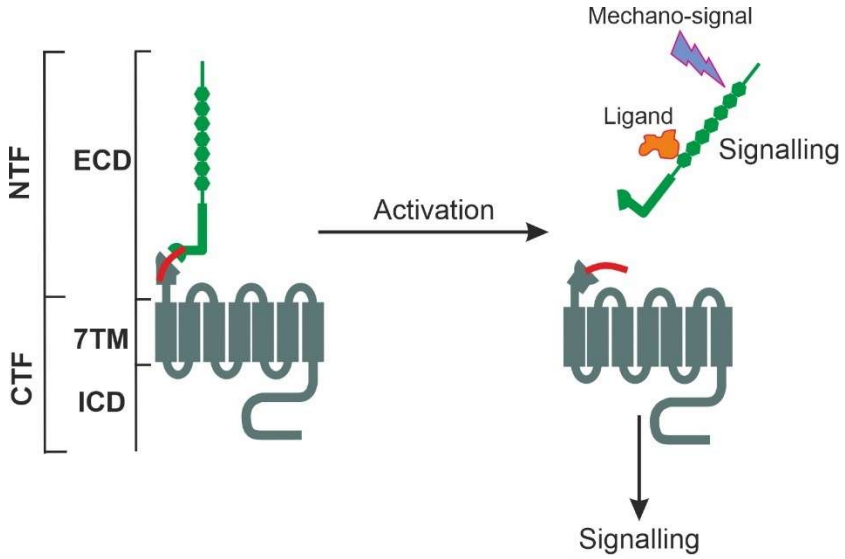

Figure 2. Activation mechanism of aGPCRs. Structurally aGPCRs contain a relatively long extracellular domain (ECD) which can be also named N-terminal fragment (NTF), a 7-serpentine transmembrane domain (TM), and a relatively short intracellular domain (ICD), together they can be named as C-terminal fragment (CTF). Typically, activation of the aGPCR receptors can be started with the dissociation or conformational changes of the NTF. Upon activation of the receptor, the "*Stachel*" sequence (red line) can be exposed in the very N-terminal region of the CTF acting as a tethered agonist of the receptor and starting the signalling (adapted from dissertation of Barbara Knapp (2017).

As mentioned above, AGPCRs can act as mechanosensors which allows cells to respond to mechanical forces sent to the cells (Langenhan, 2020). Such features indicate their importance in several different biological processes like immune response and development of the organism (references missing).

Pathogenic variants in all 33 members of aGPCRs have been implicated in various diseases including neurodegenerative disorders, cancer and, cardiovascular conditions (Folts et al., 2019; Gad and Balenga, 2020). However, due to existing challenges including the complexity of aGPCR signalling, lack of structural information and ligand information limits our understanding of aGPCR biology. Therefore, uncovering the functions of aGPCRs holds the promise of providing profound insights into their roles in health and disease. This, in turn,

may lead to innovative therapeutic strategies and diagnostic tools with significant clinical and basic impact.

1.2 Adhesion G protein-coupled receptor V1 (ADGRV1)

ADGRV1 also recognized as GPR98, MASS1, and VLGR1, is a prominent member of the GPCR family within the aGPCR family (McMillan and White, 2010; Hamann et al., 2015). The human *ADGRV1* gene consists of 90 exons and is susceptible to alternative splicing which raises up to 14 isoforms (https://www.uniprot.org). Among the various isoforms of *ADGRV1*, the full-length ADGRV1b stands out as the most substantial G protein-coupled receptor in the human body, featuring an impressive molecular weight of approximately 700 kDa and consisting of 6,306 amino acids (Figure 3) (Randy McMillan et al., 2002).

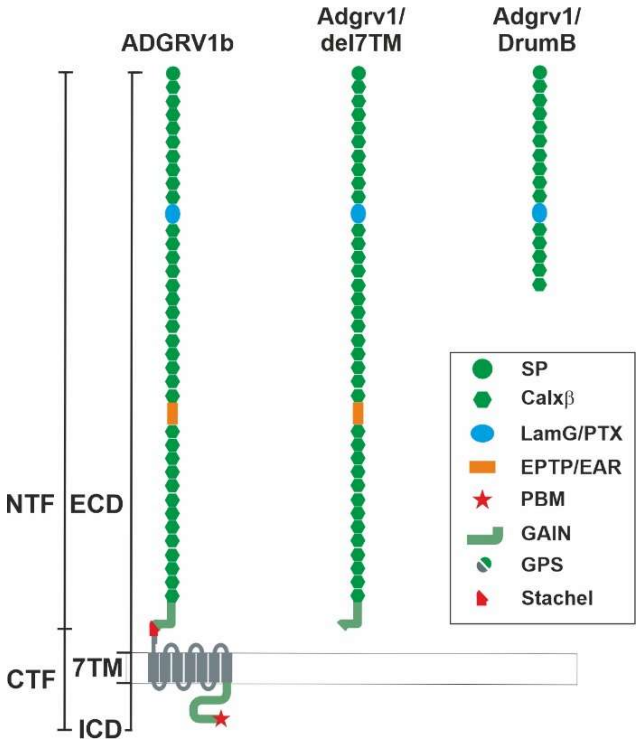

Figure 3. Domain structure of ADGRV1 in human and in Adgrv1 mouse models. ADGRV1b is composed of an extremely long extracellular domain (ECD), a 7-serpentine transmembrane domain (7TM), and a relatively short intracellular domain (ICD) with a characteristic PDZ binding motif (PBM). The ECD includes a signal peptide (SP), 35 Ca^{2+} binding calcium exchanger β motifs (Calx-β), pentaxin/laminin G-like repeats (LAMG/PTX), an epilepsy-associated/Epitemptin-like domain (EPTP/EAR), a GPCR autoproteolysis-inducing domain (GAIN) which includes the G-protein-coupled receptor proteolytic site (GPS). Autoproteolytic cleavage at the GPS can result in an N-terminal fragment (NTF) and the C-terminal fragment (CTF) and the exposition of the Stachel sequence at the very N-terminal end of the CTF which can act as a tethered agonist. ADGRV1a is composed of

35 Calx-β, 1 7TM and ICD domain. In ADGRV1/del7TM mice a nonsense mutation (by deletion of 101 bp from the 3′-terminal exon 82 and the 5′-splice donor of intron 82) introduces a STOP codon which leads to the deletion of the 7TM and ICD domains of ADGRV1 and the translation product is only the ECD. In the ADGRV1/DrumB mice, the 8554+2T>C mutation leads to a STOP codon in intron 37-38 when introns are not skipped. The translation product is a relatively short, truncated protein, which includes only 13 CalX-ß domains and the LAMG domain (Adapted from Güler et al., 2023, **Publication III**).

The autocleavage of ADGRV1 occurs at the auto-proteolysis site (GPS) situated within the GAIN (GPCR auto-proteolysis-inducing) domain gives rise to a C-terminal fragment (CTF) and an N-terminal fragment (NTF), both of which functionally independent (McMillan and White, 2010). Recent discoveries have brought to light the existence of an 11 amino acid sequence, identified as the "*Stachel*" peptide of ADGRV1 (Knapp et al., 2019). Upon autocleavage of the receptor, "*Stachel*" peptide sequence can be exposed in the very N-terminal region of CTF and is presumed to act as a tethered agonist, thereby activating aGPCRs. This autocleaveage and subsequentially activation of ADGRV1 by the "*Stachel*" sequence has been associated with a shift from Gs- to Gi-mediated signalling by ADGRV1 (Knapp et al., 2019, 2022). Our recent findings based on the Tandem affinity purification (TAP) of ADGRV1 demonstrated the association with several subunits of G-proteins. TAPs revealed that full-length ADGRV1a is associated with Gi and Gs whereas ADGRV1_CTF interacts with only Gi (Knapp et al., 2019, 2022).

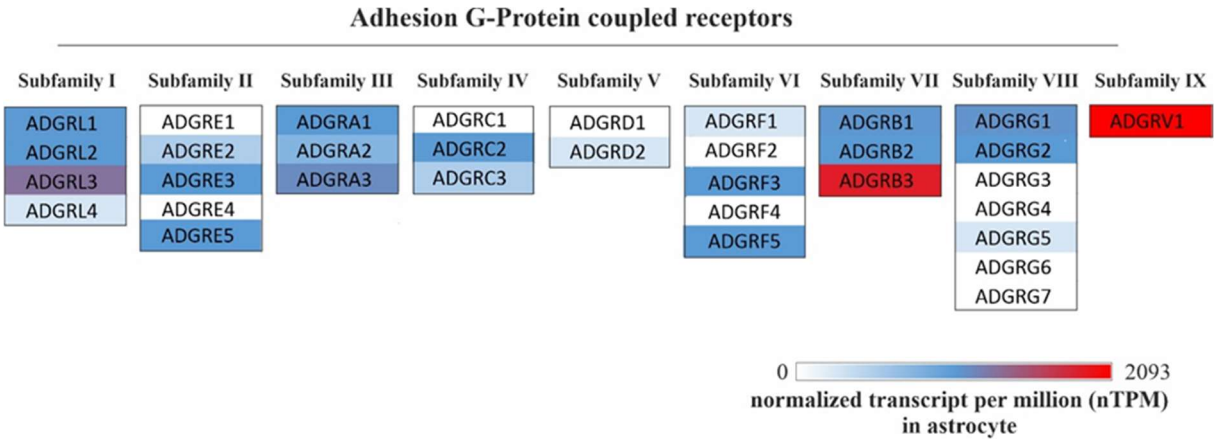

Figure 4. ADGR expression patterns in astrocytes. Heat map representation indicates aGPCRs transcripts per million (nTPM) in astrocytes (www.proteinatlas.org).

1.3 *ADGRV1* as disease causing gene

The expression of ADGRV1 is nearly ubiquitous, with heightened concentrations observed in

the central nervous system (CNS), particularly during developmental stages, as well as in the sensory cells of the eye and inner ear (https://www.proteinatlas.org/). Among the 33 ADGR members, ADGRV1 reveals the highest expression level (2093 normalized transcript per million) in astrocytes. This points to a high importance of its functions in astrocytes. (Figure 4) (www.proteinatlas.org).

Variants in *ADGRV1* have been linked to various diseases and so far, 466 pathogenic variants have been shown in humans (https://www.ncbi.nlm.nih.gov/clinvar). However, the most well-known and characterized role of *ADGRV1* is in the human Usher syndrome (USH), a hereditary deaf-blindness with a prevalence of 1:10.000 to 1:6.000 (Hope, 1997; Kimberling et al., 2010). Within the USH interactome ADGRV1 plays an indispensable role in the formation of fibrous links that span neighbouring membranes in cochlear hair cells of the inner ear and retinal photoreceptor cells (Zallocchi et al., 2012). Notably, the absence of these membrane attachment fibres can contribute to the degeneration of sensory neurons in the eye and ear, contributing to the development of USH caused by a pathogenic ADGRV1 variant.

Early studies involving mouse models for Adgrv1 have unveiled associations with audiogenic epilepsy (Randy McMillan et al., 2002; Yagi et al., 2005). During the embryonic brain development, ADGRV1 is highly expressed particularly in the ventricular zone (McMillan et al., 2002). Pathogenic variants or deficiency in ADGRV1 expression in the ventricular zone may affect neuronal migration (McMillian et al., 2004). This process highly depends on focal adhesion (FA) complexes, cell-cell contacts, and extracellular matrix (ECM) interaction during development, which may be associated with epilepsy. Adgrv1 mutant mice are not only susceptible to hearing impairments but also display a susceptibility to audiogenic seizures (AGS), indicating a potential association with epilepsy (McMillan and White, 2004; Yagi et al., 2005). The AGS are characterized by three phases which are wild running, clonic seizure, and tonic extension.

In recent years, increasing evidence has suggested that pathogenic variants of *ADGRV1* may also underlie various forms of epilepsy such as myoclonic, childhood absence and Rolandic epilepsy, as well as febrile seizures in humans (Wang et al., 2015; Myers et al., 2018; Liu et al., 2020; Leng et al., 2022; Zhou et al., 2022). Almost 3% of the confirmed epilepsy patients carry pathogenic *ADGRV1* variants (Leng et al., 2022). In patients with febrile seizures (FS) and epilepsy with prior FS, there appears to be a genotype-phenotype correlation, particularly with pathogenic *ADGRV1* variants. These variants are predominantly monoallelic and primarily concentrated within the CalX- β (calcium exchanger β) domains (Zhou et al., 2022). ADGRV1 contains 35 CalX- β repeats in its NTF suggesting its important role in

ADGRV1 function. Most of the epilepsy cases with pathogenic *ADGRV1* variants show mild prognosis. However, a recent case report showed that in a patient carrying a heterozygous missense mutation of *ADGRV1* (c.5785G> T), had severe hippocampal sclerosis characterized by neuronal cell loss and sudden unexpected death (Ji et al., 2023). It is well known that epileptic seizures, a characteristic of epilepsy, result from excessive and abnormal neuronal activity in the brain (Bou Assi et al., 2017). Nevertheless, the molecular mechanisms underlying the diverse forms of epilepsy remain largely elusive (Chong et al., 2023; Johannesen et al., 2023), and to date, nothing is known about the pathomechanism of epilepsy caused by pathogenic variants in *ADGRV1*.

1.4 Focal adhesions: macromolecular signalling hubs in cells

Focal adhesions are essential cellular structures that facilitate cell-ECM (extracellular matrix) interactions and play an important role in various cellular processes, particularly mechanotransduction and cell migration (Geiger et al., 2009; Gardel et al., 2010). These dynamic protein complexes serve as both physical anchors and signalling hubs, allowing cells to adhere to and respond to their surrounding microenvironment (Raghavan et al., 2003; Saunders et al., 2006). A set of publications (**Publication II** and **Publication III**) on the ADGRV1 function have dealt with the role of ADGRV1 in FAs. To understand the significance of ADGRV1 in FAs, it is essential to understand its role in assembly, disassembly, molecular composition, and their role in both health and disease.

FAs are highly dynamic structures that continually assemble and disassemble in response to mechanical forces and signalling cues to provide the cells migration and ECM interaction capacity (Mishra and Manavathi, 2021). Cell migration requires the continuous dynamic arrangement of FAs, the assembly of nascent FAs in the leading edge of cells and disassembly in their rear (Hu et al., 2014).

FAs play a central role in several physiological and pathological processes. In healthy tissues, they are essential for maintaining tissue integrity, regulating cell migration, and responding to mechanical cues, such as those encountered during wound healing and tissue development (Kostourou et al., 2023). However, when dysregulated, FAs are associated with numerous diseases (Mishra and Manavathi, 2021). In cancer, aberrant focal adhesions contribute to enhanced cell motility and metastasis (Maziveyi and Alahari, 2017). FA defects are also linked to cardiovascular diseases, fibrosis, and notably neurodegeneration. There is growing evidence that defects in cell migration can increase susceptibility to epilepsy (Qin et al., 2017). It has also been shown that the absence of Adgrv1 impairs the entry of Cdhr23 and

Cdhr15 expressing interneuron precursors into the cortex during embryonic cortex development in mice (Libé-Philippot et al., 2017). Therefore, understanding the intricate mechanisms of Adgrv1-driven FA dynamics and migration is critical to gain new insights into the role of ADGRV1 in CNS development and pathophysiology.

1.5 Astrocytes as regulatory cells in the central nervous system and model for ADGRV1 studies

In the central nervous system (CNS), astrocytes populate in all regions and are one of the most abundant cell types with various vital roles such as glutamate homeostasis, regulation of extracellular ion concentrations, control of energy metabolism, neuroprotection, synaptogenesis, and formation of the blood-brain-barrier (Sidoryk-Wegrzynowicz et al., 2011; Mahmoud et al., 2019; Michinaga and Koyama, 2019).

During the developmental stages, astrocytes derive from neural stem cells in the ventricular zone and subventricular zone which is a specialized reservoir for glial and neuronal progenitor cells which migrate to different layers of the brain (Tabata, 2015; Platel and Bordey, 2016). The possible role of ADGRV1 in the CNS has been indicated by McMillian and White in 2004, since they observed prominent expression of ADGRV1 during the development of the mouse brain particularly in the ventricular zone. Strikingly, of all the aGPCRs, ADGRV1 has the highest expression in astrocytes (https://www.proteinatlas.org/) which indicates its importance in astrocyte function. Therefore, utilizing the astrocytes isolated from brain can enhanced the knowledge of ADGRV1 function in CNS.

Loss of function in astrocytes or migration capacity defects during development, subsequently in post-natal and adulthood stages, may contribute to several neurodegenerative disorders in the brain such as Alzheimer's, Epilepsy and Huntington's disease (González-Reyes et al., 2017; Monterey et al., 2021; Vezzani et al., 2022).

Moreover, in tripartite synapses where astrocytes intergraded pre- and post-synapses, they regulate cross-talking between synapses via regulating ion concentration or by secreting several molecules, for instance, glutamine, glutamate and BDNF (Perea et al., 2009; Allen and Eroglu, 2017; Broadhead et al., 2022). Glutamate receptors in astrocytes regulate glutamate uptake to clear out excessive glutamate concentrations from synaptic clefts (Rose et al., 2018; Mahmoud et al., 2019). Dysregulation in glutamate uptake and release of astrocytes may cause changes in brain homeostasis, which may lead to neuronal hyperexcitability (Cho et al., 2018).

These findings highlight the importance of ADGRV1 in astrocyte physiology and eventually CNS development.

1.6 Aim of the thesis

The major goal of this thesis was to further elucidate the function of ADGRV1. To shed light on ADGRV1`s role in health and disease following scientific research objectives were pursued:

1. Establishment of a primary cellular model to study ADGRV1
2. Elucidation of the role of ADGRV1 at the focal adhesions and their dynamics
3. Deciphering the role of ADGRV1 in hippocampal astrocytes

To aim (1) Establishment of a primary cell model to study ADGRV1

Primary astrocytes have gathered attention over the decades due to their role in the CNS. Previously, astrocytes were thought to be the only helper cell types in the CNS. However, recent evidence reveals that they play active roles in regulation and maintaining CNS organization. Among all types of brain cells, astrocytes show the highest expression of ADGRV1 (https://www.proteinatlas.org/ENSG00000164199-ADGRV1), making them crucial for ADGRV1 studies. We have established a user-friendly method with high astrocyte purity to obtain primary astrocytes from Adgrv1/del7TM, Adgrv1/Drum B and WT mouse models. Most of the works included in this thesis were performed using primary astrocytes.

To aim (2) Elucidation of the role of ADGRV1 at focal adhesions

Previously, by using affinity proteomics we have shown that numerous molecules related to FAs are potentially interacting with ADGRV1 (Knapp et al., 2019, 2022). Therefore, we investigated the localization and function of ADGRV1 in the supramolecular complex of FAs. We utilized primary astrocytes as cellular models for studying the function of ADGRV1 in FAs. In **Publications II and III**, we investigated the role of ADGRV1 in astrocytes in the brain. First, we validated the localization of ADGRV1 at FAs. Furthermore, we showed that pathogenic variants in *ADGRV1* in astrocytes result in fewer FA numbers and length which eventually reduces cell migration speed. Additionally, we have also shown that ADGRV1 can function as a metabotropic mechanosensor at FAs. Our studies allowed us to identify ADGRV1 as a component of FA signalling hub and its role in the regulation of FA morphology.

Since migration of neuronal cells relies on healthy FA dynamics, investigating the role of ADGRV1 in FA dynamics is important for the understanding of CNS development. To this end, we applied two distinct approaches: the microtubule-associated FA assembly/disassembly approach and the FA recruitment approach by using live-cell imaging. These approaches showed the regulatory role of ADGRV1 in FA dynamics and recruitment.

To aim (3) Deciphering the role of ADGRV1 in hippocampal astrocytes and its impact on glutamate homeostasis

As mentioned above, affinity proteomics revealed numerous interaction partners of ADGRV1 which also regulate neuronal development and maintenance (Knapp et al., 2019, 2022). Given the fact that astrocytes are the cell types in the CNS with the highest expression of ADGRV1, we investigated the role of ADGRV1 in hippocampal astrocytes. To gain insights into the impact of ADGRV1 on astrocyte morphology and physiology, we used the Adgrv1/del7TM mouse model for *in vitro* and *in vivo* experiments. Additionally, we focused on the role of astrocytic Adgrv1 in neuronal development. The significance of this work was the elucidation of the disease-causing molecular mechanisms of ADGRV1 in the CNS.

2. Publications

Publication I

Güler BE, Krzysko J and Wolfrum U (2021). Isolation and culturing of primary mouse astrocytes for the analysis of focal adhesion dynamics. STAR Protoc. Dec 8;2(4):100954. doi: 10.1016/j.xpro.2021.100954. PMID: 34917973; PMCID: PMC8669101.

Publication II

Kusuluri DK, Güler BE, Knapp B, Horn N, Boldt K, Ueffing M, Aust G and Wolfrum U (2021). Adhesion G protein-coupled receptor VLGR1/ADGRV1 regulates cell spreading and migration by mechanosensing at focal adhesions. iScience. Mar 8;24(4):102283. doi: 10.1016/j.isci.2021.102283. PMID: 33851099; PMCID: PMC8024656.

Publication III

Güler, BE, Linnert J and Wolfrum U (2023). Monitoring paxillin in astrocytes reveals the significance of the adhesion G protein coupled receptor VLGR1/ADGRV1 for focal adhesion assembly. Basic Clin Pharmacol Toxicol. 133(4):301-312. doi: 10.1111/bcpt.13860. Epub 2023 Mar 30. PMID: 36929698.

Preprint I

Güler BE, Zorin M, Linnert J, Nagel-Wolfrum K and Wolfrum U (2024). The adhesion GPCR ADGRV1 controls glutamate homeostasis in hippocampal astrocytes supporting neuron development: first insights into to pathophysiology of ADGRV1-associated epilepsy. bioRxiv 2024.04.25.591120; doi: https://doi.org/10.1101/2024.04.25.591120.

Publication I

STAR Protocols

CellPress
OPEN ACCESS

Protocol

Isolation and culturing of primary mouse astrocytes for the analysis of focal adhesion dynamics

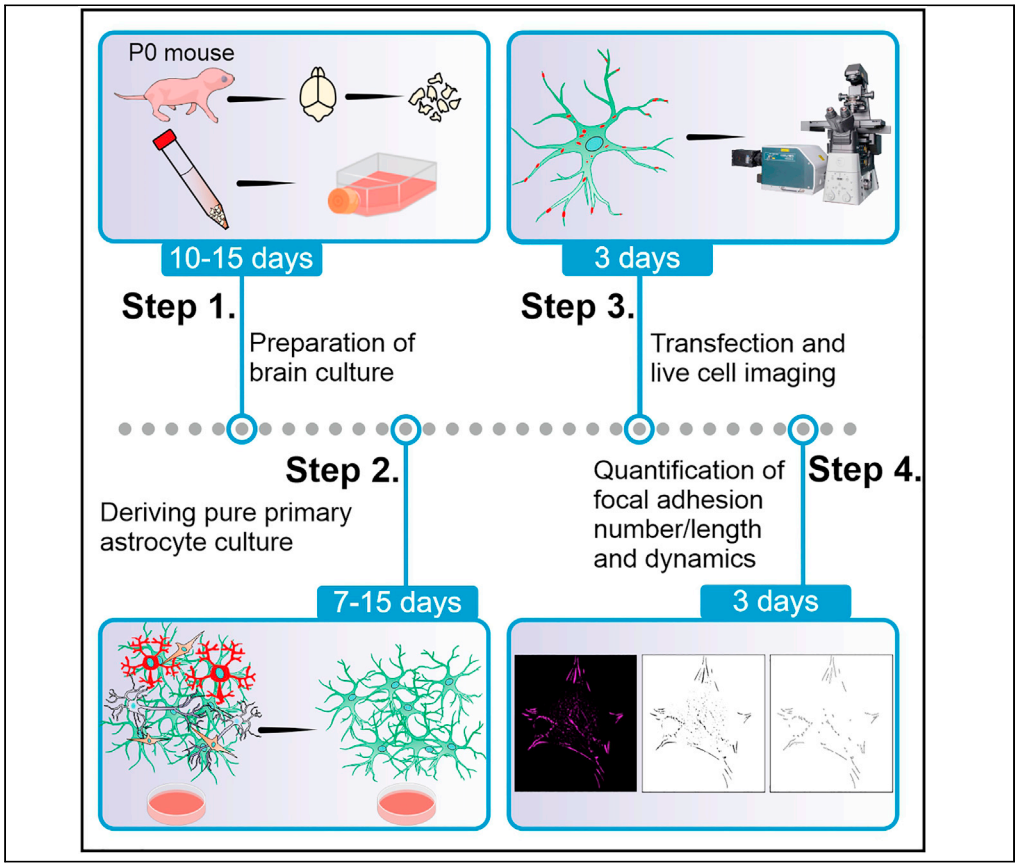

Primary astrocytes have gained attention as an important model for *in vitro* biological and biochemical research in the last decades. In this protocol, we describe a fast and cost-effective technique for isolating, culturing and maintaining primary mouse astrocytes at ~ 80% purity levels, which can be used in *in vitro* studies for migration and focal adhesion dynamics. In addition, we present an optimized transfection and manual quantification approach for focal adhesion analysis in fixed and living cells.

Baran E. Güler, Jacek Krzysko, Uwe Wolfrum

wolfrum@uni-mainz.de

Highlights

High purity of primary mouse astrocyte isolation without commercial kits

Isolated mouse primary astrocytes are functional for downstream applications

Quantitative analysis of focal adhesion properties in fixed and living astrocytes

Güler et al., STAR Protocols 2, 100954
December 17, 2021
https://doi.org/10.1016/j.xpro.2021.100954

STAR Protocols

CellPress
OPEN ACCESS

Protocol

Isolation and culturing of primary mouse astrocytes for the analysis of focal adhesion dynamics

Baran E. Güler,[1,2] Jacek Krzysko,[1] and Uwe Wolfrum[1,2,3,*]

[1]Institute of Molecular Physiology, Molecular Cell Biology, Johannes Gutenberg University of Mainz, Hanns-Dieter-Hüsch-Weg 17, 55128 Mainz, Germany

[2]Technical contact

[3]Lead contact

*Correspondence: wolfrum@uni-mainz.de
https://doi.org/10.1016/j.xpro.2021.100954

SUMMARY

Primary astrocytes have gained attention as an important model for *in vitro* biological and biochemical research in the last decades. In this protocol, we describe a fast and cost-effective technique for isolating, culturing, and maintaining primary mouse astrocytes at ~ 80% purity levels, which can be used in *in vitro* studies for migration and focal adhesion dynamics. In addition, we present an optimized transfection and manual quantification approach for focal adhesion analysis in fixed and living cells.

For complete details on the use and execution of this protocol, please refer to Kusuluri et al. (2021).

BEFORE YOU BEGIN

Dissection of mice and preparation of brain culture should be performed under sterile conditions. All equipment (Biosafety cabinet, forceps, scissors and plates, etc.) should be sterile to prevent any contamination. In this protocol, the isolation of primary astrocytes cells depends on the differential binding method which separates primary astrocytes, oligodendrocyte progenitor cells (OPCs) and microglia cells based on their different affinities for bacterial grade plastic dishes. Do not use plates that have been treated for animal cell culture because all cell types will attach to these plates with equal affinities. Primary astrocytes were isolated from brains of P0 C57BL/6J (wild type). This protocol was also successfully applied for two mouse models for Usher syndrome 2C namely *Vlgr1*/del7TM (McMillan and White, 2004) and *Drum B* mutated mice (Potter et al., 2016), bred on a C57BL/6J background and we did not observe any difference in protocol efficiency. All experiments described herein were performed in accordance with the guidelines provided by Association for Research in Vision and Ophthalmology.

Before starting the experiment several chemicals and surgical instruments should be prepared (For detailed information please see key resources table and materials and equipment section).

KEY RESOURCES TABLE

REAGENT or RESOURCE	SOURCE	IDENTIFIER
Antibodies		
Rabbit monoclonal anti-GFAP (Glial fibrillary acidic protein), working dilution 1 in 1000	DAKO-Agilent	Cat#ZO334
Mouse monoclonal anti-GFAP (Glial fibrillary acidic protein), working dilution 1 in 1000	Sigma-Aldrich	Cat#G3839

(*Continued on next page*)

Continued

REAGENT or RESOURCE	SOURCE	IDENTIFIER
Guineapig monoclonal anti-MAP2 (Microtubule associated protein), working dilution 1 in 1000	Synaptic systems	Cat#188004
Mouse monoclonal anti-Vinculin, working dilution 1 in 100	Sigma-Aldrich	Cat#V9131
Rabbit polyclonal anti- PDGFR-α, working dilution 1 in 200	Santa Cruz Biotechnology, Inc.	Cat#sc-338
Rat monoclonal anti-CD68, working dilution 1 in 200	Bio-Rad Laboratories	Cat#MCA1957
Chemicals, peptides, and recombinant proteins		
Alexa Fluor 488-conjugated goat anti-rabbit IgG, working dilution 1 in 400	Molecular Probes	Cat#A-11034
Alexa Fluor 568-conjugated goat anti-rat IgG, working dilution 1 in 400	Biotrend	Cat#20092-1
Alexa Fluor 640-conjugated goat anti-mouse IgG, working dilution 1 in 200	Biotrend	Cat#20177
Phalloidin-TRITC, working dilution 1 in 400	Sigma-Aldrich	Cat#P1951
Dulbecco's Modified Eagle Medium (DMEM)	Gibco™	Cat#31966-021
Fetal bovine serum (FBS)	Gibco™	Cat#16000044
Penicillin-streptomycin	Gibco™	Cat#15140122
10× Hanks' Balanced Salt Solution (HBSS)	Gibco™	Cat#14065-056
1 M HEPES solution	Gibco™	Cat#15630106
DNase I, recombinant, Grade II, from bovine pancreas	Merck	Cat#10104159001
0.01% Poly-L-Lysine solution	Sigma-Aldrich	Cat#25988-63-0
0.05% Trypsin-EDTA (1×)	Gibco™	Cat#25300-054
1×PBS	Gibco™	Cat#14190-094
Opti-MEM™ I Reduced Serum Medium	Thermo Fisher Scientific	Cat#31985062
GeneJuice® Transfection Reagent	Merck	Cat#70967-6
Fibronectin bovine plasma	Merck	Cat#F4759-5MG
Albumin crude from chicken egg = Ovalbumin	PanReac AppliChem	Cat#A4344
Gelatin From Cold Water Fish Skin, 40–50% in Water	Sigma-Aldrich	Cat#G7765-250ML
Deposited data		
Raw and analyzed data	This paper and Kusuluri et al. (2021)	N/A
Experimental models: organisms/strains		
Mouse: C57BL/6J (P0 age)	The Jackson Laboratory	Stock no: 000664
Mouse: *Vlgr1*/del7TM (P0 age)	Breed on a C57BL/6 background	McMillan and White (2004)
Mouse: *Drum* B (P0 age)	Breed on a C57BL/6 background	Potter et al. (2016) and Kusuluri et al. (2021)
Recombinant DNA		
RFP-Paxillin	Rudolf E. Leube, Rick Horwitz	Rudolf E. Leube, Rick Horwitz
Software and algorithms		
ImageJ software	National Institutes of Health (NIH)	http://imagej.nih.gov/ij/download.html
Focal adhesion analysis server	https://faas.bme.unc.edu	Berginski and Gomez (2013)
Other		
Stereomicroscope	Leica Microsystems	Leica WILD M3B
Cold light source	Leica Microsystems	Schott KL750
Inverted microscope	Nikon Instruments Inc.	Nikon Eclipse Ti2-E
Spinning disc unit	Yokogawa Electric Corporation	CSU-W1
Leica confocal microscope	Leica Microsystems	DM6000B
Centrifuge	Eppendorf	Centrifuge 5430 R
Medium-sized scissors	A. Dumont & Fils	Cat#T5074
Dumont #3 curved forceps	A. Dumont & Fils	Cat#T504
Dumont #4 standard tip forceps	A. Dumont & Fils	Cat#T505
Dumont #7 standard tip forceps	A. Dumont & Fils	Cat#T508
Vannas spring scissors	A. Dumont & Fils	Cat#T5322
100 mm petri dish (cell culture)	Greiner Bio-One	Cat#664160
100 mm bacterial grade petri dish	SARSTEDT AG & Co. KG	Cat#82.1472
T-75 culture flasks	Greiner Bio-One	Cat#658170
6-well culture plates	Greiner Bio-One	Cat#657160
15 mL Centrifuge Tubes	SARSTEDT AG & Co. KG	Cat#62.554.502

(*Continued on next page*)

Continued		
REAGENT or RESOURCE	SOURCE	IDENTIFIER
10 mm glass coverslips	Carl Roth GmbH +Co. KG	Cat#YX02.1
0.22 μm filter	Carl Roth GmbH +Co. KG	Cat#KH541
0.45 μm filter	Carl Roth GmbH +Co. KG	Cat#CCX9.1
μ-Slide 4 Well chamber	Ibidi GmbH	Cat#80426

MATERIALS AND EQUIPMENT

Growth medium		
Reagent	Final concentration	Amount
Dulbecco's Modified Eagle Medium (DMEM)	n/a	450 mL
Fetal bovine serum (FBS)	10%	50 mL
Penicillin-streptomycin	2%	11 mL
Total	**n/a**	**511 mL**

⚠ CRITICAL: Final antibiotic concentration may be adjusted, since different antibiotic concentrations can affect cell proliferation and differentiation.

Note: Growth medium should be kept at +4°C for a maximum of 1 month. If there is a pH level change during storage which can be distinguished by a color change, new medium should be prepared.

1× HBSS for brain tissue storage during dissection		
Reagent	Final concentration	Amount
10× HBSS	1×	100 mL
1 M HEPES	0.01 M	10 mL
ddH_2O	n/a	890 mL
Total	**n/a**	**1000 mL**

⚠ CRITICAL: Adjust pH 7.0 of buffer using 1 N HCl or 1 N NaOH and sterile medium by passing through a 0.22 μm filter.

Note: Medium should be stored at +4°C for a maximum of 1 month. If there is a pH level change during storage which can be distinguished by the color change in medium, the new medium should be prepared.

DNase I solution		
Reagent	Final concentration	Amount
DNase I	0.05%	100 mg
1× HBSS	n/a	200 mL
Total	**n/a**	**200 mL**

⚠ CRITICAL: Do not dissolve the DNase I by using vortex as mechanical force may denaturate the enzyme which can cause decrease in the activity. The solution should be prepared by pipetting and sterilized by passing through a 0.22 μm filter. To prevent any freeze/thaw

cycles which may reduce activity, 1–5 mL aliquots can be prepared and kept at –20°C or –80°C for a maximum of 6 months.

Blocking solution		
Reagent	Final concentration	Amount
Ovalbumin	0.1%	0.1 g
40–50% Fish gelatin	0.5%	1.1 g
1× PBS	n/a	100 mL
Total	**n/a**	**100 mL**

Note: Mix the Ovalbumin and 40%–50% Fish gelatin in 100 mL PBS for 12–16 h. The day after, bring the temperature of the solution to 50°C. Centrifuge for 10 min at 3000 RCF to remove undissolved particles. Sterile medium by passing through a 0.45 μm filter. In order to prevent freeze/thaw cycles, prepare 1–2 mL aliquots and keep at −20°C for a maximum of 12 months.

STEP-BY-STEP METHOD DETAILS

Preparation of primary brain culture

Timing: 10–15 days

Before starting dissection of mice pups, place 10 mL of 1× HBSS (in a 15 mL Falcon tube), 1 mL of 0.05% DNase I and 1 mL of 0.05% trypsin on ice and arrange dissection tools, microscope, a cold light source and 70% ethanol under the dissection hood. This step includes dissection and preparation of primary brain cultures. To obtain a confluent layer of primary astrocytes cells, collect 3–4 pups' brains in a 15 mL tube containing 1× HBSS solution.

Preparation of brain tissue

Timing: 15–30 min

1. Before starting the dissection, gently hold the mice pup and spray the neck with 70% of ethanol to prevent contamination.
2. Decapitation of mice can be done by using sharp scissors in one cut.

⚠ CRITICAL: Brain isolation can take time due to inexperience. In order to achieve high efficiency after the procedure and healthy brain culture, only one decapitation should be applied at a time and the remaining decapitation procedures should be carried out after step 14 is finished from the first mouse.

3. To keep the head fixed and stabile use anchoring forceps at orbital cavities (Figure 1A).
4. Make an incision of the skin at the hindbrain and follow along the midline to eye level where transverse cuts to the eye cavity will be made (Figure 1B).
5. Grasp the skin from both sides by using Dumont #5 forceps and pull it aside to reveal the skull (Figure 1C).
6. Carefully cut the cranium using a small scissors. The cut should start from the neck where the vertebral foramen is located and extended anteriorly to the nose. Make additional transverse cuts to the eye cavity.

⚠ CRITICAL: While cutting the cranium be sure that no excess pressure is applied to the brain. This may cause deformation in brain tissue and bleeding, which can lower culture purity because of contamination with red blood cells and endothelial cells.

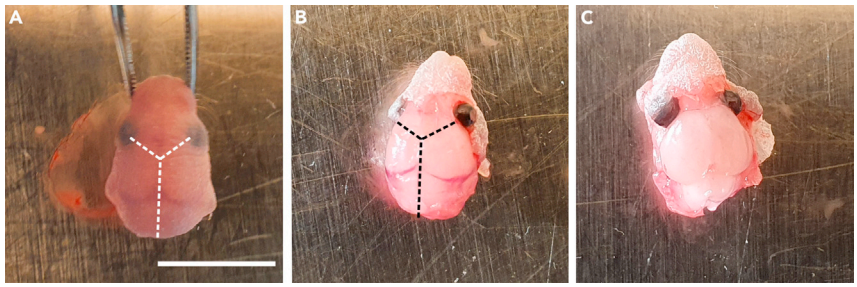

Figure 1. Dissection of the brain from PN0 mouse

(A and B) (A) Cut should be performed to remove the skin and (B) skull layers covering the brain. Dashed lines indicate the cuts using Vannas spring scissors. The cut starts from the neck where the vertebral foramen is located and extends anteriorly to the nose.

(C) Exposed brain. Scale bar: 5 mm.

7. Carefully pull apart the cranium using forceps to reveal the brain.
8. Take out the brain with the help of a small spatula. First, place the spatula under the cerebellum and gently push it towards the olfactory bulbs and scoop out by lifting. This will disconnect the brain from the skull base.
9. Transfer the brain to a 10 cm petri dish containing ice-cold 1× HBSS under sterile conditions. The brain should submerge completely in the liquid.
10. Remove olfactory bulbs in order to free the meninges. Meninges can be distinguished by their reddish color resulting from blood vessels (Figures 2A and 2B).
11. Reversing the brain and starting from the bottom side can help to remove meninges easily. Dissect the meninges from the surface of the cortical layer by using fine forceps.

Note: We observed that keeping brain integrity during the process may reduce the risk of meningeal cells and fibroblast contamination and ensure full removal.

12. Flip the brain and continue meninges removal.
13. Carefully check whether there is any meninges residue and if not, cut the brain into 6–10 pieces using forceps or sharp blades in order to increase disassociation efficiency (Figure 2C).
14. Place the brain pieces into a 15 mL tubes that contain 10 mL 1× HBSS and keep on ice (Figure 3A).

⚠ CRITICAL: Only 3–4 brains should be collected in 10 mL 1× HBSS. If more brain tissue is needed, use a 50 mL Falcon and increase the volume of 1× HBSS for 5 brains to 11 mL and for 12 brains 20 mL. If the brain pieces are not submerged completely, tap the bottom of the Falcon tube. This may help to submerge brain pieces that float on top.

Note: After obtaining meninges-free brain, repeat the steps 1–14 for the rest of the mice. Doing only one brain at a time will ensure healthy cultures.

15. Under the sterile condition, add ice cold 0.05% DNase I into the tube and gently triturate brain tissue 10–15 times with a 10 mL and 2 mL pipette, respectively.
16. Afterwards, add 0.05% trypsin, mix by using 10 mL pipette 20–30 times and incubate at room temperature (22°C–25°C) for 20 min.

⚠ CRITICAL: The amount of DNase I and trypsin can be adjusted depending on the number of brains in one tube. For 3–4 brains; 1 mL of DNase I and 1 mL of trypsin, for 5 brains; 1.5 mL of DNase I and 1.5 mL of trypsin, for 12 brains; 3 mL of DNase I and 3 mL of trypsin should be added.

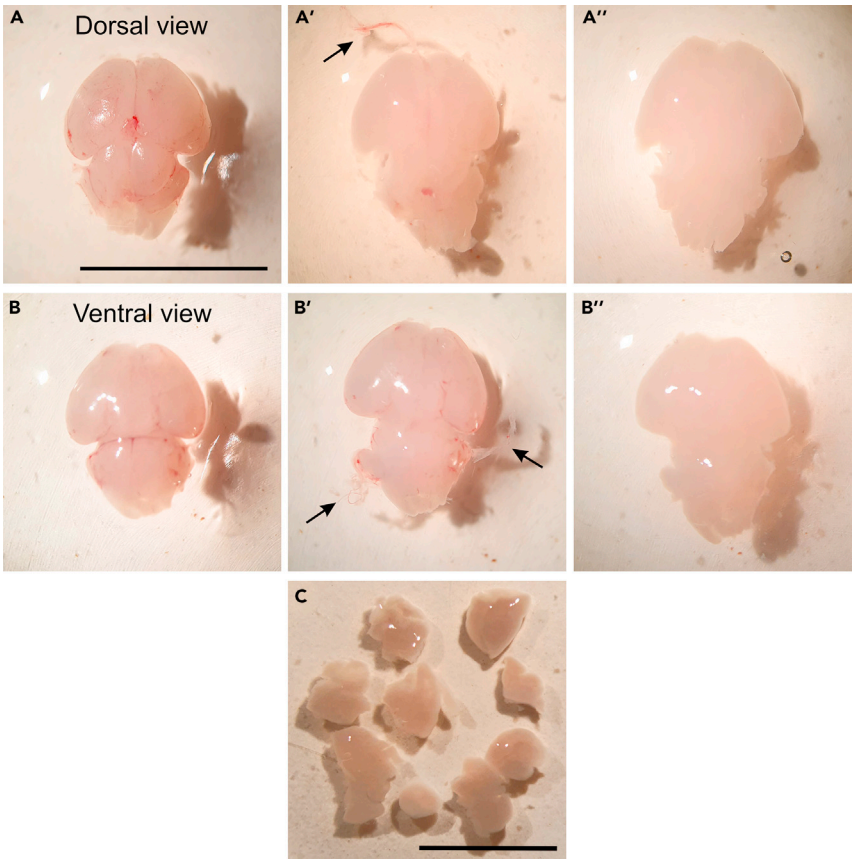

Figure 2. Dissection of mouse brain at P0

(A and B) Removing the meninges from mouse brain. (A) Dorsal view (B) and ventral view of isolated mouse brain. Meninges can be distinguished by reddish color in the cortex of the mouse brain. (A′ and B′) Meninges removal from the cortex of the mouse brain. Arrows indicate removed meninges from the cortex of the mouse brain. (A″ and B″) Dorsal and ventral view of completely meninges-free brain.

(C) Dissection of brain parts with a sharp razor blade or fine forceps. Scale bars: A and B: 10 mm; C: 5 mm.

17. During incubation time, prepare one T-75 flask for 3–4 brains and coat with 3 mL of 0.01% Poly-L-Lysine (PLL) for 20 min. Place the T-75 flask in the incubator.
18. 20 min after incubation of brain pieces mix the Falcon tube thoroughly (Figure 3B).
19. Centrifuge for 10 min at 150 RCF to the pellet brain tissue (Figure 3C).
20. After centrifugation, carefully aspirate the supernatant using a Pasteur pipette connected to a pump (Figure 3D).

Note: If there is any meninges residue or blood vessel contamination, which can be distinguished by a reddish color on top of the pellet, also aspirate and discard this layer. Resuspend pellet with 2 mL of complete growth medium and repeat centrifugation step.

21. Resuspend cell pellet with 2–4 mL of DMEM with a 10 mL pipette and mix thoroughly 10–20 times in order to obtain a single-cell suspension (Figure 3E).
22. Aspirate PLL from the T-75 flask and rinse with 10 mL of DMEM to completely wash out any residue. Add 8–10 mL of pre-warmed 37°C DMEM supplemented with 10% FBS and 2% pen/strep.
23. Plate the resuspended cell pellet and incubate at 37°C with 5% CO_2 in an incubator.
24. Change the medium on day 1, day 2 and day 7 after plating the primary cells (Figure 7A).

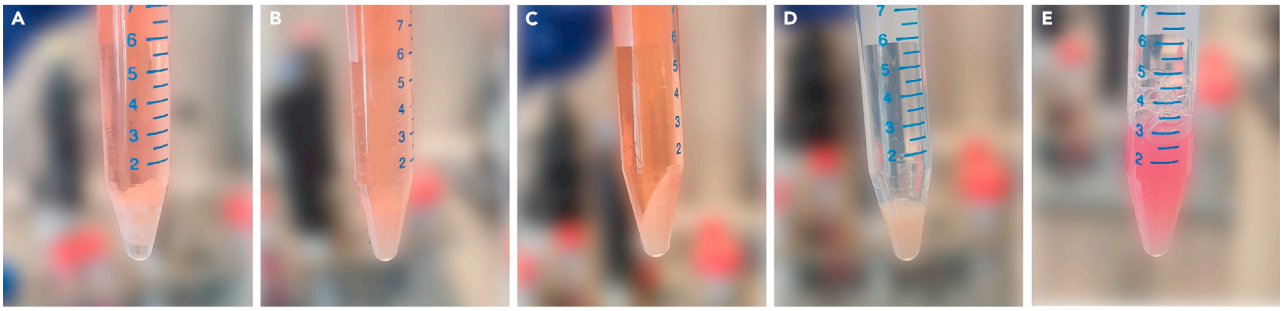

Figure 3. Dissociation of mouse brain tissue for primary cell cultivation

(A) Brain tissue dissected from wild type mice in 1× HBSS.

(B) Homogenized mouse brain tissue (MBT).

(C) MBT pellet after centrifugation.

(D) MBT pellet after removing supernatant.

(E) Resuspended MBT pellet in complete growth medium.

Note: In order to remove unattached and death cells wash the plate by using 1× PBS, before adding fresh complete growth medium.

Deriving pure primary mouse astrocyte culture

Timing: 7–15 days

This step will be used for the separation of primary astrocytes cells from oligodendrocyte progenitor cells (OPCs), microglia and neurons. In confluence, their tight arrangement at the bottom of the culture flask can distinguish primary astrocytes cells from other cell types. Widefield microcopy distinguishes microglia cells from other brain-derived cells revealing a bright and small rounded cell morphology.

Removal of oligodendrocyte progenitor cells (OPCs)

Timing: 10–20 min

25. Mixed primary cell cultures which were obtained in steps 1 to 24 reach full confluency on days 10–15. When mixed cell culture reach confluency, gently tap the flask from both sides several times in order to detach the OPCs layer. After tapping the flask, check the cells under the microscope. Detach OPCs can be distinguished as floating cells in the plate (Figure 4).

Note: In case of incomplete detachment repeat tapping several times. Tapping should be done gently so as not detach the astrocyte layer.

26. After the OPCs are released aspirate the medium completely to remove detached cells and rinse remaining cells carefully with 10 mL of complete growth medium.

Note: To avoid any loosening or loss of astrocyte layer, medium aspiration and rinsing should be done carefully. A 10 mL pipette should be placed at the corner of the flask and the medium should be slowly added against the wall of the flask and not directly onto the attached cells.

27. After removing OPCs, add 10 mL of complete growth medium and ice cold 0.5 mL DNase I to loosen the remaining cell layer and incubate 5 min at 37°C with 5% CO_2 in an incubator.
28. After DNase I treatment, the remaining OPCs are released by horizontal shaking the T-75 Flask 20–30 times.

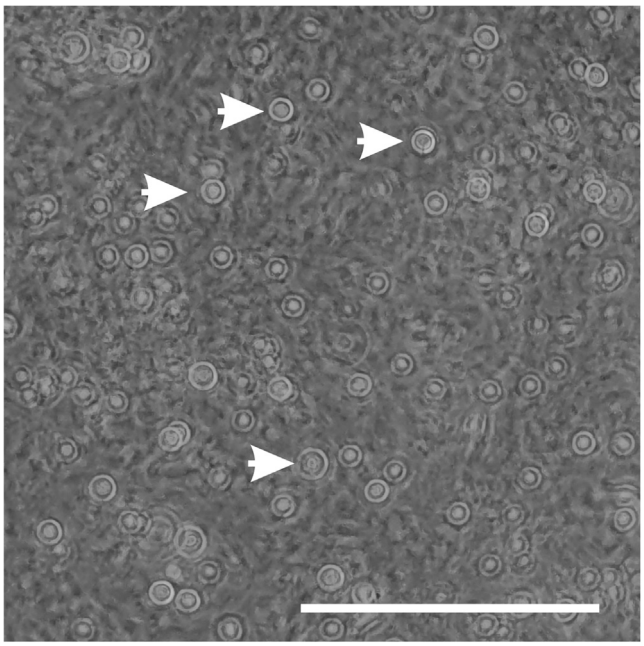

Figure 4. Detached oligodendrocyte progenitor cells after tapping the flask

OPCs are distinguished as floating cells above the monolayer of astrocytes and microglia. Arrow heads indicate round shaped floating OPCs. Scale bars: 100 μm.

Note: While too gentle shaking may cause insufficient OPCs removal, too intense shaking can damage the astrocyte layer. Shaking should be performed at a steady speed by hand.

⚠ CRITICAL: Shaking can cause foaming; therefore, the shaken flask should be held vertically for 30 s to allow the foam to float on the top.

Removal of microglia

Timing: 2–2.30 h

29. Aspirate the medium which may still contains OPCs, and wash the astrocytes and microglia layer with 3–4 mL PBS.
30. Add 3–4 mL of 0.05% trypsin and incubate 3–5 min at 37°C with 5% CO_2 in an incubator.

⚠ CRITICAL: Cells should not be incubated with trypsin for more than 5 min. Longer incubation time may harm primary astrocytes and results in an unhealthy culture.

31. After incubation, check the cells under the microscope. If there is incomplete detachment, tap the slide of the flask several times and check under the microscope again.
32. After trypsinization, add 6–7 mL of complete growth medium and resuspend the cells.
33. Transfer the suspension to a new 15 mL Falcon tube and pellet detached cells by centrifugation for 10 min at 150 rcf.
34. During centrifugation, prepare 4 sterile 10-cm bacterial grade plates. Add 2 mL of complete growth medium in each of 4 Petri dishes.
35. Aspirate the supernatant which you obtain after step 33 and resuspend cells with 4 mL of complete growth medium.
36. Add 1 mL of the cell suspension to each petri dish (Figure 5A) and incubate at 37°C with 5% CO_2 in the incubator for 20 min (Figure 5B).

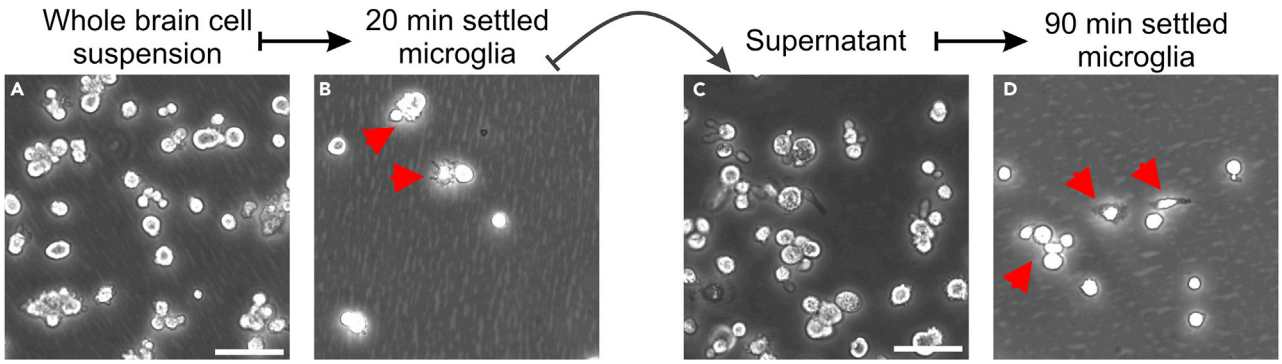

Figure 5. Differential surface binding of primary astrocytes from mouse brain

(A) Whole brain cell suspension which obtained in step 35.

(B) Red arrow heads indicate settled microglia after 20 min of incubation.

(C) Transferring the supernatant which obtained in step 37 to a new bacterial grade plate.

(D) Red arrows indicate settled microglia after 90 min of incubation. Scale bar: 50 μm.

Note: In this step, remaining microglia cells should adhere to the bacterial grade plate while primary astrocyte cells should not.

37. After incubation, collect all supernatants containing astrocytes of all 4 Petri dishes and pool them to a new 10-cm bacterial grade plate (Figure 5C).

⚠ CRITICAL: The transfer of supernatant should be performed carefully as shaking of the plate may result in loosening bound microglia. Gently tilt the plate and collect the supernatant from the side of the plate.

38. Incubate the supernatant (obtained in step 37) contains ~10–12 mL medium at 37°C with 5% CO_2 in the incubator for 90 min (Figure 5D).

Note: After incubation, check the cells under the microscope. Microglia cells should completely adhere after this step and primary astrocytes can be distinguished as floating cells in the culture medium.

39. Transfer the supernatant containing primary astrocytes into a new T-75 flask.

Note: According to volume of the obtained supernatant, add additional amount of pre-warmed complete growth medium to the T-75 flask to fill up to 20 mL.

40. Incubate the primary astrocytes for 7–15 days at 37°C with 5% CO_2 in the incubator. Primary astrocytes are reaching confluency in between day 7–15 after isolation. After culture reach confluency, primary astrocytes can be used for downstream experiments (Figure 7B).

⚠ CRITICAL: Change the complete growth medium by aspirating half of the old medium (approx. 10 mL) and replacing it with a fresh, pre-warmed complete growth medium (approx. 10 mL) every 4 days during cultivation. This will provide you with a conditioned medium that will help maintain a healthy culture.

Transfection of isolated primary astrocytes and live-cell imaging

Timing: 3 days

In these steps, we describe how to transfect primary mouse astrocytes with a focal adhesion (FA) construct namely RFP-Paxillin and how to perform live imaging to investigate FA dynamics. For live-cell imaging, we use a μ-Slide 4 Well chamber (Ibidi, Munich, Germany) and for transfection, we use GeneJuice® transfection reagent (Merck, Darmstadt, Germany).

41. First, coat the μ-Slide 4 Well chamber with 300 μL of fibronectin 5 μg/mL dissolved in dH_2O for 1 h at 37°C.
42. Next, remove the fibronectin from the wells and wash the wells once with 500 μL of sterile 1× PBS or water. After the washing, place the chamber in the incubator in order to dry it.

Note: Fibronectin solution can be used up to 3 times, therefore discarded fibronectin can be store at −20°C for further usage.

⚠ CRITICAL: If the purpose of the experiment is to study migration or focal adhesion dynamics, we strongly recommend the usage of fibronectin instead of poly-L-Lysine coating, since fibronectin may enhance cell adhesion and spreading (Blau 2013).

43. Wash the primary astrocytes when reach confluency which are cultured in T-75 flask with 1× PBS and add 3 mL of 0.05% trypsin for 5 min at 37°C to detach cells.
44. Collect the detached cells in a 15 mL tube and add 1–5 mL of growth media for preparing cell suspension. Count the number of cells and prepare 5 × 10^4 cell/mL suspension.
45. Add 700 μL (~35,000 cells) of cell suspension into each well and incubate 1 day at 37°C with 5% CO_2 in the incubator.

Note: Cell number can be adjusted based on chamber size used. Cells should be at least 50% confluent before transfection.

46. The day after incubation, change the medium to fresh 700 μL of complete growth medium.

Note: Transfection reagent volumes and DNA amount can be scaled up if more than 4 wells are needed.

47. For the single transfection of focal adhesion construct, prepare 1 Eppendorf tube and add 100 μL of Opti-MEM™ and add 6 μL of GeneJuice®. Vortex the solution thoroughly to mix it and incubate at room temperature for 5 min.
48. Add 2 μL of focal adhesion construct at a 1 μg/mL concentration into the serum-free/GeneJuice® mixture and mix it by tapping the tubes and incubate at room temperature for 15 min.

⚠ CRITICAL: Do not vortex the solution after adding the DNA construct, vigorous mixing can cause low transfection efficiency.

49. Drop-wisely add 27 μL of reagent/DNA mixture to the cells and rock the chamber to homogenize the solution in the complete growth medium.
50. After 24 h of transfection remove the old medium which contains transfection reagent and add pre-warmed complete growth medium and incubate the cells for additional 24 h at 37°C with 5% CO_2 in the incubator.
51. Before starting live-cell imaging, turn on the temperature and CO_2 controller of Nikon Eclipse Ti2-E/Yokogawa CSU-W1 Spinning disk microscope and wait till the condition stabilizes for usage.
52. Acquire the movies at 1 frame/3–5 min with 20 z-stacks at 0.5 μm step size for 1.25 h to 3-h time course (Methods video S1).

Note: Time interval between frames and z-stacks size and steps can be adjusted based on your experimental setup. After determining the parameter, all movies should be acquired using the same settings in order to provide experimental consistence.

53. Apply maximum projections to the movies and analyze focal adhesion assembly/disassembly rates by using Focal Adhesion Analysis Server (FAAS) (Figure 10) (Berginski and Gomez 2013).

Note: Microtubule induced focal adhesion disassembly experiment can be used as a control experiment in order to establish the protocol (Ezratty et al., 2005).

Immunostaining of focal adhesion molecules in fixed primary astrocytes

Timing: 4 days

We used a Leica DM6000B microscope (Leica, Bensheim, Germany) for imaging of specimens.

54. Prepare 10 mm glass coverslips in 6-well plates and coat with fibronectin as described in step 41–42.
55. Seed 1–1.5 × 10^5 cells in each well and incubate the primary astrocytes cells for 48 h at 37°C with 5% CO_2 in the incubator.
56. After the 48 h incubation, carefully remove the growth medium and wash one time rapidly with 1× PBS and do second time washing using 1× PBS for 10 min in room temperature.
57. Prepare a parafilm sheet and place it a wet chamber for keeping humidity during incubation times. Take the coverslips out from wells, place onto parafilm sheet and fix the cells by using 50 μL of 2% of PFA in 1× PBS for each coverslip for 10 min at room temperature.
58. Wash the cells 2 times for 10 min with 1× PBS to remove any remaining PFA.
59. Permeabilize the cells with 50 μL of 0.2% Triton-X-100 in PBS solution.
60. Remove the permeabilization solution and wash cells with 50 μL of 50 mM NH_4Cl in PBS for 5 min in room temperature.
61. Incubate the cells with 50 μL of blocking solution (0.1% Ovalbumin and 0.5% Fish gelatin in 1× PBS) for 60 min in room temperature.
62. After incubation, treat the cells with 50 μL of primary antibodies 12–16 h at 4°C. We used rabbit anti-GFAP (1:400 dilution) and mouse anti-vinculin (1:200 dilution) prepared in blocking solution.

Note: Primary antibodies can be incubated at room temperature for 2–3 h.

63. After primary antibody incubation, wash the cells with 1× PBS one time rapidly and two additional times for 10 min.
64. Apply the 50 μL of secondary antibodies for each coverslip. Alexa Flour 488-conjugated goat anti-rabbit 488 IgG antibody (1:400 diluted in blocking solution), Alexa Fluor 640-conjugated goat anti-mouse IgG antibody (1:400 diluted in blocking solution) and the dyes TRITC-phalloidin (1:400 diluted in blocking solution) for labeling actin filaments (F-actin) and 4′,6-Diamidino-2-Phenylindole (DAPI) (1:400 diluted in blocking solution) for counterstaining of nucleus were prepared in a 1.5 mL tube. Incubate the cells with antibodies at room temperature for 60–75 min in room temperature.
65. Wash the cells with 1× PBS one time rapidly and three times for 10 min.
66. Mount the coverslips with Mowiol.

⚠ CRITICAL: Step 63–66 should be conducted in subdued lighting to prevent bleaching of the fluorescent probes.

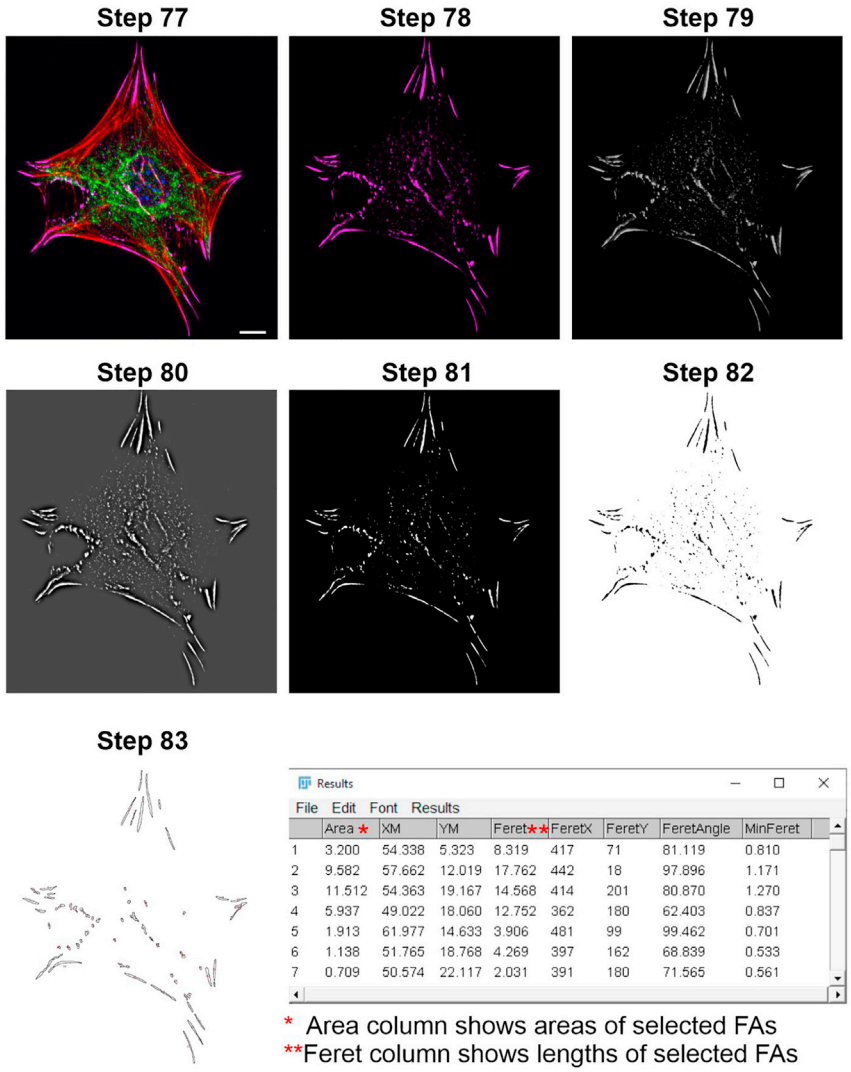

Figure 6. Step by step quantification of focal adhesion (FA) numbers and lengths

Step 77: Representative image shows merged image of primary mouse astrocytes which co-labeled with vinculin marker (magenta), actin filaments (red), GFAP (green) and for nuclear staining DAPI (blue). **Step 78:** After splitting channels, only vinculin staining is shown. **Step 79:** 8-bit image. **Step 80**: FFT Bandpass filter applied image. **Step 81–83:** Subtracting background and detecting FAs in the cell. Scale bar: 10 μm.

Quantification of number and length of focal adhesion molecules in the primary astrocyte cells

Timing: 1–2 days

Images were acquired on Leica DM6000B microscope (Leica, Bensheim, Germany) with a 63× objective and 20 cells for each condition were used for quantification. The number and length of focal adhesion molecules were quantified by using Fiji (Figure 6). For this, we modified a protocol which previously described (Horzum et al., 2014).

67. Open the images using ImageJ software.
68. If Z-projection is not created
    a. Go to Image-Stacks-Z Project-Maximum Projection.

b. Save the processed image in the folder.
69. Pick an exported and processed image from the images folder.
70. To set the scale: First, draw a straight line on the image scale bar.
    a. Go to Analyze-Set scale
    b. And mark as global.
71. Verify the scale by drawing a line on the scale bar.
72. Make a duplicate image named DUP1 for the RGB image (for comparison).
73. Draw a scale bar in the image near to the cell to be cropped.
    a. Analyze-Tools-Scale bar
74. Now, select the Rectangle box symbol from the imageJ toolbar and draw around the cell.
75. Then right-click within the drawn box and press duplicate.
    a. Go to Image-Adjust-Brightness and contrast for adjustments and then save the image in the folder.
76. Again, go to 1st duplicate RGB image and again right-click within yellow box for the FFT image.
77. Separate the merged imaged
    a. Go to Image-Color-Split channels
    b. And pick the channels which contain focal adhesion staining
78. To acquire the FFT image, change the RGB image to an 8-bit image.
    a. Image-Type 8-bit
79. In order to subtract background
    a. Process-FFT Bandpass filter
    b. Set pixel size for large structure to 20 pixels and small 1 pixel.
    c. Adjust tolerance of direction to 5%
    d. Select Autoscale after filtering
    e. Select Saturate image when autoscaling
    f. And press OK
80. Go to Image-Adjust-Brightness
    a. Adjust brightness till getting black background and save the Min/Max values for applying to other images.
    b. Adjust maximum & then minimum.
81. Save the FFT filtered image.
    a. Duplicate image.
    b. Image-Type-RGB color as in this step you cannot save 8-bit image.
    c. Close RGB image.
82. Go to Image-Adjust-Threshold
    a. Select Dark Background.
    b. In first drop-down box select-Huang.
    c. In the second drop-down box select-B&W.
    d. Then apply.
83. Run analyze particles.
    a. Set the parameter for size: 40-Infinity and for circularity 0.00–0.99.
    b. Select pixel units and show the outlines option.
    c. Select display results, clear results, summarize & include holes.
84. Quantification of focal adhesion numbers per cell area
    a. Open the image with F-actin staining.
    b. Draw a line around the cell body using the freehand tool in imageJ tool bar.
    c. Press control+M, this will give the area of the cell body.
    d. Save the results.
    e. Transfer the data to an Excel file.
    f. Count the number of focal adhesions and divide it by the total cell area.
85. Use Mann-Whitney-Wilcoxon Test for the significant test.

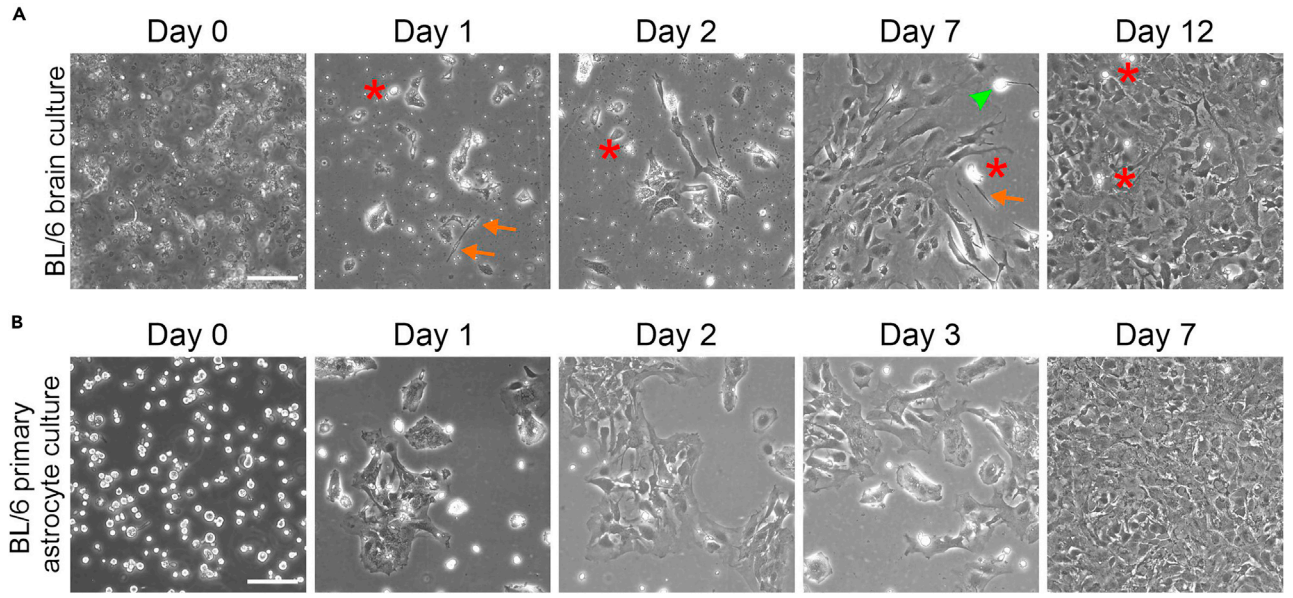

Figure 7. Growth of BL/6 mouse primary astrocyte cells in mixed brain culture and pure culture

(A) Representative differential interference contrast (DIC) images show growth of different cell types during culturing days before applying the differential binding method.

(B) Primary astrocytes in culture after applying the differential binding method. After differential binding method primary astrocytes reached the confluency. Red asterisks indicate microglia cells, arrows indicate fibroblast cells and green arrowhead indicates a neuron. Scale bars: 100 μm.

EXPECTED OUTCOMES

In this protocol, we provide a cost-efficient, reproducible isolation of primary astrocytes from P0 BL/6 mice without the requirement of commercial kits or special equipment. Applying our protocol, a healthy and easy to maintain primary astrocyte culture can be obtained from wild type or mutant mice strains (Figure 7). Furthermore, and most importantly, the purity of the primary astrocyte cell culture is suitable for studying several astrocytes dependent or related physiological processes. Isolated primary astrocytes can be identified by indirect immunofluorescence using antibodies against the glial fibrillary acidic protein (GFAP). In addition, we applied immunofluorescence staining of microtubule-associated protein (MAP2), PDGRF-alpha and CD68 as marker, respectively, for the identification primary neurons, OPC and microglia, to confirm the purity of astrocyte culture (Figure 8).

We applied our isolation protocol described above for the analysis of focal adhesion dynamics in murine isolated primary astrocytes (Figure 9). Focal adhesions (FAs) are highly dynamic molecules which serve as bi-directional signaling hub in the cell by sensing environmental (outside-in) and intracellular cues (inside-out) (Shen et al., 2012; Sun et al., 2016). With this unique bi-directional signaling feature FA molecules play essential roles in the migration and spreading (Kim et al., 2012; Kim and Wirtz 2013). Namely, size and turnover of FAs are highly important for the migration capacity of the cell. We recently showed that the adhesion G protein coupled receptor (GPCR) ADGRV1/VLGR1 (very large G protein coupled-receptor-1) is a component of FAs and mutations in *VLGR1* cause defects in FA growth and maturation processes (Kusuluri et al., 2021). In the latter study, we used isolated primary BL/6 wild-type astrocytes, *Vlgr1*/del7TM mice lacking the seven transmembrane domains (7TM) and the intracellular domain (ICD) of *Vlgr1* (McMillan and White, 2004), and mutant Drum B mice in which only a small portion of the N-terminal fragment is present and the entire C-terminal fragment is missing (Potter et al., 2016; Kusuluri et al., 2021). A significant decrease in the number and length of FAs was observed in both *Vlgr1* mutant mice compared with primary BL/6 wild-type astrocytes (Figure 10) (Kusuluri et al., 2021). For the quantifications, we applied

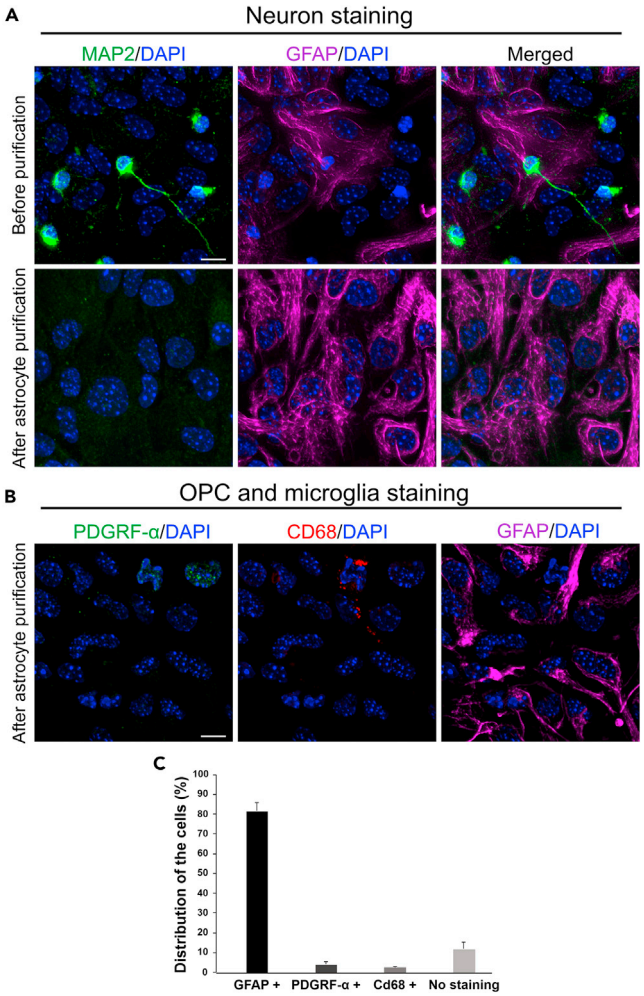

Figure 8. Representative indirect immunostaining of BL/6 mouse brain primary cell cultures

(A) Indirect immunofluorescence double staining of MAP2 (green) and primary astrocyte marker GFAP (magenta), as common markers for primary neurons and primary astrocytes, counterstained by DAPI (blue) for nuclear DNA, before and after the purification of astrocytes.

(B) Immunofluorescence staining of a primary astrocyte culture after primary astrocyte purification. OPC, microglia and primary astrocytes cells were stained by antibodies against PDGRF-α, CD68 and GFAP, respectively.

(C) Quantification of the number of GFAP, PDGRF-α and CD68-stained positive cells after astrocyte purifications demonstrates that primary astrocytes are the most prominent cell type (~80%). N = 360–490 cells per condition, 3 independent experiments. Scale bar: 10 μm.

the ImageJ protocol described above in step 67 to 85. Moreover, our study demonstrated that VLGR1 is metabotropic mechanosensor at FAs and provided novel insights into the pathomechanisms underlying VLGR1-associated diseases, such as human Usher syndrome (Reiners and Wolfrum 2006) and epilepsy (Wang et al., 2015; Myers et al., 2018).

LIMITATIONS

This protocol is designed for isolation of primary astrocytes from P0 mice and all isolation steps are optimized for this age. Nevertheless, our protocol can be adjusted for different aged mice brain culture. It might be taken under consideration that precursor and adult primary astrocyte can show different transcriptional profile which may affect experimental outcome (Zhang et al., 2016; Clarke et al., 2018; Bronzuoli et al., 2019). In addition, there might be species-specific differences between species that primary astrocyte derived may show differences in transcriptomic and protein

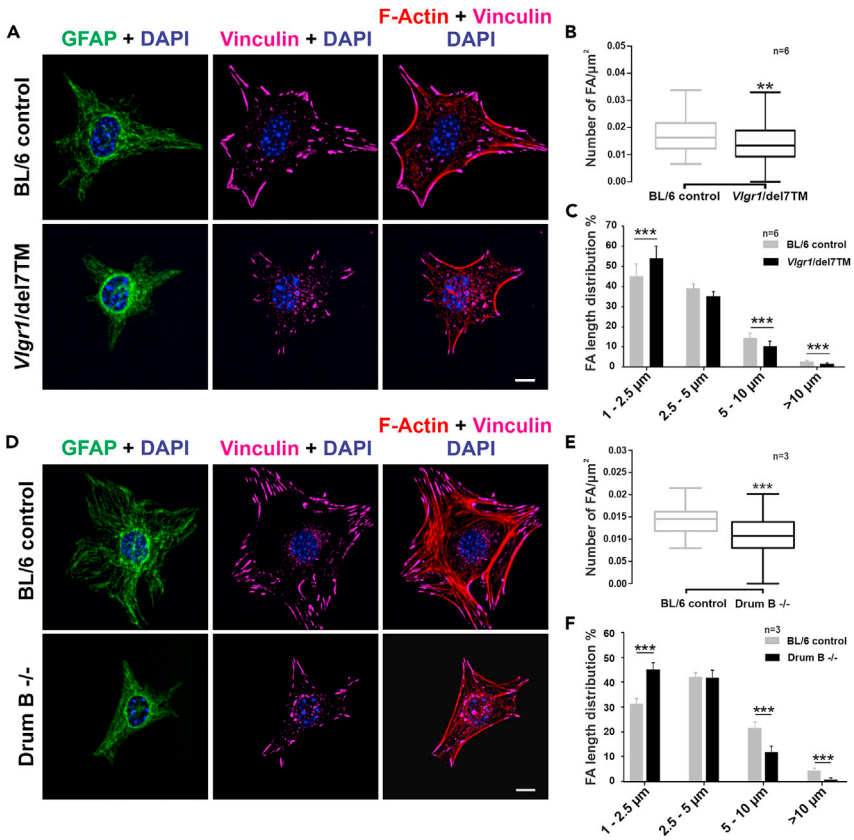

Figure 9. VLGR1 deficiency alters FA morphology

Representative images of FAs in *VLGR1*-deficient mouse primary astrocytes.

(A and D) FAs were stained for vinculin (magenta), F-actin with TRITC-phalloidin (red), and nuclei with DAPI (blue); GFAP (green) was used as an astrocyte marker. FA number and length were reduced after *VLGR1*-depletion in primary astrocytes of both *Vlgr1* mutant mouse lines.

(B and C) (B) 20 cells per condition, (C) ~1300–1700 FAs per category for control and ~200–1000 FAs for mutant astrocytes.

(E and F) (E) 20 cells per condition, (F) ~950–1250 FAs per condition for control and ~410–510 FAs for mutant astrocytes. Scale bars: (A and D) 10 µm. Data are represented in B and E are shown as box plot and statistical analyses were done using two-tailed Mann-Whitney U test. Data in C and F are represented as mean ± SD. Statistical analyses were done using Sidak's multiple comparison test; *p ≤ 0.05, **p ≤ 0.01, ***p ≤ 0.001.

(A–F). Figure is acquired and adapted from Figures 3D–3H in Kusuluri et al. (2021) with the permission of Elsevier.

interaction level. In human and mice astrocytes, it has been reported that metabolism and mitochondria related protein network was higher in mice astrocyte whereas defensive response and extracellular space related proteins were higher in human astrocytes (Li et al., 2021). In rat and mouse astrocytes, significant differences in GFAP expression level, cell proliferation and morphology has been also shown (Puschmann et al., 2010). We observed that primary astrocytes can only be subpassaged up to 3 times. As more than 3 sub passaging cause astrocyte marker (GFAP) expression loss and unhealthy cell phenotype such as poor cell growth, reduce in cell migration capacity and changes in cell morphology, we highly recommend that experiments should be planned in advance and passage 1 and passage 2 should be used. Astrocytes are one of the main parts of active information transport in central nervous system by interacting with neurons. Neuron-astrocyte interaction through messenger and signaling molecules such as Ca^{2+} and glutamate, is highly important in the CNS for function, development and pathology of the brain (Wilhelm et al., 2004; Benarroch 2005; Nimmerjahn 2009). Therefore, it should be taken under consideration that pure primary astrocyte culture may not always reflect in-vivo physiology in the absence of different cell types.

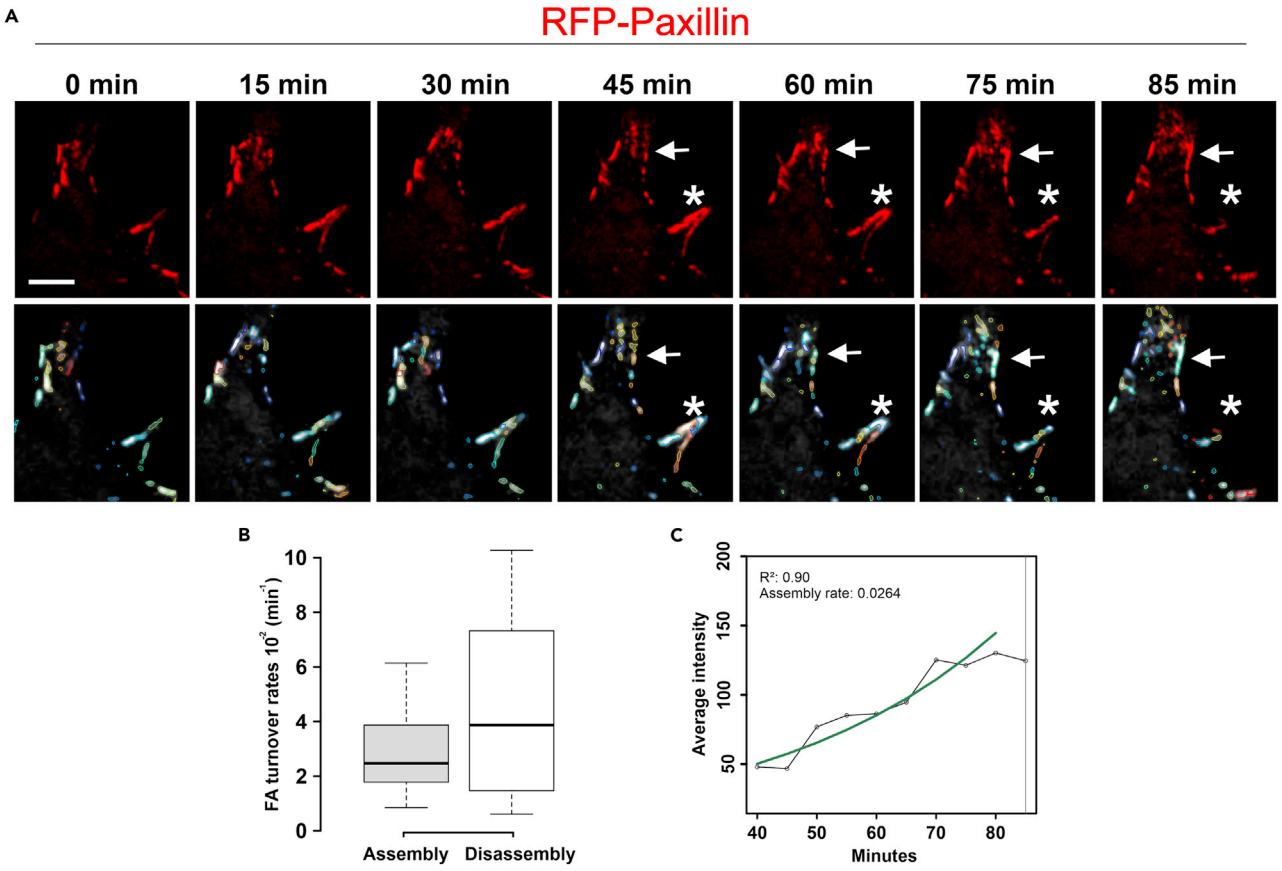

Figure 10. Analysis of assembly and disassembly of focal adhesions by life cell imaging in RFP-Paxillin transfected BL/6 mouse primary astrocytes

(A) Tracking of RFP-Paxillin molecules in focal adhesions (FAs) by live cell imaging. Images were acquired for 85 min with 3 min time intervals. Arrows point to an individual FA which assembles and asterisk indicated a FA which disassembles during the time course of imaging. Lower panel shows color coded individual FAs identified and analyzed via the Focal adhesion analysis server (FAAS) (Berginski and Gomez 2013).

(B) Assembly and disassembly rates of FAs in a single BL/6 primary mouse astrocyte.

(C) Automated intensity analysis of RFP-paxillin in an individual FAs during assembly by FAAS. Green line in the intensity plot indicates the trend line of assembling FA. Scale bar: 10 μm.

TROUBLESHOOTING

Problem 1

Contamination of fibroblast and endothelial cells in the primary cultures (step 10).

Potential solution

Fibroblast and endothelial cells are the two major cell types present in meninges. Poor handling in meningeal removing increases the contamination level in culture. These two cell types can reach confluency very rapidly which may cause a reduced number of astrocytes and purity of cultures. Meninges should peel away using fine forceps. Be sure that meninges are removed in one piece, if not there can be patches of meninges left which may cause contamination.

Problem 2

Insufficient dissociation of brain tissue (step 21).

Potential solution

When performing dissociation of brain tissue, be sure to use freshly thawed ice-cold DNase I solution as DNase I is enzymatically helping dissociation of brain tissue. Due to environmental and mechanical stress during the dissociation process DNA can leak as a result of cell damage. Released DNA is

often the cause of cell clumps that affects efficiency of dissociation. Start the resuspension of cell pellet with a 10 mL pipette and continue with 5 mL and 2 mL pipettes, respectively. Using a smaller pipette size can increase dissociation efficiency and reduce aggregation levels.

Problem 3

Cell viability is not sufficient after plating (step 24).

Potential solution

This problem may occur because of excessive Poly-L-Lysine (PLL) residue in flask. Therefore, wash the plates coated with PLL thoroughly before plating single-cell suspension. After plating single-cell suspension, cellular growth should be observed on day 1, day 2, day 7 and day 14. Differential binding should be performed when cultures reach full confluency, as insufficient cell numbers may affect the cell viability.

Problem 4

OPCs contamination in isolated astrocyte cultures (step 25).

Potential solution

After 7–15 days of culturing, primary astrocytes reach confluency. It is important to keep the astrocyte layer attached to the flask surface during the OPCs. While too gentle shaking of flask may cause lower yield of OPCs removal, too intense shanking may damage the astrocyte layer. Therefore, shaking should be done carefully.

Problem 5

Microglia contamination after differential binding (step 29).

Potential solution

After trypsinization, transfer medium containing astrocytes and potential microglia cells to the bacterial grade plates. Microglia cells are attached to the surface of bacterial grade plates whereas primary astrocytes do not. After 20 min of transferring to bacterial grade plate, check the cells, primary astrocytes can be distinguished easily as they float in the medium. Collect the medium containing primary astrocytes and repeat the step carefully for another 90 min. When collecting medium, be careful not to shake the plate or the microglia may become detached.

Problem 6

Low transfection rate (step 41).

Potential solution

An efficient transfection rate is very important for successful experiment. We have observed that transfection efficiency in primary astrocyte was the range of 15%–30%. To optimize transfection efficiency for your gene/protein of interest, you may try different transfection methods, such as transfection by electroporation or transfection by liposomes. Transfection efficiency may depend on several factors, such as DNA:transfection reagent ratio, purity and composition of the DNA, the degree of confluency of the culture and transfection method. Therefore, to achieve sufficient number of transfected cells and transfection protocol must be optimized. Plasmid DNA should be prepared by using Endotoxin-free isolation kit, as residue of bacterial toxin may lower the efficiency. After obtaining endotoxin-free DNA, different transfection reagent:DNA ratios should be tested to optimize transfection.

Problem 7

Poor migration speed during live-cell imaging (step 52).

Potential solution

Extracellular matrix is vital for migration of cells in vitro and in vivo. Primary astrocytes produce and secrete extracellular matrix (ECM) proteins such as laminin in vitro condition to provide growth and spreading condition (Chiu et al., 1991). However, in low cell density such as single cell migration study, migration speed can reduce dramatically due to lack of sufficient ECM. A potential solution to this problem is to coating the surface using fibronectin at a 5 μg/mL. Since, different ECM concentrations have an effect on migration speed and migrating cell numbers (Desban and Duband 1997; Millon-Fremillon et al., 2008), effective fibronectin concentration from 1 μg/mL to 10 μg/mL may be tested before starting the experiment. Also, providing conditioned astrocyte medium can enhance the migration speed of primary astrocyte cells as it contains ECM molecules.

RESOURCE AVAILABILITY

Lead contact

Further information and requests for resources and reagents should be directed to and will be fulfilled by the lead contact, Uwe Wolfrum (wolfrum@uni-mainz.de).

Materials availability

Reagents and resources used in this study are commercially available with the exception of RFP-paxillin plasmid which was kindly provided by Drs. Leube and Hortwitz. Nevertheless, requests for resources and reagents can be directed to and will be fulfilled by the lead contact.

Data and code availability

This study did not generate new data sets.

SUPPLEMENTAL INFORMATION

Supplemental information can be found online at https://doi.org/10.1016/j.xpro.2021.100954.

ACKNOWLEDGMENTS

This work was supported by the German Research Council DFG FOR 2149 "Elucidation of Adhesion-GPCR signaling" WO 548/8 (UW). We thank Drs Rudolf E. Leube and Rick Horwitz for kindly sharing reagents and Dr Karl R. Fath for critical reading and language corrections.

AUTHOR CONTRIBUTIONS

Conceptualization, B.E.G. and U.W.; investigation, B.E.G. and J.K.; writing – original draft, B.E.G. and U.W.; writing – review & editing, B.E.G., J.K. and U.W.

DECLARATION OF INTERESTS

The authors declare no competing interests.

REFERENCES

Benarroch, E.E. (2005). Neuron-astrocyte interactions: partnership for normal function and disease in the central nervous system. Mayo Clin. Proc. *80*, 1326–1338.

Berginski, M.E., and Gomez, S.M. (2013). The Focal Adhesion Analysis Server: a web tool for analyzing focal adhesion dynamics. F1000Res *2*, 68.

Blau, A. (2013). Cell adhesion promotion strategies for signal transduction enhancement in microelectrode array in vitro electrophysiology: an introductory overview and critical discussion. Curr. Opin. Colloid Interface Sci. *18*, 481–492.

Bronzuoli, M.R., Facchinetti, R., Valenza, M., Cassano, T., Steardo, L., and Scuderi, C. (2019). Astrocyte function is affected by aging and not Alzheimer's disease: a preliminary investigation in hippocampi of 3xTg-AD mice. Front. Pharmacol. *10*, 644.

Chiu, A.Y., Espinosa De Los Monteros, A., Cole, R.A., Loera, S., and De Vellis, J. (1991). Laminin and s-laminin are produced and released by astrocytes, Schwann cells, and schwannomas in culture. Glia *4*, 11–24.

Clarke, L.E., Liddelow, S.A., Chakraborty, C., Munch, A.E., Heiman, M., and Barres, B.A. (2018). Normal aging induces A1-like astrocyte reactivity. Proc. Natl. Acad. Sci. U S A *115*, E1896–E1905.

Desban, N., and Duband, J.L. (1997). Avian neural crest cell migration on laminin: interaction of the alpha1beta1 integrin with distinct laminin-1 domains mediates different adhesive responses. J. Cell Sci. *110*, 2729–2744.

Ezratty, E.J., Partridge, M.A., and Gundersen, G.G. (2005). Microtubule-induced focal adhesion disassembly is mediated by dynamin and focal adhesion kinase. Nat. Cell Biol. *7*, 581–590.

Horzum, U., Ozdil, B., and Pesen-Okvur, D. (2014). Step-by-step quantitative analysis of focal adhesions. MethodsX *1*, 56–59.

Kim, D.H., and Wirtz, D. (2013). Focal adhesion size uniquely predicts cell migration. FASEB J. *27*, 1351–1361.

Kim, M.C., Kim, C., Wood, L., Neal, D., Kamm, R.D., and Asada, H.H. (2012). Integrating focal adhesion dynamics, cytoskeleton remodeling, and actin motor activity for predicting cell migration on 3D curved surfaces of the extracellular matrix. Integr. Biol. *4*, 1386–1397.

Kusuluri, D.K., Guler, B.E., Knapp, B., Horn, N., Boldt, K., Ueffing, M., Aust, G., and Wolfrum, U. (2021). Adhesion G protein-coupled receptor VLGR1/ADGRV1 regulates cell spreading and migration by mechanosensing at focal adhesions. iScience *24*, 102283.

Li, J., Pan, L., Pembroke, W.G., Rexach, J.E., Godoy, M.I., Condro, M.C., Alvarado, A.G., Harteni, M., Chen, Y.W., Stiles, L., et al. (2021). Conservation and divergence of vulnerability and responses to stressors between human and mouse astrocytes. Nat. Commun. *12*, 3958.

McMillan, D.R., and White, P.C. (2004). Loss of the transmembrane and cytoplasmic domains of the very large G-protein-coupled receptor-1 (VLGR1 or Mass1) causes audiogenic seizures in mice. Mol. Cell Neurosci. *26*, 322–329.

Millon-Fremillon, A., Bouvard, D., Grichine, A., Manet-Dupe, S., Block, M.R., and Albiges-Rizo, C. (2008). Cell adaptive response to extracellular matrix density is controlled by ICAP-1-dependent beta1-integrin affinity. J. Cell Biol. *180*, 427–441.

Myers, K.A., Nasioulas, S., Boys, A., Mcmahon, J.M., Slater, H., Lockhart, P., Sart, D.D., and Scheffer, I.E. (2018). ADGRV1 is implicated in myoclonic epilepsy. Epilepsia *59*, 381–388.

Nimmerjahn, A. (2009). Astrocytes going live: advances and challenges. J. Physiol. *587*, 1639–1647.

Potter, P.K., Bowl, M.R., Jeyarajan, P., Wisby, L., Blease, A., Goldsworthy, M.E., Simon, M.M., Greenaway, S., Michel, V., Barnard, A., et al. (2016). Novel gene function revealed by mouse mutagenesis screens for models of age-related disease. Nat. Commun. *7*, 12444.

Puschmann, T.B., Dixon, K.J., and Turnley, A.M. (2010). Species differences in reactivity of mouse and rat astrocytes in vitro. Neurosignals *18*, 152–163.

Reiners, J., and Wolfrum, U. (2006). Molecular analysis of the supramolecular usher protein complex in the retina. Harmonin as the key protein of the Usher syndrome. Adv. Exp. Med. Biol. *572*, 349–353.

Shen, B., Delaney, M.K., and Du, X. (2012). Inside-out, outside-in, and inside-outside-in: G protein signaling in integrin-mediated cell adhesion, spreading, and retraction. Curr. Opin. Cell Biol. *24*, 600–606.

Sun, Z., Guo, S.S., and Fassler, R. (2016). Integrin-mediated mechanotransduction. J. Cell Biol. *215*, 445–456.

Wang, Y., Fan, X., Zhang, W., Zhang, C., Wang, J., Jiang, T., and Wang, L. (2015). Deficiency of very large G-protein-coupled receptor-1 is a risk factor of tumor-related epilepsy: a whole transcriptome sequencing analysis. J. Neurooncol. *121*, 609–616.

Wilhelm, A., Volknandt, W., Langer, D., Nolte, C., Kettenmann, H., and Zimmermann, H. (2004). Localization of SNARE proteins and secretory organelle proteins in astrocytes in vitro and in situ. Neurosci. Res. *48*, 249–257.

Zhang, Y., Sloan, S.A., Clarke, L.E., Caneda, C., Plaza, C.A., Blumenthal, P.D., Vogel, H., Steinberg, G.K., Edwards, M.S., Li, G., et al. (2016). Purification and characterization of progenitor and mature human astrocytes reveals transcriptional and functional differences with mouse. Neuron *89*, 37–53.

Publication II

iScience

CellPress
OPEN ACCESS

Article

Adhesion G protein-coupled receptor VLGR1/ADGRV1 regulates cell spreading and migration by mechanosensing at focal adhesions

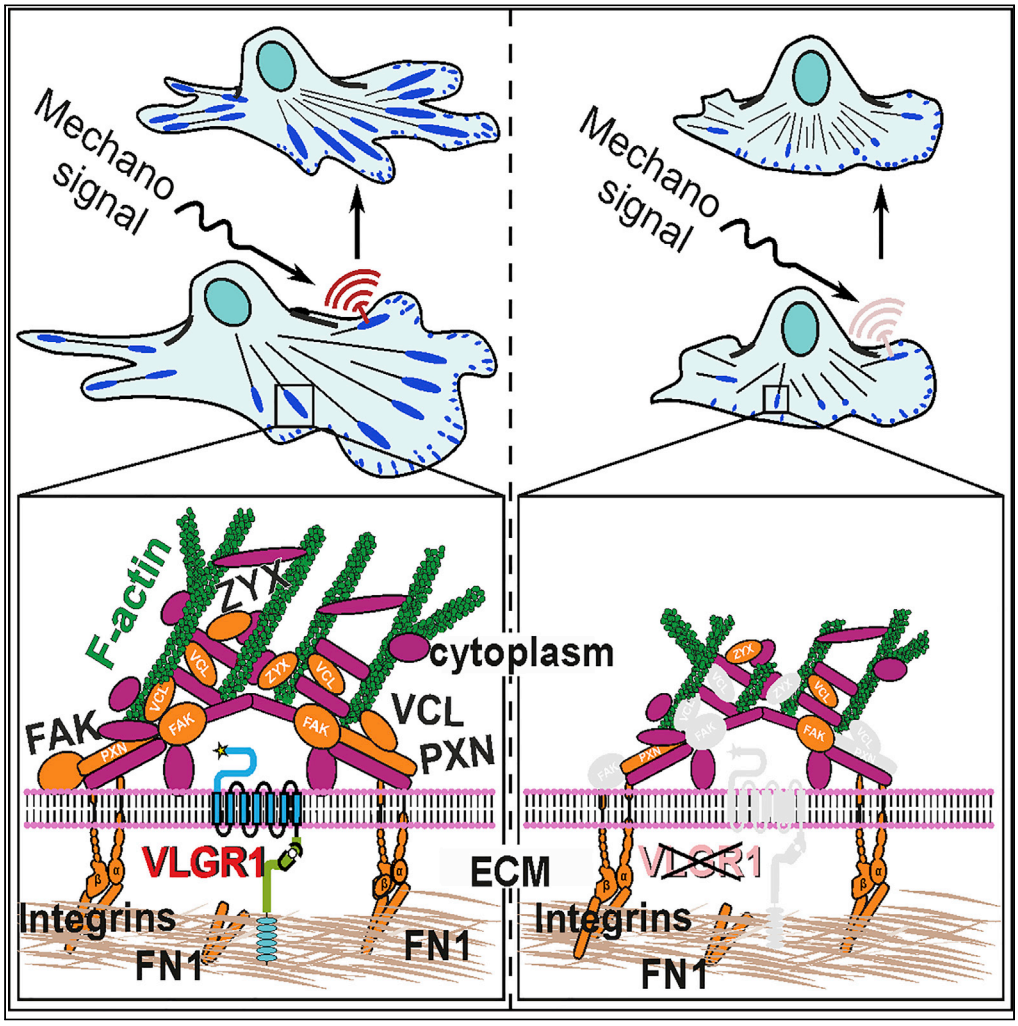

Deva K. Kusuluri, Baran E. Güler, Barbara Knapp, ..., Marius Ueffing, Gabriela Aust, Uwe Wolfrum

wolfrum@uni-mainz.de

Highlights

VLGR1 is an integral part of focal adhesions and crucial for their assembly

Absence of VLGR1 from focal adhesions alters cell spreading and cell migration

VLGR1 is a metabotropic mechanosensor in focal adhesions

Kusuluri et al., iScience 24, 102283
April 23, 2021
https://doi.org/10.1016/j.isci.2021.102283

iScience

CellPress
OPEN ACCESS

Article

Adhesion G protein-coupled receptor VLGR1/ADGRV1 regulates cell spreading and migration by mechanosensing at focal adhesions

Deva K. Kusuluri,[1] Baran E. Güler,[1] Barbara Knapp,[1] Nicola Horn,[2] Karsten Boldt,[2] Marius Ueffing,[2] Gabriela Aust,[3] and Uwe Wolfrum[1,4,*]

SUMMARY

VLGR1 (very large G protein-coupled receptor-1) is by far the largest adhesion G protein-coupled receptor in humans. Homozygous pathologic variants of *VLGR1* cause hereditary deaf blindness in Usher syndrome 2C and haploinsufficiency of *VLGR1* is associated with epilepsy. However, its molecular function remains elusive. Herein, we used affinity proteomics to identify many components of focal adhesions (FAs) in the VLGR1 interactome. VLGR1 is localized in FAs and assembles in FA protein complexes *in situ*. Depletion or loss of VLGR1 decreases the number and length of FAs in hTERT-RPE1 cells and in astrocytes of *Vlgr1* mutant mice. VLGR1 depletion reduces cell spread and migration kinetics as well as the response to mechanical stretch characterizing VLGR1 as a metabotropic mechanosensor in FAs. Our data reveal a critical role of VLGR1 in the FA function and enlighten potential pathomechanisms in diseases related to VLGR1.

INTRODUCTION

Adhesion G protein-coupled receptors (ADGRs), a unique class of the superfamily of G protein-coupled receptors (GPCRs), have been insufficiently characterized (Langenhan et al., 2016; Langenhan, 2020). Recent findings on G protein coupling, the activation mechanism by a tethered agonist (Liebscher et al., 2014), and identification of interaction partners by affinity proteomics (Knapp et al., 2019) and of their function as metabotropic mechanosensors (Scholz et al., 2015) provided prospective insights into the molecular and physiologic function of ADGRs in general (Langenhan, 2020). In the last decade, diverse physiological roles of ADGRs have been described. Several ADGRs are involved in developmental, neural, cardiovascular, immune, and endocrine processes (Knierim et al., 2019).

VLGR1 (very large G protein-coupled receptor-1)/ADGRV1, also known as GPR98 or MASS1 (monogenic audiogenic seizure susceptible-1), is by far the largest GPCR (McMillan and White, 2010). VLGR1 comprises an extremely long extracellular domain (ECD), which includes Calx-β motifs, an epilepsy-associated repeat domain, and a pentraxin domain; VLGR1 also contains the characteristic 7-transmembrane domain (7TM) and a short cytoplasmic intracellular domain (ICD) with a C-terminal PDZ (Post-synaptic density 95, Discs large, Zonula occludens-1) domain-binding motif (PBM). The ECD contains the characteristic GPCR autoproteolysis-inducing (GAIN) domain with the GPCR proteolytic site (GPS). Like other ADGRs, autocleavage at this GPS separates VLGR1 into a C-terminal fragment (CTF) and N-terminal fragment (NTF) (Hu et al., 2014). We recently found that the first 11 amino acids in the N-terminus of the CTF function as a tethered agonist that can trigger receptor activation (Knapp, et al., unpublished data). VLGR1 preferentially couples to the $G\alpha_i$ signaling pathway (Hu et al., 2014).

Several homozygous pathologic variants of the *VLGR1/ADGRV1* gene cause USH2C, a subtype of the human Usher syndrome (USH), the most common form of hereditary deaf blindness (Weston et al., 2004). Haploinsufficiency of *VLGR1/ADGRV1* associates with audiogenic epilepsy in human (Wang et al., 2015; Myers et al., 2018). Although the mechanisms underlying the epilepsy phenotypes remained unclear, so far, dysfunctions of VLGR1 related to the senso-neuronal defects in USH have been associated with fibrous linkers in membrane-membrane adhesions in retinal photoreceptor cells and auditory hair cells (McGee et al., 2006; Maerker et al., 2008) and with a putative role at the ribbon synapses of both types of sensory cells

[1]Institute of Molecular Physiology, Molecular Cell Biology, Johannes Gutenberg University, Hanns-Dieter-Hüsch-Weg 17, 55099 Mainz, Germany

[2]Medical Proteome Center, Institute for Ophthalmic Research, Eberhard Karls University of Tuebingen, 72074 Tuebingen, Germany

[3]Clinic of Visceral, Transplantation, Thoracic and Vascular Surgery & Clinic of Orthopedics, Traumatology and Plastic Surgery, Department of Surgery Research Laboratory, Leipzig University, 04301 Leipzig, Germany

[4]Lead contact

*Correspondence: wolfrum@uni-mainz.de

https://doi.org/10.1016/j.isci.2021.102283

(Reiners et al., 2005; Specht et al., 2009). At these sites, VLGR1 interacts with other USH proteins in the USH-related interactome (Mathur and Yang, 2015).

Recent and present systematic affinity proteomics analyses identified numerous new putative VLGR1 binding proteins (Knapp, et al., unpublished data, present study). Enrichment analysis and present comparisons with focal adhesion (FA) proteomes (Zaidel-Bar and Geiger, 2010; Schiller et al., 2011) and the adhesome database (http://www.adhesome.org) revealed numerous components of FAs in the VLGR1 interactome. FAs are large macromolecular assemblies arranged around transmembrane integrin dimers at the contact sites of the cell membrane with the extracellular matrix (ECM) (Geiger et al., 2009). Their dynamic assembly and disassembly play a central role in cell spreading and migration. FAs control these processes as hubs for bidirectional signaling: "inside-out" transmission of intracellular forces generated by contractions of the actin-myosin system to the ECM and *vice versa* "outside-in" signal transmission such as shear forces between the cell and the ECM from the environment to the cell interior (Shen et al., 2012; Sun et al., 2016).

The molecular composition and the dual function in adhesion and signal reception of ADGRs such as VLGR1 *per se* suggest a putative function at FAs. Here, we demonstrate that VLGR1 is an integral component of FAs essential for cell spreading and cell migration. We provide evidence that VLGR1 works as a metabotropic mechanoreceptor in FAs at the interface between the cell and its extracellular microenvironment. Our insights into the molecular and cellular function of VLGR1 in FAs enlighten the pathophysiology of the diseases related to VLGR1 dysfunction.

RESULTS

Affinity proteomics identifies FA-related proteins as putative VLGR1 interaction partners

To identify putative VLGR1-interacting proteins, we performed tandem affinity purifications (TAPs) from hTERT-RPE1 cells. We transfected these cells with Strep II Flag (SF)-tagged VLGR1 constructs (Figure 1A) and applied SF-TAP (Boldt et al., 2016). Eluted complexes were analyzed by liquid chromatography coupled with tandem mass spectrometry. Software Tool for Researching Annotations of Proteins-annotated proteomic data sets (Bhatia et al., 2009) revealed 478 proteins as putative VLGR1 interaction partners (Table S1). A comparison of these prey proteins with FA proteomes (Zaidel-Bar and Geiger, 2010; Schiller et al., 2011) and the adhesome database (http://www.adhesome.org) (Table S2) revealed 26 core FA molecules as putative interaction partners of VLGR1 (Figure 1, Table S3). Many classical FA core proteins such as integrin β1, integrin α3, and vinculin were enriched in the VLGR1 interactome of hTERT-RPE1 cells.

Integration of VLGR1 in FAs

To verify that VLGR1 is a component of FAs, we co-stained cell lines and primary cells for VLGR1, actin filaments (F-actin), and vinculin, a structural key component and molecular marker of FAs (Figure 2). Confocal microscopy of hTERT-RPE1 cells revealed VLGR1 localization in stripes at the end of F-actin bundles (Figure 2A), which were co-labeled for vinculin (Figure 2B). Quantification of VLGR1, vinculin, or F-actin staining in fluorescence intensity plots revealed substantial co-localization of these proteins (Figures 2C and 2D). We confirmed VLGR1 localization in FAs by double immunolabelling of VLGR1 and vinculin in mouse embryonic fibroblasts and primary astrocytes (Figure S1). Furthermore, we applied two additional FA markers: paxillin, present in the majority of adhesion sites including primordial focal complexes (FXs), and zyxin, absent from immature FXs but incorporated in more mature FAs (Zaidel-Bar et al., 2003). VLGR1 localized at both paxillin-associated adhesions (Figures S2A–S2C) and zyxin-labeled mature FAs (Figures S2B and S2D). The localization of VLGR1 in FAs was additionally confirmed by co-immunostaining of the FA markers vinculin or paxillin, respectively, and the two alternative VLGR1#2 and VLGR1#3 antibodies in both hTERT-RPE1 and primary astrocytes (Figure S3). Taken together, these findings indicate the presence of VLGR1 in all types of FAs, i.e., from nascent adhesions to *bona fide* FAs.

We further explored that the integration of VLGR1 in FAs using *in situ* proximity ligation assays (PLAs) (Figures 2E, S2E, and S2F). PLAs with pairs of two primary antibodies against VLGR1/vinculin, VLGR1/paxillin, and VLGR1/zyxin resulted in fluorescent PLA interaction spots indicating integration of VLGR1 into FA complexes (Figures 2E, S2E, and S2F). The PLA positive interaction spots were found near F-actin termini (Figures 2E, S2E, and S2F). In contrast, when antibodies were omitted, no PLA interaction spots were present (Figure S4). Overall, our results demonstrate that VLGR1 is part of the multi-protein complex in FAs.

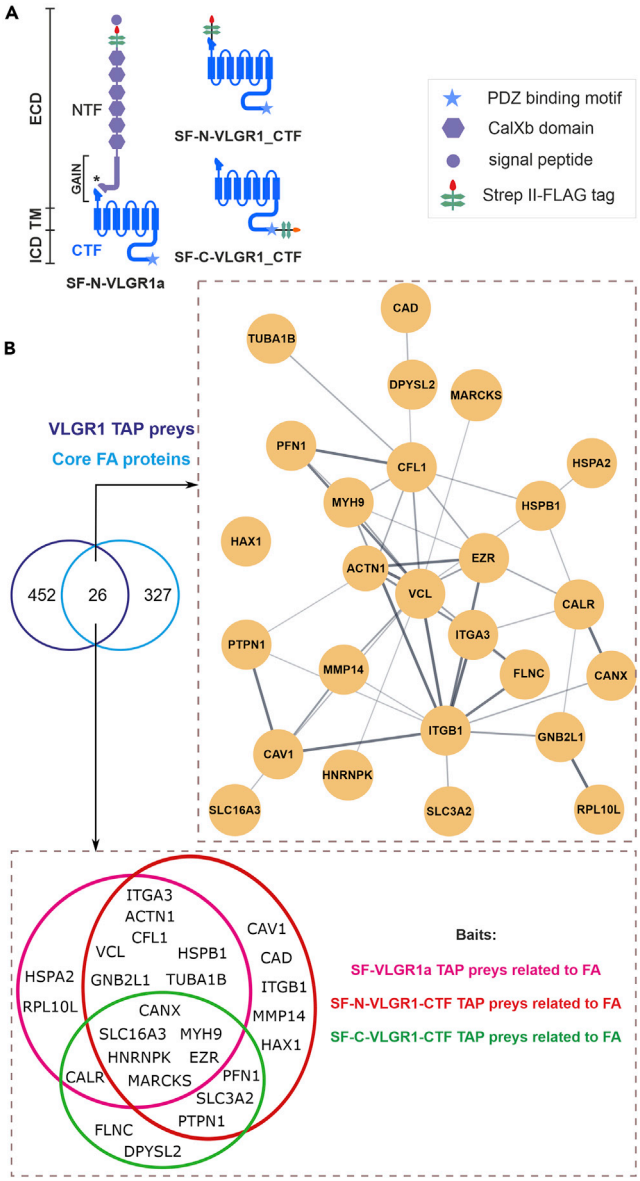

Figure 1. VLGR1 TAP associated putative FA proteins

(A) Full-length VLGR1a, N- or C- terminally VLGR1_CTF tagged with a Strep II- FLAG (SF)-tag used as baits in TAPs.

(B) Venn diagram showing an overlap of 26 proteins from VLGR1 TAP preys with previously published FA proteomes (Schiller et al., 2011; Zaidel-Bar and Geiger 2010) and the adhesome database (http://www.adhesome.org). STRING database analysis reveals the interconnection of overlapping proteins. Venn diagrams of FA preys found in the different VLGR1 TAP baits. NTF, N-terminal fragment; CTF, C-terminal fragment; ICD, intracellular domain; TM, transmembrane domain; ECD, extracellular domain; SP, signal peptide; Calxβ, Calx-β domains; PBM, PDZ-binding motif; GAIN, GPCR autoproteolysis-inducing domain; * indicates GPS, G protein-coupled receptor proteolytic site. See also Tables S1, S2, and S3.

VLGR1 deficiency or absence alters FA morphology

Next, we analyzed the effect of VLGR1 depletion on the structure and morphology of FAs in hTERT-RPE1 cells and astrocytes obtained from *Vlgr1*-deficient mutant mice. We used *Vlgr1*-del7TM mice lacking VLGR1 or the VLGR1 7TM and ICD (McMillan and White, 2004) and *Drum B* mice lacking large parts of the NTF and the entire CTF (Figure 3). For VLGR1 depletion, we transfected hTERT-RPE1 cells with non-targeting control or validated *VLGR1*-specific siRNAs (Figures 3A–3C; for *VLGR1* siRNA validation see: Figure S5). Vinculin immunostaining revealed a decrease in the number and length of FAs in *VLGR1*-depleted cells compared with control cells (Figures 3A–3C). To quantify FA lengths, we grouped FAs into four

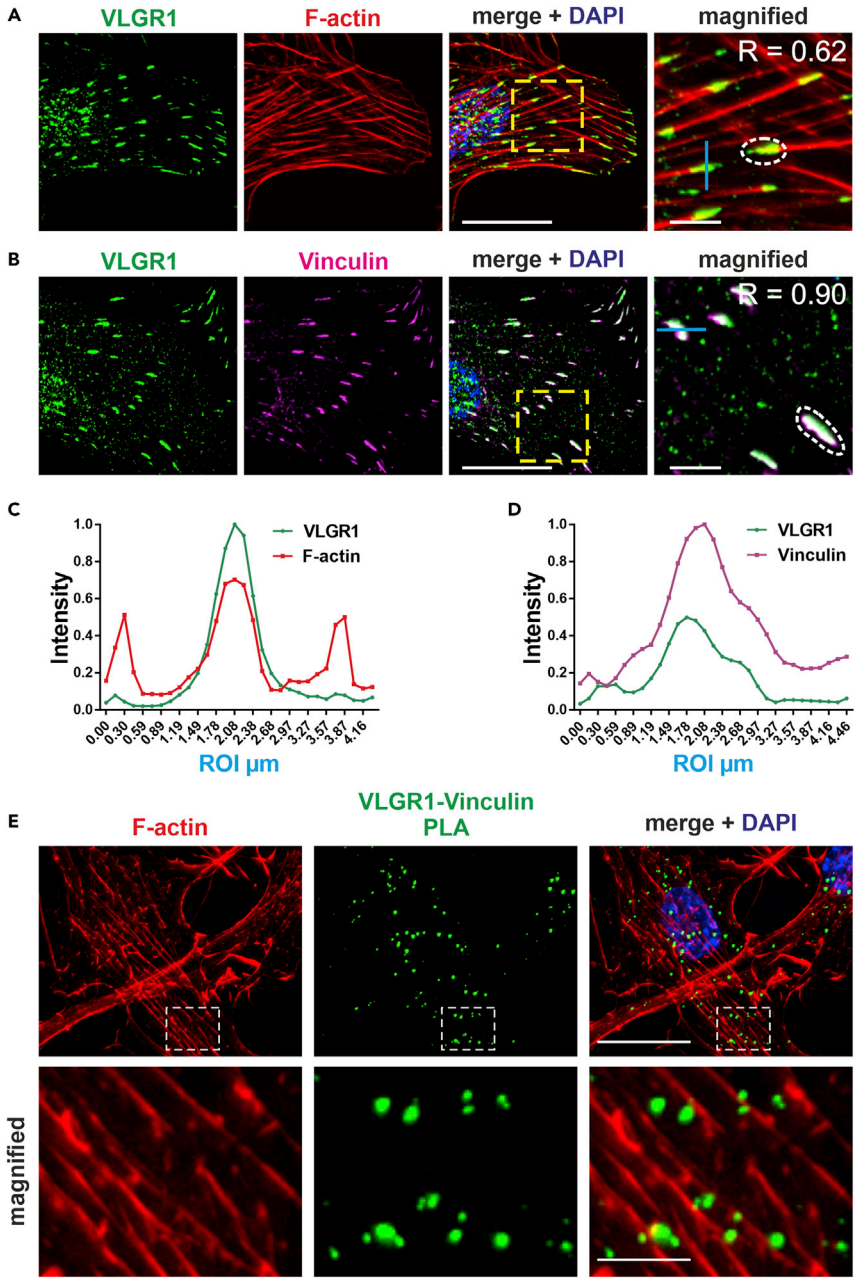

Figure 2. VLGR1 is localized at FAs

(A and B) Double labeling immunofluorescence of VLGR1 (green) and vinculin (magenta) in hTERT-RPE1 cells revealed a concentration of VLGR1 at the tip of F-actin stained by TRITC-phalloidin (red) (A) and in different forms of FAs (B). Pearson correlation coefficient R calculated in magnified images for white dotted region quantifies the degree of co-localization.

(C and D) Normalized fluorescence intensity plots of VLGR1 and F-actin (C) and VLGR1 and vinculin (D) share common peaks along the depicted blue line (ROI) in the magnified images indicating co-localization of both proteins.

(E) In a proximity ligation assay (PLA), the VLGR1-vinculin interaction dots (green) are in close proximity to F-actin. The boxed areas in the overlays are shown magnified. Nuclei are stained with DAPI (blue); scale bars: 25 µm, 5 µm magnified images. See also Figures S1–S4.

categories: nascent FXs 0-1 µm in length and more mature FAs of 1-2.5 µm, 2.5-5 µm, and 5-10 µm in length. VLGR1-depleted cells showed a higher percentage of shorter FAs 1-2.5 µm in length, while control cells contained more prominent and longer FAs (2.5-10 µm) (Figure 3C).

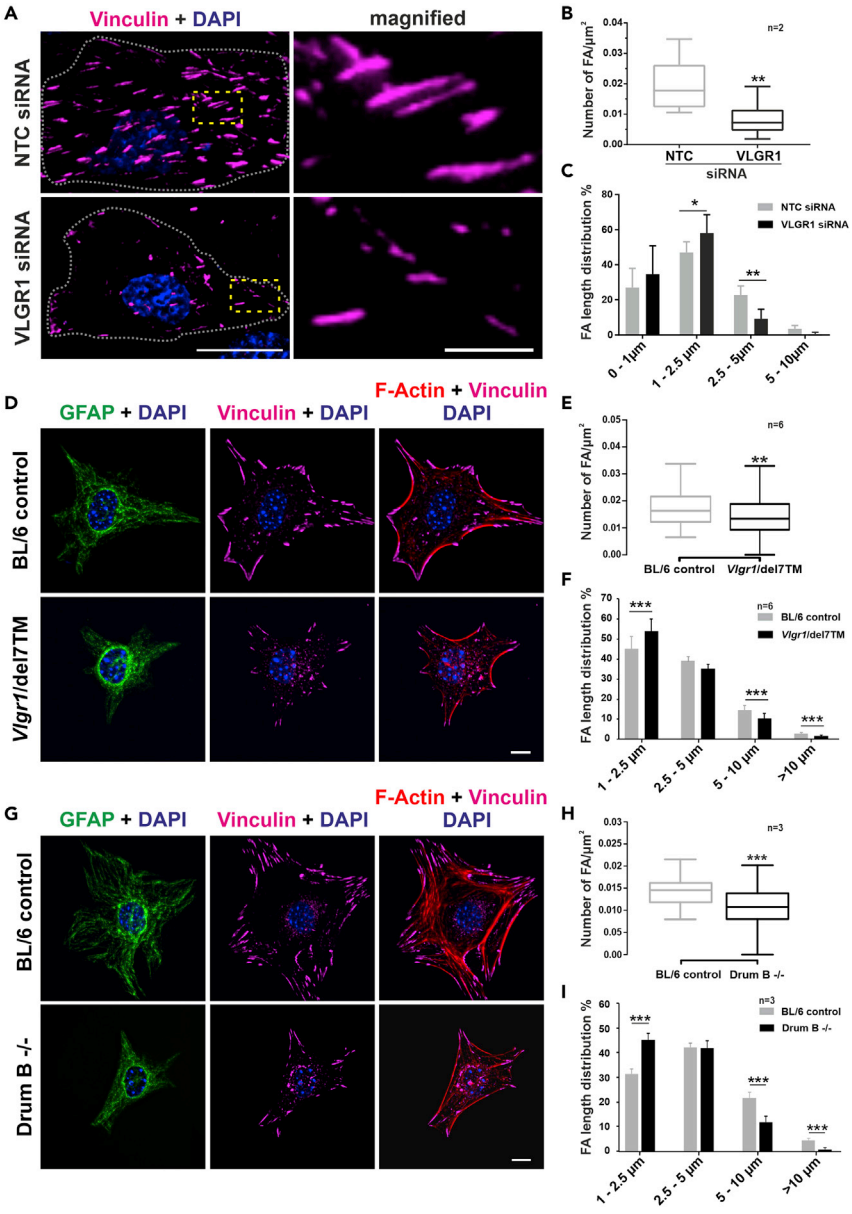

Figure 3. *VLGR1* deficiency alters FA morphology

Representative images of FAs in non-targeting control (NTC) and *VLGR1*-deficient hTERT-RPE1 cells (A–C) and in primary astrocytes from *Vlgr1*-del7TM (D–F) and *Drum B* mutant mice (G–I).

(A, D, G) FAs were stained for vinculin (magenta), F-actin with TRITC-phalloidin (red), and nuclei with DAPI (blue); GFAP (green) was used as an astrocyte marker. FA number and length were reduced after *VLGR1* depletion in hTERT-RPE1 cells (B, C) and in primary astrocytes of both *Vlgr1* mutant mouse lines (E, F, H, I). (B) Twenty-five cells per condition, (C) 900 FAs per condition. (E) Twenty cells per condition, (F) ~1300-1700 FAs per category for control and ~200-1000 FAs for mutant astrocytes. (H) Twenty cells per condition, (I) ~950-1250 FAs per condition for control and ~410-510 FAs for mutant astrocytes. Scale bars: (A) 25 µm and 5 µm in magnified images; (D), (G) 10 µm.

Data represented in (B), (E), and (H) are shown as box plot, and statistical analyses were done using two-tailed Mann-Whitney *U* test. Data in (C), (F), and (I) are represented as mean ± SD. Statistical analyses were done using Sidak's multiple comparison test; *p ≤ 0.05, **p ≤ 0.01, ***p ≤ 0.001. See also Figure S5.

In astrocytes obtained from *Vlgr1*-deficient, *Vlgr1*-del7TM, and *Drum B* mutant mice, we also observed fewer and shorter FAs compared to wild-type (WT) control astrocytes (Figures 3D–3G). The consistency of the effects on FAs in the knockdown experiments and the *Vgr1*-del7TM and *Drum B* mutant cells further

supports the specificity of the siRNAs applied. Collectively, these data demonstrate that VLGR1 is crucial for FA assembly.

VLGR1 knockdown and absence delays cell spreading

The size, shape, and spreading of cells mainly depend on FAs (Chen et al., 2003; Leiss et al., 2008). *VLGR1*-deficient and mutant cells were smaller in comparison to the control cells treated with non-targeting siRNA (Figures 3A and 3D). To address the role of VLGR1 in cell spreading more directly, control and *VLGR1*-deficient cells were allowed to spread and analyzed at different time points. Control cells formed spontaneous lamellipodia at the cell periphery, whereas the majority of the *VLGR1*-deficient cells failed to form these structures (Figure 4A). *VLGR1*-deficient cells showed abnormal morphology such as defects in blebbing, a process necessary for plasma membrane protrusion during cell spreading and migration (Norman et al., 2010).

Cell spreading goes through distinct defined subsequent phases (Gauthier et al., 2012; Greiner et al., 2013). After seeding onto an adhesive surface, cells form FAs to adhere to the ECM and proceed through phase 1 (P1, non-contractile spreading), then phase 2 (P2, contractile spreading), and finally phase 3 (P3, polarization). We defined these cell spreading phases for HEK293T cells (Figure S6). To determine the role of VLGR1 in phase progression during cell spreading, we knocked down *VLGR1* and monitored the cell shape 30 min and 2.5 hr after seeding on a poly-lysine-coated surface (Figures 4B and 4C). We found that 30 min after seeding, ~78% of the control cells had reached P2, whereas ~75% of *VLGR1*-deficient cells were still in P1 (Figures 4B–4B′). After 2.5 hr, ~80% of control cells were polarized (P3), whereas most *VLGR1*-deficient cells remained in P1 or P2 (Figures 4C–4C′).

The ECM protein fibronectin promotes cell spreading of mammalian cells (Leiss et al., 2008). On fibronectin-coated surfaces, the cell size of *VLGR1*-deficient HEK293T cells was also reduced at both time points when compared to control cells (Figures 5A, 5A′, 5B, and 5B′). In addition, primary astrocytes of both *Vlgr1*-del7TM and *Drum B* mouse mutants also had reduced surface areas compared to WT Bl6 control astrocytes (Figures 5C and 5C′). Taken together, our data demonstrate that the absence or depletion of VLGR1 causes defects in cell spreading.

VLGR1 depletion decreases total FAK expression but increases pFAK397 levels

The dynamics of FAs are regulated by the focal adhesion kinase (FAK) known as a multifunctional adapter and non-receptor tyrosine kinase involved in integrin-mediated signaling at FAs (Lawson and Schlaepfer, 2012). Phosphorylation of different amino acid residues on FAK modulates FA functions. For example, autophosphorylation of FAK at Tyr397 (pFAK-397) is a determinant step for FA disassembly (Hamadi et al., 2005; Webb et al., 2004). To determine a potential role of VLGR1-FAK interaction at FAs, we examined the expression of FAK and pFAK-397 in *VLGR1*-deficient hTERT-RPE1 cells in Western blot analyses. *VLGR1* depletion resulted in a decrease of total FAK and an increase of pFAK-397 in comparison to control cells (Figure 6). These changes suggest that FAK has roles in downstream signaling of VLGR1.

VLGR1 stimulates cell migration

Next, we investigated the role of VLGR1 in unidirectional, collective cell migration. We grew hTERT-RPE1 cells and mouse primary astrocytes cells to confluency and then "scratched" a space in the monolayer and followed the cells as they polarized and moved into the cleared area (Figure 7). In these migrating cells, VLGR1 was predominantly localized at the ends of F-actin bundles in small vinculin-positive puncta, likely FXs (Figure 7A). The localization of VLGR1-stained FAs of variable size at the leading edge of migrating cells suggests a putative role of VLGR1 in the regulation of polarized cell migration. To address such a role, we explored the effects of reducing cellular VLGR1 levels in the kinetics and extent of wound closure in two types of cells (Figure 7B). Firstly, we compared the closure rates of control hTERT-RPE1 cells with rates using hTERT-RPE1 in which we had knocked down VLGR1. We also compared the closure rates of mouse primary astrocytes from WT and Vlgr1-del7TM. Quantification revealed that wound closure was delayed at all time points in VLGR1-deficient cells compared to control cells (Figures 7B–7D). These motility assays indicate that the migration capacity is impaired in VLGR1-deficient cells and suggest a role of VLGR1 in collective cell migration regulation.

The kinetics of the closure of a wound in a monolayer is influenced both by the rate of the movement of cells into the denuded area as well as the rate of cell proliferation of new cells filling the space. Because VLGR1

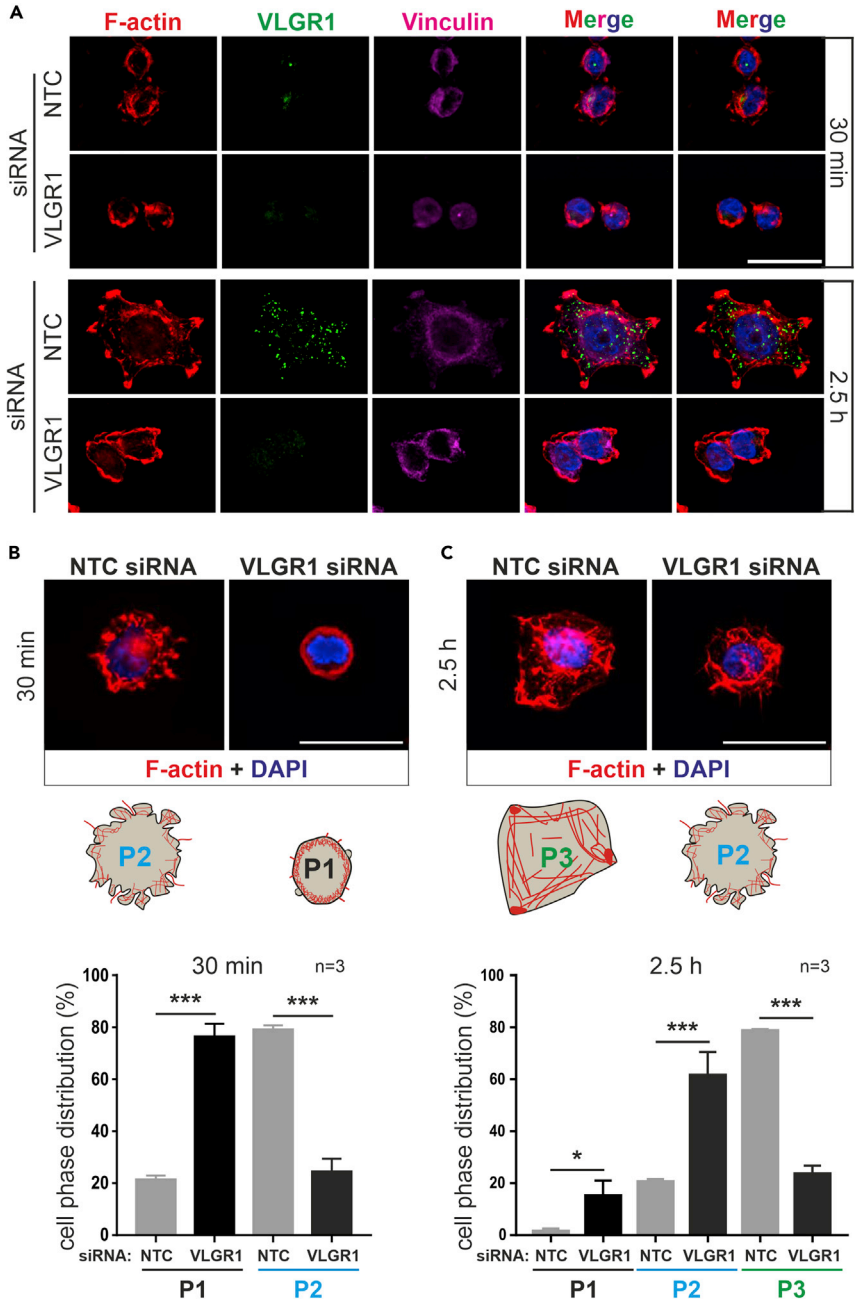

Figure 4. VLGR1-deficient cells show defects in phase progression during cell spreading

(A) Immunofluorescence staining of VLGR1 (green) of control (NTC) and VLGR1-depleted HEK293T cells subjected to cell spreading. VLGR1 is localized in the protruding cell membrane of control cells after 30 min and 2.5 hr of spreading. VLGR1 deficiency results in defective spreading. F-actin staining by TRITC-phalloidin (red) indicates cell areas. Vinculin (magenta) marks FAs.

(B and C) F-actin-stained control and VLGR1-depleted cells after 30 min (B) or 2.5 hr (C) of spreading on poly-L-coated coverslips. Cartoons represent stages of spreading for each condition. Blue: DAPI counterstain. (B′, C′) Quantification cells in different phases (P1, P2, and P3) of spreading. 300 cells per condition; scale bars, 25 μm. Data are represented as mean ± SD. Statistical evaluation was performed using Sidak's multiple comparison test; *$p \leq 0.05$, **$p \leq 0.01$, ***$p \leq 0.001$. See also Figure S6.

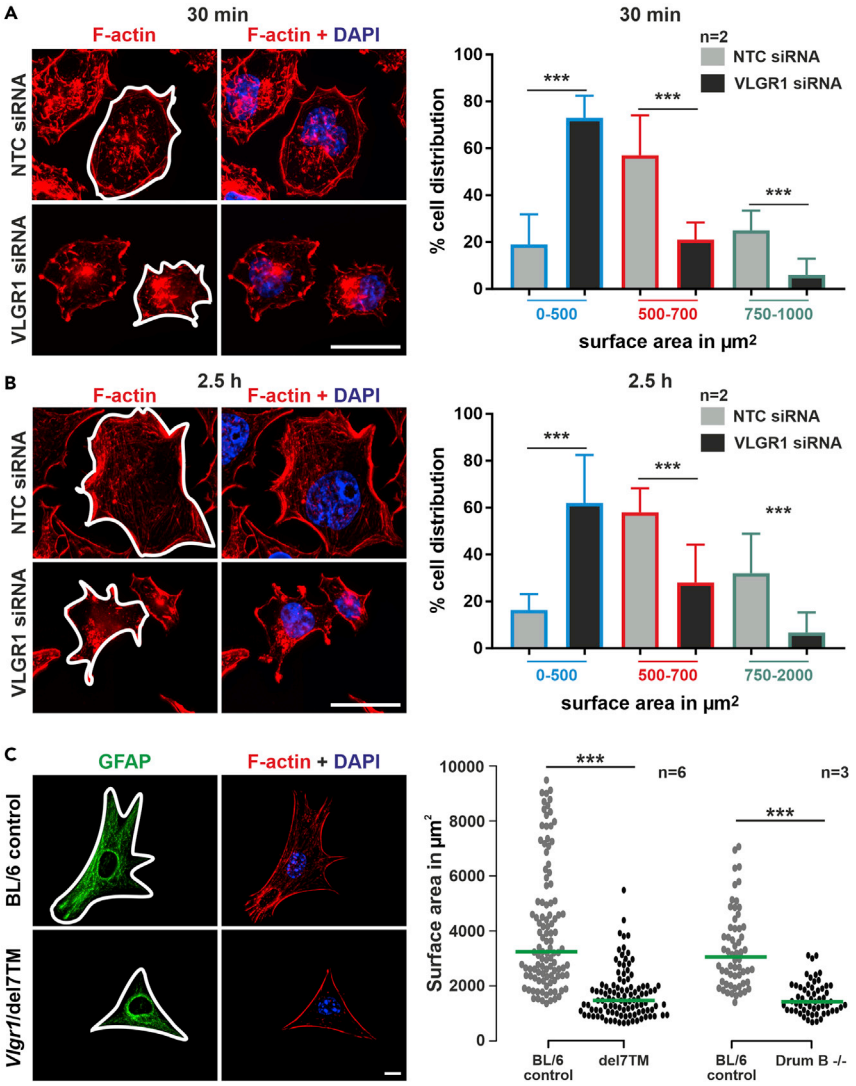

Figure 5. VLGR1 deficiency reduces cell surface area that is attached to the substrate

(A and B) HEK293T cells treated with non-targeting control (NTC) siRNA and VLGR1 siRNA were replated on fibronectin-coated coverslips and stained for F-actin (red, TRITC-phalloidin) and for nuclear DNA (blue, DAPI) at 30 min (A) and 2.5 hr (B).

(C) Primary astrocytes from *Vlgr1*-del7TM (C) stained for GFAP (green, astrocyte marker) and F-actin (red, TRITC-phalloidin); nuclei are stained with DAPI (blue). Quantifications of cell surface areas (white outline) by Fiji revealed a defect in cell spreading in VLGR1-deficient cells at both time points (A′, B′) and in primary astrocytes of *Vlgr1*-del7TM and *Drum B* mutant mice (C′). Green lines in dot plots indicate median (A′, B′) n = 400-600 cells per condition, 3 independent experiments. (C′) n = 20-40 cells per condition, 6 independent experiments for *Vlgr1*-del7TM and 3 independent experiments for *Drum B* mutant mice. Scale bars: (A), (B), 25 µm; (C), 10 µm. Data are represented as mean ± SD. Statistical evaluation was performed using Sidak's multiple comparison test in (A) and (B) and two-tailed Student's t test was applied in (C), *p ≤ 0.05, **p ≤ 0.01, ***p ≤ 0.001.

knockdown lead to a low but significant decrease of about 10% in cell proliferation (Figure S7), it is possible that the observed decrease in wound closure is a result of decreased cell proliferation and not a decreased migration. Therefore, we additionally tested the role of *VLGR1* in cell migration using live-cell imaging of single cells, which is not influenced by cell proliferation. We found that the velocity of primary astrocytes of *Vlgr1*-del7TM mice significantly decreased when compared to WT control astrocytes (Figures 7E and 7F, Videos S1 and S2). Our wound healing and single-cell imaging results suggest that cell migration in VLGR1-deficient cells is impaired and indicate an important role of the VLGR1 in controlling cell migration.

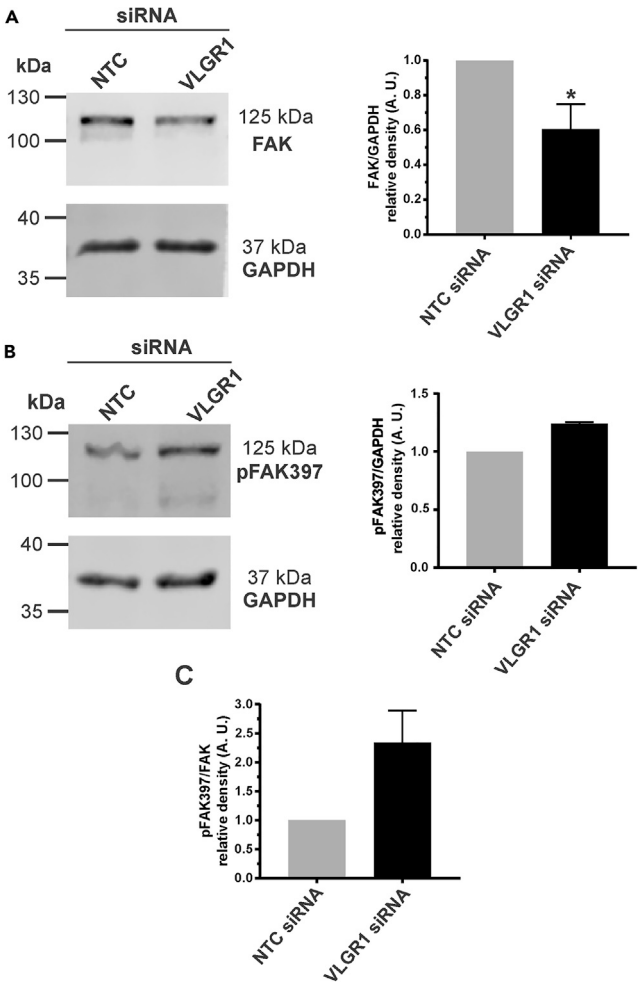

Figure 6. VLGR1 regulates FAK signaling

(A) Western blot analysis of FAK in control (NTC) and VLGR1-depleted hTERT-RPE1 cells and in the right panel, densitometric quantification of bands related to GAPDH expression in arbitrary units (A.U.).

(B) Western blot analysis of pFAK367 in control (NTC) and VLGR1-depleted hTERT-RPE1 cells and in the right panel densitometric quantification of band related to GAPDH expression in arbitrary units (A.U.).

(C) Relative expression pFAK397 and FAK. VLGR1 depletion leads to a significant decrease in total FAK and a slight increase of pFAK397. Data are represented as mean ± SD. Two-tailed Student's t test was applied, *$p < 0.05$, **$p < 0.01$, ***$p < 0.001$.

VLGR1 senses mechanical stimuli at FAs

There is growing evidence that ADGRs can act as mechanosensors that can transduce external mechanical forces into internal biochemical signals (Scholz et al., 2015). To investigate a role for VLGR1 in mechanosensing, we applied fluid shear stress to *VLGR1*-deficient and WT hTERT-RPE1 cells (Figure 8). We found that external mechanical force increased both the number and length of FAs in WT cells but not in untreated WT cells (Figures 8A–8C). Our results confirm previous studies under slightly different conditions with other cell types (Ponik and Pavalko, 2004; Lei et al., 2020). In WT cells, in addition to changes in FAs, we also observed that shear stress also decreased cell spreading on the substrate (Figure 8D). In contrast to WT cells, the number and length of FAs and cell spreading did not differ in shear stress-treated compared with untreated VLGR1-deficient hTERT-RPE1 cells (Figures 8A–8D). These findings indicate that VLGR1 participates in the transduction of mechanical force into a cellular response by remodeling FAs.

DISCUSSION

In the present study, we identified VLGR1 as an important component of FAs, highly dynamic macromolecular complexes coupled to the actin cytoskeleton (Zaidel-Bar and Geiger, 2010). FAs represent signaling

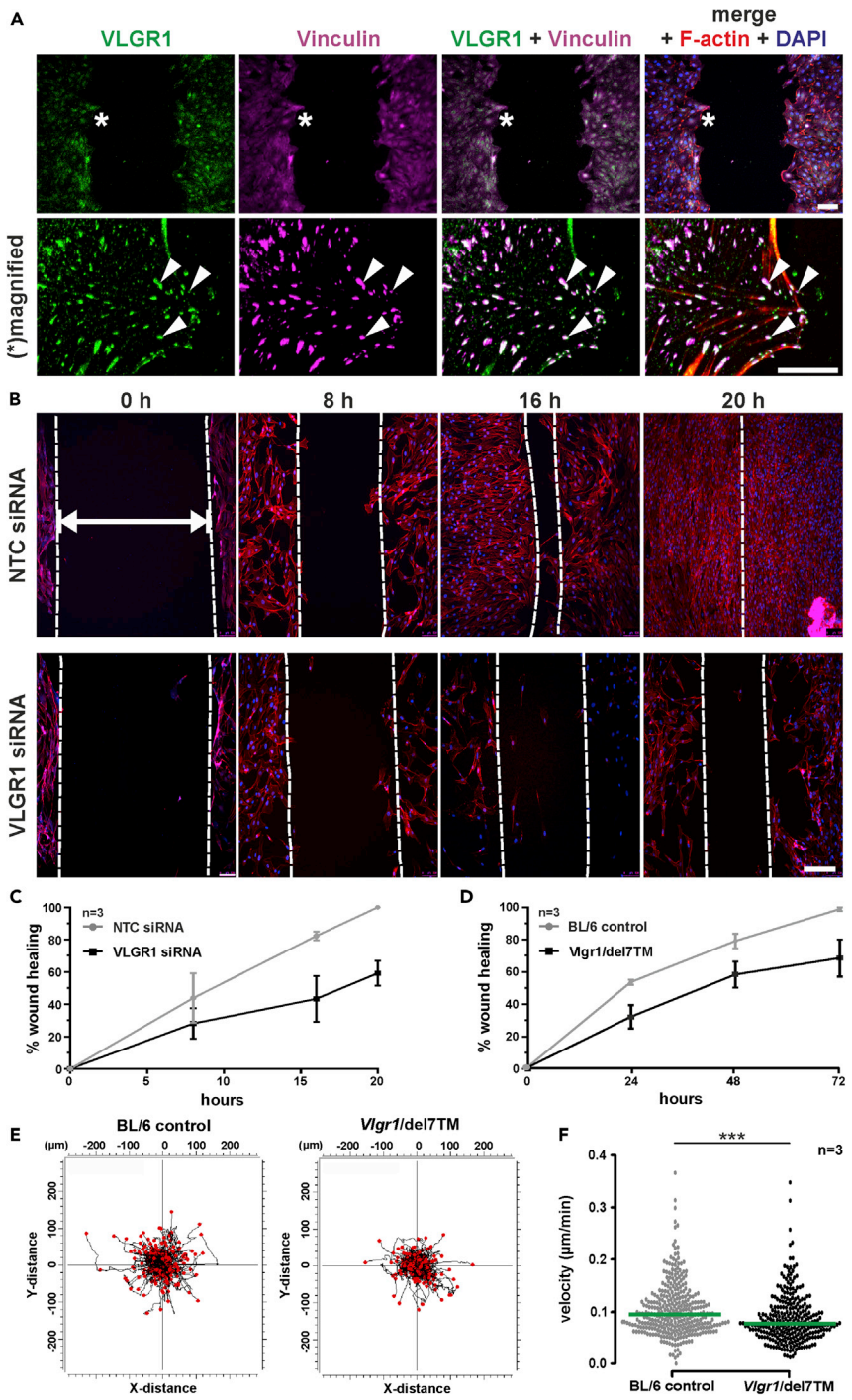

Figure 7. VLGR1 regulates cell migration

(A) VLGR1 (green) and vinculin (magenta) co-localize at the leading edge of hTERT-RPE1 cells migrating into the scratched wound area. *White asterisks* indicate the leading edge of migrating cells that are magnified in the lower panel showing focal complexes (*arrowheads*). F-actin (red); nuclear DNA (blue, DAPI).

(B) Wound closure analysis in control (NTC siRNA) and VLGR1-depleted (VLGR1 siRNA) cells at 0, 8, 16, and 20 hr. Dotted white lines indicate the wound area left open. *Double headed white arrow* indicates "wound" cleft. F-actin (red); DAPI stained nuclei (blue).

(C and D) (C) Wound closure rates in control and VLGR1-depleted hTERT-RPE1 cells and (D) in primary astrocytes of BL/6 wild-type control and *Vlgr1*-del7TM mice from 3 independent experiments each.

Figure 7. *Continued*

(E) Single-cell track plots of *Vlgr1*-del7TM and control mouse primary astrocytes; 24-hr video recorded with 15-min time interval. Each black line represents tracking paths of single cells. Red dots represent final points of migration. Images were taken at least 5 different spots; n = 329 cells for WT and n = 278 cells for *Vlgr1*-del7TM.

(F) Quantification of single cell migration revealing significant lower velocity of primary astrocytes in *Vlgr1*-del7TM mice. Green lines in dot plots indicate median. Scale bars: (A), top, 100 μm, middle, 25 μm, and bottom, 15 μm; (B), 200 μm. Data are represented as mean ± SD. Two-tailed Student's t test was applied in (C); *p ≤ 0.05, **p ≤ 0.01, ***p ≤ 0.001. See also Videos S1 and S2.

hubs that control cell adhesion and migration in response to internal or environmental cues (Geiger et al., 2009; Shen et al., 2012). Although the dual function of ADGRs in cell adhesion and sensing predestines ADGRs for signaling at cell adhesions, none of the 33 human ADGRs has been found in FAs to date.

VLGR1 associates with the FA core promoting FA maturation and dynamics

We provide several lines of evidence that VLGR1 is a component of FA. First, we identified many FA-related molecules as putative VLGR1 interacting proteins by TAP-based affinity proteomics performed in two different human cell lines (present study; Knapp et al., unpublished data), indicating that VLGR1 is a component of FAs. This is also confirmed by a quasi "reciprocal" proteomic approach, which revealed VLGR1 in the proteome of purified chemical cross-linked FAs of murine fibroblasts (Schiller et al., 2013). Secondly, VLGR1 co-localizes with molecular markers and core components of FAs present in several cell lines and primary cells. Thirdly, the physical interaction and thus close proximity of VLGR1 with other FA structural core components is strengthened by our *in situ* PLA data.

The presence of VLGR1 in immature nascent FXs at the leading edge of migrating cells suggests that its signaling may control the dynamics of FAs during their growth and maturation. Indeed, the formation of FAs is stunted in *VLGR1*-depleted cells: all analyzed cell types display smaller and less abundant FAs. A similar phenotype has been observed in cells deficient for FA core molecules known to participate in the regulation of FA dynamics and function (Raghavan et al., 2003; Saunders et al., 2006). Taken together, these findings identify VLGR1 as the first ADGR present at the protein cluster of FAs controlling FA dynamics.

VLGR1 in FA complexes establishes cell spreading and drives cell migration

FAs are signaling centers for the transformation and integration of signals between the ECM and interior of the cell, which are essential for the regulation of cell spreading and migration (Wozniak et al., 2004; Leiss et al., 2008). Here, we demonstrate that VLGR1 depletion reduces the kinetics of cell spreading and cell migration indicating that VLGR1 at FAs ensures the correct course of both processes. Defective cell spreading is a characteristic phenotype of cells deficient for FA signaling and signaling mediator molecules (Raghavan et al., 2003; Schiller et al., 2013; Thompson et al., 2014). Cell spreading is a crucial prerequisite for cell migration, and both processes require the coordination of the same subcellular molecular pathways (Kassianidou et al., 2019). Therefore, it is not surprising that VLGR1 deficiency also decreases cell migration. Consistently, cells deficient for the FA signaling molecules show decreased migration abilities (Fang et al., 2016; Colburn and Jones, 2017).

The dynamics and activity of FA components are vital for cell migration (Wozniak et al., 2004). One of the key players in the regulation of FA dynamics is FAK, and its ablation results in decreased cell migration (Sieg et al., 2000). Here, we show that VLGR1 depletion alters FAK protein expression and its physiological status, as seen by a decrease of total FAK and increase of FAK phosphorylated at tyrosine 397 (pFAK-397). VLGR1-mediated signaling may control proteostasis of the FAK protein at FAs. One potential target for this is the protease calpain, which mediates the cleavage and degradation of FAK at FAs (Chan et al., 2010). Interestingly, autophosphorylation of FAK at tyrosine 397 is a determinant step for FA disassembly (Webb et al., 2004; Hamadi et al., 2005) and correlates with the decrease in cell migration rates (Kim and Wirtz, 2013) which is line with our observations in *VLGR1*-depleted cells. Taken together, the absence of VLGR1 dysregulates FA signaling pathways and likely promotes the pathways underlying FA disassembly leading to reduced cell migration.

VLGR1 is a metabotropic mechanosensor in FAs

FAs act as supramolecular hubs for sensing and transmission of mechanical signals between the cell and its microenvironment (Gardel et al., 2010). In these adhesion complexes, integrins are key molecules of the

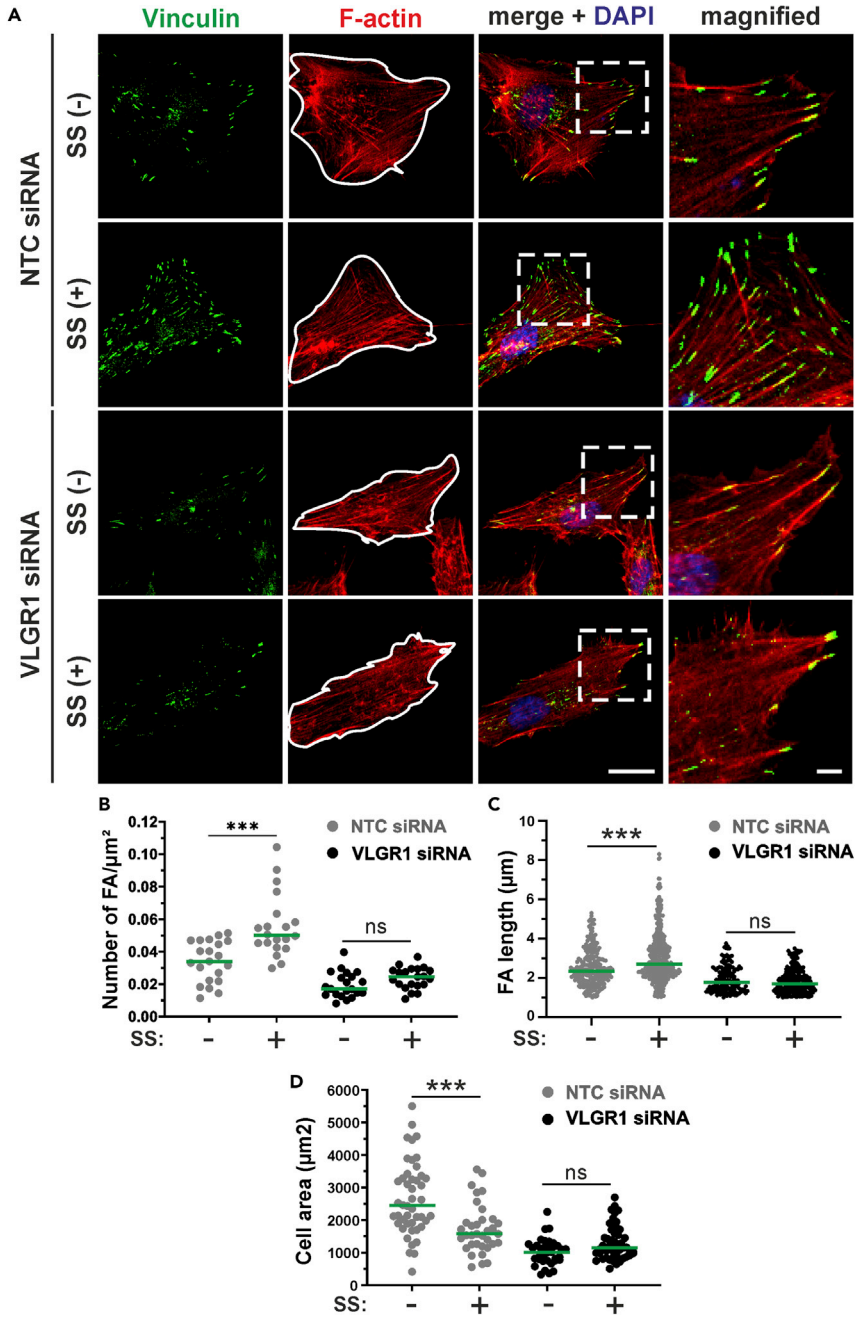

Figure 8. VLGR1 senses mechanical stimuli at FAs

(A) Analysis of FAs stained for vinculin (green) and cell area (*white lines*) in control (NTC siRNA) and VLGR1-depleted (VLGR1 siRNA) hTERT-RPE1 cells induced with (SS +) or without shear stress (SS -). Scale bars: 25 µm

(B–D) (B and C) Quantification of FA number (B), FA length (C), and of the cell area (D) in control and VLGR1-depleted cells under shear stress (SS +) and static conditions (SS -). Six hundred to 2000 FAs per condition; 50 cell areas per condition. Green lines in dot plots indicate median values. Data are represented as mean ± SD. Statistical evaluation was performed by Sidak's multiple comparison tests; *p ≤ 0.05, **p ≤ 0.01, ***p ≤ 0.001.

bidirectional mechanical signaling (Sun et al., 2016). These transmembrane dimers transmit inside-out sensing of the intracellular tension generated by the actin-myosin system to the ECM but also sense physical properties of the ECM in an outside-in manner. Tensile forces between integrins and ECM molecules are transduced via cytoskeletal adapter proteins such as the molecular clutch protein talin (Elosegui-Artola

et al., 2016). However, little is known about the participation of ADGRs in FA mechanosensation. Here, we show that VLGR1 is also essential for cells to respond to the mechanical stimuli at FAs in a shear stress paradigm. This indicates VLGR1 acts as a metabotropic mechanosensor in outside-in sensing at FAs, controlling FA assembly and function.

Our findings are consistent with emerging evidence for other ADGRs acting as mechanosensors, sensing mechanical signals from the extracellular environment (Scholz et al., 2015; Langenhan, 2020). In the peripheral nervous system, GPR126/ADGRG6 senses the mechanical property of the ECM in the basal lamina during Schwan cell development (Mogha et al., 2016). Other ADGRs also detect mechanical changes in a higher dynamic range such as shear, vibration, or stretch (Langenhan et al., 2016). In *Drosophila*, Cirl, an ADGR homolog of vertebrate latrophilins/ADGRLs, is essential for the perception of sound, stretch, or touch in mechanosensitive sensory cells (Scholz et al., 2015). VLGR1 may respond to mechanical forces in a wide dynamic range at FAs, including static mechanical forces which are present during cell spreading and assembly of FAs and more dynamic forces emerging during cell migration and shear stress, respectively.

Liebscher et al. (2014) discovered peptide sequences C-terminal to the GPS motif in the GAIN domain of ADGRs that act as a tethered endogenous agonist which is in line with their general function as mechanosensors (Langenhan et al., 2016). Mechanical forces, transmitted by the ECD, may dislodge this so-called "*Stachel*" into the extracellular grooves/surface of the 7TM domain of the receptor. Recently, we identified an 11-amino acid peptide as the *Stachel* sequence in the GAIN domain of VLGR1 (Knapp et al., unpublished data) indicating that the mechanical stimulation of VLGR1 may also occur through the conserved tethered agonism. Taken together, our findings suggest that mechanical stimuli at FAs are received and transduced by VLGR1.

VLGR1 activation likely couples to a $G\alpha_i$-mediated signaling downstream pathway (Hu et al., 2014; Knapp et al., unpublished data). Although details still remain elusive, our data indicate a cross talk between VLGR1 and FAK signaling. In any case, VLGR1 deficiency dysregulates FAK expression and activation.

How do our findings relate to diseases caused by defects in VLGR1?

At first glance, our data shown here do not provide novel insights into pathomechanisms underlying to epilepsy and USH. However, VLGR1 is highly expressed in the developing CNS (McMillan and White, 2010), in which cell migration is an important feature. Interestingly, defects in migration pathways have recently been linked to increased susceptibility to epilepsy (Qin et al., 2017; Liu et al., 2020). Accordingly, cell migration defects described here may be the cellular basis for the susceptibility to audiogenic seizures and epilepsy associated with VLGR1 dysfunction.

USH2C is characterized by hearing and vision deficiencies. In both affected sensory cells, VLGR1 is an essential component of extracellular fibers, namely the ankle links present between the neighboring stereocilia of developing hair cells (McGee et al., 2006) and fibrous links associated with sensory cilia of photoreceptors (Maerker et al., 2008). There is evidence that the ankle links sense the proximity between neighboring stereocilia, which is needed to refine and shape the typical V-form hair bundle at the hair cell surface (Richardson and Petit, 2019). Within these links, VLGR1 may serve as the mechanosensor detecing mechanical forces between neighboring stereocilia. The mechanical forces acting on the VLGR1-based fibrous links at the ciliary base of photoreceptors are even less clear. They may contribute to the alignment of the photoreceptor cilium and the outer segment toward the incoming light (Enoch, 1978; Wolfrum, 1995). However, based on the present findings, further research will be required to elucidate the pathomechanisms caused by defects in VLGR1.

Conclusion

We identified and validated VLGR1 as the first ADGR in the macromolecular cluster of proteins comprising FAs. We show that VLGR1 is vital component of FAs and provide novel insight into the molecular composition and function of FAs. VLGR1 is crucial for key functions of FAs in processes such as cell spreading and cell migration. We provide evidence that VLGR1 functions as metabotropic mechanosensor at FAs sensing mechanical cues from the extracellular environment of the cell during these processes. These findings also provide fresh basis for explaining the pathomechanisms underlying VLGR1-associated diseases.

Limitations of the study

Our study provides several lines of molecular and cellular evidence for the role of VLGR1 in FAs as a metabotropic mechanosensor that regulates cell spreading and migration. Further studies are needed to gain molecular and mechanistic insights into mechanostimulation of VLGR1 receptors in FAs, for example, using non-cleavable VLGR1 mutants to clarify whether this involves release of the NTF from its CTF base. Our data also show that a signaling pathway downstream of VLGR1 interacts with the FAK pathway. However, deciphering the details of the cross talk of FAK and integrin signaling in FAs is reserved for future studies. We propose that defective cell migration and mechanosensation that we observed in VLGR1 deficiency could trigger the development of epilepsy and USH, but further research is needed to elucidate the pathomechanisms caused by VLGR1 defects leading to these diseases.

Resource availability

Lead contact

Further information and requests for resources and data should be directed to the lead contact, Uwe Wolfrum, Institute of Molecular Physiology, Molecular Biology, Johannes Gutenberg University of Mainz, Hanns-Dieter-Hüsch-Weg 17 , D-55099 Mainz, Germany (wolfrum@uni-mainz.de).

Materials availability

This study did not generate new unique reagents.

Data and code availability

Original/source data for all figures presented in the paper are available from the lead contact upon request.

METHODS

All methods can be found in the accompanying transparent methods supplemental file.

SUPPLEMENTAL INFORMATION

Supplemental information can be found online at https://doi.org/10.1016/j.isci.2021.102283.

ACKNOWLEDGMENTS

This work was supported by the German Research Council (DFG) for 2149 "Elucidation of Adhesion-GPR signaling" WO 548/8 (U.W.) and AU132/8 (GA), European Community "SYSCILIA" [FP7/2009/241955] (M.U., U.W.), and Foundation Fighting Blindness (FFB) PPA-0717-0719-RAD (M.U., U.W.). In addition, we thank Drs. Karl Fath, Kerstin Nagel-Wolfrum, Helen May-Simera, Sarita Rani Patnaik, and Aziz El-Amraoui for helpful discussions and language editing.

AUTHOR CONTRIBUTIONS

B.K. conducted the initial TAP analysis; K.B., N.H., and M.U. carried out mass spectrometry analysis; B.K. and D.K.K. analyzed TAP datasets. B.E.G. performed the experiments with primary astrocytes including life cell imaging and D.K.K. conducted most other experiments. G.A. along with D.K.K. contributed to shear stress experiments. U.W. and D.K.K. designed the studies and wrote the manuscript. All authors read and approved the final manuscript.

DECLARATION OF INTERESTS

The authors declare that there is no conflict of interest.

Received: December 1, 2020
Revised: February 12, 2021
Accepted: March 3, 2021
Published: April 23, 2021

REFERENCES

Bhatia, V.N., Perlman, D.H., Costello, C.E., and Mccomb, M.E. (2009). Software tool for researching annotations of proteins: open-source protein annotation software with data visualization. Anal Chem. *81*, 9819–9823.

Boldt, K., Van Reeuwijk, J., Lu, Q., Koutroumpas, K., Nguyen, T.M., Texier, Y., Van Beersum, S.E., Horn, N., Willer, J.R., Mans, D.A., et al.; UK10K Rare Diseases Group (2016). An organelle-specific protein landscape identifies novel diseases and molecular mechanisms. Nat. Commun. *7*, 11491.

Chan, K.T., Bennin, D.A., and Huttenlocher, A. (2010). Regulation of adhesion dynamics by calpain-mediated proteolysis of focal adhesion kinase (FAK). J. Biol. Chem. *285*, 11418–11426.

Chen, C.S., Alonso, J.L., Ostuni, E., Whitesides, G.M., and Ingber, D.E. (2003). Cell shape provides global control of focal adhesion assembly. Biochem. Biophys. Res. Commun. *307*, 355–361.

Colburn, Z.T., and Jones, J.C. (2017). alpha6beta4 integrin regulates the collective migration of epithelial cells. Am. J. Respir. Cell Mol. Biol. *56*, 443–452.

Elosegui-Artola, A., Oria, R., Chen, Y., Kosmalska, A., Perez-Gonzalez, C., Castro, N., Zhu, C., Trepat, X., and Roca-Cusachs, P. (2016). Mechanical regulation of a molecular clutch defines force transmission and transduction in response to matrix rigidity. Nat. Cell Biol. *18*, 540–548.

Enoch, J.M. (1978). The relationship between retinal receptor orientation and photoreceptor optics. Int. Ophthalmol. Clin. *18*, 41–80.

Fang, K.P., Dai, W., Ren, Y.H., Xu, Y.C., Zhang, S.M., and Qian, Y.B. (2016). Both Talin-1 and Talin-2 correlate with malignancy potential of the human hepatocellular carcinoma MHCC-97 L cell. BMC Cancer *16*, 45.

Gardel, M.L., Schneider, I.C., Aratyn-Schaus, Y., and Waterman, C.M. (2010). Mechanical integration of actin and adhesion dynamics in cell migration. Annu. Rev. Cell Dev. Biol. *26*, 315–333.

Gauthier, N.C., Masters, T.A., and Sheetz, M.P. (2012). Mechanical feedback between membrane tension and dynamics. Trends Cell Biol. *22*, 527–535.

Geiger, B., Spatz, J.P., and Bershadsky, A.D. (2009). Environmental sensing through focal adhesions. Nat. Rev. Mol. Cell Biol. *10*, 21–33.

Greiner, A.M., Chen, H., Spatz, J.P., and Kemkemer, R. (2013). Cyclic tensile strain controls cell shape and directs actin stress fiber formation and focal adhesion alignment in spreading cells. PLoS One *8*, e77328.

Hamadi, A., Bouali, M., Dontenwill, M., Stoeckel, H., Takeda, K., and Ronde, P. (2005). Regulation of focal adhesion dynamics and disassembly by phosphorylation of FAK at tyrosine 397. J. Cell Sci. *118*, 4415–4425.

Hu, Q.X., Dong, J.H., Du, H.B., Zhang, D.L., Ren, H.Z., Ma, M.L., Cai, Y., Zhao, T.C., Yin, X.L., Yu, X., et al. (2014). Constitutive Galphai coupling activity of very large G protein-coupled receptor 1 (VLGR1) and its regulation by PDZD7 protein. J. Biol. Chem. *289*, 24215–24225.

Kassianidou, E., Probst, D., Jager, J., Lee, S., Roguet, A.L., Schwarz, U.S., and Kumar, S. (2019). Extracellular matrix geometry and initial adhesive position determine stress fiber network organization during cell spreading. Cell Rep. *27*, 1897–1909.e4.

Kim, D.H., and Wirtz, D. (2013). Focal adhesion size uniquely predicts cell migration. FASEB J. *27*, 1351–1361.

Knapp, B., Roedig, J., Boldt, K., Krzysko, J., Horn, N., Ueffing, M., and Wolfrum, U. (2019). Affinity proteomics identifies novel functional modules related to adhesion GPCRs. Ann. N Y Acad. Sci. *1456*, 144–167.

Knierim, A.B., Rothe, J., Cakir, M.V., Lede, V., Wilde, C., Liebscher, I., Thor, D., and Schoneberg, T. (2019). Genetic basis of functional variability in adhesion G protein-coupled receptors. Sci. Rep. *9*, 11036.

Langenhan, T. (2020). Adhesion G protein-coupled receptors-Candidate metabotropic mechanosensors and novel drug targets. Basic Clin. Pharmacol. Toxicol. *126* (*Suppl 6*), 5–16.

Langenhan, T., Piao, X., and Monk, K.R. (2016). Adhesion G protein-coupled receptors in nervous system development and disease. Nat. Rev. Neurosci. *17*, 550–561.

Lawson, C., and Schlaepfer, D.D. (2012). Integrin adhesions: who's on first? What's on second? Connections between FAK and talin. Cell Adhes. Migr. *6*, 302–306.

Lei, X., Wu, H., Song, Y., Liu, B., Zhang, S.S., Li, J.Q., Bi, L., and Pei, G.X. (2020). Effects of cyclic fluid stress at different frequencies on behaviors of cells incubated on titanium alloy. Biochem. Biophys. Res. Commun. *522*, 100–106.

Leiss, M., Beckmann, K., Giros, A., Costell, M., and Fassler, R. (2008). The role of integrin binding sites in fibronectin matrix assembly in vivo. Curr. Opin. Cell Biol. *20*, 502–507.

Liebscher, I., Schon, J., Petersen, S.C., Fischer, L., Auerbach, N., Demberg, L.M., Mogha, A., Coster, M., Simon, K.U., Rothemund, S., et al. (2014). A tethered agonist within the ectodomain activates the adhesion G protein-coupled receptors GPR126 and GPR133. Cell Rep. *9*, 2018–2026.

Liu, J.Y.W., Dzurova, N., Al-Kaaby, B., Mills, K., Sisodiya, S.M., and Thom, M. (2020). Granule cell dispersion in human temporal lobe epilepsy: proteomics investigation of neurodevelopmental migratory pathways. Front. Cell Neurosci. *14*, 53.

Maerker, T., Van Wijk, E., Overlack, N., Kersten, F.F., Mcgee, J., Goldmann, T., Sehn, E., Roepman, R., Walsh, E.J., Kremer, H., and Wolfrum, U. (2008). A novel Usher protein network at the periciliary reloading point between molecular transport machineries in vertebrate photoreceptor cells. Hum. Mol. Genet. *17*, 71–86.

Mathur, P., and Yang, J. (2015). Usher syndrome: hearing loss, retinal degeneration and associated abnormalities. Biochim. Biophys. Acta *1852*, 406–420.

McGee, J., Goodyear, R.J., Mcmillan, D.R., Stauffer, E.A., Holt, J.R., Locke, K.G., Birch, D.G., Legan, P.K., White, P.C., Walsh, E.J., and Richardson, G.P. (2006). The very large G-protein-coupled receptor VLGR1: a component of the ankle link complex required for the normal development of auditory hair bundles. J. Neurosci. *26*, 6543–6553.

McMillan, D.R., and White, P.C. (2004). Loss of the transmembrane and cytoplasmic domains of the very large G-protein-coupled receptor-1 (VLGR1 or Mass1) causes audiogenic seizures in mice. Mol. Cell Neurosci. *26*, 322–329.

McMillan, D.R., and White, P.C. (2010). Studies on the very large G protein-coupled receptor: from initial discovery to determining its role in sensorineural deafness in higher animals. Adv. Exp. Med. Biol. *706*, 76–86.

Mogha, A., Harty, B.L., Carlin, D., Joseph, J., Sanchez, N.E., Suter, U., Piao, X., Cavalli, V., and Monk, K.R. (2016). Gpr126/Adgrg6 has Schwann cell autonomous and nonautonomous functions in peripheral nerve injury and repair. J. Neurosci. *36*, 12351–12367.

Myers, K.A., Nasioulas, S., Boys, A., Mcmahon, J.M., Slater, H., Lockhart, P., Sart, D.D., and Scheffer, I.E. (2018). ADGRV1 is implicated in myoclonic epilepsy. Epilepsia *59*, 381–388.

Norman, L.L., Brugues, J., Sengupta, K., Sens, P., and Aranda-Espinoza, H. (2010). Cell blebbing and membrane area homeostasis in spreading and retracting cells. Biophys. J. *99*, 1726–1733.

Ponik, S.M., and Pavalko, F.M. (2004). Formation of focal adhesions on fibronectin promotes fluid shear stress induction of COX-2 and PGE2 release in MC3T3-E1 osteoblasts. J. Appl. Physiol. (1985) *97*, 135–142.

Qin, R., Cao, S., Lyu, T., Qi, C., Zhang, W., and Wang, Y. (2017). CDYL deficiency disrupts neuronal migration and increases susceptibility to epilepsy. Cell Rep. *18*, 380–390.

Raghavan, S., Vaezi, A., and Fuchs, E. (2003). A role for alphabeta1 integrins in focal adhesion function and polarized cytoskeletal dynamics. Dev. Cell *5*, 415–427.

Reiners, J., Van Wijk, E., Marker, T., Zimmermann, U., Jurgens, K., Te Brinke, H., Overlack, N., Roepman, R., Knipper, M., Kremer, H., and Wolfrum, U. (2005). Scaffold protein harmonin (USH1C) provides molecular links between Usher syndrome type 1 and type 2. Hum. Mol. Genet. *14*, 3933–3943.

Richardson, G.P., and Petit, C. (2019). Hair-bundle links: genetics as the gateway to function. Cold Spring Harb. Perspect. Med. *9*, a033142.

Saunders, R.M., Holt, M.R., Jennings, L., Sutton, D.H., Barsukov, I.L., Bobkov, A., Liddington, R.C., Adamson, E.A., Dunn, G.A., and Critchley, D.R. (2006). Role of vinculin in regulating focal adhesion turnover. Eur. J. Cell Biol. *85*, 487–500.

Schiller, H.B., Friedel, C.C., Boulegue, C., and Fassler, R. (2011). Quantitative proteomics of the integrin adhesome show a myosin II-dependent recruitment of LIM domain proteins. EMBO Rep. *12*, 259–266.

Schiller, H.B., Hermann, M.R., Polleux, J., Vignaud, T., Zanivan, S., Friedel, C.C., Sun, Z., Raducanu, A., Gottschalk, K.E., Thery, M., et al. (2013). beta1- and alphav-class integrins cooperate to regulate myosin II during rigidity sensing of fibronectin-based microenvironments. Nat. Cell Biol. *15*, 625–636.

Scholz, N., Gehring, J., Guan, C., Ljaschenko, D., Fischer, R., Lakshmanan, V., Kittel, R.J., and Langenhan, T. (2015). The adhesion GPCR latrophilin/CIRL shapes mechanosensation. Cell Rep. *11*, 866–874.

Shen, B., Delaney, M.K., and Du, X. (2012). Inside-out, outside-in, and inside-outside-in: G protein signaling in integrin-mediated cell adhesion, spreading, and retraction. Curr. Opin. Cell Biol. *24*, 600–606.

Sieg, D.J., Hauck, C.R., Ilic, D., Klingbeil, C.K., Schaefer, E., Damsky, C.H., and Schlaepfer, D.D. (2000). FAK integrates growth-factor and integrin signals to promote cell migration. Nat. Cell Biol. *2*, 249–256.

Specht, D., Wu, S.B., Turner, P., Dearden, P., Koentgen, F., Wolfrum, U., Maw, M., Brandstatter, J.H., and Tom Dieck, S. (2009). Effects of presynaptic mutations on a postsynaptic Cacna1s calcium channel colocalized with mGluR6 at mouse photoreceptor ribbon synapses. Invest Ophthalmol. Vis. Sci. *50*, 505–515.

Sun, Z., Guo, S.S., and Fassler, R. (2016). Integrin-mediated mechanotransduction. J. Cell Biol. *215*, 445–456.

Thompson, P.M., Tolbert, C.E., Shen, K., Kota, P., Palmer, S.M., Plevock, K.M., Orlova, A., Galkin, V.E., Burridge, K., Egelman, E.H., et al. (2014). Identification of an actin binding surface on vinculin that mediates mechanical cell and focal adhesion properties. Structure *22*, 697–706.

Wang, Y., Fan, X., Zhang, W., Zhang, C., Wang, J., Jiang, T., and Wang, L. (2015). Deficiency of very large G-protein-coupled receptor-1 is a risk factor of tumor-related epilepsy: a whole transcriptome sequencing analysis. J. Neurooncol. *121*, 609–616.

Webb, D.J., Donais, K., Whitmore, L.A., Thomas, S.M., Turner, C.E., Parsons, J.T., and Horwitz, A.F. (2004). FAK-Src signalling through paxillin, ERK and MLCK regulates adhesion disassembly. Nat. Cell Biol. *6*, 154–161.

Weston, M.D., Luijendijk, M.W., Humphrey, K.D., Moller, C., and Kimberling, W.J. (2004). Mutations in the VLGR1 gene implicate G-protein signaling in the pathogenesis of Usher syndrome type II. Am. J. Hum. Genet. *74*, 357–366.

Wolfrum, U. (1995). Centrin in the photoreceptor cells of mammalian retinae. Cell Motil. Cytoskeleton *32*, 55–64.

Wozniak, M.A., Modzelewska, K., Kwong, L., and Keely, P.J. (2004). Focal adhesion regulation of cell behavior. Biochim. Biophys. Acta *1692*, 103–119.

Zaidel-Bar, R., Ballestrem, C., Kam, Z., and Geiger, B. (2003). Early molecular events in the assembly of matrix adhesions at the leading edge of migrating cells. J. Cell Sci. *116*, 4605–4613.

Zaidel-Bar, R., and Geiger, B. (2010). The switchable integrin adhesome. J. Cell Sci *123*, 1385–1388.

iScience, Volume *24*

Supplemental information

Adhesion G protein-coupled receptor VLGR1/ADGRV1 regulates cell spreading and migration by mechanosensing at focal adhesions

Deva K. Kusuluri, Baran E. Güler, Barbara Knapp, Nicola Horn, Karsten Boldt, Marius Ueffing, Gabriela Aust, and Uwe Wolfrum

Supplemental Information

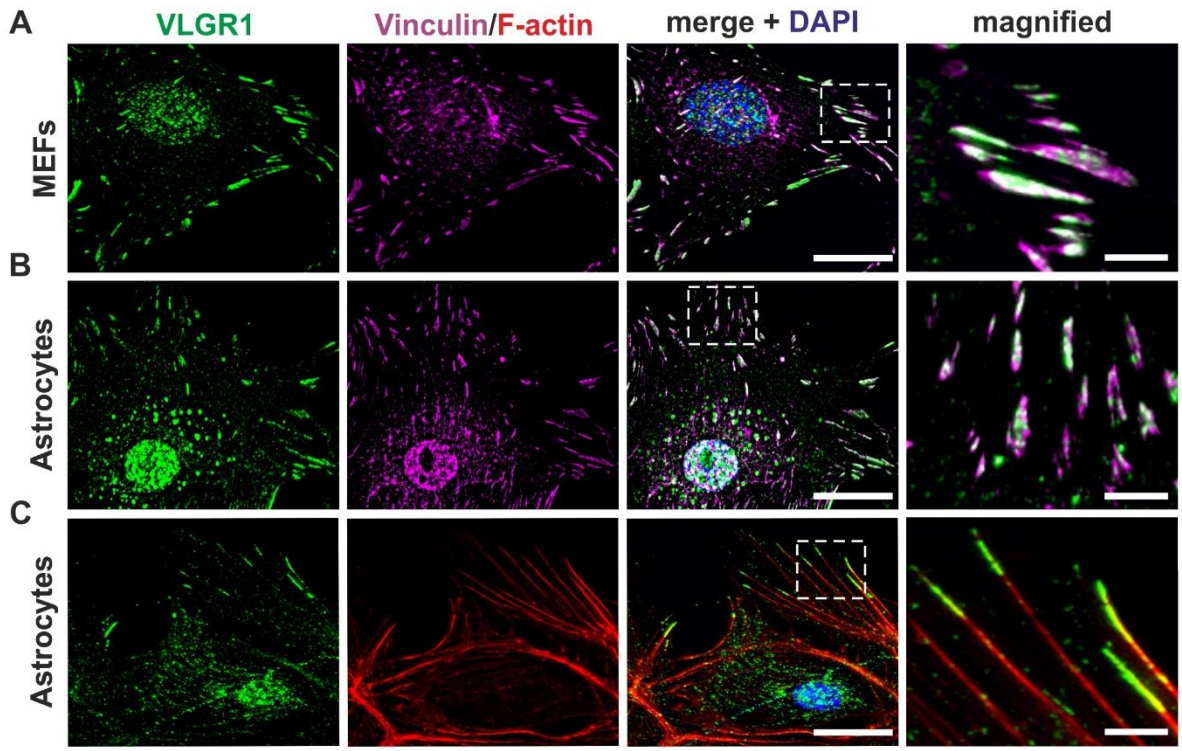

Figure S1. VLGR1 localization at FAs in different cell types, Related to Figure 2. (A) Subcellular localization of VLGR1 in FAs of cultured mouse embryonic fibroblasts (MEFs, A) and astrocytes (B). Immunofluorescence staining of VLGR1 (green), which is co-expressed with vinculin (magenta) in FAs. (C) VLGR1 localizes to the tip of F-actin in mouse astrocytes. Immunofluorescence staining of VLGR1 (green) and F-actin stained with TRITC-phalloidin (red). Scale bar, 25 μm; magnified panel, 5 μm. Nuclei were stained with DAPI (blue).

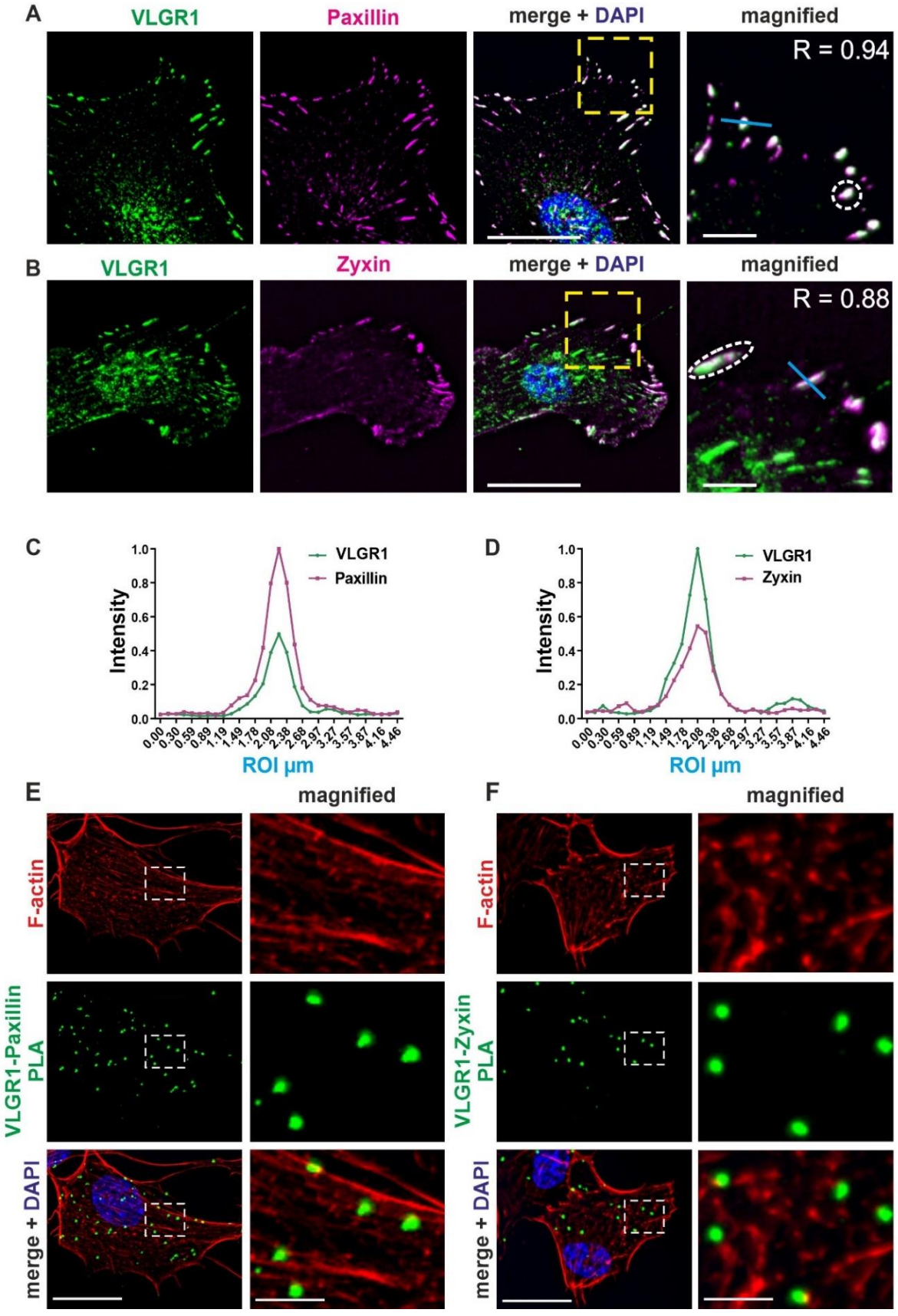
A
VLGR1
Paxillin
merge + DAPI
magnified
R = 0.94
B
VLGR1
Zyxin
merge + DAPI
magnified
R = 0.88
C
Intensity
VLGR1
Paxillin
ROI µm
D
Intensity
VLGR1
Zyxin
ROI µm
E
magnified
F-actin
VLGR1-Paxillin PLA
merge + DAPI
F
magnified
F-actin
VLGR1-Zyxin PLA
merge + DAPI

Figure S2. VLGR1 is localized at different forms of FAs, Related to Figure 2. (A-B) Immunofluorescence double labeling in hTERT-RPE1 cells revealed localization of VLGR1 (green) in nascent adhesions marked by paxillin (magenta, A), as well as mature adhesions stained with zyxin (magenta, B). The boxed areas in the overlays are shown at higher magnifications in the right column (magnified). Pearson coefficient (R) in magnified images for dotted region of interest (ROI; white) shows the degree of co-localization (positive values), indicated at the top of magnified image. Nuclei are stained with DAPI (blue). Scale bars: 25 µm, in magnified panel 5 µm. (C-D) Normalized fluorescence intensity plots of corresponding line scan (blue line) show co-localization of VLGR1 with paxillin (C), zyxin (D). (E-F) *In situ* proximity ligation assay (PLA) events (green dots) showing a close proximity localization of VLGR1 and nascent FA marker paxillin (E), VLGR1 and mature FA marker zyxin (F). TRITC-phalloidin (red) staining of F-actin was used to visualize cell area, nuclei were stained with DAPI (blue). Scale bars 25 µm, in magnified panel 5 µm.

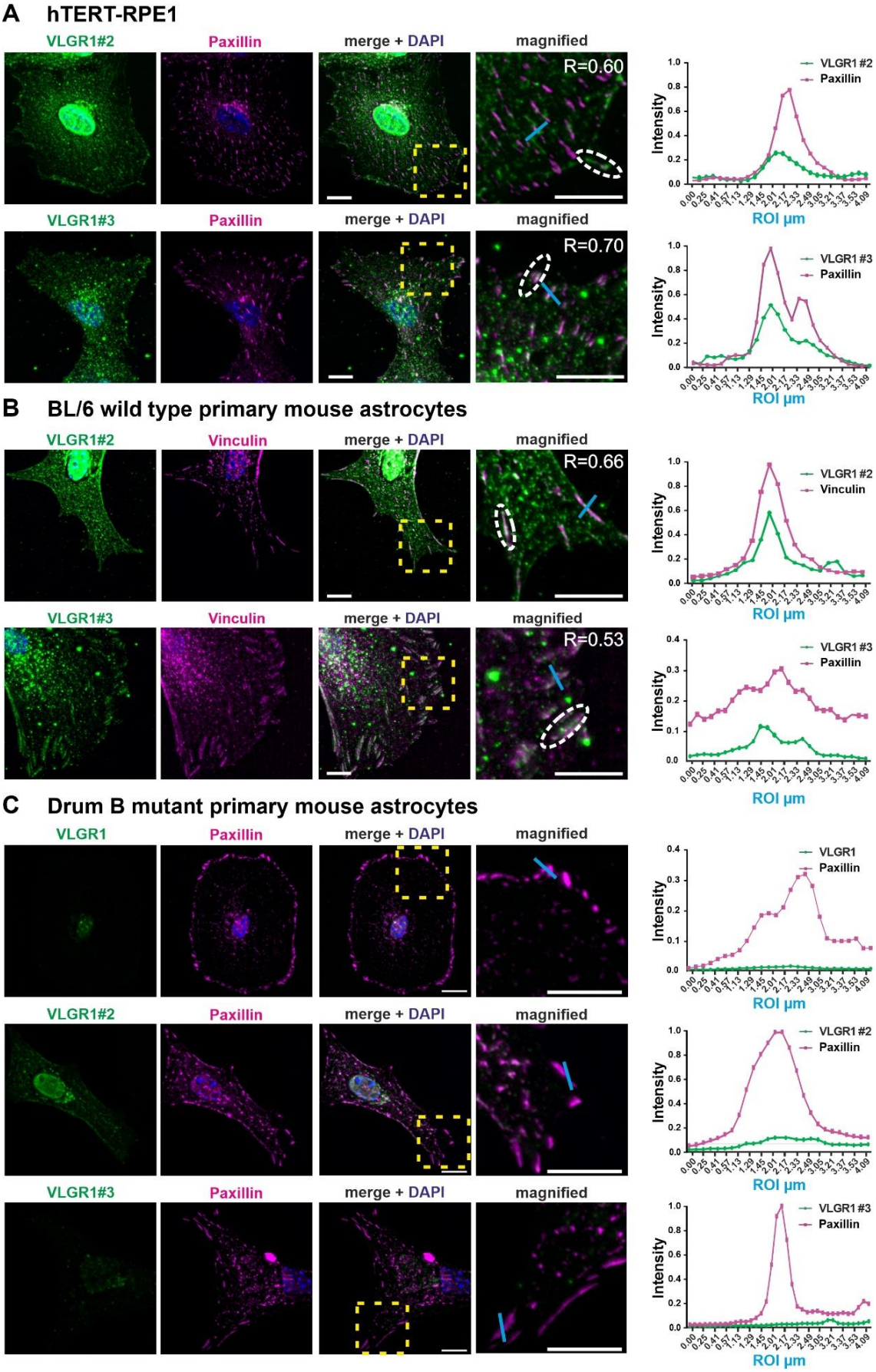
A
hTERT-RPE1
VLGR1#2
Paxillin
merge + DAPI
magnified
R=0.60
VLGR1#3
Paxillin
merge + DAPI
magnified
R=0.70
B
BL/6 wild type primary mouse astrocytes
VLGR1#2
Vinculin
merge + DAPI
magnified
R=0.66
VLGR1#3
Vinculin
merge + DAPI
magnified
R=0.53
C
Drum B mutant primary mouse astrocytes
VLGR1
Paxillin
merge + DAPI
magnified
VLGR1#2
Paxillin
merge + DAPI
magnified
VLGR1#3
Paxillin
merge + DAPI
magnified
Intensity
ROI µm
VLGR1 #2
Paxillin
VLGR1 #3
Paxillin
VLGR1 #2
Vinculin
VLGR1 #3
Paxillin
VLGR1
Paxillin
VLGR1 #2
Paxillin
VLGR1 #3
Paxillin

Figure S3. VLGR1 localization in FAs confirmed by immunostaining with alternative antibodies against VLGR1, Related to Figure 2. Immunofluorescence double labeling of paxilin or vinculin, respectively, (magenta) and of VLGR1 (green) by either the C-terminal pAb VLGR1#2 or the EAR-domain pAb VLGR1#3 in hTERT-RPE1 (A) and in primary BL/6 wildtype mouse astrocytes (B) reveal localization of VLGR1 in FAs confirming the data obtained by the C-terminal pAb VLGR1 used as standard antibody in the present paper. Positive Pearson correlation coefficient R calculated in magnified images for white dotted region indicates the degree of co-localization. Normalized fluorescence intensity plots (right hand) of VLGR1 and FA markers paxillin and vinculin, respectively share common peaks along the depicted blue line (ROI) in the magnified images indicating co-localization VLGR1 with both proteins in FAs. (C) Immunofluorescence double labeling of paxilin (magenta) and of VLGR1 (green) by either one of the three alternative antibodies used in the present study, namely VLGR1, VLGR1#2, and VLGR1#3 in primary astrocytes of VLGR1 deficient *Drum B* mice. In the absence of VLGR1 expression, all three VLGR1 antibodies do not stain FAs labeled with antibodies to paxilin, as confirmed by the normalized fluorescent intensity plots of ROIs indicated by blue lines. This demonstrates that all three antibodies specifically stain VLGR1 in FA when expressed (Fig. S1, and Fig. S3B). It is noted that the antibody staining in the nucleus, which is most pronounced by VLGR1#2 (see A and B), is reduced but not completely abolished in all three antibodies, indicating possible cross-reactivity with nuclear components.

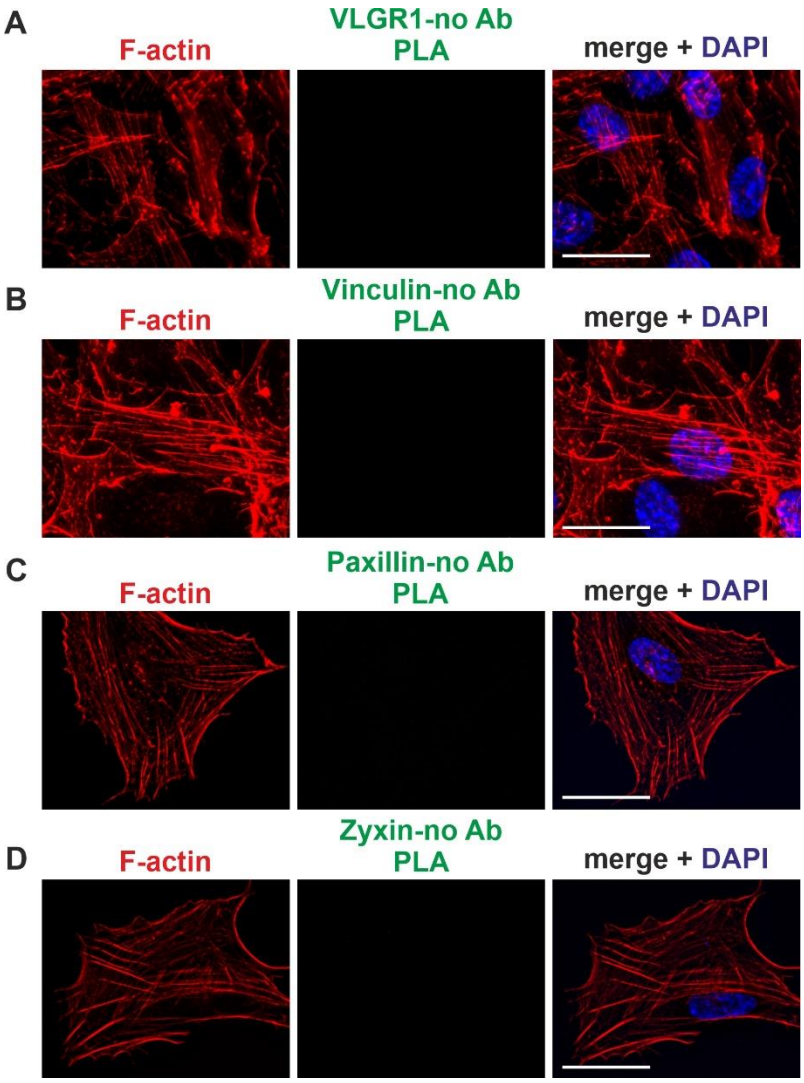

Figure S4. Controls of PLAs confirmed absence of false positive results in hTERT-RPE1 cells, Related to Figure 2. (A-D) In negative antibody controls, no PLA events could be detected (absence of green dots in second panel). TRITC-phalloidin (red) staining F-actin was used to visualize cell area, and nuclear DNA was stained with DAPI (blue). Scale bars, 25 µm.

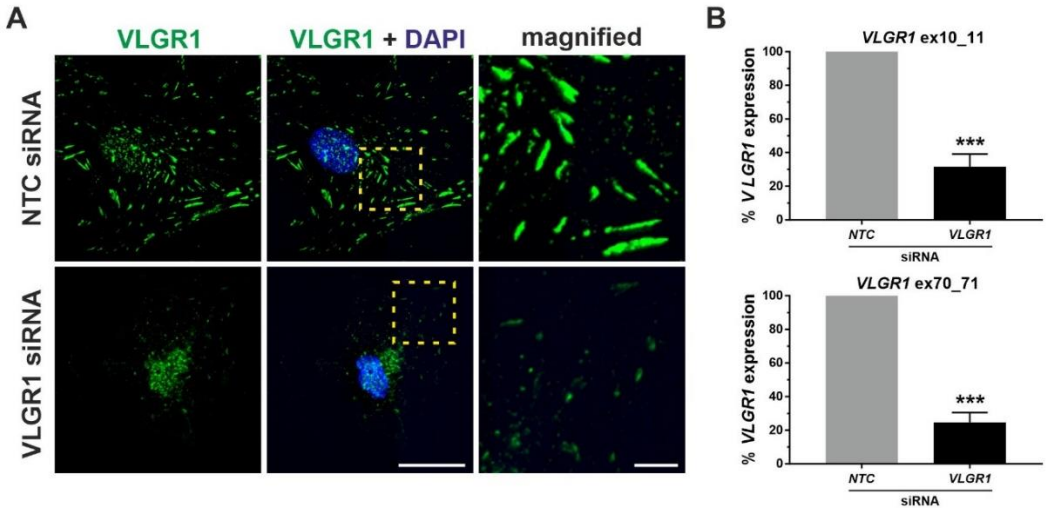

Figure S5. Validation of siRNAs for human VLGR1, Related to Figure 3. A) hTERT-RPE1 cells were transfected with a non-targeting control siRNA (NTC siRNA) or siRNA targeting *VLGR1* (*VLGR1* siRNA). 40 h after siRNA transfection, cells were fixed and immunostained for VLGR1 (green) to validate the knockdown efficacy. DAPI counterstaining in blue. (**B**) hTERT-RPE1 cells were lysed 48 h after siRNA transfection, and mRNA was extracted followed by qRT–PCR using primer sets specific to exon 10-11 and 70-71 of human *VLGR1*. *GAPDH* was used as reference. Graph shows expression levels of *VLGR1* in the knock down cells compared to that of corresponding NCT cells. Error bars show mean ± SD, three independent experiments. Statistical analyses were done using unpaired two-tailed t test.***P < 0.001.

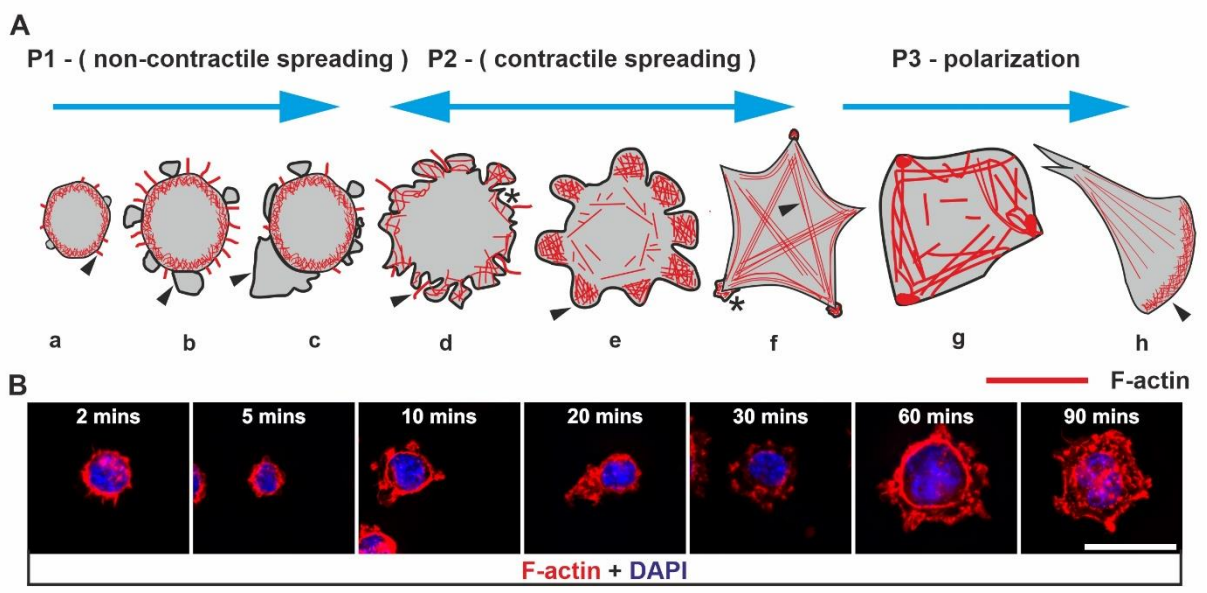

Figure S6. Phases of cell spreading, Related to Figure 4. A) Schematic representation of different phases of cell spreading phases introduced by Gauthier et al. (2012) and Greiner et al. (2013). (a) After seeding cells attach weakly to the substratum and are often rounded with very few thin F-actin microspikes emerging out (*arrow head*). (b) Cells start to spread, small membrane blebs (*arrow head*) and slightly longer microspikes are observed. (c) Thin layer of membrane starts stretching out from one side of the cell (*arrow head*) and the cell reaches its maximum adhesive area. (d) The cell progresses towards contractile spreading (P2) with alternate protrusions and retraction observed along the cell edge; occasional F-actin spikes are observed. (e) Membrane ruffles starts emerging from the edges of the cells. Stable FAs formation leads to homogenous protrusions and flower like cells are observed (*arrow head*). Cell exerts stronger forces and spreads further resulting in increased membrane area. (f) The cell experiences a drastic decrease in the membrane protrusions. Actin stress bundles (*arrow head*) become more prominent, membrane ruffles starts spreading along the edges and somewhat star-shaped cells are observed (*asterisk*). Cells start to polarize. (g) Cells protrude from one end maintaining constant membrane area. (h) Membrane protrudes towards one side forming lamellipodia (*arrowhead*) and at the rare end of the cell shrinks. The cell experiences high tension, which enables the cell to polarize. (B) HEK293T cells at different stages during cell spreading. Cells seeded on coverslips were stained for F-actin (red) after 2, 5, 10, 20, 30, 60 and 90 min to determine phases of cell spreading. DAPI (blue): nuclear DNA.

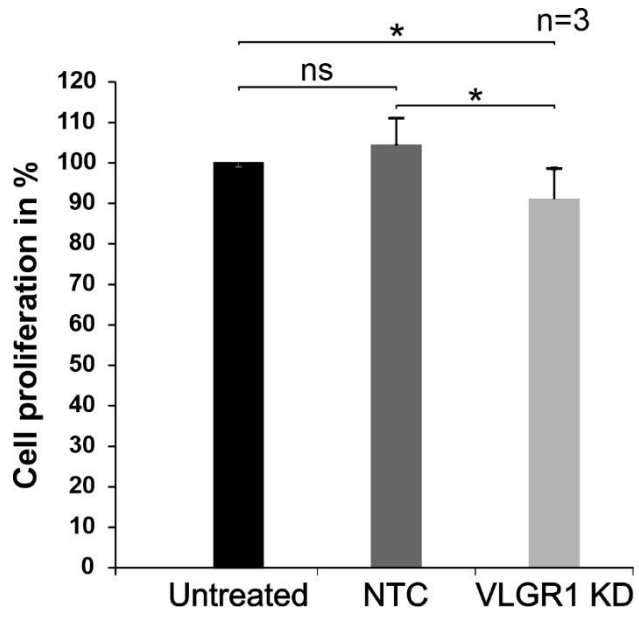

Figure S7. VLGR1 depletion affects proliferation of hTERT-RPE1 cells, Related to Figure 6. Quantification of three independent WST-1 proliferation assays revealed slightly reduced cell proliferation after siRNA-mediated VLGR1 knockdown when compared to untreated and non-targeting control (NTC) siRNA application, Data are represented as mean ± SD. Two-tailed Student's t test was applied, $*p < 0.05$, $**p < 0.01$, $***p < 0.001$.

Table S3. FA proteins identified in VLGR1 TAPs from hTERT-RPE1 cells, Related to Figure 1.

Gene name	Common protein name	Functional category
ACTN1	Alpha-actinin-1	*Actin regulation*
CFL1	Cofilin-1	*Actin regulation*
DPYSL2	Dihydropyrimidinase-like 2	*Actin regulation*
FLNC	Filamin-C	*Actin regulation*
MARCKS	Myristoylated alanine-rich C-kinase substrate	*Actin regulation*
MYH9	Myosin-9	*Actin regulation*
PTPN1	Protein tyrosine phosphatase 1B	*Actin regulation*
CAV1	Caveolin-1	*Adaptor/Cytoskeletal*
EZR	Ezrin	*Adaptor/Cytoskeletal*
GNB2L1	RACK1	*Adaptor/Cytoskeletal*
HAX1	HS1BP1	*Adaptor/Cytoskeletal*
TUBA1B	Tubulin	*Adaptor/Cytoskeletal*
VCL	Vinculin	*Adaptor/Cytoskeletal*
CALR	Calreticulin	*Chaperone*
CANX	Calnexin	*Chaperone*
HSPA2	HSP72	*Chaperone*
HSPB1	Heat shock protein beta-1	*Chaperone*
ITGB1	Integrin beta-1	*Adhesion receptor*
ITGA3	Integrin alpha-3	*Adhesion receptor*
SLC3A2	CD98	*Adhesion receptor*
CAD	Carbamoyl-phosphate synthetase 2	*Enzymes and protease*
MMP14	Matrix metalloproteinase-14	*Enzymes and protease*
PTPN1	Protein tyrosine phosphatase 1B	*Enzymes and protease*
HNRNPK	Heterogeneous nuclear ribonucleoprotein K	*RNA Metabolism*
RPL10L	Ribosomal protein L10-like;ribosomal protein 10	*RNA Metabolism*
SLC16A3	MCT4	*Channel*

Transparent Methods

Animals

All experiments described herein were performed in accordance with guidelines provided by Association for Research in Vision and Ophthalmology. *Vlgr1*-del7TM leads to the deletion of the entire 7TM domain of *Vlgr1* (McMillan and White, 2004). *Drum B* mice were identified in an ENU (N-ethyl-N-nitrosourea) mutagenesis screen (Potter et al., 2016). The c.8554+2t>c mutation the donor splice site of exon 37 resulting in a premature stop Codon in intron 37-38. Both mouse lines are bread on a C57BL/6 background.

Antibodies and dyes

Antibodies used are directed to vinculin (Merck, Darmstadt, Germany), paxillin (Abcam, Cambridge, United Kingdom), zyxin (Abcam, Cambridge, United Kingdom), FAK and pFAK397 (CST, Frankfurt, Germany). In most experiments we applied a rabbit poyclonal antibody (pAb) against the C-terminus of murine VLGR1 (aa 6198 – 6307) previously characterized in our lab (Maerker et al., 2008). We confirmed the localization of VLGR1 in FAs by using two alternative rabbit pAbs: VLGR1#2 against the C-terminus of murine VLGR1 (aa 6159–6306) and VLGR1#3 against an extracellular region of murine VLGR1 bodies against (amino acids 3249 – 3425), both kindly provided by Dr Dominic Cosgrove, Omaha, USA) (MacGee et al., 2006; Maerker et al., 2008; Zallocchi et al., 2012). Secondary antibodies conjugated to Alexa488, Alexa555, Alexa568 or Alexa647 were purchased from Molecular Probes (Life Technologies, Darmstadt, Germany) or from Rockland Inc. (Gilbertsville, PA, USA). DNA was stained with 4',6-diamidino-2-phenylindole (DAPI, Merck). F-actin was labelled with TRITC-phalloidin (Merck).

Cell culture

hTERT-RPE1 and HEK293T cells were cultured in DMEM-F12 or DMEM (ThermoFisher Scientific, Darmstadt, Germany)/10% fetal bovine serum (FBS), and 1% penicillin/streptomycin (ThermoFisher Scientific). Mouse embryonic fibroblasts (MEFs) were cultured in DMEM/10% FBS and 1% penicillin/streptomycin. Primary astrocyte cultures were prepared from cerebral cortices of C57BL/6 WT, *Vlgr1*/del7TM or *Drum B* mutant postnatal stage day 1 (PN1) mice. Mouse cortices (6-10) were enzymatically dissociated with DNase/trypsin followed by mechanical dissociation. Single cells were cultured in DMEM/10% FBS/2 mM l-glutamine 1% penicillin/streptomycin and 50 µg/ml gentamycin. Medium was changed at days 1, 2 and 7 after plating. Upon confluence, oligodendrocytes were removed. After trypsinization and DNAse treatment of still attached cells, astrocytes were passed over successive Petri dishes to get rid of microglia. Astrocytes were maintained in complete media and used after 14 days culture.

siRNA transfection

ON-TARGETplus siRNA SMARTpools for non-targeting pool (D-001810-10-05) and the siRNAs targeting human *VLGR1* (ThermoFisher Scientific) were transfected using 20 nM siRNA with Lipofectamine RNAimax (ThermoFisher Scientific).

Tandem affinity purification (TAP) and mass spectrometry

TAP was performed as described previously (Knapp et al. 2019; Boldt et al. 2016). In brief, VLGR1 domains were tagged with the tandem Strep II/FLAG tandem affinity purification tag (SF-TAP) (Fig. 1A). SF-tagged VLGR1 versions were expressed in hTERT-RPE1 cells for 48 h lysed and cleared by centrifugation. Mock-treated hTERT-RPE1 cells were used as controls. Supernatant were then subjected to a two-step purification on Strep-Tactin® Superflow® beads (IBA, Goettingen, Germany) and anti-FLAG M2 agarose beads (Merck). Competitive elution was achieved by desbiothin (IBA) in the first step and FLAG® peptide (Merck), respectively. Eluates, precipitated by methanol-chloroform were subjected to liquid chromatography coupled with tandem mass spectrometry (LC-MS/MS) (Boldt et al. 2016). Raw spectra were searched against the human SwissProt database using Mascot and results were verified by Scaffold (version Scaffold 4.02.01, Proteome Software Inc.) to validate MS/MS-based peptide and protein identifications.

Data processing

TAP data was compared to the according data for mock-transfected cells. Proteins that occurred in the mock data set were not further considered. Datasets were also compared to common control TAPs of the RAF1-protein (Gloeckner et al., 2009, Boldt et al., 2016). Gene names of preys were used as input for the Cytoscape plugins STRING and ClueGO and the STRAP software. The parameter *confidence (score) cutout* was set to 0.4 and the parameter *maximum number of interactors* was set to 0 for STRING analysis. ClueGO v2.3.3 was used for Gene Ontology (GO) term enrichment analysis. Network specificity was set to default (medium).

Immunofluorescence

Cells were fixed with 2% paraformaldehyde, washed and incubated with 50 mM NH_4Cl for 10 min. Samples were permeabilized with PBSTX (0.2% Triton-X) and blocked with 0.1% ovalbumin, 0.5% fish gelatin in PBS before primary antibodies were incubated overnight at 4°C. After washing, samples were incubated with secondary antibodies and DAPI for 1 h. After washing, cover slips were mounted in Mowiol (Roth, Germany). Specimens were analyzed on a Leica DM6000B microscope (Leica, Bensheim, Germany), images were processed, deconvoluted and co-localization profiles generated with Leica and Fiji (https://fiji.sc) image analysis software.

Cell spreading assay

24 h post siRNA transfection, 1 x 10^5 cells/well were seeded in a 6-well plate on either poly-L-lysine or fibronectin (Merck) coated coverslips. Poly-L-lysine was used for adhesion and fibronectin to promote cell spreading. After indicated periods of replating, cells were fixed and immunofluorescence analysis was performed. The area of the cells was analyzed using Fiji image analysis software.

Morphometric analysis of FAs

For the FAs morphometric analysis, vinculin was used as a marker protein. The length and number of FAs were quantified applying a modified protocol (Horzum et al., 2014). FA image analysis was implemented using Fiji. Briefly, the images were processed with fast Fourier transformation followed by a band pass filter to normalize the background. The images were thresholded, converted to binary images and analyzed using the built-in 'analyze particles' macro in Fiji, where large is defined as 40 or more pixels. This automatically generated the number and morphometric details of the FAs. The length of FAs was manually determined using the line option tool in Fiji.

Cell migration assay

Collective cell migration assay (Rodriguez et al., 2005) was performed 48 h after siRNA transfections of hTERT-RPE1 cells and in *Vlgr1*-del7TM primary astrocytes. The scratch wound was made by cutting cell monolayer longitudinally with a 200-µl or a 10-µl pipette tip in hTERT-RPE1 cells and astrocytes, respectively. Cells were allowed to migrate into the "wound" for indicated time points, fixed and stained. Image analysis to calculate wound closure was performed using Fiji. For single-cell tracking *Vlgr1-del7TM* mutant and WT Bl/6 mouse primary astrocytes were seeded on fibronectin-coated chambers at low density. Live-cell imaging performed under 5% CO_2 and at 37°C using Nikon Eclipse Ti2-E equipped with a spinning disc. D.I.C. images were acquired using a 20x microscope objective every 15 minutes for 24 h for a total in 97 time points. Cells were tracked using a Fiji manual tracking plugin and plot data were generated using Chemotaxis and Migration Tool 2.0 (Ibidi, Munich, Germany).

Proximity ligation assay (PLA)

In situ PLA was used to visualize protein – protein interactions in hTERT-RPR1 cells using Duolink In Situ FarRed Kit Mouse/Rabbit (Merck) according to the manufacturer's instruction. Cells were incubated overnight at 4°C with primary anti-bodies followed by anti-rabbit PLUS and anti-mouse MINUS secondary PLA probes. The two complementary oligonucleotides were then hybridized, ligated and amplified by rolling circle amplification, resulting in fluorescence spots when the targeted proteins were closer than 30-40 nm.

Shear-stress experiments

For shear-stress experiments, 24 h post siRNA transfections cells were replated into µ-slides (Ibidi), cultured for 24 h, and subjected to static conditions or shear stress of 20 dyn/cm^2 for 20 min using the

Ibidi pump system. Afterwards, the cells were fixed, stained and analyzed using Leica TCS SP5 confocal laser-scanning microscope (Leica) and Fiji.

Western blot analysis

Protein lysates were prepared using RIPA lysis buffer (10 mM Tris, 1mM $CaCl_2$, 150 mM NaCl, 10 mM NaF, 20 mM ß-Glycerophosphate, 0.5% Nonident P-40, 0.5% Deoxycholic acid, 0.1% SDS, pH 7.4) containing complete protease inhibitor cocktail (04693132001, Roche Diagnostics, Mannheim, Germany) and sonicated. Protein content was quantified using the BCA protein assay (Merck) and subjected to SDS-PAGE. After blotting, the polyvinylidene difluoride membranes (PVDF FL) (Millipore, Schwalbach, Germany) were blocked in AppliChem blocking reagent (AppliChem, Darmstadt, Germany) for 1 h. The membranes were incubated with primary antibodies overnight followed by appropriate secondary antibodies Alexa Flour 680 (Invitrogen) or IR Dye 800 (Rockland, Gilbertsville, USA). Scans of the blot were made employing the Odyssey infrared imaging system (LI-COR Biosciences, Bad Homburg, Germany). For densitometry analysis Fiji was used.

Quantitative Real-time PCR (qRT-PCR)

RNA from control and *VLGR1*-deficient RPE1 cells was isolated using TRIzol (ThermoFisher Scientific). 4 µg RNA was reverse transcribed to cDNA using the SuperScript III first-strand synthesis system. qRT-PCR was performed using the Platinum™ SYBR™ Green qPCR SuperMix-UDG (ThermoFisher Scientific) with the Applied Biosystems® 7500 Real-Time PCR System. The relative expression levels of the target genes were normalized *GAPDH*. Primer pairs used: *VLGR1*,
forward: 5′-CAGCCGATTGTTACCGAAAATG-3′,
reverse: 5′- AGCATCACAGTCACCAGTTG -3′;
and *GAPDH*,
forward primer: 5′-GAGGTCAAGGGATTTGGTCGT-3′,
reverse primer: 5′−TTGATTTTGGAGGGATCTCG-3′.

Statistical analyses

Statistical analyses were performed using Graphpad Prism 7.0 software (GraphPad Software Inc., San Diego, CA, USA). Differences between two groups were compared using two-tailed Student's t test. For multiple group comparisons, ANOVA followed by Dunnett's multiple comparison tests and Sidak's multiple comparison tests were performed depending on the data to be compared. Differences were considered significant at *$p < 0.05$, ** $p < 0.01$, ***$p < 0.001$. Bar plots are presented as mean ± SD. Box plots show median (middle line), edge of boxes is top and bottom quartiles (25–75%), and whiskers represent the ranges for the upper 25% and the bottom 25% of data values.

WST-1 cell proliferation assay

The cell proliferation of hTERT-RPE1 cells was tested by using the WST-1 cell proliferation assay (Roche Diagnostics). hTERT-RPE1 cells were seeded on 96 well plate at a density of $4x10^3$ cells per well as described in the manufacturer's protocol (Roche Diagnostics). After 24 h cells were treated with VLGR1 siRNA and non-targeting (NTC) siRNA for 48 h. Subsequently, 10 µl WST-1 tetrazolium salt (4-[3-(4-Iodophenyl)-2-(4-nitro-phenyl)-2H-5-tetrazolio]-1,3-benzene sulfonate) were added into wells which contain 100 µl growth medium and cells were incubated at 37°C with 5% CO_2 for 4 h. Absorbance values at 460 nm were measured using a Vario Skan Flash (ThermoFisher Scientific) plate reader. Averages of spectrophotometric absorbance values were calculated and blank control value was subtracted.

Supplemental references

Horzum, U., Ozdil, B. & Pesen-Okvur, D. 2014. Step-by-step quantitative analysis of focal adhesions. MethodsX*,* 1**,** 56-9.

Potter, P. K., Bowl, M. R., Jeyarajan, P., Wisby, L., Blease, A., Goldsworthy, M. E., Simon, M. M., Greenaway, S., Michel, V., Barnard, A., Aguilar, C., Agnew, T., Banks, G., Blake, A., Chessum, L., Dorning, J., Falcone, S., Goosey, L., Harris, S., Haynes, A., Heise, I., Hillier, R., Hough, T., Hoslin, A., Hutchison, M., King, R., Kumar, S., Lad, H. V., Law, G., Maclaren, R. E., Morse, S., Nicol, T., Parker, A., Pickford, K., Sethi, S., Starbuck, B., Stelma, F., Cheeseman, M., Cross, S. H., Foster, R. G., Jackson, I. J., Peirson, S. N., Thakker, R. V., Vincent, T., Scudamore, C., Wells, S., El-Amraoui, A., Petit, C., Acevedo-Arozena, A., Nolan, P. M., Cox, R., Mallon, A. M. & Brown, S. D. 2016. Novel gene function revealed by mouse mutagenesis screens for models of age-related disease. Nat Commun*,* 7**,** 12444.

Rodriguez, L. G., Wu, X. & Guan, J. L. 2005. Wound-healing assay. Methods Mol Biol*,* 294**,** 23-9.

Zallocchi, M., Delimont, D., Meehan, D. T. & Cosgrove, D. 2012. Regulated vesicular trafficking of specific PCDH15 and VLGR1 variants in auditory hair cells. J Neurosci*,* 32**,** 13841-59.

Publication III

Received: 3 January 2023 | Accepted: 10 March 2023

DOI: 10.1111/bcpt.13860

ORIGINAL ARTICLE

BCPT Basic & Clinical Pharmacology & Toxicology

Monitoring paxillin in astrocytes reveals the significance of the adhesion G protein coupled receptor VLGR1/ADGRV1 for focal adhesion assembly

Baran E. Güler | **Joshua Linnert** | **Uwe Wolfrum**

Institute of Molecular Physiology, Molecular Cell Biology, Johannes Gutenberg University Mainz, Mainz, Germany

Correspondence
Uwe Wolfrum, Institute of Molecular Physiology, Molecular Cell Biology, Johannes Gutenberg University Mainz, Hanns-Dieter-Hüsch-Weg 17, 55128 Mainz, Germany.
Email: wolfrum@uni-mainz.de

Funding information
Deutsche Forschungsgemeinschaft DFG FOR 2149, project number 246212759 (UW), and The Foundation Fighting Blindness (FFB) PPA-0717-0719-RAD (UW), inneruniversitäre Forschungsförderung ("Stufe I") of the Johannes Gutenberg University Mainz (UW).

Abstract

VLGR1/ADGRV1 (very large G protein-coupled receptor-1) is the largest adhesion G protein-coupled receptor (aGPCR). Mutations in *VLGR1/ADGRV1* are associated with human Usher syndrome, the most common form of deaf-blindness, and also with epilepsy in humans and mice. VLGR1 is expressed almost ubiquitously but is mainly found in the CNS and in the sensory cells of the eye and inner ear. Little is known about the pathogenesis of the diseases related to VLGR1. We previously identified VLGR1 as a vital component of focal adhesions (FAs) serving as a metabotropic mechanoreceptor controls cell spreading and migration. FAs are highly dynamic and turnover in response to internal and external signals. Here, we aimed to elucidate how VLGR1 participates in FA turnover. Nocodazole washouts and live cell imaging of paxillin-DsRed2 consistently showed that FA disassembly was not altered, but de novo assembly of FA was significantly delayed in *Vlgr1*-deficient astrocytes, indicating that VLGR1 is enrolled in FA assembly. In FRAP experiments, recovery rates were significantly reduced in *Vlgr1*-deficient FAs, indicating reduced turnover kinetics in VLGR1-deficient FAs. We showed that VLGR1 regulates cell migration by controlling the FA turnover during their assembly and expect novel insights into pathomechanisms related to pathogenic dysfunctions of VLGR1.

KEYWORDS
aGPCR, cell migration, epilepsy, focal adhesions, G protein-coupled receptors, mechanoreception, Usher syndrome

1 | INTRODUCTION

VLGR1 (very large G protein-coupled receptor-1), also known as GPR98 and MASS1 and recently renamed to ADGRV1,[1] belongs together with other 33 members to the G protein-coupled receptor (GPCR) family of adhesion G protein-coupled receptors (aGPCRs).[2] Among various VLGR1 isoforms, full-length VLGR1b is the largest G-protein coupled receptor in the human body with a molecular weight of ~700 kDa.[3] VLGR1/ADGRV1 is a

classical aGPCR characterized by a large extracellular domain (ECD), which contains 35 putative Ca^{2+}-binding calx-ß motifs, pentaxin/laminin G-like repeats (LAMG/PTX), epilepsy-associated/epitemptin-like domain (EPTP/EAR), the 7-transmembrane domain (7TM), and the relatively short cytoplasmic intracellular domain (ICD) with a class I PDZ domain-binding motif (PBM) at the very C terminal end (Figure 1). Autocleavage at the auto proteolysis site (GPS) localized within GAIN (GPCR auto-proteolysis-inducing) domain leads to a C-terminal fragment (CTF) and an N-terminal fragment (NTF), which can function independently.[4,5] There is growing evidence that after autocleavage, the short so-called "Stachel" sequence in the very N-terminal end of CTF is exposed and can act as a tethered agonist activating aGPCRs.[6,7] We have recently found an 11 amino acid sequence as the "Stachel" peptide of VLGR1.[5] We also found evidence that this activation induces a switch from Gs- to Gi-mediated signalling of VLGR1.

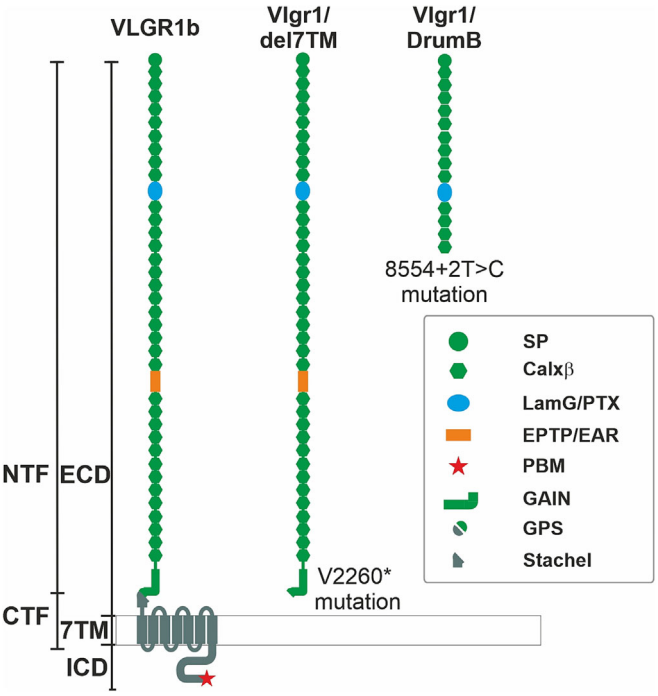

FIGURE 1 Domain structure of VLGR1/ADGRV1 and mutations in *Vlgr1* mouse models. VLGR1 is composed of an extremely long extracellular domain (ECD), 7-serpentine transmembrane domain (TM), and a relatively short intracellular domain (ICD) with a characteristic PDZ binding motif (PBM). The ECD includes a signal peptide (SP), 35 Ca^{2+} binding calcium exchanger β motifs (Calx-β), pentaxin/laminin G-like repeats (LAMG/PTX), an epilepsy-associated/Epitemptin-like domain (EPTP/EAR), a GPCR autoproteolysis-inducing domain (GAIN), which includes the G-protein-coupled receptor proteolytic site (GPS). Autoproteolytic cleavage at the GPS can result N-terminal fragment (NTF) and the C-terminal fragment (CTF) and the exposer of the Stachel sequence at the very N-terminal end of the CTF which can act as tethered agonist. In Vlgr1/del7TM mice V2260* nonsense mutation introduces a STOP codon which leads to the deletion of 7TM and ICD domains of *Vlgr1* and translation product is only ECD. In the Vlgr1/DrumB mice, the 8554+2t>c mutation leads to a STOP codon in intron 37–38. Translation product is a relatively short truncated protein, which includes only 13 CalXbeta domains and the LAMG domain.

The expression of VLGR1 is almost ubiquitously but highly concentrated in the central nervous system (CNS), especially during development and the sensory cells of the eye and inner ear[3] (Protein Atlas: https://www.proteinatlas.org/). Mutations in the *VLGR1/ADGRV1* gene cause human Usher syndrome 2C (USH), a subtype of the most common combined hereditary deaf-blindness disease.[8,9] In addition, it has been found that different mutations in mouse models for *Vlgr1/Adgrv1* are associated with audiogenic epilepsy.[3] However, over the last years, there is also growing evidence that mutations in *VLGR1/ADGRV1* also can cause different forms of epilepsy in humans.[10,11] Concrete knowledge of VLGR1's molecular function and signalling is necessary for gaining insights into the pathomechanisms and the elucidation of potential targets for therapies of diseases related to VLGR1.

In cochlear hair cells of the inner ear and the retinal photoreceptor cells, VLGR1 is essential for the formation of fibrous links spanning between neighbouring membranes.[12,13] While it is thought that the absence of these membrane attachment fibres underlie the sensory neuronal degeneration in the eye and ear causing USH, the processes leading to epilepsy due to defects in VLGR1 are completely unclear to date.

Applying affinity proteomics, we have previously identified numerous proteins related to focal adhesions (FAs) as potential interaction partners of VLGR1.[4,5,14] FAs are large supramolecular assemblies at contact sites of the cell membrane with the extracellular matrix.[15] The dynamic turnover, controlled assembly, and disassembly of FAs play a key role in cell spreading and migration. In this regard, FAs are essential for sensing and integrating intracellular signals as well as signals from the environment that control cell migration.[16] We have previously shown that VLGR1 is part of the multiprotein complex of FAs[5] and essential for their proper size and abundance in the cell.[14,17] More importantly, we have also demonstrated that VLGR1 in FAs functions as a metabotropic mechanoreceptor and controls cell spreading and migration.[14] However, it remained unknown how VLGR1 participates in the control of the dynamics of FAs during cell migration.

In the present study, we aimed to elucidate how VLGR1 controls the FA turnover during cell migration by applying nocodazole washout assays and live-cell imaging fluorescence recovery after photobleaching (FRAP) experiments. Our data conclusively demonstrate

that VLGR1 regulates cell migration by controlling the assembly of FA. From our findings, we also expect novel insights into pathomechanisms related to molecular and cellular dysfunction of VLGR1 in the developing and mature CNS.

2 | MATERIAL AND METHODS

2.1 | Animals

All animal experiments were performed per the guidelines of the Association for Research in Vision and Ophthalmology. Vlgr1/del7TM mice carry a premature STOP codon at exon 82 of *Vlgr1*, namely, the V2250* nonsense mutation of *Vlgr1*, which leads to the deletion of the entire 7TM domain and only the expression of the extracellular domain.[18] Drum B mice carry c.8554+2t>c mutation in exon 37 of Vlgr1 which results in an early STOP codon in intron 37–38 and if no splicing event occurs, the translation product only contains the first 13 CalXbeta domains and the LamG/PTX domain.[19] Both *Vlgr1*-deficient mouse lines are bred on a C57BL/6 background.

2.2 | Isolation of primary astrocytes from murine brains

Astrocytes were isolated from brains of postnatal day 0 (PN0) female and male sibling mouse pups as previously described.[17] Briefly, P0 mouse pups were dissected and cortexes were enzymatically and mechanically disassociated. Single-cell suspensions were seeded on PLL-coated T75 flasks and cultured in DMEM/10% FBS/2% penicillin/streptomycin (Thermo Fisher Scientific) for 7 to 10 days. Upon confluence, oligodendrocytes and neurons were removed by shaking the flasks. To isolate primary astrocytes from microglia cells, cultures were trypsinized and cell suspensions were seeded on successive dishes. While microglia cells attached to the surface of dishes, astrocytes could be collected from the supernatant. Isolated primary astrocytes were cultured additional 7–10 days in a complete growth medium.

2.3 | Cell culture

Primary astrocytes isolated from postnatal stage day 0 (PN0) mice were cultured in DMEM/10% FBS/20mM l-glutamine 1% penicillin/streptomycin. Half of the culture medium was changed on days 1, 2, 7, and 14 after the first isolation. Only passage 1 of astrocyte cultures was used for the experiments to maintain experimental consistency.

2.4 | Antibodies, fluorescent tools, and DNA constructs

We used the following primary antibodies: a rabbit monoclonal (ab32115) (Abcam) and a mouse monoclonal (BD Transduction Laboratories, 610 052) antibody against paxillin, and a rabbit polyclonal antibody against the C terminal of murine Adgrv1/Vlgr1.[13] Secondary antibodies conjugated to Alexa488, and Alexa647 was purchased from Molecular Probes (Life Technologies) or Rockland Immunochemicals. DNA counterstained with 4′,6-diamidino-2-phenylindole (DAPI, Merck). The Paxillin-DsRed2 plasmid was kindly provided by Drs. Rudolf E. Leube and Rick Hortwitz.[20]

2.5 | Immunocytochemistry

Primary astrocytes were fixed with 2% paraformaldehyde for 10 min. After fixations, specimens were washed twice, permeabilized with 0.2% Triton-X in PBS (Carl Roth GmbH) for 15 min, and quenched with 50-mM NH_4Cl for 5 min. Before primary antibody treatment, cells were blocked with 0.1% ovalbumin and 0.5% fish gelatin in PBS. Primary antibodies were incubated at 4°C overnight. After removing unbound antibodies by PBS washing, secondary antibodies were incubated at room temperature for 1 h, and an additional wash with H_2O, and coverslips were mounted with Mowiol 4.88 (Hoechst).

2.6 | Nocodazole-induced FA disassembly assay

FA disassembly assay was performed as described previously with slight modifications[21]; 1.5×10^5 primary murine brain astrocytes were seeded onto fibronectin-coated coverslips. After 48 h of culturing, cells were treated with 10-μM nocodazole (AppliChem GmbH) in 0.3% DMSO for 4 h in a serum-free medium. Subsequently, NDZ was washed out three times with 1× PBS, and upon washout, fresh complete growth medium was added. Coverslips were removed from the medium at time points 0, 15, 30, 45, 60, and 120 min, and cells were fixed and stained for FAs during microtubule polymerization.

2.7 | Morphometric analysis of FAs

Paxillin FA marker was used for FAs number analysis. The number of FAs was quantified as described in Güler

et al.[17] using Fiji image analysis software (https://fiji.sc). Briefly, images were converted to 8-bit images and the background was normalized with FFT Bandpass filter. Filtered images are thresholded and converted to binary images. FA numbers are analysed with the "analyse particles" built-in function. The minimum FA size is defined as 40 pixels. Finally, the total number of FAs was divided by cell area to determine FA numbers in μm^2.

2.8 | FA turnover analysis

For live-cell imaging analysis of FA turnover, ~35 000 cells were seeded on a 5 μg/ml fibronectin-coated μ-Slide 4 Well chamber (Ibidi) 72 h before imaging. The day after seeding, cells were transfected with Paxillin-DsRed2 construct with GeneJuice® transfection reagent (Merck Millipore). Transfections were performed according to the manufacturer's instructions. Cells were incubated for an additional 48 hours at 37°C with 5% CO2 in the incubator. Before starting live-cell imaging, the temperature of the incubation chamber was brought to 37°C with 5% CO_2 supply. Imaging was performed with Nikon Eclipse Ti2-E/Yokogawa CSU-W1 Spinning disk microscope using 100×/oil objectives. Live-cell movies were acquired at 1 frame/5 min with 10 z-stacks for a total 155 min. Images were analysed using Focal Adhesion Analysis Server (FAAS) (https://faas.bme.unc.edu/).[22] Maximum projections were applied to the image series and converted to 8-bit before uploading to the server. Adhesion size was defined as 10 pixels and the FA phase length was determined as five continuous image sets in the entire image analysis to provide experimental consistency. FAAS automatically detect and calculate FA assembly/disassembly rates based on changes in intensities during imaging. Life cell imaging also allowed us to determine the lifetime of FAs: The time span that encompasses the entire FA turnover cycle, that is, the time between the first appearance of an individual FA, the assembly, and the subsequent disassembly, until the disappearance of a FA.

2.9 | FRAP in primary astrocytes

For FRAP analysis, we used Paxillin-DsRed2 expressed wild type and *Vlgr1*-deficient astrocytes. Before photobleaching cells were imaged every 20 s for total 120 s to define basal bleaching rates. After 120 s of imaging, randomly selected FAs from the periphery of the cells were photobleached with 561-nm laser set to 100% power. To quantify FA kinetics, raw intensity values photobleached area (ROI1), whole cell (ROI2), and background area (ROI3) were measured with Fiji image analysis software. Intensity values were uploaded to the easyFRAP online tool (https://easyfrap.vmnet.upatras.gr/).[23] Post-bleached intensity values were normalized by subtracting pre-bleach values for bleach correction. Full-scale normalization was applied for FRAP fluorescence intensity curves and T-half time and mobile fractions were calculated with double curve fitting function. Only p values less than 0.05 are taken under consideration for quantifications. Samples were analysed with a Nikon Eclipse Ti2-E/Yokogawa CSU-W1 Spinning disk microscope using 63×/water objectives.

The study was conducted in accordance with the Basic & Clinical Pharmacology & Toxicology policy for experimental and clinical studies.[24]

3 | RESULTS

3.1 | Nocodazole washout assays revealed enrolment of VLGR1 in the assembly of FAs

We have previously shown that VLGR1 is vital for FAs affecting the size and length of FAs as well as the velocities of cell spreading and migration.[14] However, it has remained unclear/open whether VLGR1 controls migration capacity and turnover of FA during the assembly or the disassembly of FAs. We performed washout assays with the microtubule depolymerization drug nocodazole (NDZ), previously introduced to monitor the disassembly of FAs[21] (Figure 2A). We treated primary astrocytes derived from the brains of *Vlgr1*-deficient Vlgr1/DrumB mutant mice or wild type (WT) mice with either DMSO or nocodazole (NDZ) (10 μM) in DMSO. Consistent with previous reports,[21,25,26] NDZ treatment induced microtubule depolymerization leading to cell-cycle synchronization and accumulation of FAs (Figure 2A,B). After replacing the NDZ medium by a fresh medium without NDZ (NDZ washout) a phase of rapid FA disassembly was introduced which rested for approximately 45 min (Figure 2A,B). Quantifying the number of FAs after the 4-h NDZ treatment and during the FA disassembly phase, we did not observe significant differences between WT and *Vlgr1*-deficient mice in the number of FAs (Figure 2C, time points 15 to 45 min).

After 45 min of NDZ washout, the FA disassembly phase was followed by a phase of de novo assembly of FAs, characterized by increasing numbers of FAs in the primer astrocytes of mouse lines (Figure 2A,B; time points 60 and 120 min after NDZ washout).[21] Quantifying the number of FAs during this FA de novo

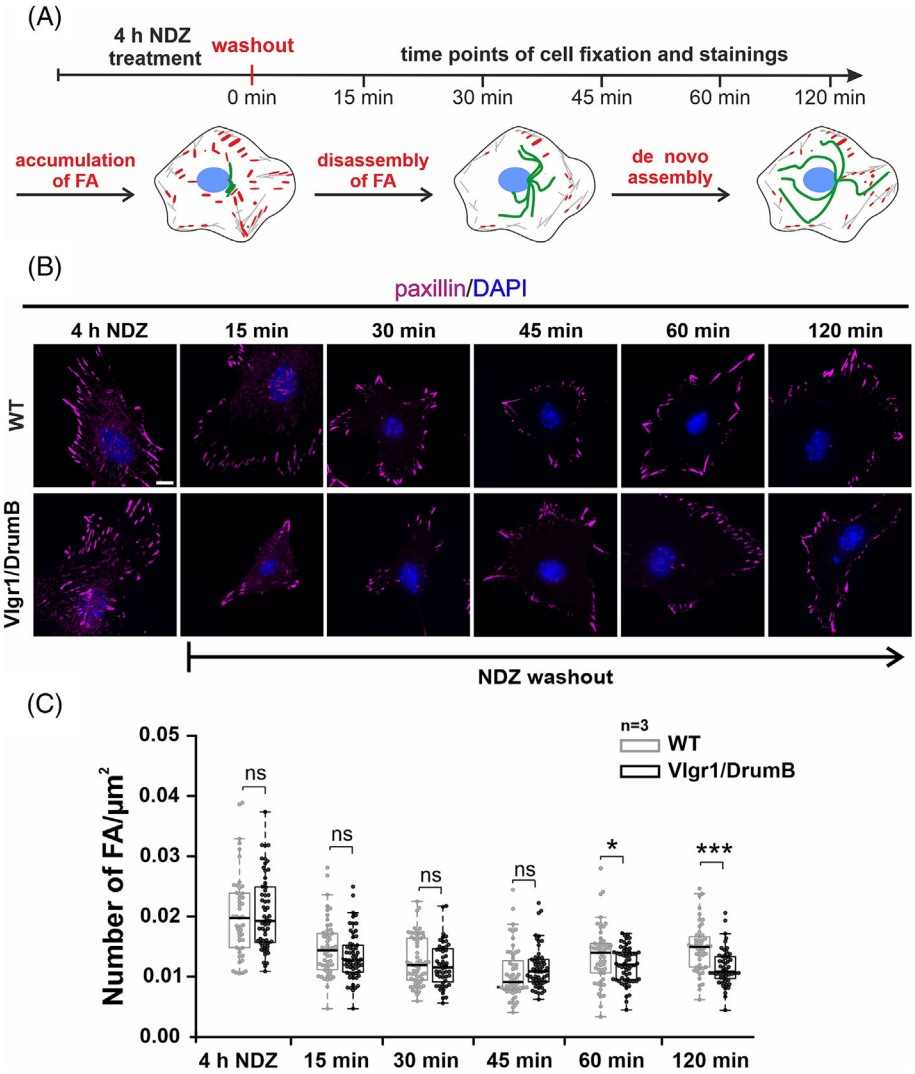

FIGURE 2 Analysis of focal adhesion (FA) turnover in primary astrocytes by nocodazole washout assays. (A) Scheme of nocodazole (NDZ) washout assay. Primary murine astrocytes were incubated with 10 uM NDZ in serum-free medium for 4 h to induce FA accumulation. Subsequent NDZ washout with complete growth medium induces FA disassembly (15–45 min), before de novo assembly starts at 60–120 min. (B) Immunostaining of the FA marker paxillin (magenta) and nuclear counterstaining of DAPI (blue) in primary astrocytes derived from wild type (WT) and *Vlgr1*-deficient Vlgr1/DrumB mouse hippocampi at different time points after NDZ washout. (C) Quantification of FA numbers after NDZ washout. In the FA disassembly phase (15–45 min after NCD washout), FA numbers steadily decreased in both WT and in *Vlgr1*-deficient Vlgr1/DrumB astrocytes without a significant difference. During the de novo assembly of FAs (60, 120 min), the number of FAs was significantly lower in *Vlgr1*-deficient Vlgr1/DrumB. $N = 47–58$ cells in WT astrocytes and 48–62 cells in Vlgr1/DrumB astrocytes per time-points were analysed in $n = 3$ independent experiments. Data are represented as mean ± SD. Statistical evaluation was performed using two-tailed Mann–Whitney *U* test, **p* % 0.05, ***p* % 0.01, ****p* % 0.001. Scale bars: 10 µm.

assembly phase revealed a significantly lower number of FAs in *Vlgr1*-deficient astrocytes when compared to WT astrocytes (Figure 2B,C). In contrast, we did not observe any changes in FA numbers in controls in which we only treated the astrocytes of both mouse lines with DMSO (Figure S1A,B). Taken together, the NDZ washout experiments showed that the absence of VLGR1 did not affect the disassembly of FAs but rather indicated a role of VLGR in the assembly of FAs.

3.2 | Live-cell imaging demonstrated that VLGR1 controls FA assembly in the living cell

Next, we analysed the FA turnover by live-cell imaging of primary astrocytes of WT and *Vlgr1*-deficient mice expressing the FA marker Paxillin-DsRed2.[17] Immunostaining of astrocytes demonstrated the co-localization of VLGR1 and Paxillin-DsRed2 confirming our previous results on VLGR1 and paxillin (Figure S2).[14]

For live-cell imaging, we recorded Paxillin-DsRed2-labelled FAs in *Vlgr1*-deficient primary astrocytes derived from Vlgr1/DrumB mice and WT astrocytes for 2 h in a spinning disc confocal microscope (Videos S1 and S2). Subsequently, we analysed and quantified the dynamics of Paxillin-DsRed2-FAs in these video tracks by applying the FAAS web tool (https://faas.bme.unc.edu)[22] (Figure 3). To eliminate putative background signals in FAAS analyses, FA sizes were defined minimum of 10 pixels and assembly/disassembly processes were

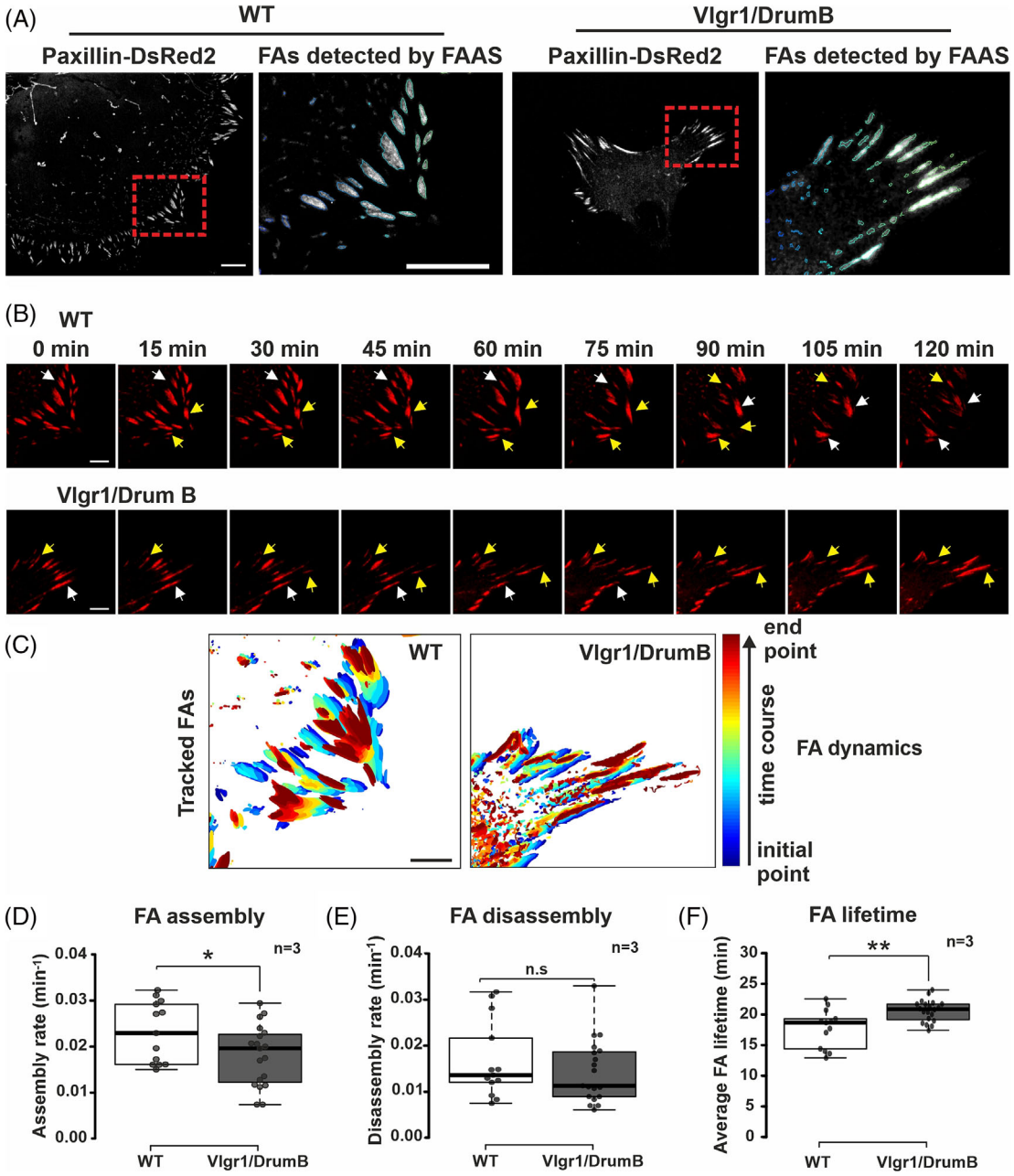

FIGURE 3 Live-cell imaging analysis of FAs turnover in primary astrocytes *Vlgr1*-deficient Vlgr1/DrumB mice. (A) Identification of FAs Paxillin-DsRed2 fluorescence image analysis by the Focal Adhesion Analysis Server (FAAS) (https://faas.bme.unc.edu) in wild type (WT) and *Vlgr1*-deficient Vlgr1/DrumB astrocytes expressing Paxillin-DsRed2. (B) Time-lapse image sequences of Paxillin-DsRed2 in FAs from WT and Vlgr1-deficient Vlgr1/DrumB astrocytes selected every 15 min from video traces recorded with a sequence of 5 min in a time course of 155 min. *Yellow arrow heads* point to assembling FAs and *white arrow heads* point to disassembling FAs. (C) Pseudo-coloured tracked FA images in WT and Vlgr1/DrumB astrocytes indicate initial and end points of assembly and disassembling FAs. Quantification of FA assembly rates (D), FA disassembly rates (E), and the average FA lifetime (F) in WT and Vlgr1/DrumB astrocytes. Cell numbers: $N = 13$ (WT), $N = 20$ (Vlgr1/DrumB) in $n = 3$ independent experiments. Data are represented as mean ± SD. Statistical evaluation was performed using two-tailed Student's t test, *p % 0.05, **p % 0.01, ***p % 0.001. Scale bars: 10 μm.

determined by using FAs, which appeared in five continuous image sets (Figure 3A). Following individual FAs (identified by FAAS) in time-lapse image sequences of Paxillin-DsRed2 in WT and Vlgr1/DrumB astrocytes, we observed that FAs undergo rapid assembly and disassembly in WT astrocytes, while the turnover of FAs was slower in Vlgr1/DrumB astrocytes (Figure 3B). The spatiotemporal dynamics in living astrocytes of WT and Vlgr1/DrumB were visualized by superposition of all FAs from microscopy image taken every 5 min during the entire time course of 155 min of colour for the set of FAs at each time point (Figure 3C).

Quantifications of all FAs in the analysed cells revealed that the assembly rate of FAs (Figure 3D) was significantly higher in WT astrocytes when compared to Vlgr1/DrumB astrocytes. In contrast, the disassembly rates did not significantly differ between both (Figure 3D). The lifetime of FAs (Figure 3F) was significantly longer in Vlgr1/DrumB astrocytes compared to WT astrocytes. To verify these results on FAs in Vlgr1/DrumB astrocytes, we also examined primary astrocytes derived from brains of Vlgr1/Del7TM mice (Figure S3), another *Vlgr1*-deficient mouse line.[18] Analogous live-cell imaging experiments showed, as in Vlgr1/DrumB astrocytes, no differences in the rate of FA disassembly but a significantly lower assembly rate of FAs in Vlgr1/Del7TM astrocytes compared with WT (Figure 3D,E; Figure S3C,D). In contrast to Vlgr1/DrumB, we did not observe differences in the life time of FAs in astrocytes of Vlgr1/del7TM (Figure S3E).

Taken together, our data show that deficiency in *Vlgr1* results in differences in turnover rates based on slower assembly rates of FAs.

3.3 | VLGR1 controls turnover kinetics of FAs by FRAP

We have shown that VLGR1 controls the assembly FA by our NDZ washout assays and live-cell imaging. We addressed next the effects of *Vlgr1*-deficiency on the kinetics of FA assembly by adhesions by FRAP (Figure 4). WT and *Vlgr1*-deficient astrocytes derived from Vlgr1/del7TM mouse brains were seeded onto fibronectin-coated surfaces and transfected them with Paxillin-DsRed2. Randomly selected FAs in the cell periphery of astrocytes were photobleached by the full power of laser of 560-nm excitation (Figure 4). Subsequently, fluorescence intensities in the bleached regions were determined by time-lapse imaging over a time period of 880 s (Video S3 and S4). Image analyses of the video tracks showed fast fluorescent intensity increases (FRAP) in WT astrocytes; already ~120 s after photobleaching Paxillin-DsRed2 fluorescence was recovered in FAs (Figure 4A,B, upper panels). In contrast, the recovery of Paxillin-DsRed2 was much slower in Vlgr1/del7TM astrocytes; we did not observe substantial FRAP until 240 s after photobleaching (Figure 4A,B, lower panels). FRAP signals were quantified by the online FRAP analysis tool EasyFRAP (https://easyfrap.vmnet.upatras.gr/).[23] For this, the FRAP intensities of bleached FA regions were normalized to the intensity values of background regions where noise signals were measured and to unbleached FAs where auto-fading values were measured. In Figure 4C, the quantitative analysis for the time course of Paxillin-DsRed2 fluorescence recovery is shown. The recovery of Paxillin-DsRed2 intensity was faster in WT astrocytes when compared to Vlgr1/del7TM astrocytes. In WT after 420 s approximately 50% of the Paxillin-DsRed2 fluorescence intensity of before bleaching levels were reached while in contrast, only 40% the Paxillin-DsRed2 fluorescence intensity was recovered in Vlgr1/del7TM astrocytes after that time (Figure 4C). In line with these results, we found a significantly slower average half-time ($t_{1/2}$) recovery of FRAP in Vlgr1/del7TM astrocytes with 338 s compared to WT astrocytes in which the $t_{1/2}$ was 223 s (Figure 4D). Nevertheless, our analysis by EasyFRAP revealed no significant differences in the calculated mobile fractions of Paxillin-DsRed2 between astrocytes of both WT and Vlgr1-deficent mice (Figure 4E).

Our FRAP data indicated that VLGR1 also participates in the recruitment of paxillin to FAs during their assembly.

The study was conducted in accordance with the Basic & Clinical Pharmacology & Toxicology policy for experimental and clinical studies.[27]

4 | DISCUSSION

The coordination and regulation of FA dynamics are central for cell migration under both healthy and pathological conditions.[16,24] Cell migration requires the continuous dynamic arrangement of FAs, the assembly of nascent FAs in the leading edge of cells, and disassembly in their rear.[28,29] In this regard, FAs are essential for sensing and integrating intracellular signals as well as for the reception of signals from the environment to control cell migration.[16] We previously showed that VLGR1 is part of the multiprotein complex of FAs and essential for their proper size and abundance in cells.[14,17] More importantly, our studies have also shown that VLGR1 is crucial for FA key functions, namely, in cell spreading and cell migration.[14] For this, the VLGR1 acts as a metabotropic mechanosensor sensing mechanical signals from the extracellular environment. So far, however, it had to

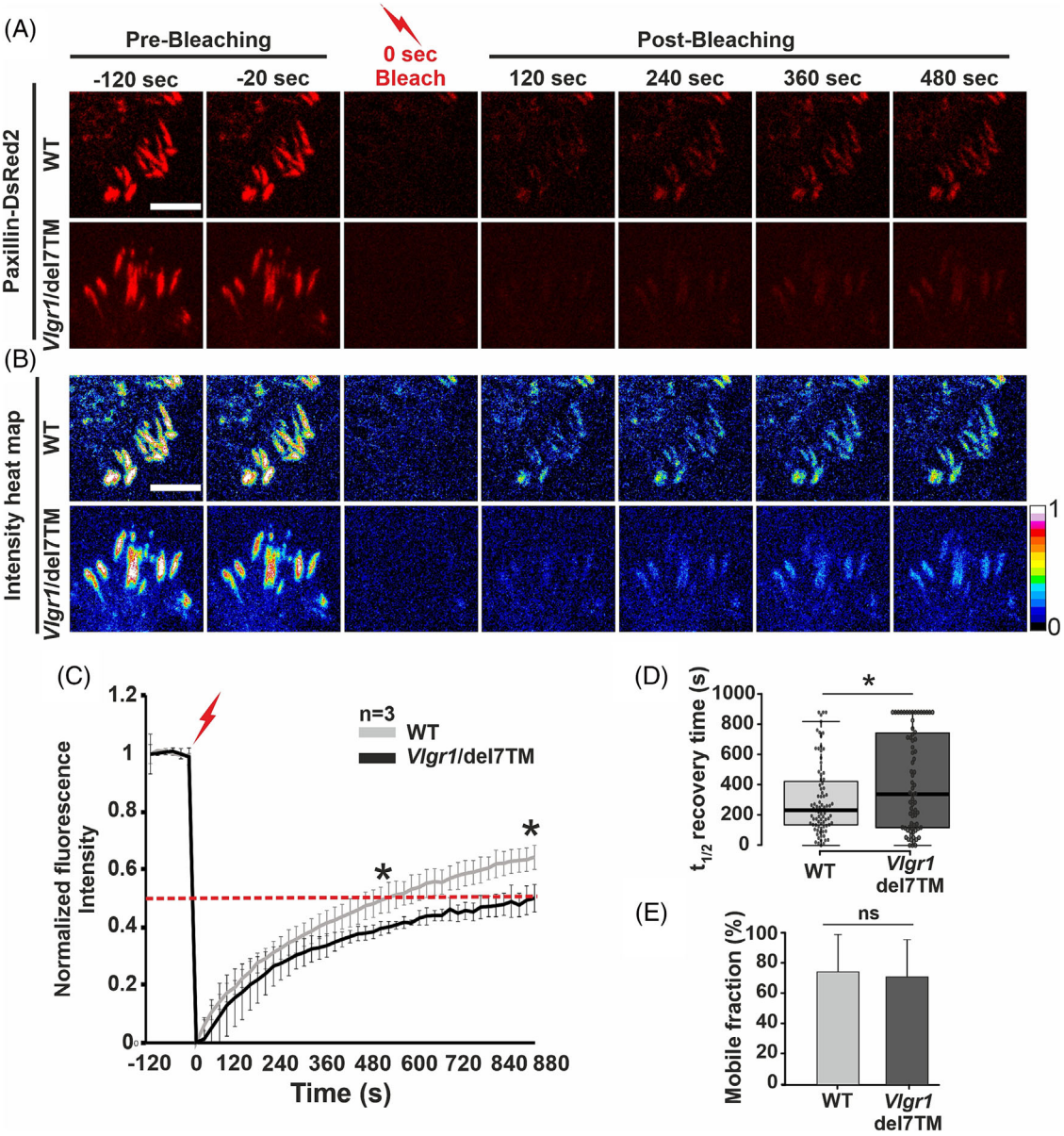

FIGURE 4 Fluorescence recovery after photo bleaching (FRAP) analysis of FAs turnover in primary astrocytes expressing Paxillin-DsRed2. (A) Representative time-lapse fluorescence images of Paxillin-DsRed2-transfected wild type (WT) and Vlgr1/del7TM primary astrocytes before and after fluorescence recovery after photobleaching (FRAP). Paxillin-DsRed2-expressed cells were imaged for 100 s before photobleaching (flash) to track basal intensity levels and bleached at 120 s. Images were acquired to record intensity recoveries for 880 s after photo bleaching. (B) Fluorescence recovery curve showing the intensity over time in the bleach ROI. From the recovery curve the immobile fraction and recovery half time can be determined. Intensity changes in individual Paxillin-DsRed2 focal adhesions during pre-bleaching and post-bleaching. (C) Normalized Paxillin-DsRed2 fluorescence intensity FRAP curves. Quantification of FRAP indicates reduction in intensity recovery in Vlgr1/del7TM astrocytes. The *red dashed line* indicates 50% of the recovery of the initial fluorescence intensity. *Asterisks* indicate significant differences in the fluorescence recovery between WT and Vlgr1/del7TM astrocytes. (D) Recovery of Paxillin-DsRed2 fluorescence after photobleaching. The recovery time after photobleaching is significantly longer Vlgr1/del7TM astrocytes (average 338 s) compared to WT astrocytes (average 233 s). (E) Mobile fractions of Paxillin-DsRed2 in WT and Vlgr1/del7TM astrocytes show no significant difference. Fluorescence recoveries normalized to pre-bleach levels and intensities of individual FA were calculated by Fiji image analysis tool and quantified by using EasyFRAP online-tool; 66–80 individual FAs were analysed in $N = 3$–7 cells of $n = 3$ experiments. Statistics: two-tailed Student's *t* test, *p % 0.05, **p % 0.01, ***p % 0.001. Scale bars: 10 μm.

remain open in which aspect of the turnover process of the dynamic macromolecular FA complexes VLGR1 participates.

In the present study, we aimed to elucidate how VLGR1 controls the FA turnover during cell migration. The turnover rate of FAs is characterized by the time

courses of their assembly and disassembly. Our data received by NDZ washout assays, live-cell imaging, and FRAP consistently provide several lines of evidence that VLGR1 regulates the turnover of FAs by participating in the assembly process of FAs. In the NDZ washout assay, FAs accumulated in response to NDZ-induced microtubule depolymerization are first rapidly degraded after NDZ washout, before FAs are reassembled.[21,25,26] Our results show that the time course of the later FA de novo assembly, but not the disassembly phase, is significantly delayed to an equal extent in the primary brain astrocytes of both *Vlgr1*-deficient mouse models studied. (Figure 2A–C; Figure S3A,B). Consistent with these findings, present live-cell imaging data acquired by monitoring the dynamics of FA turnover in living cells expressing the fluorescently tagged FA core protein paxillin[30] also demonstrated that the assembly rate but not the disassembly rate of FAs was significantly reduced in astrocytes of both *Vlgr1*-deficient mouse models (Figure 3D,E; Figure S3C,D). Present FRAP experiments also showed that the recruitment of fluorescent paxillin to FAs is slower in *Vlgr1*-deficient astrocytes (Figure 4C,D), which is in line with a reduced assembly rate of FAs as discussed above. Defects in the assembly of FAs also lead to reduced FA dynamics, which is documented by an increase of the lifetime in astrocytes of Vlgr1/DrumB mice (Figure 3F). Our data indicate that the increase of the lifespan FAs is based on a longer time span for the complete assembly of FAs as observed in Vlgr1-deficient astrocytes discussed above. All in all, these findings are consistent with the reduced migration rate in VLGR1 deficient cells that we previously found.[14]

All in all our findings on VLGR1 are consistent with the role of regulators of FA dynamics and cell migration, such as RACK1 and the phosphatidylinositol phosphate kinase type Iγ (PIPKIγ). Deficiency of VLGR1 decreases the turnover rates of the FA adaptor protein paxillin which has previously been observed for downregulation or mutations in FA regulators.[31,32]

When FAs are reassembled, integrins of disassembled FAs are recycled to the leading edge of migrating cells.[25,33,34] These integrin clusters receive signals from the extracellular matrix substrate triggering the sequential recruitment and activation of further FA components.[35–37] We have recently identified several molecules essential for the sequential assembly of FAs and related activation, such as the integrins β1, α3, α5, and α6, talin, RhoA, focal adhesion kinase (FAK), and integrin-linked kinase (ILK), as potential interacting proteins of VLGR1.[4,5,14] The absence of talin-1, one of the first FA molecules recruited to the integrin cluster, or, for example, mutations in *FAK* essential for the activation of other FA proteins, result in a delay of FA assembly but do not affect the FA disassembly rate.[25,38] This is exactly what we found in the present study for VLGR1 in *Vlgr1*-deficient cells. Taken together these data indicate that VLGR1 interplays with its interacting partners during the process of FA assembly.

The assembly of FAs as contact sites of the cell to its ECM substratum is controlled by external forces.[39] The principal membrane receptors to sense mechanical signals from the ECM are integrin dimers.[40,41] Nevertheless, there is emerging evidence that adhesion GPCRs act as mechanosensors at the cell surface, sensing mechanical forces from the extracellular environment as well.[2,42] Our recent identification of VLGR1 as a metabotropic mechanosensor in FAs,[14] in conjunction with the results found in the present study, suggests a mechanosensory role for VLGR1 in the process of FA assembly. Future studies will elucidate how the mechanosensation of integrins and VLGR1 during the assembly of FAs are coordinated.

There is growing evidence that defects in cell migration can increase susceptibility to epilepsy.[10,43] Given that the turnover of FAs is crucial for proper cell migration,[16] the altered composition rate of FAs in cells defective for VLGR1 is likely to contribute to the cellular pathophysiology in diseases caused by defects of VLGR1. VLGR1 is highly expressed in the developing CNS,[3] where the correct migration of neurons, glial cells, and their progenitors is essential.[44,45] To determine the role of VLGR1 in the turnover of FAs, we examined FA dynamics in primary brain astrocytes, which are characterized by particularly high migration properties.[46] Proper migration of astrocytes is essential for the development and maintenance of the CNS.[47] During the differentiation of the CNS, astrocytes are derived from radial glia cells in the ventricular and subventricular zone and migrate to the different layers of the brain.[47–49] In their final location, astrocytes play crucial roles in neurotransmitter clearance, synaptogenesis, and ion homeostasis and the loss of astrocyte function can lead to severe disorders of the CNS in human.[50,51] Interestingly, the loss or dysfunction of potential interacting proteins of VLGR1 in FAs, such as integrin β1, talin, or FAK can lead to astrogliosis, a hall mark in the pathogenesis of epilepsy.[52] Accordingly, VLGR1 deficiency in astrocytes may also contribute the pathophysiology underlying epilepsy, which will need to be addressed in detail in the future.

5 | CONCLUSIONS

Studying the highly mobile brain astrocytes, we validated the important role of adhesion GPCR VLGR1 in the

dynamics of FAs. Our data conclusively revealed that VLGR1 controls the kinetics of FAs by participating in the assembly of FAs, thereby the migration of the cells. For this, VLGR1 may act as a metabotropic mechanosensor sensing in parallel with integrins mechanical signals from the environment. Our findings not only elucidate the molecular and cellular function of VLGR1 in healthy brain astrocytes but also provide novel insights into the pathomechanisms of VLGR1-associated epilepsy.

ACKNOWLEDGEMENTS

We thank Drs. Rudolf E. Leube and Rick Hortwitz for kindly providing the Paxillin-DsRed2 plasmid, Dr. Kerstin Nagel-Wolfrum for fruitful discussions on the manuscript, and Susanne Wilhelm for language editing. Open Access funding enabled and organized by Projekt DEAL.

CONFLICT OF INTEREST STATEMENT

The authors declare no conflict of interest.

INSTITUTIONAL REVIEW BOARD STATEMENT

The use of mice in research was approved by the German regulation authority for the use of animals in research, the district administration Mainz-Bingen, 8341a/177-5865-§11 ZVTE, 30.04.2014.

ORCID

Baran E. Güler https://orcid.org/0000-0001-7967-9041
Uwe Wolfrum https://orcid.org/0000-0002-4756-5872

REFERENCES

1. Hamann J, Aust G, Araç D, et al. International union of basic and clinical pharmacology. XCIV. Adhesion G protein-coupled receptors. *Pharmacol Rev*. 2015;67(2):338-367. doi:10.1124/pr.114.009647
2. Lala T, Hall RA. Adhesion G protein-coupled receptors: structure, signaling, physiology, and pathophysiology. *Physiol Rev*. 2022;102(4):1587-1624. doi:10.1152/physrev.00027.2021
3. McMillan DR, White PC. Studies on the very large G protein-coupled receptor: from initial discovery to determining its role in sensorineural deafness in higher animals. *Adv Exp Med Biol*. 2010;706:76-86. doi:10.1007/978-1-4419-7913-1_6
4. Knapp B, Roedig J, Boldt K, et al. Affinity proteomics identifies novel functional modules related to adhesion GPCRs. *Ann N Y Acad Sci*. 2019;1456(1):144-167. doi:10.1111/nyas.14220
5. Knapp B, Roedig J, Roedig H, et al. Affinity proteomics identifies interaction partners and defines novel insights into the function of the adhesion GPCR VLGR1/ADGRV1. *Molecules*. 2022;27(10):3108. doi:10.3390/molecules27103108
6. Liebscher I, Schöneberg T. Tethered agonism: a common activation mechanism of adhesion GPCRs. In: *Adhesion G Protein-coupled Receptors. Handbook of Experimental Pharmacology*. Springer; 2016:111-125. doi:10.1007/978-3-319-41523-9_6
7. Liebscher I, Schöneberg T, Thor D. Stachel-mediated activation of adhesion G protein-coupled receptors: insights from cryo-EM studies. *Signal Transduct Target Ther*. 2022;7(1):227. doi:10.1038/s41392-022-01083-y
8. Fuster-García C, García-Bohórquez B, Rodríguez-Muñoz A, et al. Usher syndrome: genetics of a human ciliopathy. *Int J Mol Sci*. 2021;22(13):1-25. doi:10.3390/ijms22136723
9. Wolfrum U. Protein networks related to the Usher syndrome gain insights in the molecular basis of the disease. In: Ahuja S, ed. *Usher Syndrome: Pathogenesis, Diagnosis and Therapy*. Nova Science Publishers, Inc.; 2011:51-73.
10. Zhou P, Meng H, Liang X, et al. ADGRV1 variants in febrile seizures/epilepsy with antecedent febrile seizures and their associations with audio-visual abnormalities. *Front Mol Neurosci*. 2022;15:864074. doi:10.3389/fnmol.2022.864074
11. Dahawi M, Elmagzoub MS, A. Ahmed E, et al. Involvement of ADGRV1 gene in familial forms of genetic generalized epilepsy. *Front Neurol*. 2021;12:738272. doi:10.3389/fneur.2021.738272
12. Michel V, Goodyear RJ, Weil D, et al. Cadherin 23 is a component of the transient lateral links in the developing hair bundles of cochlear sensory cells. *Dev Biol*. 2005;280(2):281-294. doi:10.1016/j.ydbio.2005.01.014
13. Maerker T, van Wijk E, Overlack N, et al. A novel Usher protein network at the periciliary reloading point between molecular transport machineries in vertebrate photoreceptor cells. *Hum Mol Genet*. 2008;17(1):71-86. doi:10.1093/hmg/ddm285
14. Kusuluri DK, Güler BE, Knapp B, et al. Adhesion G protein-coupled receptor VLGR1/ADGRV1 regulates cell spreading and migration by mechanosensing at focal adhesions. *iScience*. 2021;24(4):102283. doi:10.1016/j.isci.2021.102283
15. Geiger B, Spatz JP, Bershadsky AD. Environmental sensing through focal adhesions. *Nat Rev Mol Cell Biol*. 2009;10(1):21-33. doi:10.1038/nrm2593
16. Mishra YG, Manavathi B. Focal adhesion dynamics in cellular function and disease. *Cell Signal*. 2021;85(May):110046. doi:10.1016/j.cellsig.2021.110046
17. Güler BE, Krzysko J, Wolfrum U. Isolation and culturing of primary mouse astrocytes for the analysis of focal adhesion dynamics. *STAR Protoc*. 2021;2(4):100954. doi:10.1016/j.xpro.2021.100954
18. McMillan DR, White PC. Loss of the transmembrane and cytoplasmic domains of the very large G-protein-coupled receptor-1 (VLGR1 or Mass1) causes audiogenic seizures in mice. *Mol Cell Neurosci*. 2004;26(2):322-329. doi:10.1016/j.mcn.2004.02.005
19. Potter PK, Bowl MR, Jeyarajan P, et al. Novel gene function revealed by mouse mutagenesis screens for models of age-related disease. *Nat Commun*. 2016;7(August):1-13. doi:10.1038/ncomms12444
20. Pora A, Yoon S, Windoffer R, Leube RE. Hemidesmosomes and focal adhesions treadmill as separate but linked entities during keratinocyte migration. *J Invest Dermatol*. 2019;139(9):1876-1888. doi:10.1016/j.jid.2019.03.1139
21. Ezratty EJ, Partridge MA, Gundersen GG. Microtubule-induced focal adhesion disassembly is mediated by dynamin

and focal adhesion kinase. *Nat Cell Biol*. 2005;7(6):581-590. doi:10.1038/ncb1262
22. Berginski ME, Vitriol EA, Hahn KM, Gomez SM. High-resolution quantification of focal adhesion spatiotemporal dynamics in living cells. *PLoS ONE*. 2011;6(7):e22025. doi:10.1371/journal.pone.0022025
23. Koulouras G, Panagopoulos A, Rapsomaniki MA, Giakoumakis NN, Taraviras S, Lygerou Z. EasyFRAP-web: a web-based tool for the analysis of fluorescence recovery after photobleaching data. *Nucleic Acids Res*. 2018;46(W1):W467-W472. doi:10.1093/nar/gky508
24. Gardel ML, Schneider IC, Aratyn-Schaus Y, Waterman CM. Mechanical integration of actin and adhesion dynamics in cell migration. *Annu Rev Cell Dev Biol*. 2010;26(1):315-333. doi:10.1146/annurev.cellbio.011209.122036
25. Nader GPF, Ezratty EJ, Gundersen GG. FAK, talin and PIPKIγ regulate endocytosed integrin activation to polarize focal adhesion assembly. *Nat Cell Biol*. 2016;18(5):491-503. doi:10.1038/ncb3333
26. Assar EA, Tumbarello DA. Loss of the essential autophagy regulators FIP200 or Atg5 leads to distinct effects on focal adhesion composition and organization. *Front Cell Dev Biol*. 2020;8(August):1-15. doi:10.3389/fcell.2020.00733
27. Tveden-Nyborg P, Bergmann TK, Jessen N, Simonsen U, Lykkesfeldt J. BCPT policy for experimental and clinical studies. *Basic Clin Pharmacol Toxicol*. 2021;128(1):4-8. doi:10.1111/bcpt.13492
28. Ridley AJ, Schwartz MA, Burridge K, et al. Cell migration: integrating signals from front to back. *Science (80-)*. 2003;302(5651):1704-1709. doi:10.1126/science.1092053
29. Parsons JT, Horwitz AR, Schwartz MA. Cell adhesion: integrating cytoskeletal dynamics and cellular tension. *Nat Rev Mol Cell Biol*. 2010;11(9):633-643. doi:10.1038/nrm2957
30. Stehbens SJ, Wittmann T. Analysis of focal adhesion turnover: a quantitative live-cell imaging example. In: *Methods in Cell Biology*. Vol.123. Academic Press; 2014:335-346. doi:10.1016/b978-0-12-420138-5.00018-5
31. Doan AT, Huttenlocher A. RACK1 regulates Src activity and modulates paxillin dynamics during cell migration. *Exp Cell Res*. 2007;313(12):2667-2679. doi:10.1016/j.yexcr.2007.05.013
32. Wu Z, Li X, Sunkara M, Spearman H, Morris AJ, Huang C. Pipkiγ regulates focal adhesion dynamics and colon cancer cell invasion. *PLoS ONE*. 2011;6(9):e24775. doi:10.1371/journal.pone.0024775
33. Caswell P, Norman J. Endocytic transport of integrins during cell migration and invasion. *Trends Cell Biol*. 2008;18(6):257-263. doi:10.1016/j.tcb.2008.03.004
34. Chao W-T, Kunz J. Focal adhesion disassembly requires clathrin-dependent endocytosis of integrins. *FEBS Lett*. 2009;583(8):1337-1343. doi:10.1016/j.febslet.2009.03.037
35. Roca-Cusachs P, Gauthier NC, Del Rio A, Sheetz MP. Clustering of α5β1 integrins determines adhesion strength whereas αvβ3 and talin enable mechanotransduction. *Proc Natl Acad Sci U S A*. 2009;106(38):16245-16250. doi:10.1073/pnas.0902818106
36. Byron A, Humphries JD, Craig SE, Knight D, Humphries MJ. Proteomic analysis of α4β1 integrin adhesion complexes reveals α-subunit-dependent protein recruitment. *Proteomics*. 2012;12(13):2107-2114. doi:10.1002/pmic.201100487
37. Baade T, Paone C, Baldrich A, Hauck CR. Clustering of integrin β cytoplasmic domains triggers nascent adhesion formation and reveals a protozoan origin of the integrin-talin interaction. *Sci Rep*. 2019;9(1):5728. doi:10.1038/s41598-019-42002-6
38. Zhu L, Plow EF, Qin J. Initiation of focal adhesion assembly by talin and kindlin: a dynamic view. *Protein Sci*. 2021;30(3):531-542. doi:10.1002/pro.4014
39. Riveline D, Zamir E, Balaban NQ, et al. Focal contacts as mechanosensors: externally applied local mechanical force induces growth of focal contacts by an mDia1-dependent and ROCK-independent mechanism. *J Cell Biol*. 2001;153(6):1175-1185. doi:10.1083/jcb.153.6.1175
40. Elosegui-Artola A, Oria R, Chen Y, et al. Mechanical regulation of a molecular clutch defines force transmission and transduction in response to matrix rigidity. *Nat Cell Biol*. 2016;18(5):540-548. doi:10.1038/ncb3336
41. Bachmann M, Schäfer M, Mykuliak VV, et al. Induction of ligand promiscuity of αVβ3 integrin by mechanical force. *J Cell Sci*. 2020;133(9):jcs242404. doi:10.1242/jcs.242404
42. Langenhan T. Adhesion G protein–coupled receptors—candidate metabotropic mechanosensors and novel drug targets. *Basic Clin Pharmacol Toxicol*. 2020;126(S6):5-16. doi:10.1111/bcpt.13223
43. Qin R, Cao S, Lyu T, Qi C, Zhang W, Wang Y. CDYL deficiency disrupts neuronal migration and increases susceptibility to epilepsy. *Cell Rep*. 2017;18(2):380-390. doi:10.1016/j.celrep.2016.12.043
44. Buchsbaum IY, Cappello S. Neuronal migration in the CNS during development and disease: insights from in vivo and in vitro models. *Development*. 2019;146(1):dev163766. doi:10.1242/dev.163766
45. Lago-Baldaia I, Fernandes VM, Ackerman SD. More than mortar: glia as architects of nervous system development and disease. *Front Cell Dev Biol*. 2020;8:611269. doi:10.3389/fcell.2020.611269
46. Zhan JS, Gao K, Chai RC, et al. Astrocytes in migration. *Neurochem Res*. 2017;42(1):272-282. doi:10.1007/s11064-016-2089-4
47. Siracusa R, Fusco R, Cuzzocrea S. Astrocytes: role and functions in brain pathologies. *Front Pharmacol*. 2019;10:1114. doi:10.3389/fphar.2019.01114
48. Tabata H. Diverse subtypes of astrocytes and their development during corticogenesis. *Front Neurosci*. 2015;9:114. doi:10.3389/fnins.2015.00114
49. Platel JC, Bordey A. The multifaceted subventricular zone astrocyte: from a metabolic and pro-neurogenic role to acting as a neural stem cell. *Neuroscience*. 2016;323:20-28. doi:10.1016/j.neuroscience.2015.10.053
50. Iram T, Ramirez-Ortiz Z, Byrne MH, et al. Megf10 is a receptor for C1Q that mediates clearance of apoptotic cells by astrocytes. *J Neurosci*. 2016;36(19):5185-5192. doi:10.1523/JNEUROSCI.3850-15.2016
51. Allen NJ, Eroglu C. Cell biology of astrocyte-synapse interactions. *Neuron*. 2017;96(3):697-708. doi:10.1016/j.neuron.2017.09.056

52. Robel S, Mori T, Zoubaa S, et al. Conditional deletion of β1-integrin in astroglia causes partial reactive gliosis. *Glia*. 2009;57(15):1630-1647. doi:10.1002/glia.20876

SUPPORTING INFORMATION

Additional supporting information can be found online in the Supporting Information section at the end of this article.

How to cite this article: Güler BE, Linnert J, Wolfrum U. Monitoring paxillin in astrocytes reveals the significance of the adhesion G protein coupled receptor VLGR1/ADGRV1 for focal adhesion assembly. *Basic Clin Pharmacol Toxicol*. 2023;1-12. doi:10.1111/bcpt.13860

Preprint I

The adhesion GPCR ADGRV1 controls glutamate homeostasis in hippocampal astrocytes supporting neuron development: first insights into to pathophysiology of *ADGRV1*-associated epilepsy

Baran E. Güler[1], Mark Zorin[1,2], Joshua Linnert[1], Kerstin Nagel-Wolfrum[1,2], Uwe Wolfrum[1*]

[1]Institute of Molecular Physiology, Molecular Cell Biology, [2]Institute of Developmental Biology and Neurobiology, Johannes Gutenberg University Mainz, 55099 Mainz, Germany.

[*]Corresponding author: Institute of Molecular Physiology, Molecular Cell Biology, Johannes Gutenberg University Mainz, Hanns-Dieter-Hüsch-Weg 17, 55128 Mainz, Germany; e-mail: wolfrum@uni-mainz.de

Short running title: ADGRV1 functions in astrocytes

Graphical Abstract

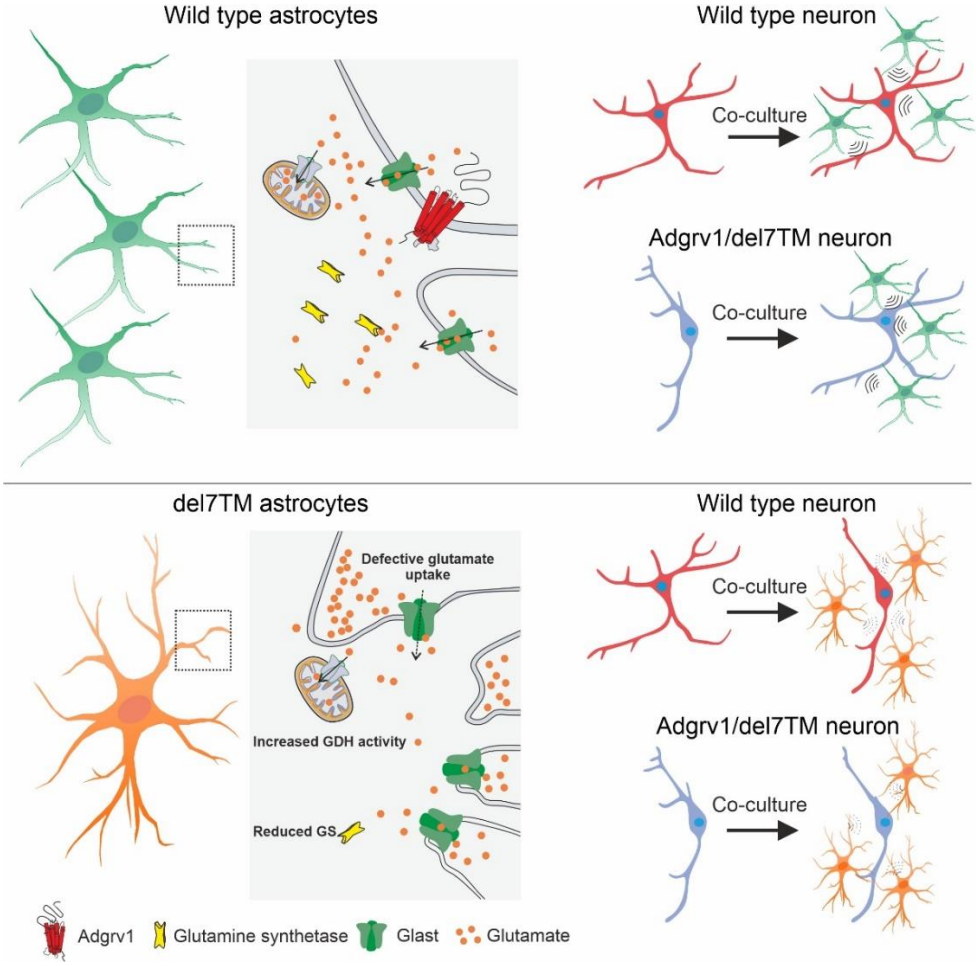

Highlights

- ADGRV1 deficiency reduces the number of astrocytes in CA1 and changes the morphology of astrocytes in the hippocampus.
- ADGRV1 interacts with numerous proteins enriched in astrocytes.
- Differential transcriptomes revealed differential expression of genes related to glutamate homeostasis and epilepsy in ADGRV1 deficient models.
- ADGRV1 controls glutamate uptake and regulates homeostasis in astrocytes.
- ADGRV1 in astrocytes is vital for neuron morphogenesis.
- First insights into the molecular pathophysiology underlying the development of epilepsy associated with mutations in ADGRV1.

Abstract

ADGRV1 is the largest member of adhesion G protein-coupled receptor (aGPCR) family. In the cell, aGPCRs have dual roles in cell adhesion and signal transduction. Mutations in *ADGRV1* have been linked not only to Usher syndrome (USH), which causes deaf-blindness, but recently also to various forms of epilepsy. While the USH defects are attributed to the loss of fiber links between membranes formed by the extracellular domain of ADGRV1, the pathomechanisms leading to epilepsy remain elusive to date.

Here, we study the specific functions of ADGRV1 in astrocytes where it is highest expressed in the nervous system. Affinity proteomics showed the interaction of ADRGV1 with proteins enriched in astrocytes. Dysregulations of cellular processes important in astrocyte function were indicated by the different transcriptomes of patient-derived cells and Adgrv1-deficent mouse hippocampi compared to appropriate controls. Alteration in morphology and reduced numbers of astrocytes in the hippocampus of Adgrv1-deficent mice. Monitoring the glutamate uptake in colorimetric assay and by live cell imaging of a genetic glutamate reporter consistently showed that glutamate uptake from the extracellular environment is significantly reduced in Adgrv1-deficent astrocytes. Expression analyses of key enzymes of the glutamate-glutamine cycle in astrocytes and the glutamate metabolism indicated imbalanced glutamate homeostasis in Adgrv1-deficient astrocytes. Finally, we provide evidence that the supportive function of astrocytes in neuronal development also relies on ADGRV1 expression in astrocytes. Our data collectively provides first insights into the molecular pathophysiology underlying the development of epilepsy associated with mutations in *ADGRV1*.

Key words: GPCR, VLGR1, epilepsy, Usher syndrome, astroglia, glutamate-glutamine cycle, glutamate metabolism, hippocampus, astrocyte-neuron interaction

INTRODUCTION

ADGRV1 (previously known as GPR98, MASS1, or VLGR1) with a molecular weight of approximately 700 kDa is the largest member of the adhesion G protein-coupled receptor (aGPCR) family consisting of 33 other members (Hamann et al., 2015). Adhesion GPCRs are structurally chimeric and contain the signature domains of seven transmembrane receptors and adhesion proteins (Langenhan, 2020). This repertoire makes them suitable to participate in cell adhesion and signaling through G protein coupled pathways (Knapp et al., 2022). Like the other aGPCRs, ADGRV1 can be autoproteolytically processed at its GAIN domain and operate as a metabotropic mechanoreceptor (Kusuluri et al., 2021). Furthermore, there is evidence that mechanosensation of ADGRV1 may trigger its cleavage and subsequent receptor activation by the tethered "Stachel" agonist inducing the switch from Gαs- to Gαi-mediated signaling (Knapp et al., 2022). ADGRV1 is a component of fibrous membrane-links, membrane contacts to the extracellular matrix, namely focal adhesions and in organelle contact sites such as the mitochondria-associated ER membranes (MAMs) (Maerker et al., 2008; Kusuluri et al., 2021; Krzysko et al., 2022; Güler et al., 2023a). There, ADGRV1 were related to the control of cell spreading and migration and the maintenance of Ca^{2+}-homeostasis.

In vertebrate hair cells and photoreceptor cells, ADGRV1 forms fiber connections between adjacent membranes ~~of neighboring stereocilia and at the ciliary pocket~~, respectively and their loss leads to USH2C, a subtype of the human Usher syndrome, the most common form of hereditary deaf blindness (Weston et al., 2004; Michalski et al., 2007; Maerker et al., 2008). However, in recent years pathogenic variants in *ADGRV1* have been also associated with various forms of epilepsy (Wang et al., 2015; Myers et al., 2018a; Liu et al., 2020; Leng et al., 2022; Zhou et al., 2022). In cohorts of patients with confirmed epilepsy, the rate of *ADGRV1* pathogenic variants was determined to be nearly 3% (Leng et al., 2022). Although most of these epilepsy cases related to *ADGRV1* haploinsufficiency have good prognoses, a recent case report of a heterozygous missense mutation of *ADGRV1* (c.5785G> T) in a patient resulted in hippocampal sclerosis characterized by neuronal cell loss and sudden unexpected death (Ji et al., 2023). It is generally accepted that the epileptic seizures which are characteristic for epilepsy are induced by excessive and abnormal neuronal activity in the brain (Bou Assi et al., 2017). However, the molecular mechanisms leading to the different forms of epilepsy remain elusive to date (Chong et al., 2023; Johannesen et al.,

2023). Also, to date, nothing is known about the molecular and cellular pathomechanisms that lead to the epileptic brain conditions caused by defects in ADGRV1.

Although ADGRV1 is expressed almost ubiquitously in many tissues, its expression is strongest in the developing and mature nervous system (McMillan and White, 2010). Of all brain cells, ADGRV1 is most strongly expressed in astrocytes (https://www.proteinatlas.org/). Astrocytes are glia cells and one of the most abundant cells in the central nervous system (CNS). Astrocytes have many roles including, regulation of extracellular ion concentration, control of energy metabolism, glutamate clearance, neuroprotection, synaptogenesis, and establishment of the blood-brain barrier (Mahmoud et al., 2019; Michinaga and Koyama, 2019). The branching of astrocytes promotes extensive contacts with neighboring cells, in particular neurons and specific association with synapses (Higashi et al., 2001). In tripartite synapses, astrocytes wrap around the pre- and post-synapses of neurons and regulate the crosstalk between synapses by balancing the ion and glutamate homeostasis (Perea et al., 2009; Allen and Eroglu, 2017; Broadhead et al., 2022). Glutamate uptake by astrocytes clears the glutamate spillover from synaptic clefts and is part of the glutamate-glutamine cycle between astrocytes and neurons preventing glutamate toxification of the neural tissue (Rose et al., 2018; Mahmoud et al., 2019). However, the uptaken glutamate can be also metabolized in the astrocytes for energy production in the mitochondrial tricarboxylic acid cycle (TCA) (Rose et al., 2020). The dysregulation of both the glutamate-glutamine cycle and the glutamate metabolism in astrocytes can cause an imbalance in brain glutamate homeostasis and lead to hyperexcitability of neurons as seen in epilepsy (Alcoreza et al., 2021). Loss of astrocyte functions or defects in their migratory capacity during development, or postnatal dysfunctions of astrocytes, have been associated not only with neurodegenerative diseases, such as Alzheimer´s and Parkinson's disease, but also with the development of various forms of epilepsy (Steinhäuser et al., 2012; Zhang et al., 2016; González-Reyes et al., 2017).

Although ADGRV1 is abundantly expressed in astrocytes, little is known about its specific function in astrocytes of the CNS. In previous studies on ADGRV1 function we made use of primary astrocytes-derived from murine brain as cellular models without a specific focus on the possibly epilepsy-relevant functions in the brain (Kusuluri et al., 2021; Krzysko et al., 2022; Güler et al., 2023b). Our studies collectively revealed insights into a variety of roles of ADGRV1 in cell functions such as cell adhesion, cell migration, mechanosensation, and the regulation of the Ca^{2+}-homeostasis at MAMs.

Our current work is focused on elucidating and understanding the specific functions of ADGRV1 in astrocytes by omics, immunohisto- and cytochemistry, biochemistry and a spectrum of cell physiology assays utilizing Adgrv1-deficient mice and human patient cells as models. We show that astrocyte morphology is altered, and their number is significantly reduced especially in the CA1 region of the hippocampus of the Adgrv1-deficient mouse brain. Omics data support the association of ADGRV1 with proteins and processes specifically enriched in astrocytes. Our data also indicates an imbalance in glutamate homeostasis in hippocampal Adgrv1-deficient astrocytes resulting in a reduced glutamate uptake from the extracellular environment and an alteration in the glutamate-glutamine cycle and glutamate metabolism. Our work in primary cultures suggests that ADGRV1 is also important for the proper development of neurons and showed that ADGRV1 substantially contributes to the beneficial support of astrocytes for neurons. Overall, our data provides first insights in the molecular pathophysiology underlying the development of epilepsy associated with mutations in *ADGRV1*.

Material and Methods

Animals

Experiments were conducted in accordance with the guidelines set forth by the Association for Research in Vision and Ophthalmology. Mice were housed in a controlled environment with a 12/12-hour light/dark cycle with unrestricted access to food and water. Adgrv1/del7TM mice, susceptible to audiogenic seizures, carry a nonsense mutation, V2250X, in the *Adgrv1* gene, leading to the loss of both its transmembrane and cytoplasmic domains (McMillan and White, 2004). The mice were bred on a C57BL/6 background. The use of mice for research purposes was granted approval by the District Administration Mainz-Bingen under reference number 41a/177-5865-§11 ZVTE on April 30, 2014.

Antibodies

The following antibodies were used: rabbit anti-GFAP (DAKO agilent, ZO334), rabbit anti-SOX9 (Abcam, ab185966), guinea pig anti-MAP2 (Sysy, 188004), rabbit anti-GLAST (Almone lab, AGC-021), mouse anti-Gapdh (Abcam, ab9484), rabbit anti-Glutamine synthetase (Abcam, ab49873), mouse anti-Glutamine synthetase (Abcam, ab64613), rabbit anti-Homer1 (Sysy, 160011), mouse anti-Gephyrin (Sysy, 147021). Secondary antibodies conjugated to Alexa488, Alexa568 and Alexa647 were purchased from Molecular Probes (Life Technologies). Nuclear

DNA was stained with DAPI (4′,6-diamidino-2-phenylindole, 1 mg/ml, Sigma-Aldrich, 10236276001).

Transcardiac perfusion fixation of mouse brains and immunohistochemistry analysis

Mice were anesthetized with an injection of 40 to 80 mg/kg of pentobarbital. Then transcardiac perfusion was performed with cold 0.1 M phosphate buffer (pH 7.4) (PBS) containing 0.0025 g/50 ml heparin solution following by 4% paraformaldehyde (PFA) in phosphate buffer (Gage et al., 2012). Dissected brains were post-fixed in buffered 4% PFA overnight, infiltrated stepwise with 10%, 20% and, 30% sucrose in PBS, and embedded in Tissue-Tek OCT before frozen in melting isopentane (Wolfrum, 1991). 16 µm thick cryosections and placed onto Poly-L-Lysine (Sigma-Aldrich, P4832-50ML) coated coverslips. After permeabilization in 0.2% Triton X-100 for 10 min (Sigma-Aldrich, 102533092) in PBS, immunostaining performed as previously described (Arévalo et al., 2022). Fluorescence intensity immunoreactivity in mouse hippocampi was analyzed using a build-in ImageJ/Fiji plugin (https://fiji.sc/).

Morphometric analysis of hippocampal astrocytes

The morphology of astrocytes and neurons was quantified as previously published (Young and Morrison, 2018). In brief, cryosections through the hippocampus of mice were stained for astrocytes by anti-GFAP and counterstained with DAPI. Hippocampal subregions were identified by the Allen mouse brain atlas (https://mouse.brain-map.org/) (Figure S1). Z-stacked images were maximum intensity projected, converted to 8-bit using ImageJ/Fiji, and pre-processed with an FFT bandpass filter (filter up to 5 pixels, down to 40). Individual astrocytes were cropped, skeletonized, and quantified using AnalyzeSkeleton(2D/3D) and FracLac analysis plugins (Arganda-Carreras et al., 2010).

Astrocyte number analysis

GFAP and SOX9 positive astrocyte numbers were counted in different hippocampal subregions in immunostained cryosections of mice brains. GFAP and DAPI positive cells were marked with the image counter plugin of ImageJ/Fiji. For the analysis of SOX9-positive cells, images were converted to 8-bit and “huang dark” threshold was applied, converted to binary, and watershed was applied. Particles analysis was performed with the sizes defined as 100 to infinity and circularity was defined as 0.4 to 1.00. Counted cells were exported and processed in GraphPad prism.

Mouse hippocampi transcriptome analysis

PN40 wild type and Adgrv1/del7TM mice were sacrificed by cervical dislocation. The hippocampus was dissected from the brain and flash-frozen using liquid nitrogen. mRNA was

isolated according to the instructions of the Qiagen RNeasy Mini kit. The quality and quantity of RNAs were measured with a Nanodrop 2000 spectrophotometer (Thermo Fischer Scientific). Sequencing was performed with Illumina NovaSeq 6000 Sequencing Systems (Novogene). Analysis was performed using Conda package manager v.23.5.2 (Grüning et al., 2018). All packages were installed in separate environments and an analysis pipeline was written in Snakemake v.7.32.3 (Mölder et al., 2021). First, we performed a quality control analysis of raw paired end reads using FastQC v.0.12.1 (https://www.bioinformatics.babraham.ac.uk/projects/fastqc/). Then we trimmed our reads using Trimmomatic v.0.39 (Bolger et al., 2014) with HEADCROP:15 parameter. After trimming, we performed contamination check analysis using FastQ Screen v.0.15.3 (Wingett and Andrews, 2018) software and reference genomes: *Escherichia coli* strain K-12 (ASM584v2), *Homo sapiens* (GRCh38.p14), *Metamycoplasma orale* strain NCTC10112 (50465_D02-3), *Mus musculus* (GRCm39), *Staphylococcus aureus* (ASM1342v1). During contamination check, we used Bowtie2 v.2.5.1 as an aligner. Reads that did not match to any mammalian genome or aligned to *E. coli*, *M. orale* or *S. aureus* were excluded from subsequent analysis. Then, we aligned the filtered reads to the reference mouse genome (GRCm39) using Hisat2 v.2.2.1 (Kim et al., 2019) software, sorted and recorded them in the bam format using Samtools v.1.17 (Li et al., 2009). To quantify the number of reads that mapped to each gene we used the featureCounts program that included in Subread v.2.0.6 (Liao et al., 2014) package. In the following analysis we used only genes with more than 5 mapped reads. After filtering files, we performed a differential expression analysis using DESeq2 v.1.40.2 (Love et al., 2014). In further analysis we used only genes with adjusted p-value less than 0.05. Three biological replicates of WT and Adgrv1/del7TM mice were used. However, during the analysis of the raw data, we observed high ingroup variation in Adgrv1/del7TM. Therefore, to identify the differences between WT and Adgrv1/del7TM group, we excluded the outlier biological replicate to decrease ingroup variation.

Human fibroblast transcriptome analysis

Dermal primary fibroblast lines were expanded from skin biopsies of human subjects (ethics vote: Landesärztekammer Rhineland-Palatinate to KNW). Fibroblasts from the skin biopsies of a 57-year-old male patient with clinically confirmed Usher syndrome 2C caused by a nonsense mutation in the *ADGRV1* gene (g.[90006848C>T], R2959*) were kindly provided by Dr Erwin van Wijk (Radboud University Medical Center, Nijmegen). Fibroblasts derived from the patient and from a healthy individual were maintained in DMEM/10% FBS (Thermo Fischer Scientific, 31966-021)

before the RNA isolation, isolated fibroblast RNAs were subjected to RNAseq analysis with Illumina NovaSeq 6000 Sequencing Systems (Novogene) previously described (Schäfer et al., 2023).

Analysis of tandem affinity purification (TAP) data sets and Gene Ontology (GO) analysis

Data sets obtained by tandem affinity purification (TAP) from HEK293T cells lysates expressing Strep II/ Strep-Tactin tagged ADGRV1 constructs (Figure S2A, B) were previously published in (Knapp et al., 2022). We categorized the TAP hits by using Gene Ontology (GO) term analysis following by Cytoscape (http://www.cytoscape.org; accessed on 09 September 2023) plugin ClueGO (Bindea et al., 2009). Functional protein association networks were prepared by using String database v10 (Szklarczyk et al., 2015). For transmembrane transporter activity related genes in fibroblasts were screened in the web application of the Amigo2 (https://amigo.geneontology.org/amigo/search/bioentity?q=transmembrane%20transporter%20activity).

Isolation of primary astrocytes

Astrocytes were isolated from newborn female and male sibling mouse pups on postnatal day 0 (PN0), as previously described (Güler et al., 2021). Briefly, PN0 mouse pups were dissected, and their brains enzymatically and mechanically dissociated. The resulting single-cell mixtures were plated on Poly-L-Lysine-coated (PLL) flasks and cultured in DMEM/10% FBS/2% penicillin/streptomycin for 7 to 10 days. Upon reaching confluence, flasks were agitated to remove oligodendrocytes and neurons. To separate primary astrocytes from microglia cells, cultures were trypsinized and plated on sequential bacterial-grade dishes. Microglia cells adhered to the dish surfaces, while astrocytes were recovered from the supernatant. Isolated primary astrocytes were cultured for an additional 7 to 10 days in complete growth medium.

Isolation of primary neurons

Primary neurons were isolated from the mouse hippocampus on embryonic day E18.5. Hippocampal tissues were dissected and kept in ice-cold HBSS buffer. After washing twice with HBSS to remove dead cells, tissues were trypsinized for 5 min at 37°C. Single-cell solutions were prepared using fire-polished Pasteur pipettes with varying opening diameters. After trituration, 5 ml HBSS was added to stop the enzymatic reaction. Cell suspensions were allowed to settle for 5 min before aspirating the HBSS/trypsin mixture. Cell pellets were then triturated with 2 ml cold HBSS, and cell numbers were counted. Cells were seeded on PLL coated coverslips and cultured

in neuron growth medium containing B27 supplement, L-glutamine, penicillin-streptomycin, and glutamate in Neurobasal medium (ThermoFisher Scientific, 21103049).

Astrocyte-neuron co-culture

Primary astrocytes were cultured in PLL coated coverslips in a 6 well plate for 2 days at a density of $3x10^5$ cells per well in DMEM/10% FBS/2% penicillin/streptomycin medium. After two days of cultivation, primary neurons were isolated and seeded on top of the lawn of astrocytes at a density of $3x10^5$ neurons per well. In these co-cultures, the DMEM medium was replaced by neuron growth medium.

Immunocytochemistry

Primary astrocytes and neurons were processed for immunocytochemistry as previously described (Kusuluri et al., 2021; Güler et al., 2023b).

Western blot analyses

Protein lysates from tissue and primary cells were prepared as previously described (Krzysko et al., 2022) and densitometry analysis was performed by using an Odyssey imaging system (LI-COR Biosciences).

Glutamate uptake and Glutamate dehydrogenase (GDH) activity assays

Glutamate uptake assays were performed as previously described (Mahmoud et al., 2019). Briefly, primary astrocytes were seeded at a density of $2x10^5$ cells per well of 12 well plate. After 72 h in DMEM medium, astrocytes were treated with serum free Opti-MEM medium for 2 h. Opti-MEM was removed by 3 PBS washes. Cells were exposed to 100 or 200 µM Glutamate solution in Hank´s Balanced Salt Solution (HBSS) containing Ca^{2+} buffer for 4 h. Cell culture supernatants were analyzed in a Glutamate assay kit (Sigma-Aldrich, MAK004) following the manufacturer's instructions. GDH activities in primary astrocytes were determined with glutamate dehydrogenase activity assay kit following with the manufacturer´s instructions (Abcam, ab102527).

Stachel peptide synthesis

The "Stachel" peptide (SVYAVYARTDN) (Knapp et al., 2022) and a randomized control peptide (ATSVRYDNAYV) were synthesized from C- to N-terminus by solid phase peptide chemistry, HPLC purified and analyzed by mass spectrometry (Chempeptide limited). Lyophilized peptide was solubilized in 100% DMSO and diluted in 80% ddH_20 and 20% HNO_3 (20% v/v) to obtain a 10 mM stock solution.

Live cell imaging and "Stachel" peptide application

Glutamate was monitored in primary astrocytes using the fluorescent reporter for glutamate pAAV.GFAP.iGluSnFR3.v857.GPI (Addgene plasmid # 178338) which was a gift from Kaspar Podgorski (Aggarwal et al., 2023). Images were acquired by Nikon eclipse Ti2 microscope (Nikon Instruments Inc) equipped with CSU-W1-T2 automatic Spinning Disk Confocal Scanning unit with 63x water objective (Yokogawa Electric Corporation). Dyes were excited with a 488 nm laser. The exposure time was kept at 250 ms and image sequences were obtained every 700 milliseconds for a total of 300 seconds. 1 mM "Stachel" peptide applied to the HBSS medium to evoke the Adgrv1 signaling at 98th sec of imaging. Fluorescence values were normalized to the first 98 frames of images (F_0). Calculation of intensity changes was done by following formula $(F-F_0)/ F_0$.

Morphometric analysis of neurons

To analyze neuronal dendritic complexity, Sholl analysis method was used as previously described (Ferreira et al., 2014). Briefly, images of MAP2 positive neurons were exported to ImageJ/Fiji and converted to 8-bit images and "IsoData" thresholding was applied to images. Thresholded images were converted to Mask and fill hole function applied. Binarized images were loaded into the SNT plugin in ImageJ/Fiji. Branches of neuritis were selected and semi-autonomous branch detection option of SNT used. Intersection numbers were exported to Excel and Sholl plots were generated using R Studio.

Synaptic puncta analysis in cultured neurons

Primary neurons isolated from WT and Adgrv1/del7TM mice hippocampi were cultured for 14 days. For the quantification of the number of synaptic puncta along the MAP2 positive dendrites, SynapCountJ and NeuronJ Fiji/ImageJ plugins were used (Mata et al., 2016). Briefly, dendrites from individual neurons were tracked using NeuronJ plugin and dendritic structures saved as a tab-limited text file (Txt). Next, dendritic branch information and images with synaptic channels were uploaded to SynapCountJ plugin. Images were manually thresholded and threshold values kept constant throughout the analysis. Synaptic densities were calculated per 100 µm dendritic length. Synaptic puncta sizes were analyzed with another Fiji/ImageJ plugin Synapse Counter (Dzyubenko et al., 2016). Images were thresholded with Triangle and synaptic particle size was limited from 20 px^2 to 400 px^2 using the batch mode function of the plugin.

Microscopy

Images were acquired using a Leica DM6000B Microscope (Leica-Bensheim) or a Nikon eclipse Ti2-E microscope (Nikon Instruments Inc) equipped with CSU-W1-T2 automatic Spinning Disk Confocal Scanning unit (Yokogawa Electric Corporation).

Statistical analyses

Statistical analyses were performed with Graphpad Prism 9.0 software (GraphPad Software Inc.). Differences between two sets of data were assessed via a two-tailed Student's t-test. In the case of multiple group comparisons, one way ANOVA was employed, followed by either Dunnett's multiple comparison tests or Sidak's multiple comparison tests, chosen based on the specific data being compared. Significance levels were defined as *$p < 0.05$, **$p < 0.01$, and ***$p < 0.001$. The bar plots display means with standard deviations (mean ± SD). The box plots exhibit the median (central line), while the edges of the boxes represent the interquartile range (25^{th}-75^{th} percentile). The whiskers depict the range for the upper 25% and lower 25% of the data points.

RESULTS

Adgrv1 controls astrocyte morphology in the mature mouse hippocampus

We have previously shown that the morphology of primary astrocytes is altered in Adgrv1/del7TM mice (Kusuluri et al., 2021). To examine the astrocyte morphology *in situ,* we stained cryosections of the hippocampus of mature Adgrv1/del7TM and control wild-type (WT) mice for the astrocyte marker glial fibrillary protein (GFAP) (Figures 1B, and S1). We then quantified the branching, the circularity, and the convex-hull area of astrocytes in the different subregions of the hippocampus (Figure 1C). The number of branches in astrocytes was significantly increased in all three *Cornu ammonis* regions of the hippocampus (CA1, CA2, and CA3) in Adgrv1/del7TM compared to WT (Figures 1D-F). The circularity (polarization) and convex-hull area of the astrocytes were significantly reduced in CA1 and CA2, but not in CA3 (Figures 1E, F). These data suggest that the lack of Adgrv1 results in morphological changes in astrocytes, predominantly in the CA1 region of the hippocampus.

Loss of astrocytes in hippocampus regions of Adgrv1/del7TM mice

Next, we examined whether the number of astrocytes in the hippocampus is altered in Adgrv1/del7TM mice. The number estimated by determining the level of expression of the astrocyte-specific markers GFAP and SOX9 in Western blots of hippocampus tissue (Figures 2A, B). Quantification of Western blot bands showed a slight decrease of GFAP and SOX9 expression in the hippocampus of Adgrv1/del7TM mice. We subsequently stained cryosections through the hippocampus for GFAP, SOX9, and DAPI and counted the immunostained astrocytes in the

different regions (Figures 2C, D). There were no significant changes in the number of astrocytes in the CA2, CA3, and dentate gyrus region, but a significant decrease in the number of astrocytes in the CA1 region of Adgrv1/del7TM hippocampi compared to WT controls.

Affinity proteomics reveals the interaction of ADGRV1 with proteins enriched in astrocytes

We have previously identified numerous putative interacting proteins of ADGRV1 by affinity proteomics capture approaches based on tandem affinity purifications (TAP) combined with mass spectrometry (Figure S2A) (Knapp et al., 2019, 2022). Re-analyzing our TAP datasets previously obtained in HEK293T and hTERT-RPE1 cells (PXD042629), we identified 289 proteins which are enriched in the proteome of astrocytes (Batiuk et al., 2020) as potential interacting proteins to ADGRV1 (Table S1, subtitle 1: Enriched protein annotations; Figure S2B). GO term analysis of these astrocyte proteins showed that in total 52 proteins are clustered in the GO term "*Transmembrane transporter activity*" (Table S1, subtitle 2: Biological function analysis; Figure S2C). Interestingly, five of these potentially interacting proteins of ADGRV1 were also found under the GO term *"L-glutamate import"* (subtitle Table S1; Figure S2C, D) suggesting a link to the glutamate homeostasis, a major function of astrocytes in the CNS. In particular, the two plasma membrane proteins, namely the excitatory amino acid transporters SLC1A1/EAAT3 and SLC1A3/EAAT1/GLAST1 are core proteins of the glutamate uptake machinery in astrocytes (Cuellar-Santoyo et al., 2023) and the three mitochondrial carrier family proteins, SLC25A12/Aralar, SLC25A13, and SLC25A22 are related to the glutamate metabolization in the TCA (Table S1, subtitle 3: Transporters and L-Glutamate import; Figure S2D) (Hillen and Heine, 2020). These findings indicated that ADGRV1 potentially interacts with numerous proteins that are important for the astrocyte functions in the nervous system.

Transcriptome analysis reveals differentially expressed genes (DEGs) related to glutamate homeostasis and epilepsy in the hippocampus of Adgrv1/del7TM mice

Next, we performed genome-wide mRNA sequencing from hippocampus tissue dissected from Adgrv1/del7TM and WT mice. The comparison of transcriptomes revealed 80 differentially expressed genes (DEGs) in the hippocampus of Adgrv1/del7TM in relation to WT mice (Table S2). The removal of the non-coding RNAs from the list of DEGs due to incomplete genome annotation (Boivin et al., 2020) resulted in 25 and 31 protein-coding genes being significantly up or down regulated, respectively (Figure 3A, B; Table S2).

Gene set enrichment analysis (GSEA) of the term "*cellular compartment"* showed that DEGs in the hippocampus of Adgrv1/del7TM mice are associated with "*cellular endomembrane system entity*", "*cytoplasmic intracellular vesicle*", "*plasma cell bounded projection*", "*intracellular non-membrane-bounded organelle"* and "*cytoplasm membrane-bounded anatomical structure*" (Figure 3C) (date of analysis: 24.08.2023). GSEA of "*biological function"* showed that DEGs in Adgrv1/del7TM hippocampus are associated with functions related to "*cell signaling*", "*cellular response to stimulus*", "*regulation of biological processes*", "*establishment of nitrogen compound transport*" and "*protein cellular macromolecule localization*" (Figure 3D) (date of analysis: 24.08.2023).

In screens of the Harmonizome 3.0 database (Rouillard et al., 2016) (date of analysis: 22.12.2023) we found 6 DEGs associated with epilepsy diseases in Adgrv1/del7TM hippocampus. Of these genes, 4 were found to be upregulated (*Nudt3*, *Adar*, *Adgrv1*, *Hif3a*) while 2 were downregulated (*Trh*, *Grm4*). Interestingly we found that epilepsy associated genes *Adar*, *Hif3a*, *Trh*, and *Grm4* also play a role in glutamate receptor and metabolism regulation. In addition to those DEGs, we identified *Pcdh17*, *Chrm5*, *Gabra2*, and *Ptpn5* which function as glutamate receptor and metabolism regulatory proteins (Figure 3B).

Transcriptome analysis of human patient-derived cells confirmed DEGs related to glutamate homeostasis and epilepsy

Next, we performed genome-wide mRNA sequencing of dermal fibroblasts of a confirmed USH2C patient and a healthy individual by Illumina platform and pair end reads were mapped and quantified (Figure 4). Our DEG analysis of the transcriptomes revealed a total of 1,319 DEGs (Table S3, subtitle 1: All DEGs of patient vs healthy fibroblasts). By GO term analysis applying the web application of the amigo2 and previously reported epilepsy-associated genes (Macnee et al., 2023) we identified in 87 genes related to "transporter activity" and 63 genes related to "epilepsy associated", respectively (Table S4, subtitle 2: Transporter activity genes, subtitle 3: Epilepsy associated genes). (https://amigo.geneontology.org/amigo) (Figure 4A, B). 24 of these DEGs (15 up-regulated and 9 down-regulated) were identified as being common to genes involved in transporter activity and to genes associated with epilepsy. (Figure 4B, Table S3, subtitle 4: Common in Transporter activity and epilepsy associated gene). For further GSEA analysis, we combined "transporter activity" and "epilepsy associated genes" which was a total number of 125 DEGs. Of these DEGs, 74 genes were up- and 51 genes were downregulated (Figure 4A, S3, Table

S3, subtitle 5: DEGs in epilepsy and transport). A comparison with of these DEGs with those found in the Adgrv1/del7TM hippocampus revealed that the solute carrier proteins *SLC2A1, SLC4A3,* and *SLC19A3* were present as DEGs in both transcriptomes (Figure 4A, B, S3).

We additionally performed GSEA on the DEGs which were detected in the patient fibroblasts. The *cellular compartment* GSEA showed that DEGs are related to "*AMPA ionotropic glutamate complex*", "*neurotransmitter receptor complex*", "*plasma membrane signaling complex*", "*organelle envelope*" and "*nuclear membrane envelope*" (Figure 4C). GSEA of *biological function* showed that DEGs in patient fibroblast are associated with "*calcium response*", "*regulation potassium ion transport*", "*adult cognition locomotory behavior* "*forebrain, hippocampus, limbic and pallium development*" and "*cation monoatomic transporter activity*" (Figure 4D). GSEA of the "*biological function"* subclusters showed that DEGs in patient fibroblast are also related to "*nerve development and neuron migration"* as well as the "*development of the brain regions",* such as the forebrain, hippocampus, and telencephalon (Figure 4D).

Altogether, Adgrv1 deficiency causes the dysregulation of genes related to glutamate homeostasis and epilepsy in mouse hippocampus and patient-derived cells.

Glutamate uptake of primary brain astrocytes depends on Adgrv1 activation

Our omics data analysis suggested that ADGRV1 may play an important role in glutamate homeostasis in hippocampal astrocytes. To confirm the data at a functional level, we accessed glutamate uptake in primary astrocytes *in vitro* using a glutamate uptake assay introduced by (Mahmoud et al., 2019). Primary astrocytes were isolated from Adgrv1/del7TM and WT p0 mice and incubated with either 100 or 200 µM glutamate in a Ca^{2+} containing cell culture medium. Colorimetric analysis of the supernatants demonstrated the dose-dependent reduction in glutamate uptake by Adgrv1/del7TM astrocytes compared to WT controls (Figure 5A).

To follow the uptake of glutamate from the media into the primary astrocytes, we used the genetically encoded glutamate reporter GFAP.iGluSnFR3.v857.GPI (Aggarwal et al., 2023). This glutamate reporter contains a glycosylphosphatidylinositol anchor that allows it to bind to glycosylphosphatidylinositols in biological membranes and thereby to monitor changes in glutamate concentration (Kinoshita and Fujita, 2016). In the first set of experiments, we confirmed that the glutamate reporter activity can be induced in both primary WT and Adgrv1/del7TM astrocytes by the addition of 10 mM glutamate to the culture medium (Figure S4). Next, we activated Adgrv1 using the "Stachel" of ADGRV1, an 11-amino acid peptide SVYAVYARTDN,

which we had previously identified as the tethered agonist of the receptor (Knapp et al., 2022) to the culture medium of GFAP.iGluSnFR3.v857.GPI expressing primary astrocytes. Activation of Adgrv1 by the spike peptide led to an increase in reporter fluorescence in primary WT astrocytes, but not in astrocytes derived from Adgrv1-deficient Adgrv1/del7TM (Figure 5B, C). A control peptide, which consisted of a randomized amino acid sequence and should not activate Adgrv1, did not cause an increase in fluorescence in WT astrocytes (data not shown). Collectively, our data demonstrate that glutamate uptake into primary brain astrocytes depends on the activation of Adgrv1.

The catabolism of internalized glutamate is increased in Adgrv1/del7TM hippocampal astrocytes

Alternative to its detoxification in the glutamate-glutamine cycle, glutamate can be also metabolized in astrocytes by TCA in mitochondria (Nissen et al., 2015). In the TCA, glutamate dehydrogenase (GDH) is the key enzyme, and its activity is a benchmark for glutamate metabolization. Measuring the GDH in cultured astrocytes with a colorimetric assay revealed an almost 1.5-fold increase in GDH activity in Adgrv1/del7TM astrocytes compared to WT astrocytes (Figure 5D).

Expression of glutamine synthetase is reduced in hippocampus of Adgrv1/del7TM mice

Next, we analyzed the protein expression of key components of the glutamate-glutamine cycle in astrocytes of the hippocampal CA1 region: the glutamate transporter GLAST which imports glutamate from the extracellular space (Zhou et al., 2014) and the glutamine synthetase (GS) catalyzes the glutamine synthesis from glutamate in the cell (Papageorgiou et al., 2018) (Figure 6). We immunostained sections through the hippocampal CA1 region of Adgrv1/del7TM and WT mice for GS, GFAP, and DAPI (Figure 6A). Confocal microscopy demonstrated bright immunofluorescence of GS in GFAP-positive astrocytes of WT mice, and a greatly reduced fluorescence in astrocytes of Adgrv1/del7TM mice (Figure 6B). Quantification of anti-GS Western blots of hippocampus reveals a significant decrease in Adgrv1/del7TM mice (Figure 6C). In contrast, we observed only a minor and not significant increase in GLAST expression in the hippocampus of Adgrv1/del7TM neither by immunohistochemistry nor Western blotting (Figure 6D-F).

Adgrv1 affects neurite morphogenesis in neurons

To investigate the effects of Adgrv1 in neurons, we analyzed single neuron cultures from brains of Adgrv1/del7TM and WT mice on day 1 *in vitro* (DIV1) and day 3 *in vitro* (DIV3) by staining for the neuronal marker MAP2 and with DAPI (Figures 7).

Morphological analysis of neurites in fluorescent microscopy images for neurite intersections (Sholl analysis), convex area, and maximal branch length revealed that all parameters were reduced in Adgrv1/del7TM neurons at both DIV1 and DIV3 (Figure 7C, H). All quantification analyses revealed significant differences (Figure 7D, I), except for the maximum branch length measurements in DIV3, which shows only a tendency in reduced length in Adgrv1/del7TM neurons (*p* value: 0.70) (Figure 7J). These findings suggest that Adgrv1 is not only important in astrocyte morphology (Figure 1C-F) but also has an additional significant influence on neuronal morphogenesis.

Astrocyte Adgrv1 affects neurite morphogenesis

Astrocytes cooperate with neurons and support them in a variety of ways to maintain and nurture the neuronal microenvironment and help to control neuronal migration during development (Sidoryk-Wegrzynowicz et al., 2011). To investigate the effects of Adgrv1 in astrocytes on neurons, we analyzed cocultures of primary astrocyte and neurons from brains of Adgrv1/del7TM and WT mice at DIV1 and DIV3 and identified neurons and astrocytes with immunostaining of MAP2 and GFAP, respectively (Figures 8 and 9).

Sholl analysis of the fluorescence images indicated a significant increase in the number of neurite intersections in WT neurons when co-cultured with WT astrocytes at both DIV1 and DIV3, indicating a synergistic effect on neuronal development (Figure 8B, F). In contrast, co-culturing WT neurons with Adgrv1/del7TM astrocytes led to fewer neurite intersections at both stages, with the most pronounced effect at DIV3 (Figure 8B, F). Furthermore, the convex area of neurites in WT neurons was significantly increased by WT astrocytes at DIV1 but not at DIV3, suggesting a temporal influence on neurite morphology (Figure 8C, G). Interestingly, DIV3 cultures with Adgrv1/del7TM astrocytes exhibited a decrease in convex area compared to WT neuron cultures alone, highlighting the impact of Adgrv1 deficiency on neurite development (Figure 8C, G). However, the maximum branch length analysis revealed no significant differences in WT neurons when co-cultured with either WT or Adgrv1/del7TM astrocytes at DIV1 and DIV3 (Figure 8D, H).

Next, we explored the role of astrocyte Adgrv1 expression on Adgrv1-deficient neurons. Sholl analysis revealed a substantial increase in neurite numbers in the presence of WT astrocytes at both DIV1 and DIV3 (Figure 9B, F). Additionally, WT astrocytes significantly increased the convex area of neurites in WT neurons at DIV1, though not at DIV3, indicating a dynamic interplay between astrocytic Adgrv1 expression and neurite morphology (Figures 9C, G). Moreover, maximum branch length analysis of Adgrv1/del7TM neurons showed an initial increase at DIV1 followed by a significant decrease at DIV3 in the presence of WT astrocytes (Figure 9D, H). However, Adgrv1/del7TM astrocytes showed an opposite effect on Adgrv1/del7TM neurons, namely an increase of the number of intersection numbers and of convex area of neurites at DIV1 (Figure 9B, C) but inducing a significant decrease at DIV3 cultures (Figure 9F, G).

In summary, Adgrv1 in astrocytes supports the beneficial role of astrocytes in neurite morphogenesis during neuronal development and the dysfunctions of Adgrv1-deficient astrocytes exacerbate defective neurite morphogenesis in Adgrv1-deficient neurons.

Adgrv1 functions in the astrocyte-neuron crosstalk affecting synaptogenesis

Astrocytes promote synapse formation in a variety of ways (Baldwin and Eroglu, 2017). To determine whether Adgrv1 in astrocytes plays a role in synaptogenesis in neurons, we isolated primary neurons and astrocytes derived from the hippocampus of WT or Adgrv1/del7TM mice and cultured primary neurons alone or together with primary astrocytes, respectively. In DIV14 cultures, we immunostained neurons for homer, a post synaptic density (PSD) marker for excitatory synapses, gephyrin as a PSD marker for inhibitory synapses, and the neurite marker MAP2. This triple labelling allowed us to determine the number of PSD per 100 µm neurite length ~ (synaptic density) and sizes of the PSD puncta (~ synaptic strength) (Holler et al., 2021), and to distinguish between the excitatory and inhibitory synapses in neurites (Figure 10A).

In neuron-only cultures of WT or Adgrv1/del7TM mice, there were no differences in the density of excitatory PSDs (homer puncta) on neurites while the density of inhibitory PSDs (gephyrin puncta) was slightly increased (Figure 10B, C). In co-cultures of WT neurons with astrocytes from either WT and Adgrv1/del7TM mice, the density of synaptic puncta was significantly increased in both excitatory and inhibitory synapses (Figure 10B, C) compared to neuron-only cultures. Co-culturing of Adgrv1/del7TM neurons with both WT and Adgrv1/del7TM astrocytes, respectively, did not affect the inhibitory PSD puncta density on neurites (Figure 10C). However, excitatory PSD puncta density on Adgrv1/del7TM neurites increased to the level of WT

neurites in co-cultures with WT astrocytes but decreased in co-cultures with Adgrv1/del7TM astrocytes (Figure 10B). Our data suggest that Adgrv1 in astrocytes controls the frequency of excitatory synapses on neurites but has only a modest effect on the frequency of inhibitory synapses. This may lead to an imbalance of excitatory-inhibitory (E/I) synapses which has been previously correlated with neurological diseases such as epilepsy (Bonansco and Fuenzalida, 2016).

Next, we measured and quantified the size of the synaptic puncta stained for homer and gephyrin, a feature previously shown to be related with synaptic strength (Holler et al., 2021) (Figure 10D, E). In WT neurons the puncta size for both excitatory and inhibitory PSDs was not affected by co-cultured WT and Adgrv1/del7TM astrocytes. However, in neuron-only cultures, the sizes of the excitatory and inhibitory PSDs were significantly decreased (*p*-value $1.29987e^{-19}$ and $1.79652e^{-18}$, respectively) in Adgrv1/del7TM compared to WT control mice. This was compensated in co-cultures with Adgrv1/del7TM or WT astrocytes but were more prominent by WT astrocytes (Figure 10D, E).

In summary, our data demonstrate that Adgrv1 expression in neurons significantly affects the size of PSDs which correlates with a reduced synaptic strength in Adgrv1-deficient neurons. Furthermore, our data show that the synaptic strength in Adgrv1-deficient neurites increases by the interaction with astrocytes and that Adgrv1 in astrocytes can potentiate this effect.

DISCUSSION

The high expression of ADGRV1 in astrocytes is indicative of its major importance for astrocyte functions which was confirmed by our omics data: Using affinity proteomics, we identified nearly 300 proteins enriched in the proteome of human and mouse astrocytes (Batiuk et al., 2020) as potential interacting proteins of ADGRV1. In addition, transcriptome analyses of mouse hippocampus and human cells deficient for ADGRV1 revealed that numerous genes encoding for proteins with important functions in astrocytes were differentially expressed.

Furthermore, our omics data analysis suggests that ADGRV1 is associated with signaling pathways that are highly specific for astrocytes and essential for their proper function. One of the major functions of astrocytes in the brain is the rapid clearance of excitatory neurotransmitter glutamate from the synaptic cleft after its release from the pre-synapse to prevent glutamate

neurotoxicity (Armbruster et al., 2016; Langer et al., 2017). Strikingly, we identified the glutamate transporters EAAT3 and EAAT1 (GLAST1) as potential interacting partners of ADGRV1 (Zhou et al., 2014; Piepgras et al., 2022). Although we did not find altered protein expression of glutamate transporters in Adgrv1-deficient cells, the interaction of ADGRV1 with these core proteins of the glutamate uptake machinery suggests a role in the regulation of glutamate uptake processes in astrocytes. Indeed, in *in vitro* glutamate uptake assays and by live cell imaging using a glutamate reporter, we found consistently reduced glutamate uptake in primary astrocytes deficient for Adgrv1 confirming that ADGRV1 participates in glutamate uptake in astrocytes. Interestingly, glutamate uptake by astrocytes could be triggered by the synthetic activator mimicking the tethered agonist peptide, (Knapp et al., 2022). This stimulation suggests that glutamate uptake is controlled by the activation of the CTF receptor part of ADGRV1 and is not due to its cell adhesion function. Failure in glutamate uptake by astrocytes and thereby of the clearance of glutamate form the extracellular environment can lead to glutamate toxification in the brain and lead to glia and neuron cell death (Kritis et al., 2015). The toxicity of excess glutamate in the extracellular *milieu* is probably the cause for the astrocyte depletion found in in the hippocampus Adgrv1/del7TM mice.

After uptake by astrocytes, glutamate can be converted into the non-toxic essential amino acid glutamine catalyzed by GS as part of the glutamate-glutamine cycle between astrocytes and neurons (Papageorgiou et al., 2018). Alternatively, glutamate can be also metabolized in astrocytes by the TCA cycle which operates inside the mitochondria (Rose et al., 2020). A balanced interaction of the two pathways is vital for glutamate homeostasis in astrocytes and globally in the brain (Robinson et al., 2020). The identification of potential interacting proteins of ADGRV1 and DEGs in Adgrv1/del7TM mice related to both pathways collectively support a vital role of ADGRV1 in glutamate homeostasis. This role is further supported by the dysregulation of two key enzymes of the two pathways in Adgrv1-deficient astrocytes, namely an increase of the activity of the glutamate dehydrogenase (GDH) in the TCA and the glutamate synthetase (GS) a pivotal enzyme in the glutamate-glutamine cycle.

Interestingly, the increase of the activity of the TCA enzyme GDH is accompanied in Adgrv1-deficient astrocytes by a drastic reduction in the expression of the GS protein, a key enzyme in the glutamate-glutamine cycle. The downregulation of GS in ADGRV1-deficient hippocampal astrocytes is likely due to deficient glutamate uptake, as described in previous studies, leading to accumulation of toxic intracellular glutamate in astrocytes (Trabelsi et al., 2017). Intriguingly, a decrease of GS expression accompanied with an increase of GDH activity was

previously described in patients with myoclonic absence epilepsy with sclerotic hippocampus (D.M. et al., 2005; Bahi-Buisson et al., 2008; Chan et al., 2019) a clinical condition that also occurs in ADGRV1-associated epilepsy (Leng et al., 2022). Overall, our results suggest that ADGRV1 is significantly involved in the control of glutamate homeostasis, which is imbalanced by defects in ADGRV1, which is proven to be disease relevant (Onaolapo and Onaolapo, 2020).

In the brain, ADGRV1 is strongly expressed in neurons, but highest in astrocytes (McMillan and White, 2010) Here, we observed that deficiency of ADGRV1 leads to decreased abundance and altered morphology of astrocytes in the CA1 region of the hippocampus, most likely due to an imbalanced glutamate homeostasis. Corresponding changes in astrocyte morphology and number have been observed in diseases in which astrocytes are known to be involved in the pathogenesis such as acute brain trauma and chronic neuropathies, *e.g.*, Alzheimer's disease, but also in the development of epilepsy (Wu et al., 2021; Hayashi et al., 2022; de Sousa et al., 2023). The increase in branching or convex hull area of astrocytes is thought to be a consequence of the reduced number of cells in the diseased brain due to their exploratory attempts to contact the remaining neurons.

In the present study, we demonstrate that ADGRV1 is not only important for the functions of astrocytes but also of neurons. In developing neurons, the lack of ADGRV1 compromises neurite synaptogenesis. This is consistent with previously found interactions of ADGRV1 with numerous components of the pre- and post-synapse and with molecules important for synaptic signaling and neurotransmitter vesicle cycle (Knapp et al., 2019). The previously identified interactions of ADGRV1 with other synaptic molecules such as latrophillin 2 (ADGRL2) another aGPCR (Anderson et al., 2017), might be vital for synaptic function and synaptogenesis. This hypothesis supports our finding that expression of Adgrv1 in astrocytes is crucial for the size of excitatory and inhibitory synapses and thereby for synaptic strength (Chung et al., 2015; Gürth et al., 2020). Interestingly, the presence of Adgrv1 in astrocytes influences only the abundance of excitatory synapses on neurites, but not of inhibitory synapses. This possibly leads to an imbalance of excitatory-inhibitory (E/I) synapses previously correlated with neurological diseases such as epilepsy (Bonansco and Fuenzalida, 2016).

In addition, we found that neurite branching was significantly reduced in ADGRV1-deficient neurons. This reduction is consistent with the identification of DEGs in patient cells with mutations in *ADGRV1* that encode proteins related to neuronal development and neuronal

migration as well as the development of brain regions. These results demonstrate a possible role of ADGRV1 in neurite outgrowth during neurogenesis previously proposed (Knapp et al., 2022).

The molecular crosstalk between astrocytes and neurons is crucial for the correct development, function, and maintenance of the proper health of the CNS (Allen and Eroglu, 2017; Perez-Catalan et al., 2021). Here, we studied the contribution of ADGRV1 in astrocyte-neuron communication in co-cultures of primary cells from the mouse hippocampus. We found that developing primary WT neurons were supported in their development by the presence WT astrocytes but not by Adgrv1-deficent astrocytes. In addition, the defective development of Adgrv1/del7TM primary neurons was rescued by the presence of WT primary astrocytes but was potentiated by Adgrv1-deficent astrocytes. Our findings suggest the bidirectional interaction of ADGRV1 in astrocyte-neuron communication supportive for the correct development of neurons.

Pathogenic variants of *ADGRV1* cause quite distinct diseases such as human Usher syndrome type 2 leading to hereditary deaf blindness (Weston et al., 2004) and various forms of epilepsy in human and rodents (McMillan and White, 2010; Wang et al., 2015; Myers et al., 2018; Liu et al., 2020; Leng et al., 2022; Zhou et al., 2022). It can be assumed that the loss of the fibrous membrane links formed by the extracellular domain of ADGRV1 cause crucial defects in the sensory cells of the inner ear and eye leading to USH2C (Lefèvre et al., 2008; Maerker et al., 2008). It is possible, but no current evidence suggests, that dysfunctions of ADGRV1 in astrocytes may also contribute to the USH disease in eye and the inner ear links.

The data presented in this paper provides first insights into the molecular and cellular basis underlying epilepsy associated with mutations in *ADGRV1*. Present omics data identified molecules as potential interaction partners of ADGRV1 related to glutamate homeostasis (see above) have been previously also associated with epilepsy (Lechan and Fekete, 2006; Poduri et al., 2013; Falk et al., 2014; Saleh et al., 2020; Sachs et al., 2023). The absence of ADGRV1 from these protein complexes may also result in pathways altered in epilepsy. This is consistent with our finding that DEGs found in the hippocampus of Adgrv1/delTM7 mice and in patient-derived cells with ADGRV1 deficiency have previously been associated with epilepsy. Interestingly, the morphological and physiological alterations in astrocytes were pronounced especially in the CA1 of the hippocampus, a region which is vulnerable to glutamate toxicity (Ouyang et al., 2007), where recently astrocyte loss was related to early epileptogenesis (Wu et al., 2021). Cumulatively, our data support the hypothesis that the molecular origin of ADGRV1-associated epilepsy lies in the

dysfunction of astrocytes in the hippocampus due to impaired glutamate homeostasis and its consequences caused by ADGRV1 deficits.

Conclusion

We show here that ADGRV1 is crucial for the morphology and physiology of hippocampal astrocytes. ADGRV1 deficiency imbalances the glutamate homeostasis possibly leading to glutamate toxification in the cell and neuronal tissue. The resulting consequences presumably lead to impaired neuronal development and to impaired communication between astrocytes and neurons in the brain. These molecular dysfunctions of ADGRV1-deficent astrocytes provide first clues to understanding the pathomechanisms in epilepsy associated with mutations in *ADGRV1* and will be essential in the development of future therapies. Future studies aimed at the physiology of receptor complexes in astrocytes and neurons related to ADGRV1 and the pathways downstream to activated ADGRV1 could assist to defining the precise mechanisms of ADGRV1 functions in the CNS in health and disease. This should also provide further targets for therapies and offer prospects for the future treatment and cure of ADGRV1-related epilepsy.

Acknowledgements

We thank Ulrike Maas, and Yvonne Kerner for excellent technical assistance, and Drs. Filip Maciag for critical discussion of the data. We also thank Kevin Peter Langenberg and Selina Kröll for their support in the analysis of neuron morphology. We thank Dr. Erwin van Wijk for kindly providing patient fibroblasts for the present study.

Supplementary Materials

Table S1. Biological function analysis of astrocyte related proteins in ADGRV1 TAPs and protein annotations. Subtitle 1 shows the astrocytes enriched proteins and their annotations. Subtitle 2 shows biological functions of astrocytes enriched proteins. Subtitle 3 shows transporter activity and L-glutamate import related proteins.

Table S2. DEGs in WT and Adgrv1/del7TM mouse hippocampi.

Table S3. The result of RNAseq analysis in fibroblast derived from patient. Subtitle 1 shows DEGs in patient-derived fibroblast. Subtitle 2 shows transporter activity genes found in patient derived fibroblasts. Subtitle 3 shows epilepsy associated genes DEGs found in patient fibroblasts. Subtitle 4 indicates common DEGs in transporter activity and epilepsy associated genes. Subtitle 5 shows total 126 DEGs found in transporter activity and epilepsy associated genes.

Funding

This work was supported by the Deutsche Forschungsgemeinschaft (DFG): FOR 2149 Elucidation of Adhesion-GPCR signaling, project number 246212759 (UW) and SPP2127 - Gene and Cell based therapies to counteract neuroretinal degeneration, project numbers: 399443882 (KNW), 399487434 (UW), The Foundation Fighting Blindness (FFB) PPA-0717-0719-RAD (UW), FAUN Stiftung (Nuremberg), and inneruniversitäre Forschungsförderung („Stufe I“) of the Johannes Gutenberg University Mainz.

Institutional Review Board Statement: The use of mice in research was approved by the German regulation authority for the use of animals in research, the district administration Mainz-Bingen, 8341a/177-5865-§11 ZVTE, 30.04.2014.

Data availability statement

Full Western blots presented in the study are included in the article/Supplementary Material. TAP data have been deposited to the ProteomeXchange Consortium via the PRIDE partner repository with the dataset identifier PXD042629. Codes for the RNA-sequencing analysis can be found at https://github.com/LabWolfrum.

Author contributions

All authors contributed to the article and approved the submitted version. B.E.G. conducted most of the experiments, analyzed tandem affinity purification data sets, and prepared all the figures for publication. J.L. helped with the isolation of hippocampus RNA samples and contributed to TAP data analysis. M.Z. performed the analysis of RNA sequencing. B.E.G. and U.W. conceptualized the study and wrote the manuscript. K.N.-W. supervised M.Z., contributed with patient-derived fibroblast cultures, discussing data and writing.

Competing Interests

The authors declare that the research was conducted in the absence of any commercial or financial relationships that could be construed as a potential conflict of interest.

References

Aggarwal A, Liu R, Chen Y, Ralowicz AJ, Bergerson SJ, Tomaska F, Mohar B, Hanson TL, Hasseman JP, Reep D, Tsegaye G, Yao P, Ji X, Kloos M, Walpita D, Patel R, Mohr MA, Tillberg PW, Looger LL, Marvin JS, Hoppa MB, Konnerth A, Kleinfeld D, Schreiter ER, Podgorski K. 2023. Glutamate indicators with improved activation kinetics and localization for imaging synaptic transmission. Nat Methods 20:925–934.

Alcoreza OB, Patel DC, Tewari BP, Sontheimer H. 2021. Dysregulation of Ambient Glutamate and Glutamate Receptors in Epilepsy: An Astrocytic Perspective. Front Neurol 12.

Allen NJ, Eroglu C. 2017. Cell Biology of Astrocyte-Synapse Interactions. Neuron 96:697–708.

Anderson GR, Maxeiner S, Sando R, Tsetsenis T, Malenka RC, Südhof TC. 2017. Postsynaptic adhesion GPCR latrophilin-2 mediates target recognition in entorhinal-hippocampal synapse assembly. J Cell Biol 216:3831–3846.

Arévalo AP, Lutz AK, Atanasova E, Boeckers TM. 2022. Trans-cardiac perfusion of neonatal mice and immunofluorescence of the whole body as a method to study nervous system development. PLoS One 17:1–8.

Arganda-Carreras I, Fernández-González R, Muñoz-Barrutia A, Ortiz-De-Solorzano C. 2010. 3D reconstruction of histological sections: Application to mammary gland tissue. Microsc Res Tech 73:1019–1029.

Armbruster M, Hanson E, Dulla CG. 2016. Glutamate clearance is locally modulated by presynaptic neuronal activity in the cerebral cortex. J Neurosci 36:10404–10415.

Bahi-Buisson N, El Sabbagh S, Soufflet C, Escande F, Boddaert N, Valayannopoulos V, Bellané-Chantelot C, Lascelles K, Dulac O, Plouin P, de Lonlay P. 2008. Myoclonic absence epilepsy with photosensitivity and a gain of function mutation in glutamate dehydrogenase. Seizure 17:658–664.

Baldwin KT, Eroglu C. 2017. Molecular mechanisms of astrocyte-induced synaptogenesis. Curr Opin Neurobiol 45:113–120.

Batiuk MY, Martirosyan A, Wahis J, de Vin F, Marneffe C, Kusserow C, Koeppen J, Viana JF, Oliveira JF, Voet T, Ponting CP, Belgard TG, Holt MG. 2020. Identification of region-specific astrocyte subtypes at single cell resolution. Nat Commun 11:1220.

Bindea G, Mlecnik B, Hackl H, Charoentong P, Tosolini M, Kirilovsky A, Fridman WH, Pagès F, Trajanoski Z, Galon J. 2009. ClueGO: A Cytoscape plug-in to decipher functionally grouped gene ontology and pathway annotation networks. Bioinformatics 25:1091–1093.

Boivin V, Reulet G, Boisvert O, Couture S, Elela SA, Scott MS. 2020. Reducing the structure bias of RNA-Seq reveals a large number of non-annotated non-coding RNA. Nucleic Acids Res 48:2271–2286.

Bolger AM, Lohse M, Usadel B. 2014. Trimmomatic: A flexible trimmer for Illumina sequence data. Bioinformatics 30:2114–2120.

Bonansco C, Fuenzalida M. 2016. Plasticity of hippocampal excitatory-inhibitory balance: Missing the synaptic control in the epileptic brain. Neural Plast 2016.

Bou Assi E, Nguyen DK, Rihana S, Sawan M. 2017. Towards accurate prediction of epileptic seizures: A review. Biomed Signal Process Control 34:144–157.

Broadhead MJ, Bonthron C, Waddington J, Smith W V., Lopez MF, Burley S, Valli J, Zhu F, Komiyama NH, Smith C, Grant SGN, Miles GB. 2022. Selective vulnerability of tripartite synapses in amyotrophic lateral sclerosis. Acta Neuropathol 143:471–486.

Chan F, Lax NZ, Voss CM, Aldana BI, Whyte S, Jenkins A, Nicholson C, Nichols S, Tilley E, Powell Z, Waagepetersen HS, Davies CH, Turnbull DM, Cunningham MO. 2019. The role of astrocytes in seizure generation: Insights from a novel in vitro seizure model based on mitochondrial dysfunction. Brain 142:391–411.

Chong D, Jones NC, Schittenhelm RB, Anderson A, Casillas-Espinosa PM. 2023. Multi-omics integration and epilepsy: Towards a better understanding of biological mechanisms. Prog Neurobiol 227:102480.

Chung W, Allen NJ, Eroglu C. 2015. Astrocytes Control Synapse Formation, Function, and Elimination. Cold Spring Harb Perspect Biol 7:a020370.

Cuellar-Santoyo AO, Ruiz-Rodríguez VM, Mares-Barbosa TB, Patrón-Soberano A, Howe AG, Portales-Pérez DP, Miquelajáuregui Graf A, Estrada-Sánchez AM. 2023. Revealing the contribution of astrocytes to glutamatergic neuronal transmission. Front Cell Neurosci 16:1–15.

Raizen DM, Brooks-Kayal A, Steinkrauss L, Tennekoon GI, Stanley CA, Kelly A 2005. Central nervous system hyperexcitability associated with glutamate dehydrogenase gain of function mutations. J Pediatr 146:388–394.

Dzyubenko E, Rozenberg A, Hermann DM, Faissner A. 2016. Colocalization of synapse marker proteins evaluated by STED-microscopy reveals patterns of neuronal synapse distribution in vitro. J Neurosci Methods 273:149–159.

Falk MJ, Li D, Gai X, McCormick E, Place E, Lasorsa FM, Otieno FG, Hou C, Kim CE, Abdel-Magid N, Vazquez L, Mentch FD, Chiavacci R, Liang J, Liu X, Jiang H, Giannuzzi G, Marsh ED, Yiran G, Tian L, Palmieri F, Hakonarson H. 2014. AGC1 Deficiency Causes Infantile Epilepsy, Abnormal Myelination, and Reduced N-Acetylaspartate. In: JIMD Reports. Vol. 4. . p 77–85.

Ferreira TA, Blackman A V., Oyrer J, Jayabal S, Chung AJ, Watt AJ, Sjöström PJ, Van Meyel DJ. 2014. Neuronal morphometry directly from bitmap images. Nat Methods 11:982–984.

Gage GJ, Kipke DR, Shain W. 2012. Whole animal perfusion fixation for rodents. J Vis Exp:1–9.

González-Reyes RE, Nava-Mesa MO, Vargas-Sánchez K, Ariza-Salamanca D, Mora-Muñoz L. 2017. Involvement of astrocytes in Alzheimer's disease from a neuroinflammatory and oxidative stress perspective. Front Mol Neurosci 10:1–20.

Grüning B, Chilton J, Köster J, Dale R, Soranzo N, van den Beek M, Goecks J, Backofen R, Nekrutenko A, Taylor J. 2018. Practical Computational Reproducibility in the Life Sciences. Cell Syst 6:631–635.

Güler BE, Krzysko J, Wolfrum U. 2021. Isolation and culturing of primary mouse astrocytes for the analysis of focal adhesion dynamics. STAR Protoc 2.

Güler BE, Linnert J, Wolfrum U. 2023a. Monitoring paxillin in astrocytes reveals the significance of the adhesion GPCR VLGR1/ADGRV1 for focal adhesion assembly. Basic Clin Pharmacol Toxicol:1–12.

Güler BE, Linnert J, Wolfrum U. 2023b. Monitoring paxillin in astrocytes reveals the significance of the adhesion GPCR VLGR1/ADGRV1 for focal adhesion assembly. Basic Clin Pharmacol Toxicol:1–12.

Gürth CM, Dankovich TM, Rizzoli SO, D'Este E. 2020. Synaptic activity and strength are reflected by changes in the post-synaptic secretory pathway. Sci Rep 10:1–13.

Hamann J, Aust G, Araç D, Engel FB, Formstone C, Fredriksson R, Hall RA, Harty BL, Kirchhoff C, Knapp B, Krishnan A, Liebscher I, Lin HH, Martinelli DC, Monk KR, Peeters MC, Piao X, Prömel S, Schöneberg T, Schwartz TW, Singer K, Stacey M, Ushkaryov YA, Vallon M, Wolfrum U, Wright MW, Xu L, Langenhan T, Schiöth HB. 2015. International union of basic and clinical pharmacology. XCIV. adhesion G protein-coupled receptors. Pharmacol Rev 67:338–367.

Hayashi MK, Sato K, Sekino Y. 2022. Neurons Induce Tiled Astrocytes with Branches That Avoid Each Other. Int J Mol Sci 23.

Higashi K, Fujita A, Inanobe A, Tanemoto M, Doi K, Kubo T, Kurachi Y. 2001. An inwardly rectifying K+ channel, Kir4.1, expressed in astrocytes surrounds synapses and blood vessels in brain. Am J Physiol Cell Physiol 281:922–931.

Hillen AEJ, Heine VM. 2020. Glutamate Carrier Involvement in Mitochondrial Dysfunctioning in the Brain White Matter. Front Mol Biosci 7:1–8.

Holler S, Köstinger G, Martin KAC, Schuhknecht GFP, Stratford KJ. 2021. Structure and function of a neocortical synapse. Nature 591:111–116.

Ji T, Downs AW, Dorris L, Zhong N. 2023. De novo ADGRV1 variant in a patient with ictal asystole provides novel clues for increased risk of SUDEP. Acta Epileptologica 5.

Johannesen KM, Tümer Z, Weckhuysen S, Barakat TS, Bayat A. 2023. Solving the unsolved genetic epilepsies: Current and future perspectives. Epilepsia 64:3143–3154.

Kim D, Paggi JM, Park C, Bennett C, Salzberg SL. 2019. Graph-based genome alignment and genotyping with HISAT2 and HISAT-genotype. Nat Biotechnol 37:907–915.

Kinoshita T, Fujita M. 2016. Biosynthesis of GPI-anchored proteins: Special emphasis on GPI lipid remodeling. J Lipid Res 57:6–24.

Knapp B, Roedig J, Boldt K, Krzysko J, Horn N, Ueffing M, Wolfrum U. 2019. Affinity proteomics identifies novel functional modules related to adhesion GPCRs. Ann N Y Acad Sci 1456:144–167.

Knapp B, Roedig J, Roedig H, Krzysko J, Horn N, Güler BE, Kusuluri DK, Yildirim A, Boldt K, Ueffing M, Liebscher I, Wolfrum U. 2022. Affinity Proteomics Identifies Interaction Partners and Defines Novel Insights into the Function of the Adhesion GPCR VLGR1/ADGRV1. Molecules 27.

Kritis AA, Stamoula EG, Paniskaki KA, Vavilis TD. 2015. Researching glutamate – induced cytotoxicity in different cell lines: A comparative/collective analysis/study. Front Cell Neurosci 9:1–18.

Krzysko J, Maciag F, Mertens A, Güler BE, Linnert J, Boldt K, Ueffing M, Nagel-Wolfrum K, Heine M, Wolfrum U. 2022. The Adhesion GPCR VLGR1/ADGRV1 Regulates the Ca2+ Homeostasis at Mitochondria-Associated ER Membranes. Cells 11:1–20.

Kusuluri DK, Güler BE, Knapp B, Horn N, Boldt K, Ueffing M, Aust G, Wolfrum U. 2021. Adhesion G protein-coupled receptor VLGR1/ADGRV1 regulates cell spreading and migration by mechanosensing at focal adhesions. iScience 24.

Langenhan T. 2020. Adhesion G protein–coupled receptors—Candidate metabotropic mechanosensors and novel drug targets. Basic Clin Pharmacol Toxicol 126:5–16.

Langer J, Gerkau NJ, Derouiche A, Kleinhans C, Moshrefi-Ravasdjani B, Fredrich M, Kafitz KW, Seifert G, Steinhäuser C, Rose CR. 2017. Rapid sodium signaling couples glutamate uptake to breakdown of ATP in perivascular astrocyte endfeet. Glia 65:293–308.

Lechan RM, Fekete C. 2006. Chapter 12: The TRH neuron: a hypothalamic integrator of energy metabolism. Prog Brain Res 153:209–235.

Lefèvre G, Michel V, Weil D, Lepelletier L, Bizard E, Wolfrum U, Hardelin JP, Petit C. 2008. A core cochlear phenotype in USH1 mouse mutants implicates fibrous links of the hair bundle in its cohesion, orientation and differential growth. Development 135:1427–1437.

Leng X, Zhang T, Guan Y, Tang M. 2022. Genotype and phenotype analysis of epilepsy caused by ADGRV1 mutations in Chinese children. Seizure 103:108–114.

Li H, Handsaker B, Wysoker A, Fennell T, Ruan J, Homer N, Marth G, Abecasis G, Durbin R. 2009. The Sequence Alignment/Map format and SAMtools. Bioinformatics 25:2078–2079.

Liao Y, Smyth GK, Shi W. 2014. FeatureCounts: An efficient general purpose program for assigning sequence reads to genomic features. Bioinformatics 30:923–930.

Liu JYW, Dzurova N, Al-Kaaby B, Mills K, Sisodiya SM, Thom M. 2020. Granule Cell Dispersion in Human Temporal Lobe Epilepsy: Proteomics Investigation of Neurodevelopmental Migratory Pathways. Front Cell Neurosci 14.

Love MI, Huber W, Anders S. 2014. Moderated estimation of fold change and dispersion for RNA-seq data with DESeq2. Genome Biol 15:1–21.

Maerker T, van Wijk E, Overlack N, Kersten FFJ, Mcgee J, Goldmann T, Sehn E, Roepman R, Walsh EJ, Kremer H, Wolfrum U. 2008. A novel Usher protein network at the periciliary reloading point between molecular transport machineries in vertebrate photoreceptor cells. Hum Mol Genet 17:71–86.

Mahmoud S, Gharagozloo M, Simard C, Amrani A, Gris D. 2019. NLRX1 enhances glutamate uptake and inhibits glutamate release by astrocytes. Cells 8:1–16.

Mata G, Heras J, Morales M, Romero A, Rubio J. 2016. SynapCountJ: A tool for analyzing synaptic densities in neurons. BIOIMAGING 2016 - 3rd International Conference on Bioimaging, Proceedings; Part of 9th International Joint Conference on Biomedical Engineering Systems and Technologies, BIOSTEC 2016:25–31.

McMillan DR, White PC. 2004. Loss of the transmembrane and cytoplasmic domains of the very large G-protein-coupled receptor-1 (VLGR1 or Mass1) causes audiogenic seizures in mice. Mol Cell Neurosci 26:322–329.

McMillan DR, White PC. 2010. Studies on the very large G protein-coupled receptor: from initial discovery to determining its role in sensorineural deafness in higher animals. Adv Exp Med Biol 706:76–86.

Michalski N, Michel V, Bahloul A, Lefèvre G, Barral J, Yagi H, Chardenoux S, Weil D, Martin P, Hardelin JP, Sato M, Petit C. 2007. Molecular characterization of the ankle-link complex in cochlear hair cells and its role in the hair bundle functioning. Journal of Neuroscience 27:6478–6488.

Michinaga S, Koyama Y. 2019. Dual roles of astrocyte-derived factors in regulation of blood-brain barrier function after brain damage. Int J Mol Sci 20:1–22.

Mölder F, Jablonski KP, Letcher B, Hall MB, Tomkins-Tinch CH, Sochat V, Forster J, Lee S, Twardziok SO, Kanitz A, Wilm A, Holtgrewe M, Rahmann S, Nahnsen S, Köster J. 2021. Sustainable data analysis with Snakemake [version 2; peer review: 2 approved]. F1000Res 10:1–29.

Myers KA, Nasioulas S, Boys A, McMahon JM, Slater H, Lockhart P, Sart D du, Scheffer IE. 2018a. ADGRV1 is implicated in myoclonic epilepsy. Epilepsia 59:381–388.

Nissen JD, Pajęcka K, Stridh MH, Skytt DM, Waagepetersen HS. 2015. Dysfunctional TCA-Cycle Metabolism in Glutamate Dehydrogenase Deficient Astrocytes. Glia 63:2313–2326.

Onaolapo AY, Onaolapo OJ. 2020. Peripheral and Central Glutamate Dyshomeostasis in Neurodegenerative Disorders. Curr Neuropharmacol 19:1069–1089.

Ouyang YB, Voloboueva LA, Xu LJ, Giffard RG. 2007. Selective dysfunction of hippocampal CA1 astrocytes contributes to delayed neuronal damage after transient forebrain ischemia. Journal of Neuroscience 27:4253–4260.

Papageorgiou IE, Valous NA, Lahrmann B, Janova H, Klaft Z, Koch A, Schneider UC, Vajkoczy P, Heppner FL, Grabe N, Halama N, Heinemann U, Kann O. 2018. Astrocytic glutamine synthetase is expressed in the neuronal somatic layers and down-regulated proportionally to neuronal loss in the human epileptic hippocampus. Glia 66:920–933.

Perea G, Navarrete M, Araque A. 2009. Tripartite synapses: astrocytes process and control synaptic information. Trends Neurosci 32:421–431.

Perez-Catalan NA, Doe CQ, Ackerman SD. 2021. The role of astrocyte-mediated plasticity in neural circuit development and function. Neural Dev 16:1–14.

Piepgras J, Rohrbeck A, Just I, Bittner S, Ahnert-Hilger G, Höltje M. 2022. Enhancement of Phosphorylation and Transport Activity of the Neuronal Glutamate Transporter Excitatory Amino Acid Transporter 3 by C3bot and a 26mer C3bot Peptide. Front Cell Neurosci 16:1–14.

Poduri A, Heinzen EL, Chitsazzadeh V, Lasorsa FM, Elhosary PC, LaCoursiere CM, Martin E, Yuskaitis CJ, Hill RS, Atabay KD, Barry B, Partlow JN, Bashiri FA, Zeidan RM, Elmalik SA, Kabiraj MMU, Kothare S, Stödberg T, McTague A, Kurian MA, Scheffer IE, Barkovich AJ, Palmieri F, Salih MA, Walsh CA. 2013. SLC25A22 is a novel gene for migrating partial seizures in infancy. Ann Neurol 74:873–882.

Robinson MB, Lee ML, DaSilva S. 2020. Glutamate Transporters and Mitochondria: Signaling, Co-compartmentalization, Functional Coupling, and Future Directions. Neurochem Res 45:526–540.

Rose CR, Felix L, Zeug A, Dietrich D, Reiner A, Henneberger C. 2018. Astroglial glutamate signaling and uptake in the hippocampus. Front Mol Neurosci 10:1–20.

Rose J, Brian C, Pappa A, Panayiotidis MI, Franco R. 2020. Mitochondrial Metabolism in Astrocytes Regulates Brain Bioenergetics, Neurotransmission and Redox Balance. Front Neurosci 14:1–20.

Rouillard AD, Gundersen GW, Fernandez NF, Wang Z, Monteiro CD, McDermott MG, Ma'ayan A. 2016. The harmonizome: a collection of processed datasets gathered to serve and mine knowledge about genes and proteins. Database (Oxford) 2016:1–16.

Sachs N, Wechsberg O, Landau YE, Krause I, Elgali II, Darawshe M, Shomron N, Lidzbarsky G, Orenstein N. 2023. A novel SLC25A13 gene splice site variant causes Citrin deficiency in an infant. Gene 874:147483.

Saleh M, Helmi M, Yacop B. 2020. A Novel Nonsense Gene Variant Responsible for Early Infantile Epileptic Encephalopathy Type 39: Case Report. Pak J Biol Sci 23:973–976.

Sidoryk-Wegrzynowicz M, Wegrzynowicz M, Lee E, Bowman AB, Aschner M. 2011. Role of Astrocytes in Brain Function and Disease. Toxicol Pathol 39:115–123.

de Sousa DMB, Benedetti A, Altendorfer B, Mrowetz H, Unger MS, Schallmoser K, Aigner L, Kniewallner KM. 2023. Immune-mediated platelet depletion augments Alzheimer's disease neuropathological hallmarks in APP-PS1 mice. Aging 15:630–649.

Steinhäuser C, Seifert G, Bedner P. 2012. Astrocyte dysfunction in temporal lobe epilepsy: K + channels and gap junction coupling. Glia 60:1192–1202.

Szklarczyk D, Franceschini A, Wyder S, Forslund K, Heller D, Huerta-Cepas J, Simonovic M, Roth A, Santos A, Tsafou KP, Kuhn M, Bork P, Jensen LJ, Von Mering C. 2015. STRING v10: Protein-protein interaction networks, integrated over the tree of life. Nucleic Acids Res 43:D447–D452.

Trabelsi Y, Amri M, Becq H, Molinari F, Aniksztejn L. 2017. The conversion of glutamate by glutamine synthase in neocortical astrocytes from juvenile rat is important to limit glutamate spillover and peri/extrasynaptic activation of NMDA receptors. Glia 65:401–415.

Wang Y, Fan X, Zhang W, Zhang C, Wang J, Jiang T, Wang L. 2015. Deficiency of very large G-protein-coupled receptor-1 is a risk factor of tumor-related epilepsy: a whole transcriptome sequencing analysis. J Neurooncol 121:609–616.

Weston MD, Luijendijk MWJ, Humphrey KD, Möller C, Kimberling WJ. 2004. Mutations in the VLGR1 Gene Implicate G-Protein Signaling in the Pathogenesis of Usher Syndrome Type II. Am J Hum Genet 74:357–366.

Wingett SW, Andrews S. 2018. Fastq screen: A tool for multi-genome mapping and quality control. F1000Res 7:1–14.

Wolfrum U. 1991. Distribution of F-actin in the compound eye of the blowfly, Calliphora erythrocephala (Diptera, Insecta). Cell Tissue Res 263:399–403.

Wu Z, Deshpande T, Henning L, Bedner P, Seifert G, Steinhäuser C. 2021. Cell death of hippocampal CA1 astrocytes during early epileptogenesis. Epilepsia 62:1569–1583.

Young K, Morrison H. 2018. Quantifying microglia morphology from photomicrographs of immunohistochemistry prepared tissue using imagej. JOVE 2018:1–9.

Zhang Y, Sloan SA, Clarke LE, Caneda C, Plaza CA, Blumenthal PD, Vogel H, Steinberg GK, Edwards MSB, Li G, Duncan JA, Cheshier SH, Shuer LM, Chang EF, Grant GA, Gephart MGH, Barres BA. 2016. Purification and Characterization of Progenitor and Mature Human Astrocytes Reveals Transcriptional and Functional Differences with Mouse. Neuron 89:37–53.

Zhou P, Meng H, Liang X, Lei X, Zhang J, Bian W, He N, Lin Z, Song X, Zhu W, Hu B, Li B, Yan L, Tang B, Su T, Liu H, Mao Y, Zhai Q, Yi Y. 2022. ADGRV1 Variants in Febrile Seizures/Epilepsy With Antecedent Febrile Seizures and Their Associations With Audio-Visual Abnormalities. Front Mol Neurosci 15.

Zhou Y, Wang X, Tzingounis A V., Danbolt NC, Larsson HP. 2014. EAAT2 (GLT-1; slc1a2) glutamate transporters reconstituted in liposomes argues against heteroexchange being substantially faster than net uptake. Journal of Neuroscience 34:13472–13485.

Figures and Legends

Figure 1

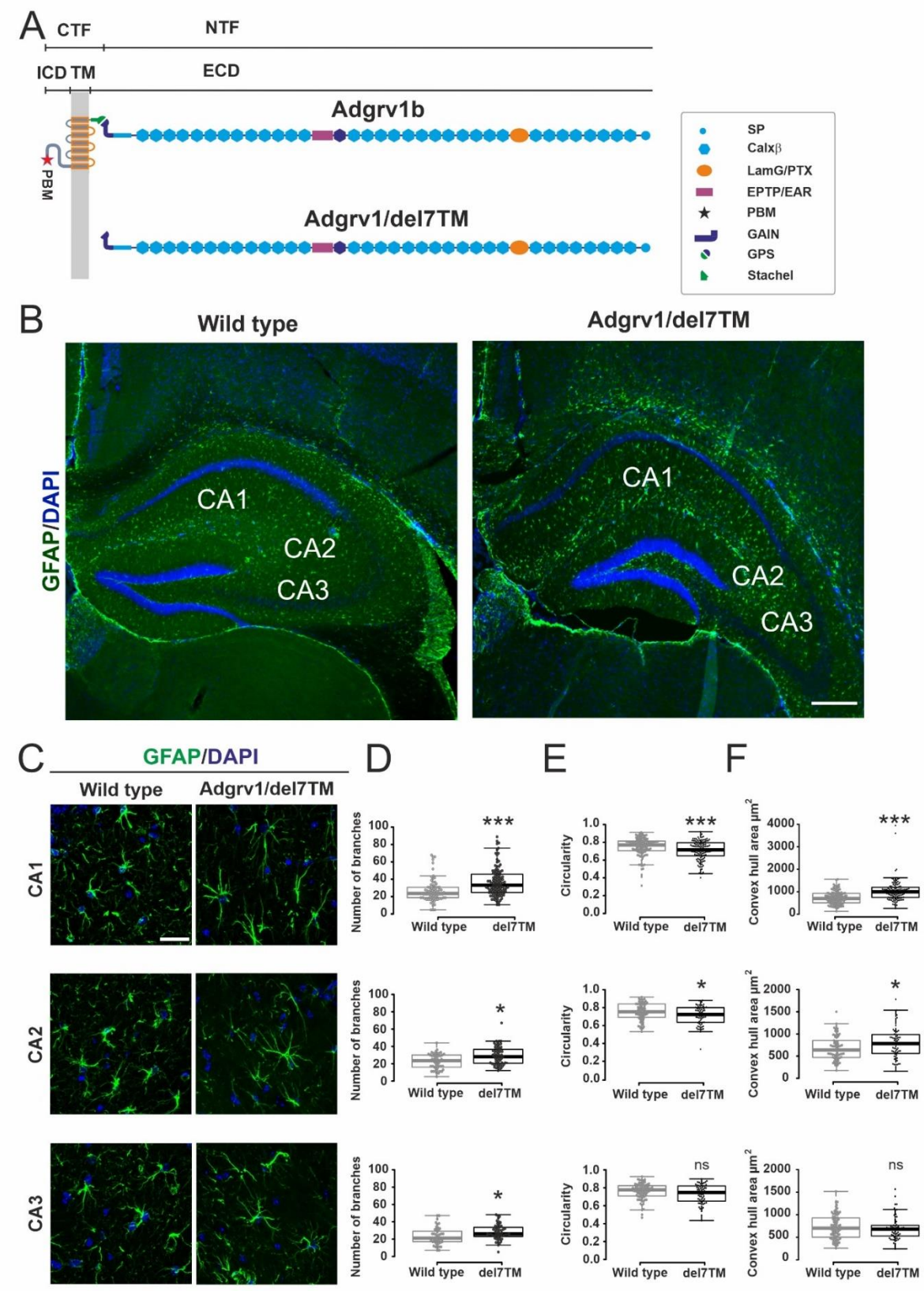

Figure 1. Morphological analysis reveals differences between astrocytes in WT and Adgrv1/del7TM mouse hippocampi. (A) Domain structures of ADGRV1 full length and Adgrv1/del7TM proteins. The cleavage of the full-length molecule from the highly conserved GPCR proteolytic site (GPS) in the GAIN (autoproteolysis-inducing) domain results in relative short C-terminal fragment (CTF) which contains 7-transmembrane (7TM) and intracellular domain (ICD) and extra-large N-terminal fragment (NTF). Extra-large N-terminal fragment contains calcium binding Calxß repeats, seven epilepsy-associated/Epimptin like (EAR/EPTP) repeats, and pentaxin/laminin G-like domain (Lamg/PTX). Adgrv1/del7TM mice carry a nonsense mutation in V2260* which results in STOP codon and leads to deletion 7TM and ICD domains. **(B)** Overview of hippocampal sections from WT and Adgrv1/del7TM hippocampus through the CA (*Cornu ammonis*) 1, CA2 and CA3 subregions of the hippocampus stained for GFAP and for nuclear DNA by DAPI. **(C)** Anti-GFAP stained astrocytes in the three different CA1-3 regions of the hippocampus and the quantification of **(D)** branching, **(E)** circularity and **(F)** convex hull areas. n = 3 per mouse group, 3 continuous sections were analysed. In total 150-160 cells from CA1, 80-85 cells from CA2 and 75-85 cells from CA3 were used for the quantification. Scale bar: 25 µm. Statistics: two-tailed Student´s t test; *$p \leq 0.05$, **$p \leq 0.01$, ***$p \leq 0.001$.

Figure 2

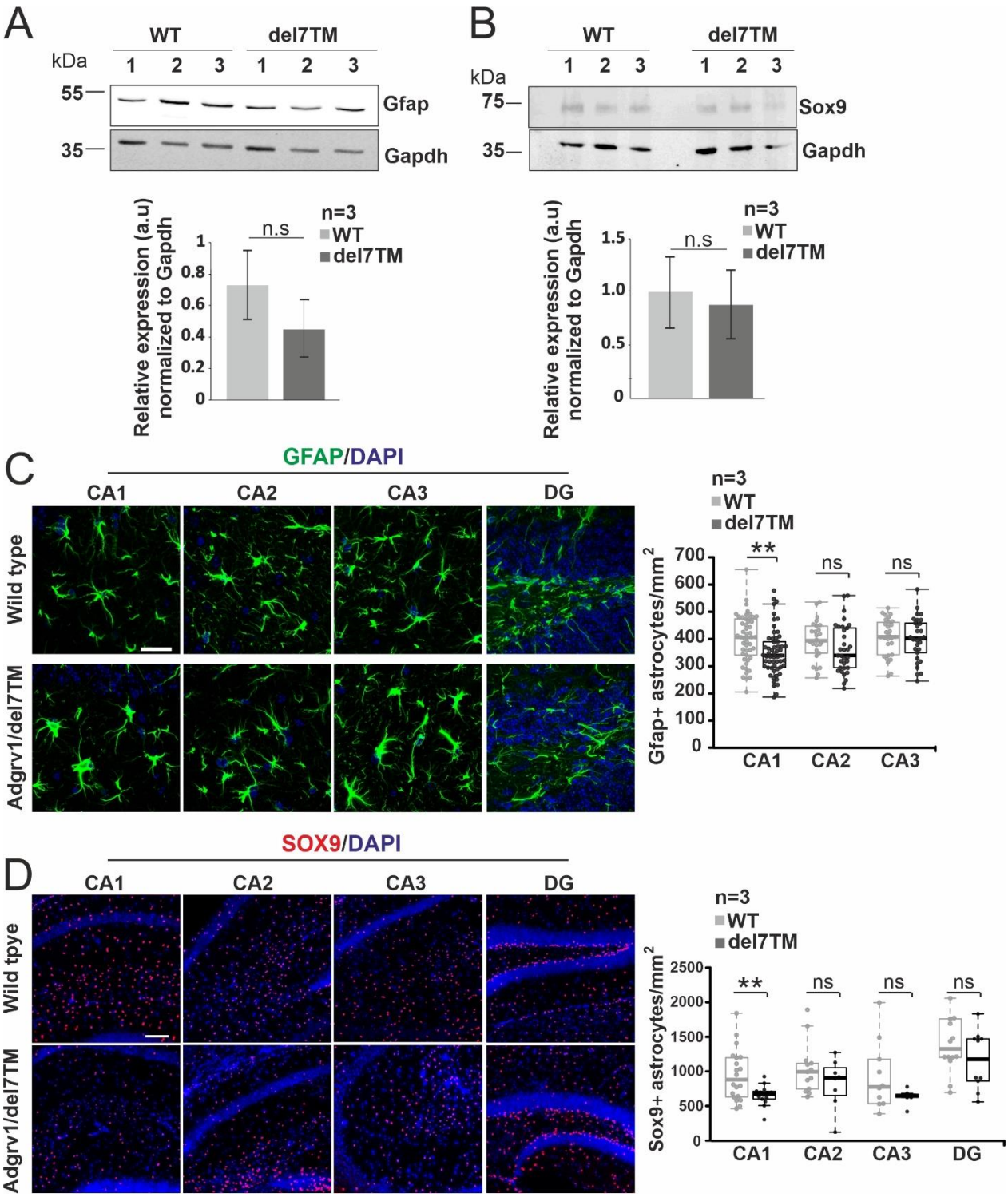

Figure 2. Analysis of the abundance of astrocytes in the hippocampus of Adgrv1/del7TM and wild type mice. (A, B) Quantitative Western blot analyses of the astrocyte marker proteins GFAP **(A)** and SOX9 **(B)** demonstrate the decrease of the expression of both proteins in the hippocampus of Adgrv1/del7TM mice. **(C, D)** Immunofluorescence staining of GFAP **(C)** and SOX9 **(D)**, counterstained by DAPI for nuclear DNA in cryosections through the hippocampus of Adrgv1/del7TM and WT control mice. Quantification of GFAP-positive and SOX9-positive astrocytes revealed the significant decrease in the number of astrocytes only in the hippocampus CA1 region of Adgrv1/del7TM mouse compared to WT. n = 3 per mice group, 3 continuous sections were analysed. Scale bars: C: 25 µm; D: 200 µm. Statistical evaluation by two-tailed Student´s t test; *$p \leq 0.05$, **$p \leq 0.01$, ***$p \leq 0.001$.

Figure 3.

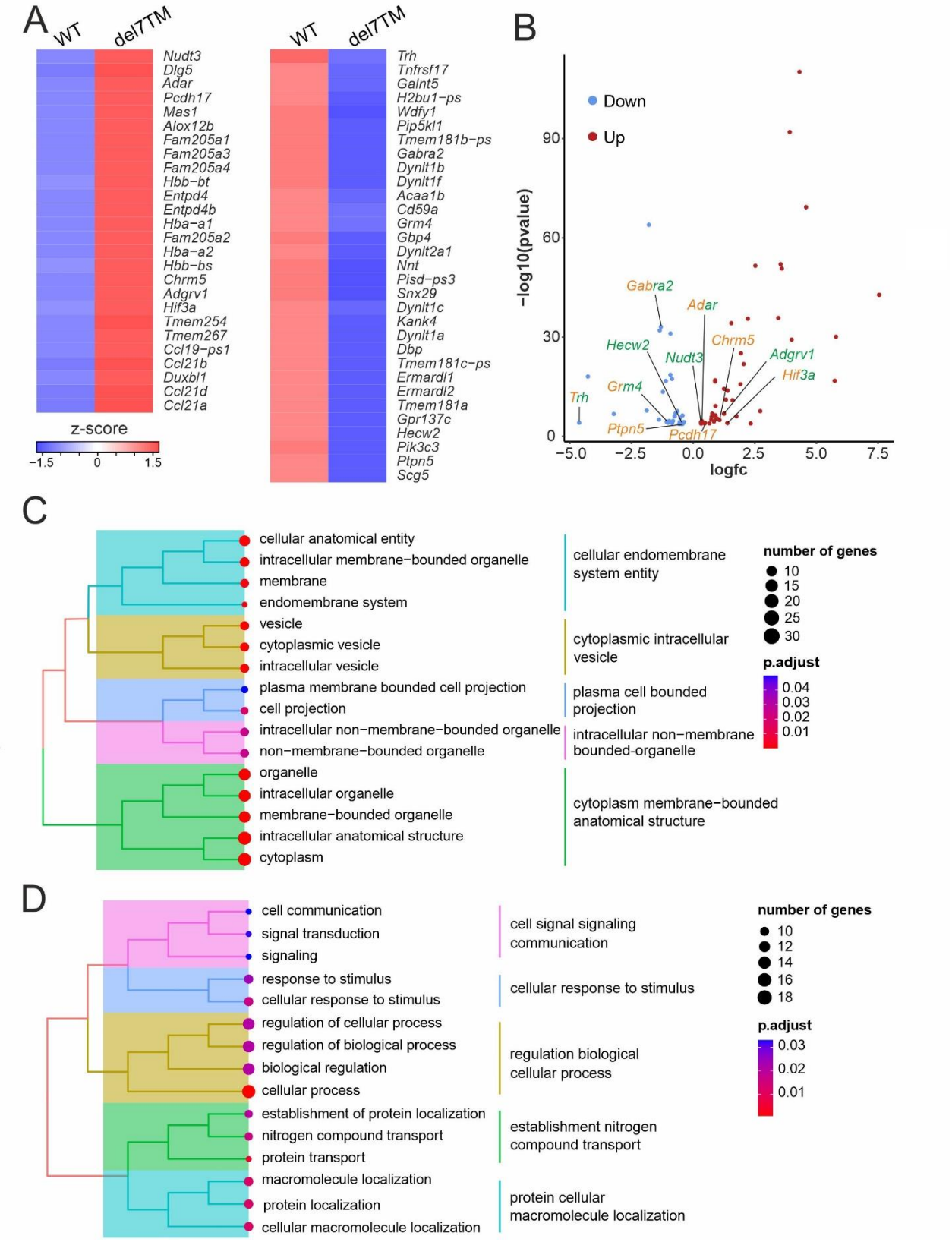

Figure 3. Transcriptome analysis of the hippocampus of Adgrv1/del7TM and WT mice. (A) Heatmap of differentially expressed genes (DEG) in the hippocampus of wild type control (WT) and Adgrv1/del7TM (del7TM) mice. Red, upregulated, and blue, downregulated genes in Adgrv1/del7TM compared to WT. Only adjusted p-values less than 0.05 are shown. **(B)** Volcano plot of DEGs associated to epilepsy (green) and related to transporter activity (orange) in the hippocampus Adgrv1/del7TM mice. **(C)** Gene set enrichment (GSE) analysis for the biological function of the DEGs shown in clusters. **(D)** GSE for the cellular compartment analysis of DEGs. *n*=3 biological replicates for WT and *n*=2 biological replicates for del7TM.

Figure 4.

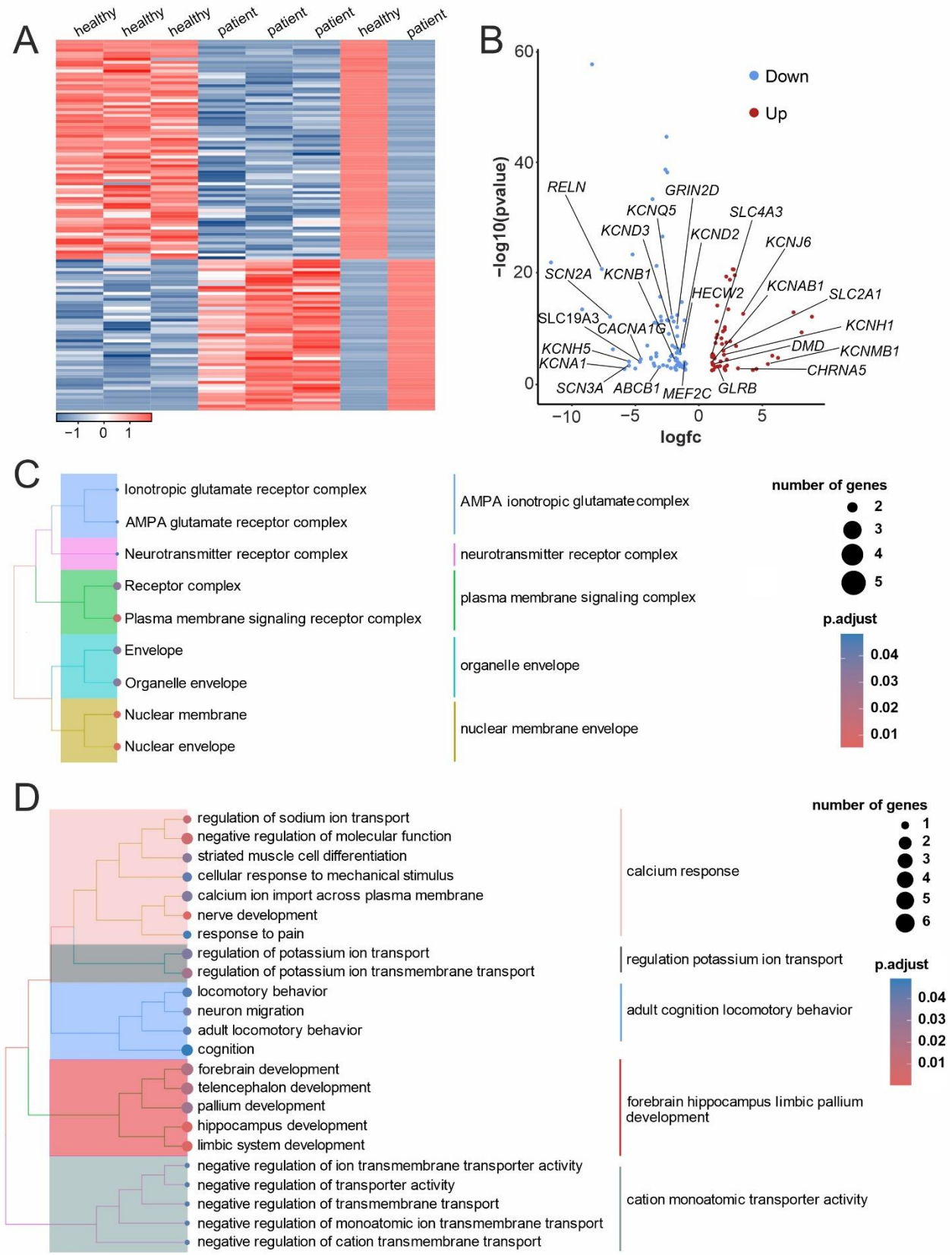

Figure 4. Transcriptome analysis of fibroblasts derived from patient and a healthy individuum. (A) DEGs of epilepsy-associated and transporter activity genes in patient derived fibroblasts are shown in heatmap analysis. Red color cells indicate upregulated genes and blue color cells indicate downregulated genes. **(B)** Volcano plot of DEGs shows the genes are common in epilepsy-associated genes and transporter activity related genes in patient-derived fibroblast. **(C)** Gene set enrichment (GSE) in total 125 DEGs shown in clusters. **(D)** GSE for "*cellular compartment*" analysis of differentially expressed genes. Only adjusted p-values less than 0.05 are shown. *n*=3 replicates for the analysis of healthy and USH2C fibroblasts.

Figure 5.

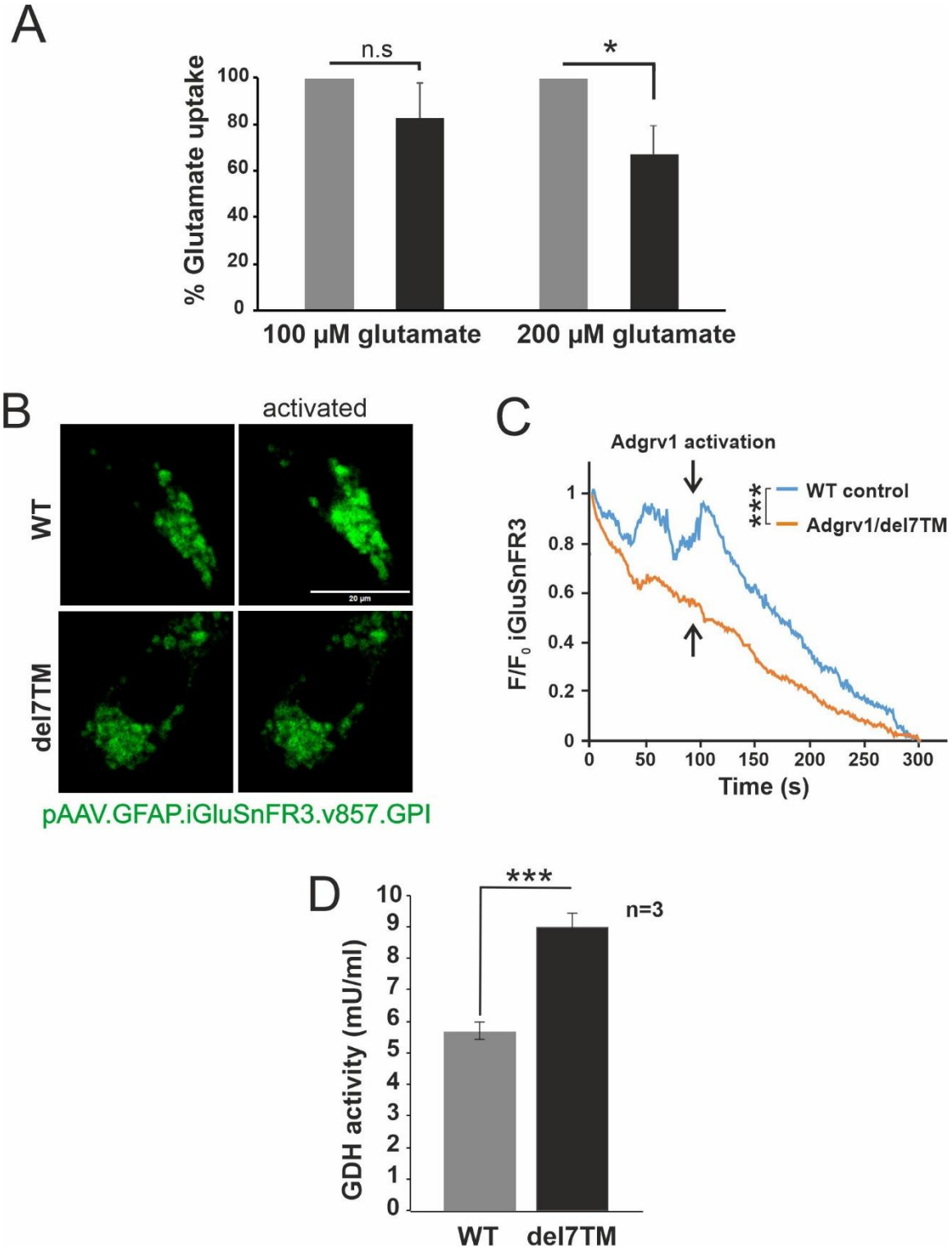

Figure 5. Glutamate uptake is mediated by Adgrv1 in primary astrocytes. (**A)** Glutamate uptake assay showing a dose-dependent reduction in Adgrv1/del7TM primary astrocytes. **(B)** Live-cell imaging of pAAV.GFAP.iGluSnFR3.v857.GPI transfected primary astrocytes derived from WT and Adgrv1/del7TM mice. Time-lapse image sequences of the fluorescent glutamate reporter were recorded with a sequence of 700 ms in a time course of 300 seconds with and without activation by the Statchel peptide. **(C)** Fluorescence intensity changes were calculated with F/F_0 formula to obtain before and after application changes in fluorescence intensities. The yellow line indicates application of 1 mM "Stachel" peptide for receptor activation. F/F_0 iGluSnFR3 intensity changes revealed an increase in WT astrocytes after Stachel peptide application, whereas there was no change observed in Adgrv1/del7TM astrocytes. (**D)** Glutamate dehydrogenase activity significantly increases in Adgrv1/del7TM astrocytes. For glutamate dehydrogenase activity assay 3 technical and 3 biological replicates were used for the quantification. For iGluSnFR3 intensity analysis *n*=7 (WT) and *n*=9 (Adgrv1/del7TM) in n=3 independent experiments were used. Data are represented as mean ± SD. Statistical evaluations were performed for bar plots using two-tailed Student's t test and using Kruskal-Wallis test for iGluSnFr3 curves**p* % 0.05, ***p* % 0.01, ****p* % 0.001. Scale bars: 20 µm.

Figure 6.

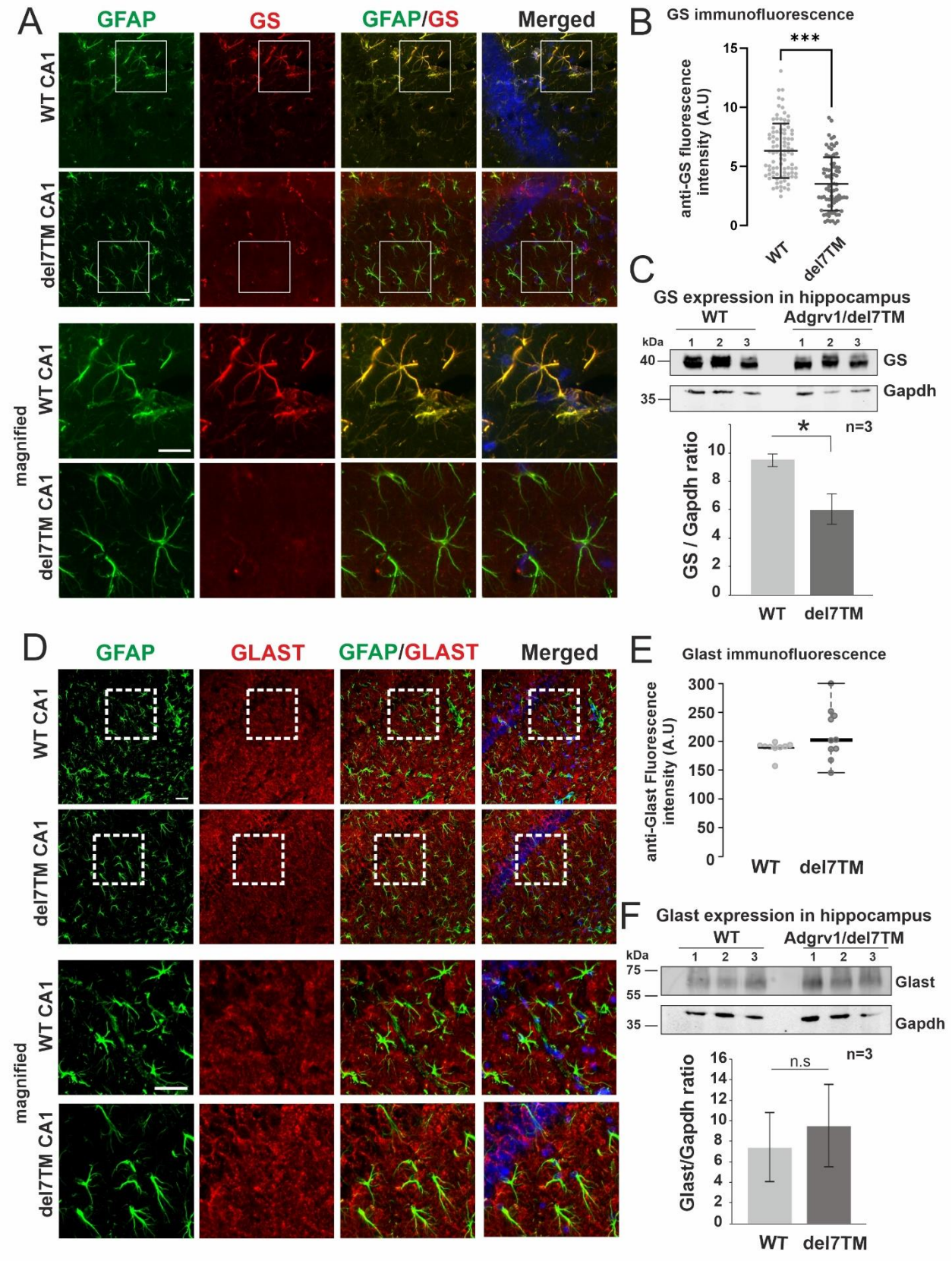

Figure 6. Expression analysis of glutamine synthetase (GS) and GLAST in astrocytes of the hippocampus of Adgrv1/del7TM and wild type control mice. (A) Double immunofluorescence staining for GS (red) and for the astrocyte marker GFAP (green) in sections through the CA1 region of the hippocampus counterstained for nuclear DNA by DAPI (blue). Merged images revealed localization and abundant expression of GS in GFAP-positive astrocytes in WT mice which is almost absent in Adgrv1/del7TM mice. **(B)** Quantification of anti-GS immunofluorescence intensity in in GFAP-positive astrocytes of hippocampal CA1 region reveals a high significant decrease in Adgrv1/del7TM mice. **(C)** Anti-GS Western blot analysis of hippocampal lysates demonstrates the significant decrease of GS protein expression in Adgrv1/del7TM mice. **(D)** Indirect immunofluorescence staining for GFAP (green) and glutamate transporter GLAST (red) counterstained by DAPI (blue) in the CA1 region of the hippocampus of Adgr1/del7TM (del7TM) and wild type (WT) mice. **(E)** Quantification of anti-GLAST immunofluorescence intensity in GFAP-positive astocytes of hippocampal CA1 region shows slight but not significant increase in Adgrv1/del7TM. *n*=3, number of sections quantified: 3 continuous sections per group. **(F)** Anti-GLAST Western blot analysis of hippocampal lysates of Adgrv1/del7TM and WT mice. Densitometry analysis related to Gapdh expression (A.U) showed tentative but an no upregulation of GLAST expression in Adgrv1/del7TM. *n*=3 animals and 3 continuous sections per group were used. Statistics: two-tailed Student´s t test, One way-ANOVA test; *$p \leq 0.05$, **$p \leq 0.01$, ***$p \leq 0.001$. Scale bars: 20 µm. Magnified images Scale bars: 200 µm and 20 µm.

Figure 7.

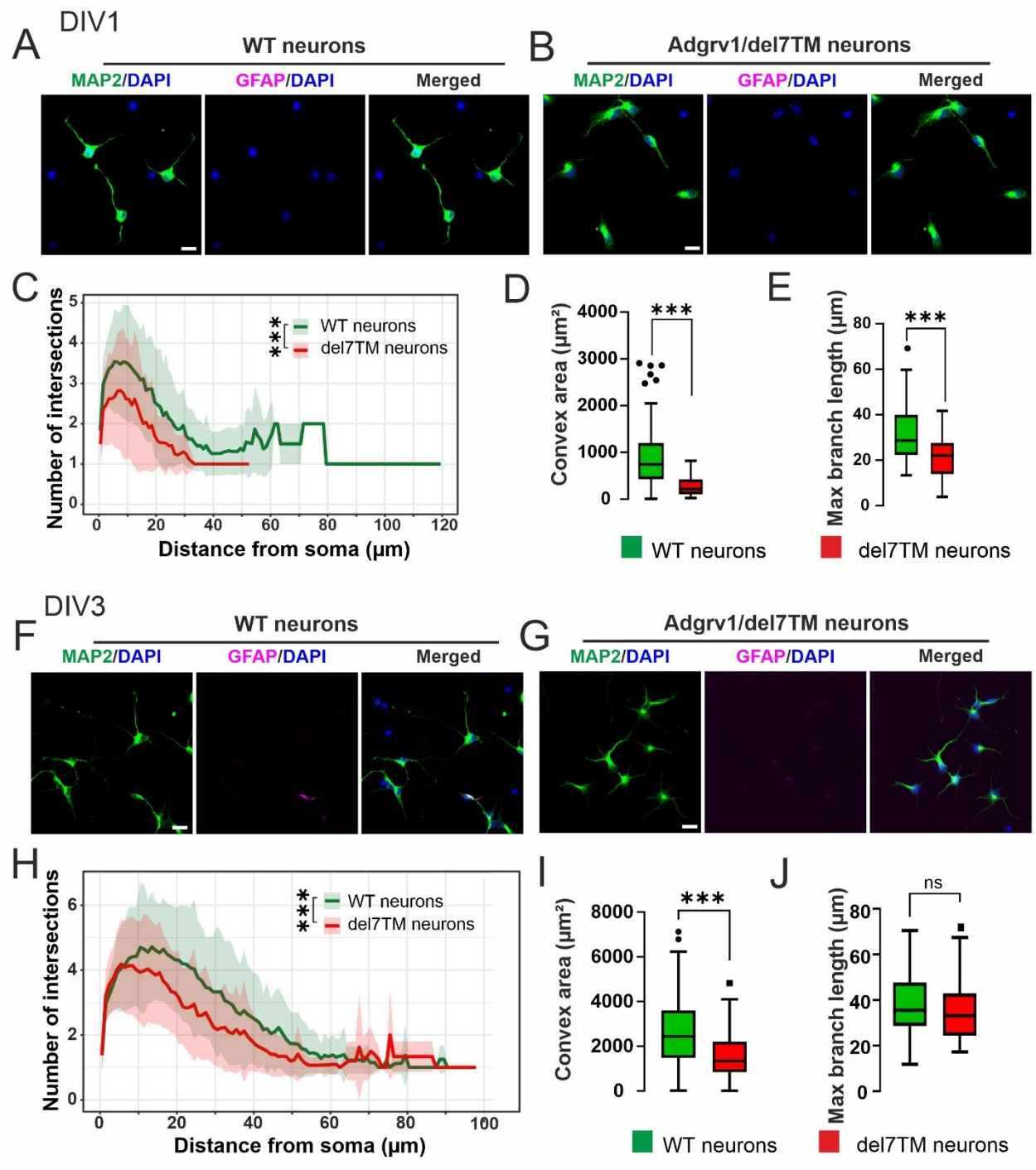

Figure 7. Morphometric characterization of primary neurons derived from WT and Adgrv1 mouse hippocampi. (A, B) Primary neurons isolated from the E18.5 WT and Adgrv1/del7TM mouse hippocampi were cultured for 1 day and stained with anti-MAP2 (green) and anti-GFAP (magenta) to visualize neurites of neurons and astrocytes, respectively. **(C)** Sholl analysis method applied for the quantification of intersection numbers of WT (green line) and Adgrv1/del7TM (red line) neuron cultures. A significant decrease in the number of neuronal intersections were observed in Adgrv1/del7TM neurons only cultures compared to the WT neuron cultures in day *in vitro* 1 (DIV1). **(D)** Analysis of Convex area showed a significant reduction in area of Adgrv1/del7TM neurons compared to WT neurons. **(E)** Maximum branch length of intersection in Adgrv1/del7TM neurons were also reduced. **(F)** WT and Adgrv1/del7TM neurons were cultured for 3 days in vitro (DIV 3). Neurons were identified with anti-MAP2 (green) and possible astrocyte contamination were detected with anti-GFAP (magenta) antibodies. **(H)** Quantification of **i**ntersection numbers by sholl analysis showed that Adgrv1/del7TM neurons have significantly less intersection numbers compared to WT neurons in DIV3. **(I)** Convex area quantification revealed that reduction in the area of Adgrv1/del7TM neurons persisted in DIV3 compared to WT neurons. **(G)** Maximum branch length of intersection analysis in DIV3 showed tentative decrease but no significant differences in between Adgrv1/del7TM and WT neurons. 60-70 cells in total for n=3 experiments. Statistics: One way-ANOVA test; *$p \leq 0.05$, **$p \leq 0.01$, ***$p \leq 0.001$. Scale bar: 10 μm.

Figure 8.

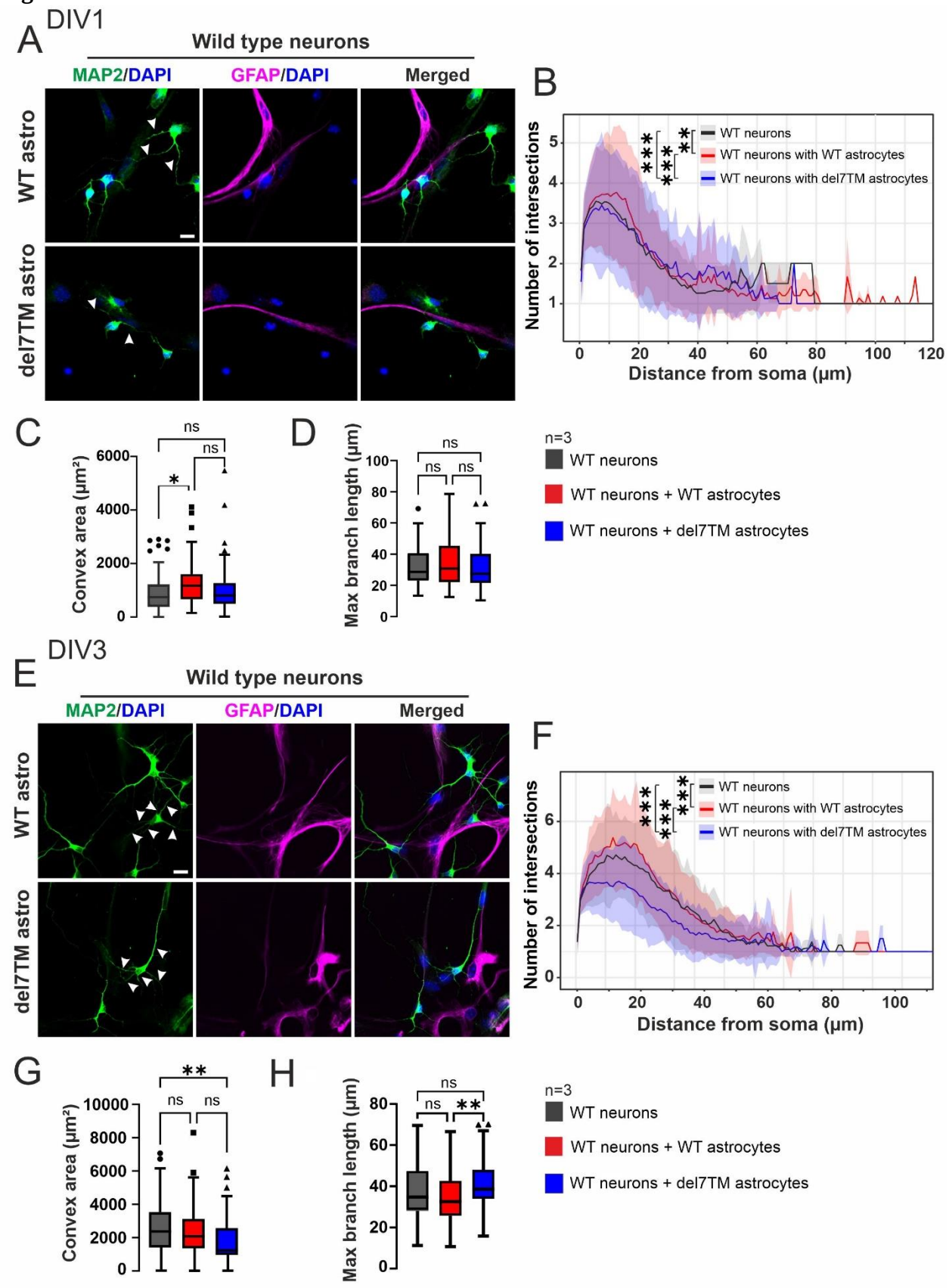

Figure 8. Morphometric characterization of primary neurons derived from WT mouse hippocampi co-cultured with WT and Adgrv1/del7TM astrocytes. **(A)** Primary neurons isolated from the WT E18.5 mouse hippocampus were cultured alone and together with WT or Adgrv1/del7TM astrocytes for DIV1. Anti-MAP2 (green) and anti-GFAP (magenta) were used for the visualization of neuronal neurites and astrocytes, respectively. Arrow heads indicate the neurites of primary neurons. (**B)** Sholl analysis revealed that co-culturing of WT neurons with WT astrocytes (red line) resulted in significant increase of intersection numbers of WT neurons. On contrary, co-culturing of WT neurons with Adgrv1/del7TM astrocytes (blue line) showed slight but significant decrease compared to WT neuron only cultures (black line). (**C)** Convex area analysis showed a notable increase in area of WT neurons co-cultured with WT astrocytes. However, no significant changes were observed in co-cultures with Adgrv1/del7TM astrocytes. (**D)** Maximum branch length of intersection in WT neurons did not change on both co-cultured together with WT and Adgrv1/del7TM astrocytes. (**E)** Immunofluorescence staining of neuronal neurites and astrocytes using Anti-MAP2 (green) and anti-GFAP (magenta), respectively in DIV3. (**F)** Total number of the intersections in WT neurons co-cultured with WT astrocytes (red line) showed the highest neurite numbers in DIV3 similar to DIV1 cultures. The analysis revealed that compared to WT neurons only cultures (black line) and WT neurons with WT astrocyte cultures (red line), co-culturing of WT neurons with Adgrv1/del7TM astrocytes (blue line) resulted in the lowest intersection numbers in DIV3 of culture. (**G)** Convex area quantification showed a significant decrease in WT neuron areas co-cultured with Adgrv1/del7TM astrocytes in DIV3. However no significant changes were observed in the WT neuron area when co-cultered with WT astrocytes. **(G)** Maximum branch length of intersections in WT neurons did not change in both co-cultures together with WT and Adgrv1/del7TM astrocytes in DIV3. However, analysis revealed that WT neurons with WT astrocytes co-cultures have significantly smaller areas compared to WT neurons with Adgrv1/del7TM astrocytes. 60-70 cells in total for n=3 experiments. Statistics: One way-ANOVA test; *$p \leq 0.05$, **$p \leq 0.01$, ***$p \leq 0.001$. Scale bar: 10 µm.

Figure 9.

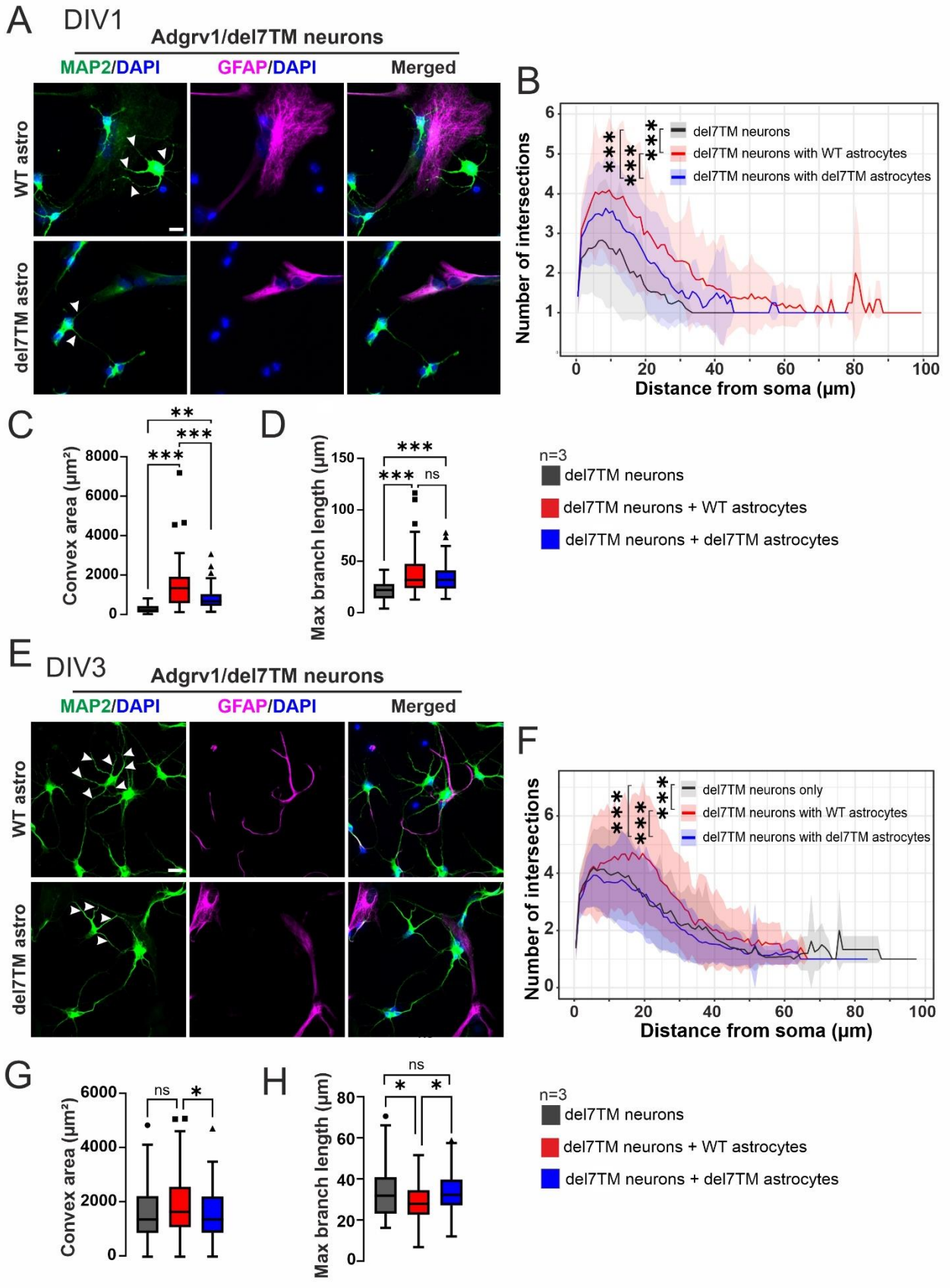

Figure 9. Morphometric characterization of primary neurons derived from Adgrv1/del7TM mouse hippocampi co-cultured with WT and Adgrv1/del7TM astrocytes. (A) Primary neurons isolated from the Adgrv1/del7TM E18.5 mouse hippocampus were cultured alone or together with WT or Adgrv1/del7TM astrocytes for DIV1. Anti-MAP2 (green) and anti-GFAP (magenta) were used for the visualization of neuronal neurites and astrocytes, respectively. Arrow heads indicate the neurites of neurons. (B) Sholl analysis of Adgrv1/del7TM neurons only cultures (black line) revealed the least intersection numbers. Co-culturing of the Adgrv1/del7TM neurons with WT (red line) or Adgrv1/del7TM (blue line) resulted in significant increase in intersection numbers. The most prominent increase in intersection numbers was observed in Adgrv1/del7TM neurons co-cultured with WT astrocytes. (**C)** Co-cultures of Adgrv1/del7TM neurons with WT or Adgrv1/del7TM astrocytes significantly increased the area of Adgrv1/del7TM neurons. The most prominent increases in the Adgrv1/del7TM neuron areas were observed in co-cultures with WT astrocytes. (**D)** Maximum branch length of intersection in Adgrv1/del7TM neurons significantly increased in both co-cultured together with WT and Adgrv1/del7TM astrocytes in DIV1. (**E)** Double immunofluorescence staining of neuronal neurites and astrocytes using Anti-MAP2 (green) and anti-GFAP (magenta), respectively in DIV3. (**F)** The highest intersection numbers were observed in Adgrv1/del7TM neurons when co-cultured with WT astrocytes (red line). Adgrv1/del7TM neurons co-cultured with Adgrv1/del7TM astrocytes (blue line) showed a significantly lowest intersection numbers compared to both Adgrv1/del7TM neuron only cultures (black line) and Adgrv1/del7TM neurons/WT astrocyte co-cultures in DIV3. (**G)** Co-culturing the Adgrv1/delTM neurons with both WT and Adgrv1/del7TM astrocytes did not change the area of Adgrv1/del7TM neurons. However, a significant reduction observed in Adgrv1/del7TM neuron and Adgrv1/del7TM astrocyte co-cultures compared to co-cultures with WT astrocytes in DIV3. **(G)** Maximum branch length of intersections in Adgrv1/del7TM neurons co-cultured with WT astrocytes showed significant reduction compared to Adgrv1/del7TM neuron only and Adgrv1/del7TM neuron co-cultured with Adgrv1/del7TM astrocytes in DIV3. 60-70 cells in total for n=3 experiments. Statistics: One way-ANOVA test; *$p \leq 0.05$, **$p \leq 0.01$, ***$p \leq 0.001$. Scale bar: 10 µm.

Figure 10.

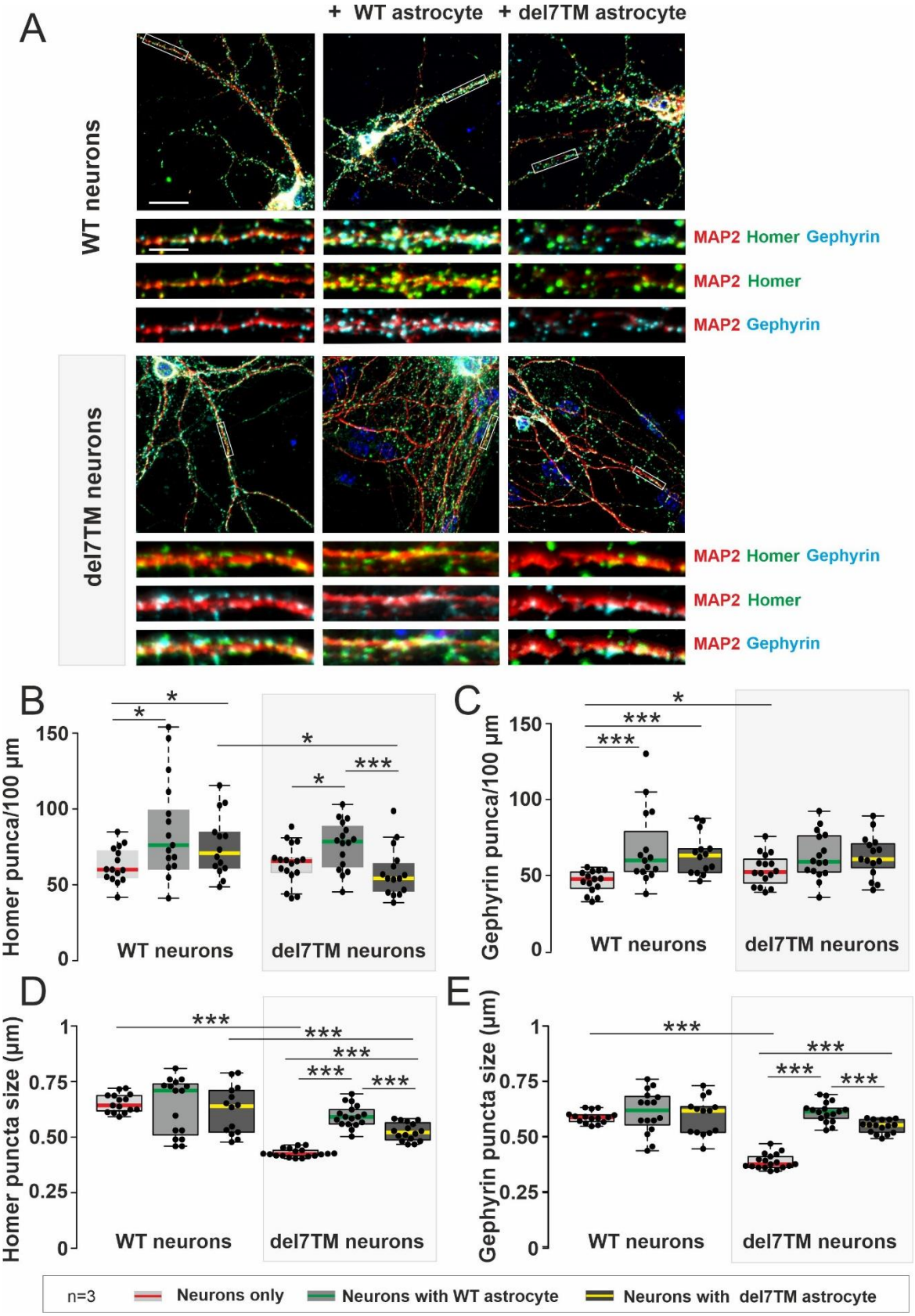

Figure 10. Co-culturing of WT and Adgrv1/del7TM neurons with WT astrocytes increases synaptic numbers and sizes. (A) Hippocampal neurons from WT and Adgrv1/del7TM mice were immunolabelled with anti-Homer (Green), anti-Gephyrin (Cyan) and anti-MAP2 (red). Nucleus was counter-stained with DAPI. **(B)** Quantification of excitatory post-synaptic puncta revealed that similar Homer puncta in WT and Adgrv1/del7TM neuron cultures. WT astrocyte and neuron co-cultures increased the Homer puncta number in both neuron cultures. The lowest homer puncta number was observed in Adgrv1/del7TM astrocyte-neuron co-cultures. **(C)** Quantification of inhibitory post-synaptic puncta using Gephyrin staining showed significantly more puncta in Adgrv1/del7TM neuron only cultures compared to WT neuron cultures. While astrocyte co-cultures increased the numbers of inhibitory synaptic puncta in WT neuron co-cultures, no differences observed in Adgrv1/del7TM neuron co-cultures. **(D)** Excitatory post-synaptic puncta size did not change in WT neuron co-cultures with WT or Adgrv1/del7TM astrocytes. Adgrv1/del7TM neurons showed significantly smaller size of Homer puncta. Smaller size observed in Adgrv1/del7TM neurons were increased by co-culturing with WT or Adgrv1/del7TM astrocytes. **(E)** Similar to excitatory synapses quantification, there was a significant decrease in inhibitory synaptic puncta in Adgrv1/del7TM neurons. Highest puncta sizes were observed in neurons with WT astrocyte co-cultures. Scale bar: 10 and 20 µm. 15-16 cells in total for n=3 experiments were used, and statistical evaluation was performed using Student´s t-test analysis: *$p \leq 0.05$, **$p \leq 0.01$, ***$p \leq 0.001$.

Supplemental Figures

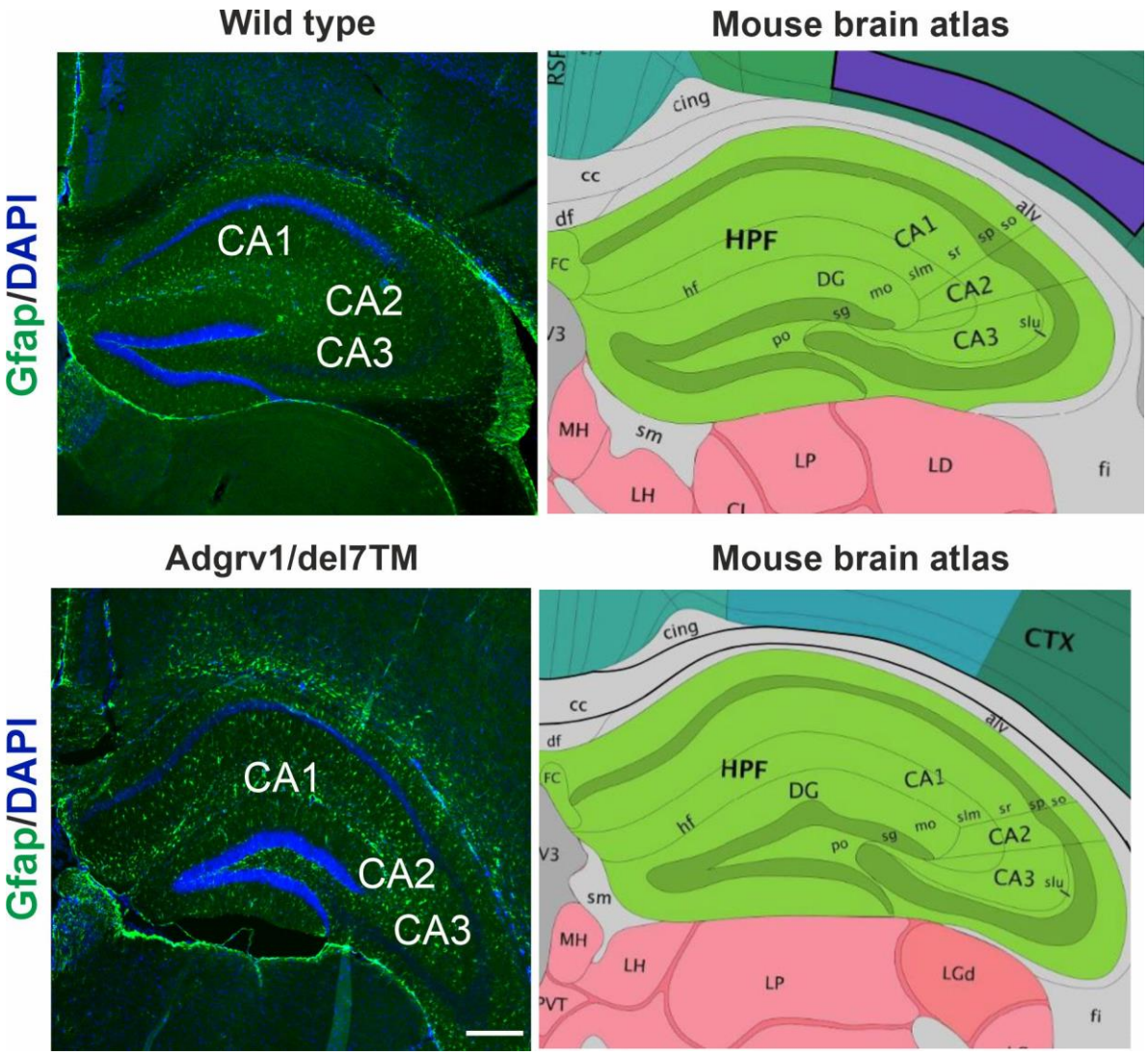

Figure S1. Reference coronal brain sections from mouse brain atlas for the identification of hippocampus subregions.

The subregions of the mouse hippocampus sections were identified using the Allen mouse brain atlas (https://mouse.brain-map.org/) during the image analysis. Scale bar: 25 μm.

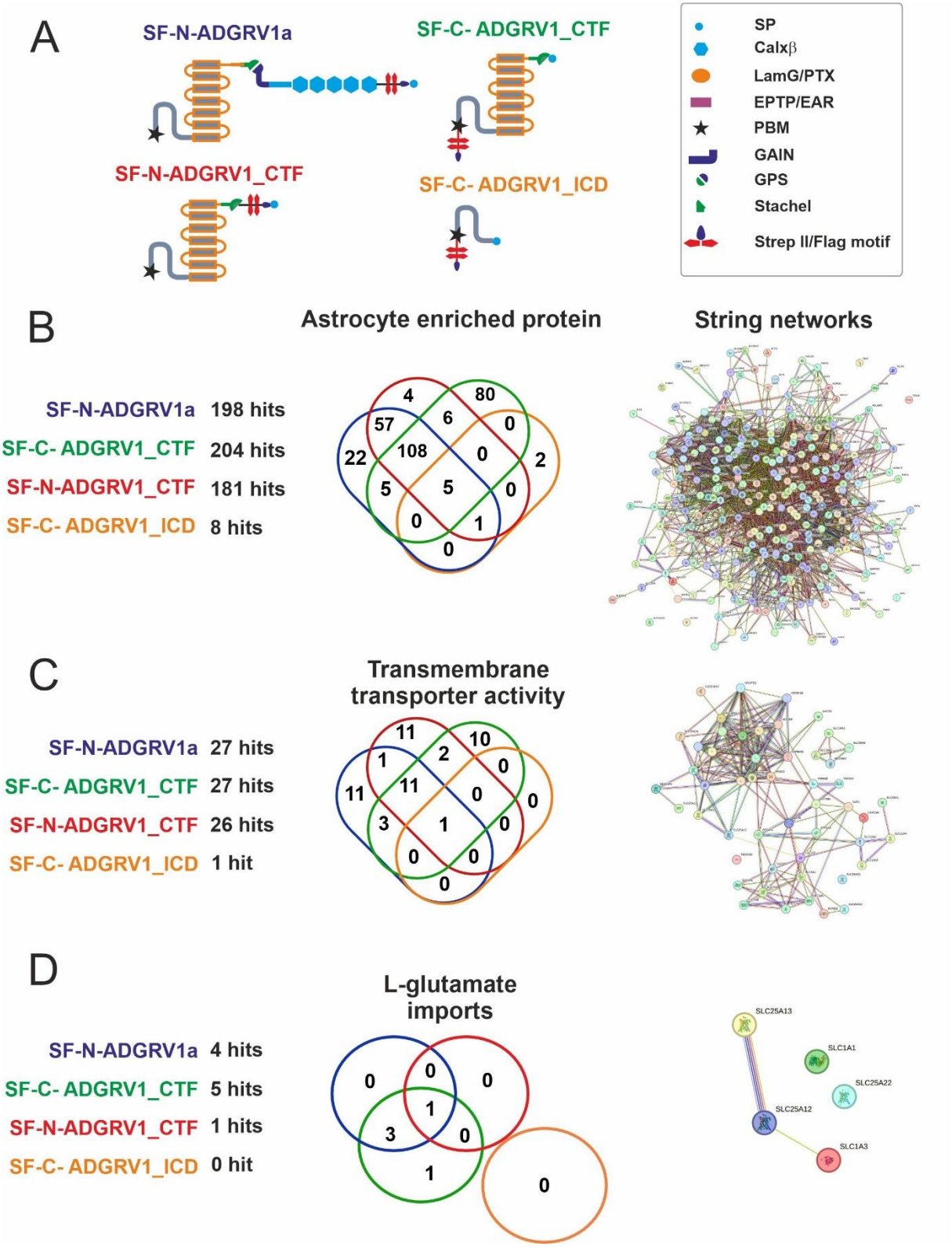

Figure S2. TAP analysis reveals a complex protein network related to ADGRV1 protein

(A) Different Strep II/FLAG (SF)-tagged ADGRV1 constructs used as a prey in Tanden affinity purification (TAP) to revealing potential interaction partners of ADGRV1 using HEK293T cells. ADGRV1 constructs were tagged from C or N terminals to eliminate false binding partners and changes in receptor structure. (**B**) GO term analysis revealed astrocyte enriched protein in ADGRV1 TAP analysis. The Venn-diagram shows a high overlap in astrocyte enriched proteins in 4 different ADGRV1 constructs, and string network analysis shows interactions. (**C**) Transmembrane transporter activity related proteins highly overlapped in SF-N-ADGRV1a, SF-N-ADGRV1_CTF and SF-C-ADGRV1 preys. (**D**) L-glutamate import related proteins have enriched in SF-N-ADGRV1a and SF-C-ADGRV1 preys.

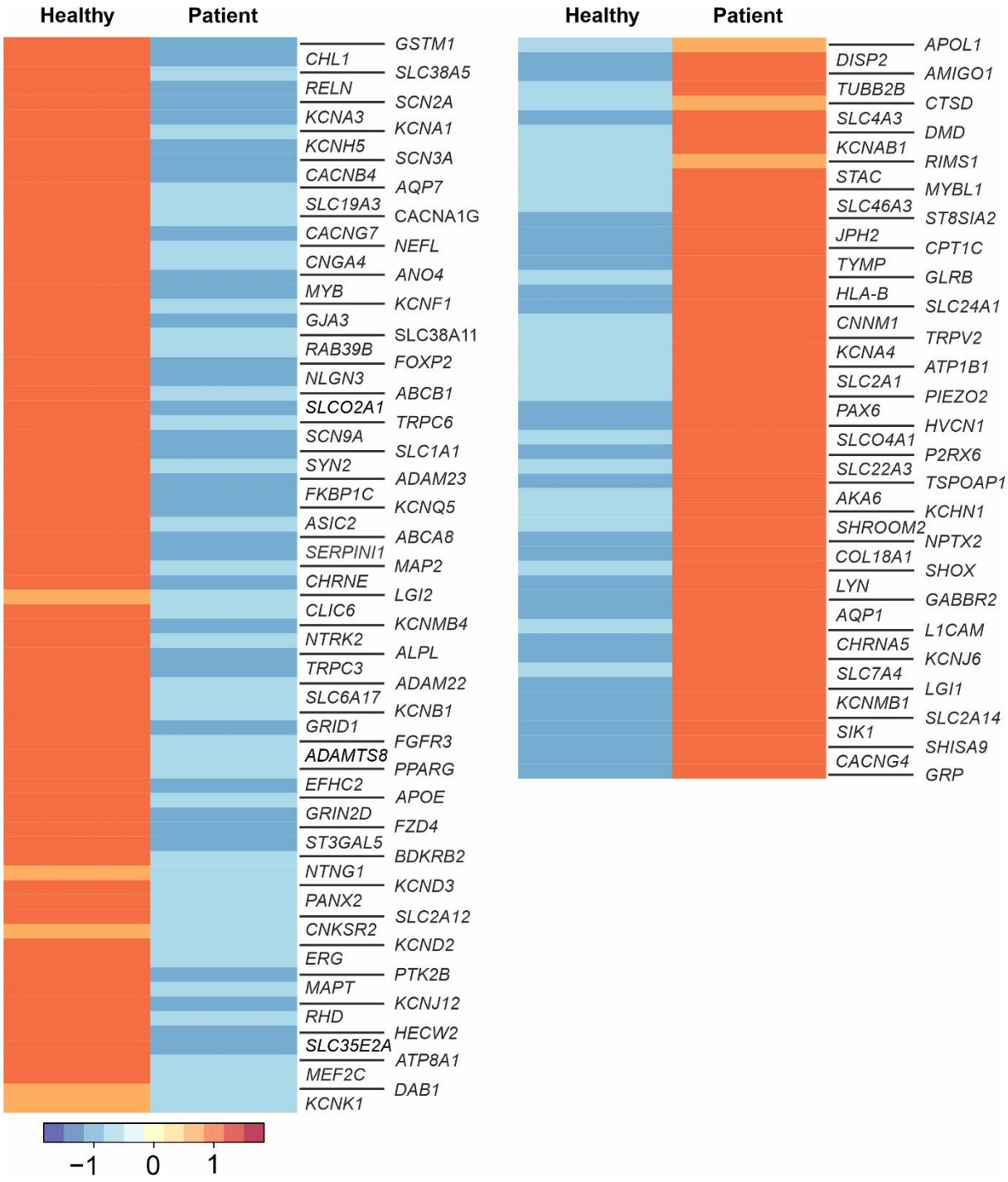

Figure S3. Differential expressed genes (DEGs) in patient-derived fibroblasts compared to fibroblasts from a healthy individuum. The average expression profiles from 3 replicates of healthy individuum and patient fibroblasts. Blue color shows downregulated genes and red color shows upregulated genes in patient-derived fibroblasts compared to healthy individuals.

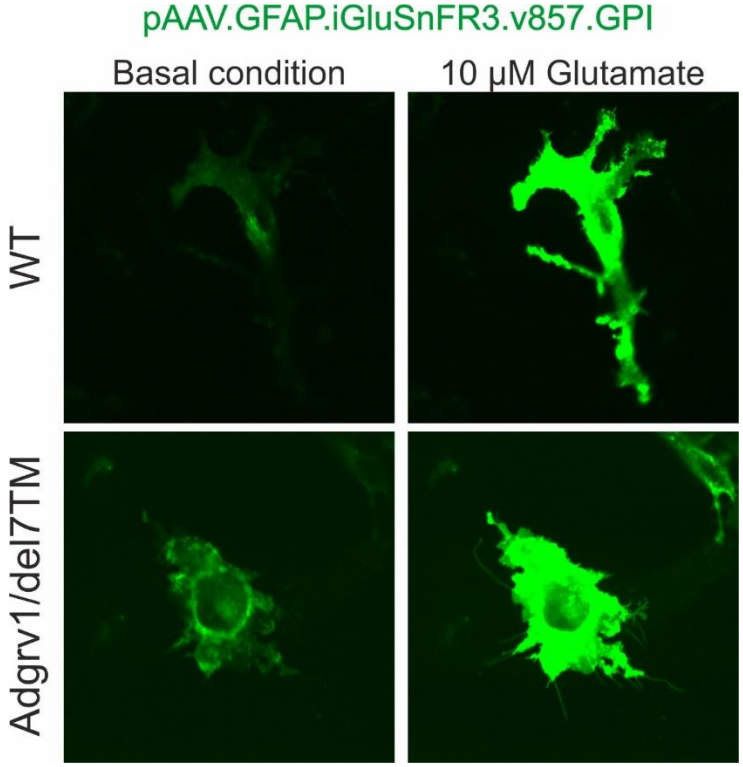

Figure S4. Images from live-cell imaging of pAAV.GFAP.iGluSnFR3.v857.GPI (green) expressing WT and Adgrv1/del7TM astrocytes.

Time-lapse image sequences of pAAV.GFAP.iGluSnFR3.v857.GPI was recorded with 700 ms intervals for a total of 300 seconds. 10 µM glutamate was applied to the cells in 98th image of the sequence.

3. Summary of results and general discussions

In my cumulative PhD thesis, I have investigated the function of ADGRV1 in FAs, utilizing primary astrocytes derived from mouse brain tissue Publications I and II and its additional functions in hippocampal astrocytes. While several studies have explored GPCR activities in astrocyte physiology and their impact on the CNS, there has been limited research specifically examining the role of aGPCRs in astrocyte. To elucidate ADGRV1 function, we have therefore developed a robust method for isolating primary astrocytes (**Publication I**). The localization of ADGRV1 at focal adhesion (FA) molecules has been validated, with evidence indicating its function as a metabotropic mechanosensory receptor (**Publication II**). The role of ADGRV1 in dynamic regulation of FA arrangement and recruitment has been shown using live-cell imaging methods in migrating primary astrocytes. We have shown that ADGRV1 controls the assembly but not disassembly of FAs and regulates their recruitment to the FA macromolecular complex. (**Publication III**). Finally, the role of ADGRV1 in the mouse hippocampus was shown by using molecular and morphological approaches (**Preprint I**). This study revealed that ADGRV1 expression in astrocytes controls hippocampal astrocyte morphology and abundance. Furthermore, it has been demonstrated that ADGRV1 controls glutamate uptake. Finally, we provided evidence that the supportive function of astrocytes in the development of neurons is also dependent on the expression of ADGRV1 in astrocytes.

3.1. Establishment of the primary cell model to study ADGRV1

Primary cell culture holds paramount significance in research for its ability to maintain the physiological relevance of cells, preserving their natural characteristics and interactions (Richter et al., 2021). This method is important for disease modelling, as the cells isolated from their natural environment, thereby aiding the study of tissue-specific pathologies. Furthermore, primary cell cultures contribute significantly to our understanding of cellular signalling pathways, gene expression regulation, and molecular events that underpin various biological processes (Januszyk et al., 2015). Primary cell culture offers several advantages such as physiological relevance, cellular heterogeneity, disease modelling and reduced genetic drift (Caires et al., 2018). This enhances the reliability and reproducibility of experimental results. In summary, the advantages of primary cell culture lie in its ability to provide a more biologically relevant and realistic representation of cellular behaviour, making it an indispensable tool in advancing our understanding of biology, disease, and potential therapeutic interventions.

Throughout my studies, we used astrocytes as a model for studying ADGRV1 functions. Astrocytes are a key cell type in the CNS to regulate signalling and interaction between neurons. However, isolating astrocytes, like isolating many other cell types, can be a complex and resource-intensive process, adding to the overall expense. We present a cost-effective and reliable method to isolate primary astrocytes from P0 mouse pups that eliminates the need for specialized equipment or commercially available kits. By using our protocol, we established a robust culture of primary astrocytes from both WT and mutant mouse strains such as Adgrv1/del7TM and Adgrv1/Drum B (**Publication I**).

3.2. The role of ADGRV1 in FAs and their dynamics

Affinity proteomics which previously performed by (Knapp et al., 2019, 2022) revealed the possible role of ADGRV1 in adhesion complexes namely FAs. In **Publication II and III**, we focused on the validation of ADGRV1 localization at FAs and its regulatory roles in these supramolecular complexes.

3.2.1. ADGRV1 localize at focal adhesion macromolecular complex and regulates the size, abundance and kinetics

We first validated the localization of ADGRV1 together with core FA molecules such as vinculin, paxillin and zyxin (**Publication II**). For this purpose, we used different cell models such as hTERT-RPE1 cells and primary astrocytes isolated from mice brains to strengthen our findings. We used in *situ PLA* analysis which allowed us to detect the proximity of proteins which are in less than 40 nm distance to each other. *In situ* PLA analysis revealed that ADGRV1 interacts with other FA molecules in proximity. After revealing the localization of ADGRV1 at FAs, we next focused on whether loss-of-function in ADGRV1 causes alteration in FA size and abundance. In this research, hTERT-RPE1 cells were utilized in which ADGRV1 was knocked down and alongside primary astrocytes isolated from Adgrv1/del7TM and Adgrv1/DrumB mouse brains. The analysis revealed that ADGRV1 depletion from hTERT-RPE1 cells or primary astrocytes causes disruptions in FA size and abundance. Quantification of the FA marker vinculin in those cells showed that smaller and fewer FAs highlight the role of ADGRV1 in FA assembly (**Publication II**). Additionally, by applying fluid shear stress, we have shown that ADGRV1 acts as a metabotropic mechanosensor in these cells.

We investigated how ADGRV1 regulates FA turnover in primary astrocytes during cell migration (**Publication III**). Results obtained from nocodazole (NDZ) washout assays, live-cell imaging, and FRAP consistently provided evidence that ADGRV1 regulates FA turnover

by actively participating in the assembly process. In NDZ washout assays which rely on microtubule depolymerization, the *de novo* assembly of FAs was notably delayed in ADGRV1-deficient astrocytes. Live-cell imaging using a Paxillin_dsRed2 construct to track FAs confirmed a reduced assembly rate in these cells. Defects in FA assembly also led to an increased FA lifetime in ADGRV1-deficient astrocytes. Fluorescence recovery after photobleaching (FRAP) also confirmed that the recruitment of Paxillin_dsRed2 is significantly delayed in Adgrv1/del7TM astrocytes, which shows that ADGRV1 plays a role in the recruitment of core FA molecules to the FA sides (**Publication III**). Our findings align with the roles of other regulators of FA dynamics, such as RACK1 and phosphatidylinositol phosphate kinase type Iγ (PIPKIγ) (Doan and Huttenlocher, 2007; Wu et al., 2011). Additionally, it has been shown in *drosophila* CNS that FA molecules are important for the astrocytic morphology and their coverage of synapses and thereby regulate their hyperexcitability (Cho et al., 2018b). The absence or dysfunction of FA proteins that potentially interact with ADGRV1 at focal adhesions, such as integrin β1, talin or FAK, can result in astrogliosis, an important feature in the development of epilepsy. Therefore, ADGRV1 deficiency in astrocytes may play a role in the mechanisms that cause epilepsy, and this issue will be thoroughly explained in the next chapters.

3.2.2 Deficiency of ADGRV1 disrupts the astrocyte migration

It has been previously shown that FA size strictly controls the migration capacity of the cell (DiMilla et al., 1991; Kim and Wirtz, 2013). Since we showed that ADGRV1 is an integral component of the FA complex and crucial for maintaining their proper size, abundance, and dynamics in primary astrocytes, we additionally investigated the migration capacity of primary astrocytes (**Publication II**). The effective coordination and regulation of FA dynamics are vital for cell migration in both normal and pathological conditions. Cell migration relies on the continuous rearrangement of FAs, involving the assembly of nascent FAs at the leading edge and their disassembly at the rear (Yamaguchi and Knaut, 2022). With the indication of a regulatory role of ADGRV1 in FA sides of the cells, it is not surprising that migration can also be altered. Therefore, using different approaches we wanted to validate ADGRV1´s role in cell migration.

Firstly, we showed that ADGRV1 depletion from hTERT-RPE1 and primary astrocytes reduces the cell spreading which gives an additional clue about the role of ADGRV1 in cell migration. Using a unidirectional migration assay in hTERT-RPE1 cells showed that ADGRV1 colocalizes with FAs in the leading edges. Additionally, a motility assay showed that Adgrv1

depletion from hTERT-RPE1 cells and in Adgrv1-deficient primary astrocytes impairs the migration capacity. We further showed with live-cell imaging in Adgrv1/del7TM astrocytes and WT astrocytes, that ADGRV1 is also vital for single-cell migration. Single-cell migration only relies on extracellular cues, since no cell-cell contact events occur (Lintz et al., 2017; Pawluchin and Galic, 2022). Overall, we show that ADGRV1 is an important molecule which controls cell migration likewise other reporter aGPCRs such as ADGRC1 and ADGRG1 (Curtin et al., 2003; Li et al., 2008).

It has been previously shown that FAs regulate neuronal growth during embryonic development (Monje et al., 2012). The growth cone of the axons is highly dependent on functional FA structures and the ECM for guidance. As neurons, astrocyte migration is also highly dependent on the ECM and FA dynamics during development and adulthood in the CNS (Hillen and Heine, 2020). During cortical development, neurons interact with radial glial fibres to establish precise laminar organization through integrins. Integrins containing β1 subunits, which associate with paxillin in FAs, play a crucial role in the proper development of the cortex. Specifically, the α3β1 integrin likely participates in radial glial fibre recognition by migrating neurons (Dulabon et al., 2000), while α5β1 integrin is essential for radial glia migration (Marchetti et al., 2010). Given the fact that ADGRV1 has the highest expression level in astrocytes in the CNS and it is potentially interacting with integrins α3, α5, and β1 (**Publication II**) raises a question about the importance of ADGRV1 in the CNS and its pathophysiology.

As defects in cell migration and disrupted CNS organizations are linked to diseases like epilepsy, alterations in FA composition due to ADGRV1 deficiency may contribute to the pathophysiology of diseases associated with ADGRV1 defects in CNS (Qin et al., 2017).

3.3. Importance of astrocytic ADGRV1 expression in CNS

Neuron-astrocyte interaction through messenger and signalling molecules such as Ca^{2+} and glutamate, is highly important in the CNS for function, development, and pathology of the brain (Benarroch, 2005; Nimmerjahn and Bergles, 2015).

In our studies in **Publication II and III** we elucidated the impact of ADGRV1 on astrocyte morphology and FA dynamics. Additionally, our previous research demonstrated that ADGRV1 regulates calcium homeostasis at the mitochondria-endoplasmic reticulum (ER) interface, mitochondria-associated membranes (MAMs), and autophagy in primary astrocytes derived from Adgrv1/del7TM mouse brain. These findings emphasize the important regulatory role of ADGRV1 in astrocyte morphology and physiology (Krzysko et al., 2022; Linnert et al., 2023).

Therefore, we focused on the role of ADGRV1 in astrocyte morphology in the mouse hippocampus **(Preprint I)**. We showed that Adgrv1 expression is important for the proper morphology of astrocytes. Furthermore, we demonstrated that loss of Adgrv1 from astrocytes results in fewer cell numbers in the Cornu ammonis (CA) 1 region of the Adgrv1/del7TM mouse hippocampus. Then, we showed that Adgrv1 can act in the physiology and morphology of astrocytes, as demonstrated by proteomic and transcriptomic analyses. We revealed that Adgrv1 functions in glutamate homeostasis in astrocytes, which is vital for the clearance of extracellular glutamate from synaptic clefts. Application of the "*Stachel*" mimetic peptide revealed that activation of Adgrv1 controls glutamate uptake in primary astrocytes. Finally, in neuron-astrocyte co-culture experiments, we provide evidence that ADGRV1 also functions in neuronal development and is crucial for the beneficial support of astrocytes for neurons.

3.3.1 ADGRV1 controls the morphology and abundance of astrocytes in hippocampus

We have shown for the first time that Adgrv1 controls astrocyte morphology and abundance in the hippocampi of mice. We found that astrocytes in the Adgrv1/del7TM mice hippocampus show significant morphological differences which predominantly occur in Cornu ammonis (CA) 1 (**Preprint I**). Next, we questioned whether Adgrv1 loss causes different morphology due to the loss of cells from the hippocampus. Quantification of astrocyte numbers in the hippocampus of mouse models with GFAP (glial fibrillary acidic protein) and Sox9 stainings, revealed a significant decrease in astrocyte numbers in CA1 of hippocampi but no other regions. We additionally revealed that Adgrv1 deficiency results in increased branch numbers in astrocytes.

Astrocytic branches reach to the synapses and control neuronal signalling with the participating synapses and these special compartments are called “tripartite synapses” (Perea et al., 2009). In the hippocampus, astrocytic branches cover nearly 60% of the synapses and the synaptic coverage depends on the spine size and local efficacy of the glutamate uptake (Ventura and Harris, 1999; Herde et al., 2020). Astrocyte loss or dysfunction in hippocampus CA1 has been associated with acute and chronic diseases such as ischemia and epilepsy. Moreover, the early astrocyte response to ischemic injury has shown that CA1 astrocytes have a selective vulnerability (Ouyang et al., 2014). In kainate-mediated induction of status epilepticus (SE) in rodent models, astrocyte density was shown to decrease, especially in CA1 of the hippocampus, due to necroptosis and increased autophagy (Wu et al., 2021).

Altogether, the loss of astrocytic cells and morphologic alterations are classically known as hallmarks of a pathological condition in many neurological disorders (Zhou et al., 2019).

Our findings lead to the hypothesis that CA1 astrocytic cell loss in Adgrv1/del7TM mice hippocampi may eventually result in seizures observed in Adgrv1/del7TM mice and eventually in patients with epilepsy (**Preprint I**).

3.2.2 Physiological function of ADGRV1 in astrocytes

In our affinity proteomics data, we could identify furthermore a high number of astrocyte-associated putative interaction partners (Knapp et al., 2019, 2022). This highlights the role of ADGRV1 in astrocytes. Among these proteins, we found several proteins associated with the regulation of glutamate homeostasis and epilepsy. In addition to proteomic analysis, bulk RNAseq of patient fibroblast and Adgrv1/del7TM hippocampi unveiled around 1300 and 80 differentially expressed genes (DEGs), respectively. Among those DEGs, we identified in total 24 common genes in both patient cells and Adgrv1/del7TM mouse hippocampi which play a role in epilepsy and transporter activity (Table 1).

Table 1. Epilepsy and transporter activity revealed differentially expressed genes in patient-derived fibroblasts and Adgrv1/del7TM mouse hippocampi (Blue color indicates downregulated and black color indicates upregulated genes).

Gene	Protein name	Protein function	Reference
RELN	Reelin	Regulation of neuronal migration	(Förster et al., 2010)
SCN2A	Sodium voltage-gated channel alpha subunit 2	Depolarizing phase of the action potential	(George et al., 1992)
KCNA1	Potassium voltage-gated channel shaker-related subfamily member 1	Membrane potential and nerve signaling	(Feria Pliego and Pedroarena, 2020)
KCNH5	Potassium voltage-gated channel eag-related subfamily member 5	Action potential, and in neuronal excitability and plasticity	(Niday and Tzingounis, 2018)
SCN3A	Sodium voltage-gated channel alpha subunit 3	Depolarizing phase of the action potential	(Chen et al., 2015)
SLC19A3	Solute carrier family 19-member 3	Transports reduced folate into mammalian cells	(Zhao and Goldman, 2013)
CACNA1G	Calcium voltage-gated channel subunit alpha1 G	Stabilizing the calcium channel	(Singh et al., 2007)
ABCB1	ATP-binding cassette sub-family B member 1	ATP dependent efflux pump	(Ambudkar et al., 2006)
KCNQ5	Potassium voltage-gated channel KQT-like subfamily member 5	Returning the depolarized cell to a resting state.	(Lehman et al., 2017)
KCNB1	Potassium voltage-gated channel shaw-related subfamily member 1	Transmembrane potassium transport	(Kang et al., 2019)
GRIN2D	Glutamate ionotropic receptor NMDA type subunit 2D	Synaptic communication	(Camp and Yuan, 2020)
KCND3	Potassium voltage-gated channel Shal-related subfamily member 3	Ion channel	(Pollini et al., 2020)
KCND2	Potassium voltage-gated channel Shal-related subfamily member 2	Ion channel	(Lee et al., 2014)
HECW2	E3 ubiquitin-protein ligase HECT, C2 and WW domain-containing protein 2	ubiquitin-dependent protein catabolic process	(Halvardson et al., 2016)
MEF2C	Myocyte-specific enhancer factor 2C	RNA processing	(Barbosa et al., 2008)
SLC4A3	Solute carrier family 4-member 3	Bicarbonate (HCO3-) transport	(Alper, 2006)
DMD	Dystrophin	Suppress the toxicities of toxins	(Duan et al., 2021)
KCNAB1	Potassium voltage-gated channel subfamily A member regulatory beta subunit 1	Shaping the action potential, plasticity	(Tiong et al., 2019)

GLRB	Glycine receptor beta	Neurotransmitter ligand-gated ion channels	(Lemoine et al., 2012)
SLC2A1	Solute carrier family 2-member 1	Sugar transporting	(Larsen et al., 2015)
KCNH1	Potassium voltage-gated channel Eag-related subfamily member 1	Potassium ion transport	(Simons et al., 2015)
CHRNA5	Cholinergic receptor nicotinic alpha 5	Proteolysis	(Steinlein, 2000)
KCNJ6	Potassium inwardly rectifying channel subfamily J member 6	Potassium ion transport	(Cooper et al., 2012)
KCNMB 1	Calcium-activated potassium channel subunit beta-1	Potassium ion transport	(Toro et al., 2006)
Pcd17	Protocadherin 17	homophilic cell adhesion	(Hayashi et al., 2014)
Chrm5	Muscarinic acetylcholine receptor M5	G-protein coupled receptors	(Pedersen et al., 2018)
Gabra2	Gamma-aminobutyric acid receptor subunit alpha-2	Mediating fast inhibitory synaptic transmission	(Butler et al., 2018)
Ptpn5	Tyrosine-protein phosphatase non-receptor type 5	Catalyze the dephosphorylation of phosphotyrosine peptides	(Tautermann et al., 2019)
Nudt3	Nudix hydrolase 3	Pyrophosphatase activity	(Grudzien-Nogalska et al., 2016)
Adar	Adenosine deaminase acting on RNA	RNA editing	(Jin and Nachury, 2009)
Adgrv1	Adhesion G protein-coupled receptor V1	G-protein signalling, AC regulation	(McMillan and White, 2004)
Hif3a	Hypoxia-inducible factor 3 alpha	Regulation of hypoxia-inducible gene expression	(Suzuki et al., 2017)
Trh	Thyrotropin-releasing hormone	Neuromodulator in the central nervous system	(Lechan and Fekete, 2006)
Grm4	Metabotropic glutamate receptor 4	Glutamatergic neurotransmission	(Muhle Hiltrud et al., 2010)

Gene set enrichment analysis (GSEA) focusing on biological function demonstrated that DEGs in Adgrv1/del7TM hippocampi and patient-derived USH2C fibroblast were associated with entities such as the "establishment of nitrogen compound transport" and "cation monoatomic transporter activity" which aligns with our proteomic data that ADGRV1 can be important for astrocytic glutamate homeostasis and epilepsy pathophysiology.

Altogether, this observation led us to investigate the homeostasis of glutamate in astrocytes. One of the main excitatory neurotransmitters in the CNS is glutamate and its homeostasis is strictly controlled by astrocytes in the brain. Reduced astrocytic cell number and synaptic coverage by astrocytic tiling can lead to extracellular glutamate concentrations which may rise to 1 mM at synapses (Zheng et al., 2008). High glutamate presence can exceed the capacity of glutamate transporters which may explain the astrocytic cell loss in CA1 of Adgrv1/del7TM hippocampus. We showed that Adgrv1-deficiency leads to a decrease in glutamate uptake which eventually can lead to accumulation of neurotoxic glutamate levels in CNS. Investigation of the key glutamate homeostasis proteins glutamate synthetase (GS) and, Glast/EAAT1 an interaction partner of Adgrv1, showed that loss of Adgrv1 expression leads to defective GS expression in both *in vitro* and *in vivo* conditions but not for Glast/EAAT1. We showed in this study (**Preprint I**) that mitochondrial glutamate dehydrogenase (GDH) activity,

which is important for the TCA cycle, increases its activity to almost 1.5-fold in Adgrv1/del7TM astrocytes.

The activation of Adgrv1 with the "*Stachel*" mimicking peptide, which acts as a tethered agonist, resulted in the activation of glutamate uptake in primary astrocytes. Consistent with our discoveries, previous research has indicated a correlation between mitochondrial membrane potential, glutamate uptake, and neuronal death in the CA1 region of the rat hippocampus (Ouyang et al., 2014). It's worth noting that previous studies have also reported a correlation between reduced GS expression and heightened GDH activity in individuals diagnosed with myoclonic absence epilepsy featuring hippocampal sclerosis (Bahi-Buisson et al., 2008; Chan et al., 2019; Raizen et al., 2005). In conclusion, our results may offer insights into the phenotypic and physiological alterations observed in Adgrv1/del7TM astrocytes. All together we showed that Adgrv1 is vital for not only glutamate uptake from ECM but also for glutamate homeostasis which can be relevant to epilepsy pathophysiology.

3.3.3 ADGRV1 function in neuron dendritogenesis and synaptogenesis

Additionally, we studied the impact of Adgrv1 deficiency on neuronal development. In the brain, astrocytic branches occupy and penetrate the synapse where no other astrocytic branching overlaps and this phenomenon is called an astrocytic tile (Hayashi et al., 2022). Astrocytic tiles are mostly controlled by neuronal cells through extracellular signalling molecules such as glutamate. Synaptic release of glutamate by neurons may induce the branching of astrocytes and neurons in the CNS (Hayashi et al., 2014). However, the exact mechanism behind the astrocytic tiling event is so far unknown.

To understand the role of the astrocytic Adgrv1 expression on neuron health we conducted astrocyte-neuron co-culture experiments. Strikingly, Adgrv1/del7TM neurons only cultures exhibited reduced neurite development, convex area, and maximum branch length compared to WT neurons which shows an additional role of Adgrv1 in neurons. Co-culturing Adgrv1/del7TM neurons with WT astrocytes improved their phenotype, while Adgrv1/del7TM astrocytes negatively affected both WT and Adgrv1/del7TM neurons. These results showed the important role of astrocytic Adgrv1 expression over neuronal dendrite development. After showing the effect of Adgrv1 expression on neuron morphogenesis, we focused on its role in synaptogenesis. Previously, we found that several aGPCRs namely ADGRL2 (Latrophillin 2), ADGRAs, ADGRBs (BAI) and finally ADGRV1 potentially interact with synaptic scaffold proteins (Knapp et al., 2019). Interestingly, ADGRV1 potentially interacts with the postsynaptic vesicle protein SNAP23, which localizes at postsynaptic density and regulates the

exocytosis of glutamate receptors (Suh et al., 2010; Knapp et al., 2019), which overlaps with our current findings (**Preprint I**). ADGRL2 is one of the interaction partners of ADGRV1 and is known to regulate hippocampal postsynaptic assembly in the CA1 region and acts as a synaptic target-recognition molecule (Anderson et al., 2017). Additionally, our affitinity analysis indicated several presynaptic molecules which potentially interact with ADGRV1 such as SNAP47, VDAC1, VDAC2 and BSN. In addition to presynaptic molecules, we have found post-synaptic molecules such as ADAM10, ITGB1, SLC1A3, SLC29A1 SIGMA1R and NPTN (Knapp et al., 2019). This wide range of potential interaction partners showed the importance of ADGRV1 in synaptic signalling and synaptogenesis.

In this line, we next investigated the role of Adgrv1 in synaptogenesis. In neuron-only cultures, gephyrin inhibitory PSDs were significantly higher in Adgrv1/del7TM neuron-only cultures when compared to WT neuron cultures. Co-culturing WT neurons with astrocytes increased gephyrin PSDs, while Adgrv1/del7TM neurons showed no significant changes with either astrocyte type. The size of synaptic puncta, indicative of synaptic strength, was smaller in Adgrv1/del7TM neuron-only cultures compared to WT. Co-culturing with astrocytes from both WT and deficient mice increased the size of homer and gephyrin-positive PSDs in Adgrv1/del7TM neurons. However, co-culturing with Adgrv1/del7TM astrocytes resulted in decreased excitatory and inhibitory synaptic puncta size compared to co-culturing with WT astrocytes. Given the fact that depletion of Adgrv1 either from neurons or astrocytes shows a deficiency in synaptogenesis, it underlines the dual role of Adgrv1 in the CNS. In conclusion, our findings further support the role of Adgrv1 expression during CNS development.

3.4. Relevance of present findings for the role ADGRV1 in the development of brain pathophysiology

Pathogenic variants of *ADGRV1* cause quite distinct diseases in human: hereditary deaf blindness in the human Usher syndrome type 2 (Weston et al., 2004) and various forms of epilepsy (Wang et al., 2015; Myers et al., 2018; Liu et al., 2020; Leng et al., 2022; Zhou et al., 2022). The present study only contributed few new facts to the understanding of the pathophysiology in USH2C. However, the data gathered in **Preprint I** provide the first significant insights into the pathophysiology of epilepsy associated with mutations in *ADGRV1* (*see page 15*). We present cumulative evidence that the absence or defects of ADGRV1 disrupts glutamate homeostasis in astrocytes of the hippocampus CA1 region, leading to their loss which has previously been related to the development epilepsy (Wu et al., 2021). The epilepsy relation of ADGRV1 was further confirmed and corroborated by omics data on patient-derived cells

and the ADGRV1-deficient mouse brain revealing the transcriptional dysregulation of genes and the interaction of ADGRV1 with molecules associated with epilepsy. In addition, deficiency of Adgrv1 in astrocytes resulted in an imbalance of excitatory-inhibitory synapses in neurons which was also previously related epilepsy (Bonansco and Fuenzalida, 2016).

However, were already findings presented in **Publications II** and **III** which confirm an association of dysfunction of ADGRV1 in astrocytes to epilepsy (*see page 13 and 14*). ADGRV1, identified as a FA resident protein, plays a critical role in cell migration. Deficiency in ADGRV1 controls FA morphology and its deficiency causing astrocyte migration defects. There is robust evidence that deficient cell migration increases CNS vulnerability and contributes to epileptogenesis (Qin et al., 2021; Zou et al., 2022). Present study showed that ADGRV1 controls astrocyte migration by the recruitment and assembly of paxillin (**Publication III**). Paxillin and integrin β1 containing FA components are critical for cortical development and neuronal migration (Dulabon et al., 2000; Schmid et al., 2004; Marchetti et al., 2010). The migration of neurons through the recognition of glial pathways is mediated by astrocytic FA molecules and its dysregulation associated with epileptogenesis (Gall and Lynch 2004). Astrocytic FA components holds significant importance for healthy CNS maintenance and pathophysiology of brain. Integrins containing α3β1 subunits are involved in the recognition of radial glial fibres by migrating neurons (Dulabon et al., 2000; Schmid et al., 2004), α5β1 integrin is required for radial migration (Marchetti et al., 2010). ADGRV1 as a metabotropic mechanosensory can sense extracellular cues in parallel with integrins and regulate migration of cells in CNS which disorganization causes epilepsy.

The important molecular dysfunctions observed in ADGRV1-deficient astrocytes provide a promising starting point for unravelling the underlying pathomechanisms of epilepsy associated with *ADGRV1* mutations. Even though we do not have unveiled the role of *ADGRV1* as USH causing gene, this study can also provide new evidence on the role of *ADGRV1* in human Usher syndrome. These initial findings are crucial for advancing our understanding of ADGRV1-associated diseases.

4. Future perspectives for deepening the understanding of ADGRV1 function in the CNS and disease

We have demonstrated the localization of focal adhesions (FAs) in primary astrocytes and their regulation of abundance, size, and dynamics by ADGRV1. This ultimately influences migratory capacities. The latter part of this thesis highlights the crucial role of astrocytic Adgrv1

expression in maintaining the health of astrocytes and, consequently, hippocampal neurons. However, additional studies are required to fully unravel ADGRV1's role in CNS development.

Given our findings that ADGRV1 is essential for FA structure and dynamic organization, influencing migration, it is prudent to expand these investigations to the developing CNS of mouse brains. The proper organization of the CNS relies heavily on the migration of neuronal cells for brain formation. Crossbreeding Adgrv1-deficient or wild-type mouse strains with GFAP-EGFP or CaMKIIα-RFP mouse models can facilitate the tracking of migrating astrocytes or neurons in developing mouse brains, respectively. This mouse brain study presents an opportune avenue for exploring the role of ADGRV1 in cell migration during brain development.

Beyond ADGRV1's involvement in FAs, we observed that its deficiency results in fewer astrocytes with increased branching. However, we have not confirmed whether the loss of astrocytes in the CA1 hippocampus leads to neuronal cell death or insufficient neuron activity. Hence, there is a pressing need to validate, under *in vivo* conditions, whether astrocyte loss culminates in neuronal death or compromised neuron activity. To comprehend ADGRV1's role in neurons, particularly in the Adgrv1/del7TM hippocampus where astrocyte loss occurs, whole-cell voltage-clamp recordings from different regions of acutely sliced hippocampal tissues can provide insights into potential differences in evoked and miniature Electric excitatory postsynaptic currents. Additionally, synaptic coverage of astrocytic branches in different regions of the hippocampus can be investigated by electron microscopy. To further understand ADGRV1's impact on astrocytes and its function in neuron physiology and networks, multi-electrode array (MEA) measurements can be employed. Exploring different co-culture setups, such as WT astrocytes with Adgrv1/del7TM neurons or vice versa, can shed light on the dual role of ADGRV1 in neuronal networks.

In primary astrocytes expressing pAAV.GFAP.iGluSnFR3, we observed that activation of Adgrv1 by the tethered agonist “Satchel” peptide induces glutamate signalling in intracellular membranes. The use of pAAV.GFAP.iGluSnFR3, allowing the visualization of glutamate kinetics, can be extended to WT and Adgrv1/del7TM mouse models' hippocampus to observe glutamate release activities from neurons.

Our results reveal alterations in dendritic arborization and synaptic formation in Adgrv1/delTM hippocampal neurons, with rescue potential by WT astrocytes. This implies a dual role of ADGRV1 in both astrocytes and neurons. Notably, our prior TAP analysis suggested potential interactions between ADGRV1 and proteins regulating neurogenesis (e.g., SLIT2, FN1, NPTN) (Knapp et al., 2019, 2022). Furthermore, ADGRV1 potentially interacts

with synaptic proteins, indicating a role in synaptogenesis in neurons. Validating synaptic interaction partners and determining synaptic localization is crucial for understanding ADGRV1's role in the CNS.

In parallel with mouse studies, investigating patient-derived fibroblasts can provide more relevant insights into role of *ADGRV1* in humans. Induced pluripotent stem cells (iPSCs) derived from patient fibroblasts can generate neurons, astrocytes, or 3D brain organoids. RNAseq data from patient-derived fibroblasts suggest promising gene set enrichment (GSE) results, with overlaps in categories like "*hippocampus development*," "*neuron migration*," and "*nerve development*" with previous TAP results. Expressing ADGRV1 minigenes with shortened domain structures in organoids or neurons can elucidate the functional domain structures of ADGRV1 in CNS development.

We have previously shown that ADGRV1 is a vital component for primary cilia and showed that primary astrocytes from Adgrv1/del7TM hippocampi show significantly fewer and shorter cilia. It has been shown that primary cilia lengths show differences in astrocytes from different cortical layers which indicates a specific arrangement and need for cilia in different regions of the brain (Wu et al., 2023). In the brain, primary cilia play an important role in neurogenesis, neuron survival and different signalling pathways such as WNT and hedgehog (Shim et al., 2023). Investigating the role of ADGRV1 in primary cilia in astrocytes or neurons in the mouse hippocampus or patient-derived organoids may unveil previously unknown roles in CNS signalling and maintenance, especially within "tetrapartite synapses" where post- and pre-synapses meet with astrocytes and cilia.

5. Summary

In this cumulative dissertation, the physiological and molecular functions of the adhesion GPCR ADGRV1 in astrocytes of the brain are analysed. Pathogenic variants of ADGRV1 lead to Usher syndrome (USH) in humans, the most common hereditary deaf-blindness. There is also increasing evidence that a defect in ADGRV1 is associated with various forms of epilepsy in humans. The molecular and cellular causes of ADGRV1 defects in the development of epilepsy are completely unknown. Investigation of the molecular function of the ADGRV1 protein in astrocytes should provide important insights into its disease relevance in the CNS.

In **Publication I**, we developed a robust method for the isolation of primary astrocytes from the mouse brain. This was subsequently used to isolate primary astrocytes from Adgrv1/del7TM and Adgrv1/DrumB mouse models and control animals to understand the role of ADGRV1 in its function in hippocampal astrocytes.

In **Publications II** and **III**, we investigated the role of ADGRV1 in focal adhesions (FA). FAs are dynamic supramolecular complexes that mediate cell attachment and whose signalling plays a crucial role in the control of cell migration. Our analyses showed that ADGRV1 is an important component of FAs and that its deficiency in different cell models leads to changes in cell morphology and disruption of their migration. We found that ADGRV1 acts as a metabotropic mechanosensor on FAs. Using live cell microscopy, we also found that ADGRV1 controls the dynamics of FA turnover during their assembly.

In **Preprint I**, we deepened our understanding of the role of ADGRV1 in hippocampal astrocytes. Our analysis in the mouse brain showed that the loss of ADGRV1 leads to a reduction in the number of astrocytes in CA1 of the hippocampus and to significant morphological changes in the remaining astrocytes. Furthermore, using molecular approaches, we confirmed that ADGRV1 controls glutamate uptake and regulates key molecules of the glutamate-glutamine cycle. Finally, we showed effects of Adgrv1 in astrocytes on neuronal development and synaptogenesis.

In summary, ADGRV1 is crucial for the development and physiology of primary astrocytes and is involved in several different compartments. Above all, these findings provide the first valuable insights into the pathogenesis of ADGRV1 dysfunction in epilepsy. The elucidation of ADGRV1 as a regulatory molecule in the CNS could contribute to the understanding of the pathomechanisms underlying epilepsy or other neurological diseases.

6. Zusammenfassung

In der vorliegenden kumulative Dissertationsschrift werden die physiologischen und molekularen Funktionen des Adhäsion GPCR ADGRV1 in Astrozyten des Gehirns untersucht. Pathogene Varianten von *ADGRV1* führen zum Usher-Syndrom (USH) des Menschen, der häufigsten erblichen Taubblindheit. Zudem mehren sich die Hinweise, dass eine das Defekte in *ADGRV1* mit verschiedenen Formen von Epilepsie beim Menschen assoziiert sind. Die molekularen und zellulären Ursachen die bei *ADGRV1*-Defekten sind für die Entstehung Epilepsie vollkommen unbekannt. Untersuchung zur molekularen Funktion des ADGRV1-Proteins in Astrozyten sollten wichtige Einblicke in seine Krankheitsrelevanz im ZNS ergeben.

In **Publikation I** haben wir eine robuste Methode zur Isolierung von primären Astrozyten aus dem Gehirn der Maus entwickelt. Diese wurde im Folgenden zur Isolation von primären Astrozyten aus Adgrv1/del7TM und Adgrv1/DrumB Mausmodellen sowie Kontrolltieren eingesetzt, um die Rolle von ADGRV1 bei seiner Funktion in den Astrozyten des Hippocampus zu verstehen.

In den **Publikationen II und III** untersuchten wir die Rolle von ADGRV1 in fokalen Adhäsionen (FA). FA sind dynamische supramolekulare Komplexe, die die Anheftung der Zelle vermitteln und deren Signaling insbesondere bei der Kontrolle der Zellmigration eine entscheidende Rolle spielen. Unsere Analysen zeigten, dass ADGRV1 wichtige eine Komponente in FAs ist und seine Defizienz in verschieden Zellmodellen zu Änderung der Zellmorphologie und zu Störung in ihrer Migration führt. Dabei konnten wir herausarbeiten, dass ADGRV1 als metabotroper Mechanosensor an FAs fungiert. Durch Lebendzellmikroskopie fanden wir zudem heraus, dass ADGRV1 die Dynamik der FAs bei ihren Turnover während ihres Aufbaus kontrolliert.

In **Preprint I** vertieften wir unser Verständnis der Rolle von ADGRV1 in den Astrozyten des Hippocampus. Dabei zeigten unsere Analyse im Gehirn der Maus, dass der Verlust von ADGRV1 zu einer Verringerung der Anzahl von Astrozyten in CA1 des Hippocampus und in den noch vorblieben Astrozyten zu signifikanten morphologischen Veränderungen führt. Darüber hinaus konnten wir mittels molekularer Ansätze bestätigt, dass ADGRV1 die Glutamataufnahme kontrolliert und die Schlüsselmoleküle des Glutamat-Glutamin-Zyklus reguliert. Schließlich zeigten wir Auswirkungen von Adgrv1 in Astrozyten auf die neuronale Entwicklung und Synaptogenese.

Zusammenfassend lässt sich sagen, dass ADGRV1 für die Entwicklung und Physiologie der primären Astrozyten von entscheidender Bedeutung ist und an mehreren verschiedenen Kompartimenten beteiligt ist. Diese Erkenntnisse geben vor allem erste wertvoll Einblicke in

die Pathogenese der ADGRV1-Dysfunktion bei Epilepsie. Die Aufklärung von ADGRV1 als regulatorisches Molekül im ZNS könnte zum Verständnis der Pathomechanismen beitragen, die der Epilepsie oder anderen neurologischen Erkrankungen zugrunde liegen.

7. Appendix

7.1 References

Allen NJ, Eroglu C. 2017. Cell Biology of Astrocyte-Synapse Interactions. Neuron 96:697–708.

Alper SL. 2006. Molecular physiology of SLC4 anion exchangers. Exp Physiol 91:153–161.

Ambudkar S V., Kim IW, Sauna ZE. 2006. The power of the pump: Mechanisms of action of P-glycoprotein (ABCB1). European Journal of Pharmaceutical Sciences 27:392–400.

Anderson GR, Maxeiner S, Sando R, Tsetsenis T, Malenka RC, Südhof TC. 2017. Postsynaptic adhesion GPCR latrophilin-2 mediates target recognition in entorhinal-hippocampal synapse assembly. Journal of Cell Biology 216:3831–3846.

Araç D, Boucard AA, Bolliger MF, Nguyen J, Soltis SM, Südhof TC, Brunger AT. 2012. A novel evolutionarily conserved domain of cell-adhesion GPCRs mediates autoproteolysis. EMBO Journal 31:1364–1378.

Bahi-Buisson N, El Sabbagh S, Soufflet C, Escande F, Boddaert N, Valayannopoulos V, Bellané-Chantelot C, Lascelles K, Dulac O, Plouin P, de Lonlay P. 2008. Myoclonic absence epilepsy with photosensitivity and a gain of function mutation in glutamate dehydrogenase. Seizure 17:658–664.

Barbosa AC, Kim MS, Ertunc M, Adachi M, Nelson ED, McAnally J, Richardson JA, Kavalali ET, Monteggia LM, Bassel-Duby R, Olson EN. 2008. MEF2C, a transcription factor that facilitates learning and memory by negative regulation of synapse numbers and function. Proc Natl Acad Sci U S A 105:9391–9396.

Benarroch EE. 2005. Neuron-astrocyte interactions: Partnership for normal function and disease in the central nervous system. Mayo Clin Proc 80:1326–1338.

Bou Assi E, Nguyen DK, Rihana S, Sawan M. 2017. Towards accurate prediction of epileptic seizures: A review. Biomed Signal Process Control 34:144–157.

Broadhead MJ, Bonthron C, Waddington J, Smith W V., Lopez MF, Burley S, Valli J, Zhu F, Komiyama NH, Smith C, Grant SGN, Miles GB. 2022. Selective vulnerability of tripartite synapses in amyotrophic lateral sclerosis. Acta Neuropathol 143:471–486.

Butler KM, Moody OA, Schuler E, Coryell J, Alexander JJ, Jenkins A, Escayg A. 2018. De novo variants in GABRA2 and GABRA5 alter receptor function and contribute to early-onset epilepsy. Brain 141:2392–2405.

Caires HR, Barros da Silva P, Barbosa MA, Almeida CR. 2018. A co-culture system with three different primary human cell populations reveals that biomaterials and MSC modulate macrophage-driven fibroblast recruitment. J Tissue Eng Regen Med 12:e1433–e1440.

Camp CR, Yuan H. 2020. GRIN2D/GluN2D NMDA receptor: Unique features and its contribution to pediatric developmental and epileptic encephalopathy. European Journal of Paediatric Neurology 24:89–99.

Chan F, Lax NZ, Voss CM, Aldana BI, Whyte S, Jenkins A, Nicholson C, Nichols S, Tilley E, Powell Z, Waagepetersen HS, Davies CH, Turnbull DM, Cunningham MO. 2019. The role of astrocytes in seizure generation: Insights from a novel in vitro seizure model based on mitochondrial dysfunction. Brain 142:391–411.

Chen YJ, Shi YW, Xu HQ, Chen ML, Gao MM, Sun WW, Tang B, Zeng Y, Liao WP. 2015. Electrophysiological Differences between the Same Pore Region Mutation in SCN1A and SCN3A. Mol Neurobiol 51:1263–1270.

Cho S, Muthukumar AK, Stork T, Coutinho-Budd JC, Freeman MR. 2018a. Focal adhesion molecules regulate astrocyte morphology and glutamate transporters to suppress seizure-like behavior. Proc Natl Acad Sci U S A 115:11316–11321.

Cho S, Muthukumar AK, Stork T, Coutinho-Budd JC, Freeman MR. 2018b. Focal adhesion molecules regulate astrocyte morphology and glutamate transporters to suppress seizure-like behavior. Proceedings of the National Academy of Sciences 115:11316–11321.

Chong D, Jones NC, Schittenhelm RB, Anderson A, Casillas-Espinosa PM. 2023. Multi-omics integration and epilepsy: Towards a better understanding of biological mechanisms. Prog Neurobiol 227:102480.

Cooper A, Grigoryan G, Guy-David L, Tsoory MM, Chen A, Reuveny E. 2012. Trisomy of the G protein-coupled K + channel gene, Kcnj6, affects reward mechanisms, cognitive functions, and synaptic plasticity in mice. Proc Natl Acad Sci U S A 109:2642–2647.

Curtin JA, Quint E, Tsipouri V, Arkell RM, Cattanach B, Copp AJ, Henderson DJ, Spurr N, Stanier P, Fisher EM, Nolan PM, Steel KP, Brown SDM, Gray IC, Murdoch JN. 2003. Mutation of Celsr1 Disrupts Planar Polarity of Inner Ear Hair Cells and Causes Severe Neural Tube Defects in the Mouse. Current Biology 13:1129–1133.

Demberg LM, Winkler J, Wilde C, Simon KU, Schön J, Rothemund S, Schöneberg T, Prömel S, Liebscher I. 2017. Activation of adhesion G protein-coupled receptors: Agonist specificity of Stachel sequence-derived peptides. Journal of Biological Chemistry 292:4383–4394.

DiMilla PA, Barbee K, Lauffenburger DA. 1991. Mathematical model for the effects of adhesion and mechanics on cell migration speed. Biophys J 60:15–37.

Raizen DM, Brooks-Kayal A, Steinkrauss L, Tennekoon GI, Stanley CA, Kelly A2005. Central nervous system hyperexcitability associated with glutamate dehydrogenase gain of function mutations. Journal of Pediatrics 146:388–394.

Duan D, Goemans N, Takeda S, Mercuri E, Aartsma-Rus A. 2021. Duchenne muscular dystrophy. Nat Rev Dis Primers 7:13.

Favara DM, Banham AH, Harris AL. 2014. A review of ELTD1, a pro-angiogenic adhesion GPCR. Biochem Soc Trans 42:1658–1664.

Feria Pliego JA, Pedroarena CM. 2020. Kv1 potassium channels control action potential firing of putative GABAergic deep cerebellar nuclear neurons. Sci Rep 10:1–13.

Folts CJ, Giera S, Li T, Piao X. 2019. Adhesion G Protein-Coupled Receptors as Drug Targets for Neurological Diseases. Trends Pharmacol Sci 40:278–293.

Förster E, Bock HH, Herz J, Chai X, Frotscher M, Zhao S. 2010. Emerging topics in Reelin function. European Journal of Neuroscience 31:1511–1518.

Fredriksson R, Lagerström MC, Lundin LG, Schiöth HB. 2003. The G-protein-coupled receptors in the human genome form five main families. Phylogenetic analysis, paralogon groups, and fingerprints. Mol Pharmacol 63:1256–1272.

Gad AA, Balenga N. 2020. The Emerging Role of Adhesion GPCRs in Cancer. ACS Pharmacol Transl Sci 3:29–42.

Gardel ML, Schneider IC, Aratyn-Schaus Y, Waterman CM. 2010. Mechanical integration of actin and adhesion dynamics in cell migration. Annu Rev Cell Dev Biol 26:315–333.

Geiger B, Spatz JP, Bershadsky AD. 2009. Environmental sensing through focal adhesions. Nat Rev Mol Cell Biol 10:21–33.

George AL, Knittle TJ, Tamkun MM. 1992. Molecular cloning of an atypical voltage-gated sodium channel expressed in human heart and uterus: Evidence for a distinct gene family. Proc Natl Acad Sci U S A 89:4893–4897.

Glukhova A, Draper-Joyce CJ, Sunahara RK, Christopoulos A, Wootten D, Sexton PM. 2018. Rules of Engagement: GPCRs and G Proteins. ACS Pharmacol Transl Sci 1:73–83.

González-Reyes RE, Nava-Mesa MO, Vargas-Sánchez K, Ariza-Salamanca D, Mora-Muñoz L. 2017. Involvement of astrocytes in Alzheimer's disease from a neuroinflammatory and oxidative stress perspective. Front Mol Neurosci 10:1–20.

Grudzien-Nogalska E, Jiao X, Song MG, Hart RP, Kiledjian M. 2016. Nudt3 is an mRNA decapping enzyme that modulates cell migration. Rna 22:773–781.

Halvardson J, Zhao JJ, Zaghlool A, Wentzel C, Georgii-Hemming P, Månsson E, Sävmarker HE, Brandberg G, Zander CS, Thuresson AC, Feuk L. 2016. Mutations in HECW2 are associated with intellectual disability and epilepsy. J Med Genet 53:697–704.

Hamann J, Aust G, Araç D, Engel FB, Formstone C, Fredriksson R, Hall RA, Harty BL, Kirchhoff C, Knapp B, Krishnan A, Liebscher I, Lin HH, Martinelli DC, Monk KR, Peeters MC, Piao X, Prömel S, Schöneberg T, Schwartz TW, Singer K, Stacey M, Ushkaryov YA, Vallon M, Wolfrum U, Wright MW, Xu L, Langenhan T, Schiöth HB. 2015. International union of basic and clinical pharmacology. XCIV. adhesion G protein-coupled receptors. Pharmacol Rev 67:338–367.

Hayashi MK, Sato K, Sekino Y. 2022. Neurons Induce Tiled Astrocytes with Branches That Avoid Each Other. Int J Mol Sci 23.

Hayashi S, Inoue Y, Kiyonari H, Abe T, Misaki K, Moriguchi H, Tanaka Y, Takeichi M. 2014. Protocadherin-17 Mediates Collective Axon Extension by Recruiting Actin Regulator Complexes to Interaxonal Contacts. Dev Cell 30:673–687.

Herde MK, Bohmbach K, Domingos C, Vana N, Komorowska-Müller JA, Passlick S, Schwarz I, Jackson CJ, Dietrich D, Schwarz MK, Henneberger C. 2020. Local Efficacy of Glutamate Uptake Decreases with Synapse Size. Cell Rep 32.

Hu Q-X, Dong J-H, Du H-B, Zhang D-L, Ren H-Z, Ma M-L, Cai Y, Zhao T-C, Yin X-L, Yu X, Xue T, Xu Z-G, Sun J-P. 2014a. Constitutive Gαi Coupling Activity of Very Large G Protein-coupled Receptor 1 (VLGR1) and Its Regulation by PDZD7 Protein. Journal of Biological Chemistry 289:24215–24225.

Hu YL, Lu S, Szeto KW, Sun J, Wang Y, Lasheras JC, Chien S. 2014b. FAK and paxillin dynamics at focal adhesions in the protrusions of migrating cells. Sci Rep 4:1–7.

Jang W, Lu S, Xu X, Wu G, Lambert NA. 2023. selectivity. 19:687–694.

Januszyk M, Rennert R, Sorkin M, Maan Z, Wong L, Whittam A, Whitmore A, Duscher D, Gurtner G. 2015. Evaluating the Effect of Cell Culture on Gene Expression in Primary Tissue Samples Using Microfluidic-Based Single Cell Transcriptional Analysis. Microarrays 4:540–550.

Ji T, Downs AW, Dorris L, Zhong N. 2023. De novo ADGRV1 variant in a patient with ictal asystole provides novel clues for increased risk of SUDEP. Acta Epileptologica 5.

Jin H, Nachury M V. 2009. The BBSome. Current Biology 19:472–473.

Johannesen KM, Tümer Z, Weckhuysen S, Barakat TS, Bayat A. 2023. Solving the unsolved genetic epilepsies: Current and future perspectives. Epilepsia 64:3143–3154.

Kang SK, Vanoye CG, Misra SN, Echevarria DM, Calhoun JD, O'Connor JB, Fabre KL, McKnight D, Demmer L, Goldenberg P, Grote LE, Thiffault I, Saunders C, Strauss KA, Torkamani A, van der Smagt J, van Gassen K, Carson RP, Diaz J, Leon E, Jacher JE, Hannibal MC, Litwin J, Friedman NR, Schreiber A, Lynch B, Poduri A, Marsh ED, Goldberg EM, Millichap JJ, George AL, Kearney JA. 2019. Spectrum of K V 2.1 Dysfunction in KCNB1 -Associated Neurodevelopmental Disorders. Ann Neurol 86:899–912.

Kim DH, Wirtz D. 2013. Focal adhesion size uniquely predicts cell migration. FASEB Journal 27:1351–1361.

Knapp B, Roedig J, Boldt K, Krzysko J, Horn N, Ueffing M, Wolfrum U. 2019. Affinity proteomics identifies novel functional modules related to adhesion GPCRs. Ann N Y Acad Sci 1456:144–167.

Knapp B, Roedig J, Roedig H, Krzysko J, Horn N, Güler BE, Kusuluri DK, Yildirim A, Boldt K, Ueffing M, Liebscher I, Wolfrum U. 2022. Affinity Proteomics Identifies Interaction Partners and Defines Novel Insights into the Function of the Adhesion GPCR VLGR1/ADGRV1. Molecules 27.

Kostourou V, Goult BT, Ambriović-Ristov A. 2023. Editorial: Integrin adhesion receptors in health and disease. Front Cell Dev Biol 11:1–3.

Kuhn CK, Stenzel U, Berndt S, Liebscher I, Schöneberg T, Horn S. 2024. The repertoire and structure of adhesion GPCR transcript variants assembled from publicly available deep-sequenced human samples. Nucleic Acids Res.

Langenhan T. 2020. Adhesion G protein–coupled receptors—Candidate metabotropic mechanosensors and novel drug targets. Basic Clin Pharmacol Toxicol 126:5–16.

Larsen J, Johannesen KM, Ek J, Tang S, Marini C, Blichfeldt S, Kibæk M, Von Spiczak S, Weckhuysen S, Frangu M, Neubauer BA, Uldall P, Striano P, Zara F, Kleiss R, Simpson M, Muhle H, Nikanorova M, Jepsen B, Tommerup N, Stephani U, Guerrini R, Duno M, Hjalgrim H, Pal D, Helbig I, Møller RS, Craiu DC, Caglayan HS, Talvik T, Weber YG, Barisic N. 2015. The role of SLC2A1 mutations in myoclonic astatic epilepsy and absence epilepsy, and the estimated frequency of GLUT1 deficiency syndrome. Epilepsia 56:e203–e208.

Lechan RM, Fekete C. 2006. Chapter 12: The TRH neuron: a hypothalamic integrator of energy metabolism. Prog Brain Res 153:209–235.

Lee H, Lin M chin A, Kornblum HI, Papazian DM, Nelson SF. 2014. Exome sequencing identifies de novo gain of function missense mutation in KCND2 in identical twins with autism and seizures that slows potassium channel inactivation. Hum Mol Genet 23:3481–3489.

Lehman A, Thouta S, Mancini GMS, Naidu S, van Slegtenhorst M, McWalter K, Person R, Mwenifumbo J, Salvarinova R, Adam S, du Souich C, Elliott AM, Nelson TN, van Karnebeek C, Friedman JM, Boelman C, Bolbocean C, Buerki SE, Candido T, Eydoux P, Evans DM, Gibson W, Horvath G, Huh L, Sinclair G, Tarling T, Toyota EB, Townsend KN, Van Allen MI, Vercauteren S, Guella I, McKenzie MB, Datta A, Connolly MB, Kalkhoran SM, Poburko D, Farrer MJ, Demos M, Desai S, Claydon T. 2017. Loss-of-Function and Gain-of-Function Mutations in KCNQ5 Cause Intellectual Disability or Epileptic Encephalopathy. Am J Hum Genet 101:65–74.

Lemoine D, Jiang R, Taly A, Chataigneau T, Specht A, Grutter T. 2012. Ligand-gated ion channels: New insights into neurological disorders and ligand recognition. Chem Rev 112:6285–6318.

Leng X, Zhang T, Guan Y, Tang M. 2022. Genotype and phenotype analysis of epilepsy caused by ADGRV1 mutations in Chinese children. Seizure 103:108–114.

Li S, Jin Z, Koirala S, Bu L, Xu L, Hynes RO, Walsh CA, Corfas G, Piao X. 2008. GPR56 regulates pial basement membrane integrity and cortical lamination. Journal of Neuroscience 28:5817–5826.

Liebscher I, Schön J, Petersen SC, Fischer L, Auerbach N, Demberg LM, Mogha A, Cöster M, Simon KU, Rothemund S, Monk KR, Schöneberg T. 2014. A Tethered Agonist within the Ectodomain Activates the Adhesion G Protein-Coupled Receptors GPR126 and GPR133. Cell Rep 9:2018–2026.

Lintz M, Muñoz A, Reinhart-King CA. 2017. The Mechanics of Single Cell and Collective Migration of Tumor Cells. J Biomech Eng 139:1–9.

Liu JYW, Dzurova N, Al-Kaaby B, Mills K, Sisodiya SM, Thom M. 2020. Granule Cell Dispersion in Human Temporal Lobe Epilepsy: Proteomics Investigation of Neurodevelopmental Migratory Pathways. Front Cell Neurosci 14.

Mahmoud S, Gharagozloo M, Simard C, Gris D. 2019. Astrocytes maintain glutamate homeostasis in the cns by controlling the balance between glutamate uptake and release. Cells 8:1–27.

Maziveyi M, Alahari SK. 2017. Shiho shoshi pafekuto kako mondaishu. 2022-8. 8:48471–48487.

McMillan DR, White PC. 2004. Loss of the transmembrane and cytoplasmic domains of the very large G-protein-coupled receptor-1 (VLGR1 or Mass1) causes audiogenic seizures in mice. Molecular and Cellular Neuroscience 26:322–329.

McMillan DR, White PC. 2010. Studies on the very large G protein-coupled receptor: from initial discovery to determining its role in sensorineural deafness in higher animals. Adv Exp Med Biol 706:76–86.

Michinaga S, Koyama Y. 2019. Dual roles of astrocyte-derived factors in regulation of blood-brain barrier function after brain damage. Int J Mol Sci 20:1–22.

Mishra YG, Manavathi B. 2021. Focal adhesion dynamics in cellular function and disease. Cell Signal 85:110046.

Monterey MD, Wei H, Wu X, Wu JQ. 2021. The Many Faces of Astrocytes in Alzheimer's Disease. Front Neurol 12:1–12.

Muhle Hiltrud H, von Spiczak S, Gaus V, Kara S, Helbig I, Hampe J, Franke A, Weber Y, Lerche H, Kleefuss-Lie AA, Elger CE, Schreiber S, Stephani U, Sander T. 2010. Role of GRM4 in idiopathic generalized epilepsies analysed by genetic association and sequence analysis. Epilepsy Res 89:319–326.

Myers KA, Nasioulas S, Boys A, McMahon JM, Slater H, Lockhart P, du Sart D, Scheffer IE. 2018. ADGRV1 is implicated in myoclonic epilepsy. Epilepsia 59:381–388.

Niday Z, Tzingounis A V. 2018. Potassium Channel Gain of Function in Epilepsy: An Unresolved Paradox. Neuroscientist 24:368–380.

Nimmerjahn A, Bergles DE. 2015. Large-scale recording of astrocyte activity. Curr Opin Neurobiol 32:95–106.

Odoemelam CS, Percival B, Wallis H, Chang MW, Ahmad Z, Scholey D, Burton E, Williams IH, Kamerlin CL, Wilson PB. 2020. G-Protein coupled receptors: Structure and function in drug discovery. RSC Adv 10:36337–36348.

Okajima D, Kudo G, Yokota H. 2010. Brain-specific angiogenesis inhibitor 2 (BAI2) may be activated by proteolytic processing. Journal of Receptors and Signal Transduction 30:143–153.

Ouyang Y-B, Xu L, Liu S, Giffard RG. 2014. Role of Astrocytes in Delayed Neuronal Death: GLT-1 and its Novel Regulation by MicroRNAs. :171–188.

Paavola KJ, Stephenson JR, Ritter SL, Alter SP, Hall RA. 2011. The N terminus of the adhesion G protein-coupled receptor GPR56 controls receptor signaling activity. Journal of Biological Chemistry 286:28914–28921.

Pawluchin A, Galic M. 2022. Moving through a changing world: Single cell migration in 2D vs. 3D. Front Cell Dev Biol 10:1–14.

Pedersen JE, Bergqvist CA, Larhammar D. 2018. Evolution of the muscarinic acetylcholine receptors in vertebrates. eNeuro 5:1–12.

Perea G, Navarrete M, Araque A. 2009. Tripartite synapses: astrocytes process and control synaptic information. Trends Neurosci 32:421–431.

Platel JC, Bordey A. 2016. The multifaceted subventricular zone astrocyte: From a metabolic and pro-neurogenic role to acting as a neural stem cell. Neuroscience 323:20–28.

Pollini L, Galosi S, Tolve M, Caputi C, Carducci C, Angeloni A, Leuzzi V. 2020. KCND3-related neurological disorders: From old to emerging clinical phenotypes. Int J Mol Sci 21:1–15.

Qin R, Cao S, Lyu T, Qi C, Zhang W, Wang Y. 2017. CDYL Deficiency Disrupts Neuronal Migration and Increases Susceptibility to Epilepsy. Cell Rep 18:380–390.

Raghavan S, Vaezi A, Fuchs E. 2003. A role for αβ1 integrins in focal adhesion function and polarized cytoskeletal dynamics. Dev Cell 5:415–427.

Randy McMillan D, Kayes-Wandover KM, Richardson JA, White PC. 2002. Very large G protein-coupled receptor-1, the largest known cell surface protein, is highly expressed in the developing central nervous system. Journal of Biological Chemistry 277:785–792.

Richter M, Piwocka O, Musielak M, Piotrowski I, Suchorska WM, Trzeciak T. 2021. From Donor to the Lab: A Fascinating Journey of Primary Cell Lines. Front Cell Dev Biol 9:1–11.

Rose CR, Felix L, Zeug A, Dietrich D, Reiner A, Henneberger C. 2018. Astroglial glutamate signaling and uptake in the hippocampus. Front Mol Neurosci 10:1–20.

Rosenbaum DM, Rasmussen SGF, Kobilka BK. 2009. The structure and function of G-protein-coupled receptors. Nature 459:356–363.

Sakurai T, Kamakura S, Hayase J, Kohda A, Nakamura M, Sumimoto H. 2022. GPR125 (ADGRA3) is an autocleavable adhesion GPCR that traffics with Dlg1 to the basolateral membrane and regulates epithelial apicobasal polarity. Journal of Biological Chemistry 298:102475.

Saunders RM, Holt MR, Jennings L, Sutton DH, Barsukov IL, Bobkov A, Liddington RC, Adamson EA, Dunn GA, Critchley DR. 2006. Role of vinculin in regulating focal adhesion turnover. Eur J Cell Biol 85:487–500.

Shim S, Goyal R, Panoutsopoulos AA, Balashova OA, Lee D, Borodinsky LN. 2023. Calcium dynamics at the neural cell primary cilium regulate Hedgehog signaling–dependent neurogenesis in the embryonic neural tube. Proceedings of the National Academy of Sciences 120:2017.

Sidoryk-Wegrzynowicz M, Wegrzynowicz M, Lee E, Bowman AB, Aschner M. 2011. Role of Astrocytes in Brain Function and Disease. Toxicol Pathol 39:115–123.

Simons C, Rash LD, Crawford J, Ma L, Cristofori-Armstrong B, Miller D, Ru K, Baillie GJ, Alanay Y, Jacquinet A, Debray FG, Verloes A, Shen J, Yesil G, Guler S, Yuksel A, Cleary JG, Grimmond SM, McGaughran J, King GF, Gabbett MT, Taft RJ. 2015. Mutations in the voltage-gated potassium channel gene KCNH1 cause Temple-Baraitser syndrome and epilepsy. Nat Genet 47:73–77.

Singh B, Monteil A, Bidaud I, Sugimoto Y, Suzuki T, Hamano S ichiro, Oguni H, Osawa M, Alonso ME, Delgado-Escueta A V., Inoue Y, Yasui-Furukori N, Kaneko S, Lory P, Yamakawa K. 2007. Mutational analysis of CACNA1G in idiopathic generalized epilepsy. Mutation in brief #962. Online. Hum Mutat 28:524–525.

Steinlein OK. 2000. Neuronal nicotinic receptors in human epilepsy. Eur J Pharmacol 393:243–247.

Stoveken HM, Hajduczok AG, Xu L, Tall GG. 2015. Adhesion G protein-coupled receptors are activated by exposure of a cryptic tethered agonist. Proc Natl Acad Sci U S A 112:6194–6199.

Suh YH, Terashima A, Petralia RS, Wenthold RJ, Isaac JTR, Roche KW, Roche PA. 2010. A neuronal role for SNAP-23 in postsynaptic glutamate receptor trafficking. Nat Neurosci 13:338–343.

Suzuki N, Gradin K, Poellinger L, Yamamoto M. 2017. Regulation of hypoxia-inducible gene expression after HIF activation. Exp Cell Res 356:182–186.

Tabata H. 2015. Diverse subtypes of astrocytes and their development during corticogenesis. Front Neurosci 9:1–7.

Tautermann CS, Binder F, Büttner FH, Eickmeier C, Fiegen D, Gross U, Grundl MA, Heilker R, Hobson S, Hoerer S, Luippold A, Mack V, Montel F, Peters S, Bhattacharya S, Vaidehi N, Schnapp G, Thamm S, Zeeb M. 2019. Allosteric Activation of Striatal-Enriched Protein Tyrosine Phosphatase (STEP, PTPN5) by a Fragment-like Molecule. J Med Chem 62:306–316.

Tiong SYX, Oka Y, Sasaki T, Taniguchi M, Doi M, Akiyama H, Sato M. 2019. Kcnab1 is expressed in subplate neurons with unilateral long-range inter-areal projections. Front Neuroanat 13:1–16.

Toro B, Cox N, Wilson RJ, Garrido-Sanabria E, Stefani E, Toro L, Zarei MM. 2006. KCNMB1 regulates surface expression of a voltage and Ca2+-activated K+ channel via endocytic trafficking signals. Neuroscience 142:661–669.

Ventura R, Harris KM. 1999. Three-dimensional relationships between hippocampal synapses and astrocytes. Journal of Neuroscience 19:6897–6906.

Vezzani A, Ravizza T, Bedner P, Aronica E, Steinhäuser C, Boison D. 2022. Astrocytes in the initiation and progression of epilepsy. Nat Rev Neurol 18:707–722.

Wang Y, Fan X, Zhang W, Zhang C, Wang J, Jiang T, Wang L. 2015. Deficiency of very large G-protein-coupled receptor-1 is a risk factor of tumor-related epilepsy: a whole transcriptome sequencing analysis. J Neurooncol 121:609–616.

Weston MD, Luijendijk MWJ, Humphrey KD, Möller C, Kimberling WJ. 2004. Mutations in the VLGR1 Gene Implicate G-Protein Signaling in the Pathogenesis of Usher Syndrome Type II. Am J Hum Genet 74:357–366.

Wu JY, Cho SJ, Descant K, Li PH, Shapson-Coe A, Januszewski M, Berger DR, Meyer C, Casingal C, Huda A, Liu J, Ghashghaei T, Brenman M, Jiang M, Scarborough J, Pope A, Jain V, Stein JL, Guo J, Yasuda R, Lichtman JW, Anton ES. 2023. Mapping of neuronal and glial primary cilia contactome and connectome in the human cerebral cortex. Neuron:1–15.

Wu Z, Deshpande T, Henning L, Bedner P, Seifert G, Steinhäuser C. 2021. Cell death of hippocampal CA1 astrocytes during early epileptogenesis. Epilepsia 62:1569–1583.

Yagi H, Takamura Y, Yoneda T, Konno D, Akagi Y, Yoshida K, Sato M. 2005. Vlgr1 knockout mice show audiogenic seizure susceptibility. J Neurochem 92:191–202.

Yamaguchi N, Knaut H. 2022. Focal adhesion-mediated cell anchoring and migration: from in vitro to in vivo. Development 149.

Zhao R, Goldman ID. 2013. Folate and thiamine transporters mediated by facilitative carriers (SLC19A1-3 and SLC46A1) and folate receptors. Mol Aspects Med 34:373–385.

Zheng K, Scimemi A, Rusakov DA. 2008. Receptor actions of synaptically released glutamate: The role of transporters on the scale from nanometers to microns. Biophys J 95:4584–4596.

Zhou B, Zuo YX, Jiang RT. 2019. Astrocyte morphology: Diversity, plasticity, and role in neurological diseases. CNS Neurosci Ther 25:665–673.

Zhou P, Meng H, Liang X, Lei X, Zhang J, Bian W, He N, Lin Z, Song X, Zhu W, Hu B, Li B, Yan L, Tang B, Su T, Liu H, Mao Y, Zhai Q, Yi Y. 2022a. ADGRV1 Variants in Febrile Seizures/Epilepsy With Antecedent Febrile Seizures and Their Associations With Audio-Visual Abnormalities. Front Mol Neurosci 15.

Zhou P, Meng H, Liang X, Lei X, Zhang J, Bian W, He N, Lin Z, Song X, Zhu W, Hu B, Li B, Yan L, Tang B, Su T, Liu H, Mao Y, Zhai Q, Yi Y. 2022b. ADGRV1 Variants in Febrile Seizures/Epilepsy With Antecedent Febrile Seizures and Their Associations With Audio-Visual Abnormalities. Front Mol Neurosci 15.

7.2 Contributions made to the individual publications

This cumulative thesis consists of a total of four publications. The contributions were made by me, and other colleagues outlined in the following sections.

In **Publication I**, Güler et al., 2022, we developed and optimized a method for isolating primary astrocytes which were facilitated in this cumulative thesis. Dr. Jacek Krysko helped during the optimization of the protocol in all steps. Isolation of the primary brain cells and differential bindings were conducted by me and Dr. Krysko. Maintenance and the storage of the cells were conducted by me. The figures through the publication were prepared by me.

In **Publication II**, Kusuluri et al., 2021, All mass spectrometric measurements work were done by our cooperation partner Dr. Karsten Boldt and Dr. Nicola Horn (working group of Prof. Marius Ueffing) in Tübingen. The raw data for the TAP analysis were generated by Dr. Barbara Knapp and all the experiment in hTERT-RPE1 cells were conducted by Dr. Deva Kurupakar Kusuluri. This study has been outlined and designed by Prof. Uwe Wolfrum and Dr. Deva Kurupakar Kusuluri. My contribution to this publication was limited to experiments related to primary astrocytes which were isolated from Adgrv1/del7TM and Adgrv1/DrumB mice brain. The figures related to analysis of ADGRV1 in primary astrocytes were prepared by me (Publication I, Fig. 3 D-I, Fig. 5C, Fig. 7D-F, Fig. S3, Fig. S7).

In **Publication III**, Güler et al., 2023, we intensively used live-cell imaging method for the analysis of FA kinetics. Live-cell imaging was performed in the lab of Prof. Claire Jacob. Technical guidance for the live cell imaging has been provided by Dr. Gianuligi Nocera. All figures and experiments were performed by me. Primary astrocyte isolation and culturing was performed by me and Joshua Linnert.

In **Preprint I**, Güler et al., 2024, perfusion fixation of the Adgrv1/del7TM and WT mice were performed in the lab of Prof. Clarie Jacob. During the perfusion fixation Dr. Gianluigi Nocera and Nadège Hertzog assisted me. Western blots have been performed by me and Ulrike Maas. Cryosections for immunohistochemistry staining were prepared by me and Yvonne Kerner and subsequently microscopically analysed and documented by me. The RNA isolation and RNAseq procedures were performed by me and Joshua Linnert. The whole transcriptome analysis of mouse hippocampus was reanalysed by Mark Zorin. The RNA isolation for the USH2C patient-derived fibroblast (Patient-derived fibroblasts provided by Dr. Erwin van Wijk), was conducted by Joshua Linnert. Neuron cultures were prepared by me with the help of Prof. Martin Heine´s group members Dr. Arthur Bikbaev and Dr. Filip Maciag.

7.3 Acknowledgement

I would like to express my gratitude to Prof. Uwe Wolfrum for providing me an independent working environment and support throughout my doctoral studies. I am grateful for accepting me into his research group and leading the way in opening a new chapter in my career and life.

I would like to extend my sincere thanks to the ADGRV1 team members Dr. Jacek Krysko and Joshua Linnert. Throughout my doctoral studies, all the conversations and discussions we had significantly contributed to the formation of this doctoral thesis in its current state. Dr. Krysko deserves special thanks not only for being an office and teammate but also for being a good friend.

I also would like to express my sincere thanks to all former members of Prof. Dr. Wolfrum's group whom I had the privilege to meet and current members for all the times we spent together during this journey. I want to thank Ulli Maas, Yvonne Kerner, and the late Elisabeth Sehn for their technical and moral support.

I also thank Prof. Clarie Jacob and her laboratory members for their invaluable assistance and guidance in the field of live-cell imaging microscopy. Additionally, I would like to acknowledge Dr. Erwin van Wijk for providing us with patient-derived cells, which have contributed to our deeper understanding of ADGRV1 dysfunction.

I want to express special thanks to my mother and father. I hope this doctoral thesis may help to alleviate, even if only a bit, the fatigue brought on by the sleepless nights and intense labor they have experienced to raise me. Finally, I also want to express my gratitude to my elder brothers for all the humanitarian values and philosophical perspectives they have imparted to me.

7.4 Curriculum Vitae

PERSONAL INFORMATION

Date of Birth : 26.09.1992

Place of Birth: Ankara / TURKEY

Nationality : Turkish

Marital Status: Single

EDUCATION

PhD

2019-2024 : Institute of Molecular Pysiologie, Johannes Gutenberg University-Mainz, **Dissertation:** The molecular role of the adhesion GPCR ADGRV1 in astrocytes: from morphology to functionality

MSc

2015- 2017 : Uludag University, Graduate School of Natural and Applied Sciences, Department of Biology (Molecular Biology), GPA: 4.00, TURKEY

2016 - 2017 : University of Bialystok, Faculty of Biology and Chemistry (ERASMUS+ Student Exchange Programme), POLAND

BSc

2010- 2015 : Uludag University, Faculty of Science and Art, Biology Department, GPA: 3.17 finished 3th in the place, TURKEY

ACADEMIC/ TEACHING EXPERIENCE

2016- Teaching Assistant, Uludag University Biology Department

2019-2024 Research assistant (doctoral student)- AG Wolfrum
Johannes Gutenberg University- Mainz

- Molecular biology methods (Cloning, PCR, qPCR, RNAseq, Transformation, Transfection)
- Microscopic methods (Confocal microscopy, live cell imaging)
- Immunocytochemistry, immunohistochemistry methods,
- Animal model studies
- Supervision of, bachelor's and master's students
- Participation in writing scientific publications

REVIEWING ACTIVITIES

2023

iScience – Cell Press

2022-

Star Protocols – Cell Press

Journal of Neurochemistry – Wiley Reviewer in training

8. Decleration

I affirm that this thesis is the result of my own original research efforts. It has not been submitted for any degree at this university or any other institution before. I have duly credited and referenced all verbatim excerpts or content derived from published or unpublished works by others. Throughout the research described in this dissertation, I have adhered to the principles of ethical scientific conduct as outlined by Johannes Gutenberg University of Mainz.

Baran Enes Güler

Mainz, Germany